



ULPGC
Universidad de
Las Palmas de
Gran Canaria

Contribution to Optical Camera Communication using
multispectral cameras and LED's thermal effect

Juan Daniel Moreno Gázquez

Doctoral thesis
to achieve the academic degree of

Doctor of Philosophy
(*Ph.D.*)

in the doctorate program
EmTIC - Empresa, Internet y Tecnologías de las Comunicaciones

IDeTIC - Instituto Universitario para el Desarrollo Tecnológico y la Innovación en
Comunicaciones

Universidad de Las Palmas de Gran Canaria

Date: January 2024

Supervisors

Prof. Dr. José Alberto Rabadán Borges
IDeTIC, Universidad de Las Palmas de Gran Canaria

Dr. Julio Francisco Rufo Torres
Universidad de La Laguna

D. JOSÉ A. RABADÁN BORGES
COORDINADOR DEL PROGRAMA DE DOCTORADO
EMPRESA, INTERNET Y TECNOLOGÍAS DE LAS COMUNICACIONES DE LA
UNIVERSIDAD DE LAS PALMAS DE GRAN CANARIA

INFORMA,

De que la Comisión Académica del Programa de Doctorado, en su sesión de fecha tomó el acuerdo de dar el consentimiento para su tramitación, a la tesis doctoral titulada “*Contribution to Optical Camera Communication using multispectral cameras and LED’s thermal effect*” presentada por el/la doctorando/a D. Juan Daniel Moreno Gázquez y dirigida por los Doctores José Alberto Rabadán Borges y Julio Francisco Rufo Torres.

Y para que así conste, y a efectos de lo previsto en el Art.º 11 del Reglamento de Estudios de Doctorado (BOULPGC 04/03/2019) de la Universidad de Las Palmas de Gran Canaria, firmo la presente en Las Palmas de Gran Canaria, a de.....de dos mil veintitrés.

UNIVERSIDAD DE LAS PALMAS DE GRAN CANARIA
ESCUELA DE DOCTORADO

Programa de doctorado: Empresa, Internet y Tecnologías de las Comunicaciones.

Título de la Tesis: Contribution to Optical Camera Communication using multispectral cameras and LED's thermal effect.

Tesis Doctoral presentada por D. Juan Daniel Moreno Gázquez.

Dirigida por el Prof. Dr. José Alberto Rabadán Borges.

Codirigida por el Dr. Julio Francisco Rufo Torres.

En Las Palmas de Gran Canaria, a de de 2023.

El/la Directora/a,

El/la Codirector/a,

El/la Doctorando/a,

Dedication

Quiero agradecer a mis directores de tesis, el Dr. José Rabadán y el Dr. Julio Rufo, por el apoyo recibido durante todo el transcurso de este trabajo, así como la confianza depositada en mí.

Además de mis directores, quisiera mostrar mi gratitud a los doctores Víctor Guerra, por su inestimable ayuda en cualquier cuestión, y Rafael Pérez, por sus útiles consejos.

También agradezco a mis compañeros y compañeras del IDeTIC por los buenos momentos vividos y por amenizar diariamente cada descanso en el trabajo.

Fuera del mundo académico, aprecio mucho el apoyo de mis amigos, Mario, Sergio y Dani, por poder confiar en ellos en cualquier circunstancia y compartir memorables vivencias en su compañía.

Asimismo, durante esta etapa conocí a una persona muy importante en mi vida, Cristina, la cual es un gran pilar para mí, por lo que agradezco su disposición a ayudarme y sus ganas de compartir su vida conmigo.

Por último, gracias a mi familia, mi madre, mi padre y mi hermana, por todo el esfuerzo que han realizado que ha permitido que yo pueda presentar esta tesis. Es un privilegio sentir que ellos siempre están ahí cuando los necesito.

Acknowledgments

Funding

This work was benefit from the Universidad de Las Palmas's Trainee Predoctoral Research Staff Program, 2019.

Collaborators

The author thanks the technical contributions and active support from the team members at the IDeTIC in Las Palmas de Gran Canaria, Spain, listed as follows:

- **Main supervisor:** Prof. Dr. José Alberto Rabadán Borges (IDeTIC).
- **Second supervisor:** Dr. Julio Francisco Rufo Torres (ULL).
- **Academic staff:**
 - Dr. Víctor Guerra Yáñez (IDeTIC).
 - Prof. Dr. Rafael Pérez Jiménez (IDeTIC).
- **Technical support:**
 - Behnaz Majlesein (Lightbee, S.L.).

Optical wireless communication (OWC) is progressively emerging as a pivotal technology in upcoming communication networks and is believed to be poised for a revolution within both industry and research sectors. Its capacity to offer huge bandwidth, rapid deployment, and low power consumption has attracted significant attention. Hence, these characteristics position OWC as a compelling candidate to meet the requirements of future communication systems.

Among the principal technologies encompassing OWC, optical camera communication (OCC) has experienced a pronounced increase in recent years owing to the proliferation of camera-equipped devices. Consequently, the widespread adoption of these devices, along with the advances in image sensors, has boosted the interest of OCC. This technology overcomes the limitation of visible light communication (VLC) and light fidelity (LiFi) against path loss and eases the complexity of the implementation with respect to free-space optical (FSO) links. However, one of the major challenges of OCC lies in increasing the data rate, which has led to the development of new techniques and approaches to improve it. In this context, the use of non-conventional cameras is leveraged in order to improve the OCC system performance. Given that the data rate is partially defined by half of the camera's frame rate, high-speed cameras (more than 120 fps) are the predominant choice for increasing the data rate.

Despite that constraint, certain applications prioritize factors other than data rate, making them well-suited for the incorporation of different types of camera to enhance overall system performance. To the best of the author's knowledge, the use of high-spectral-resolution cameras as receivers in OCC

systems remains relatively unexplored. Multispectral (MS) and hyperspectral (HS) cameras provide more bands than conventional red, green, and blue (RGB) types by using narrow band-pass filters. The number of bands, as well as their spectral width, determines the camera's spectral resolution. Those characteristics make these kinds of cameras a valuable tool in several applications, such as remote sensing, agriculture, and medicine. Specifically, MS and HS cameras are set to become a vital factor in precision farming due to the increasing demands in food production, making it necessary to optimize farming practices sustainably. This considerable interest and the particular features of these devices open up a variety of opportunities for communication. Notably, this operating principle of this type of cameras permits capturing the spectral response curve, also known as spectral signature, of different elements of an image. Thus, using light-emitting diodes (LEDs) with different peak wavelengths transmitting certain data, the MS camera captures the signals and could separate them taking advantage of their distinct spectral signature, to decode the information ultimately.

On the other hand, the employment of LEDs has considerably increased in the last decade. Developments in this type of device have caused improvements in their efficiency, allowing high luminous intensity with low power consumption. As a result, it has raised the LED demands in several sectors, such as industrial, commercial, and residential. This increase has also heightened the OWC attention because they are customarily used as the transmitter light source. The key feature that makes these devices helpful for communication is their rapid switching capability that allows modulating light.

Moreover, LEDs are sensitive to temperature variations that affect their performance and spectral features. In general, luminous efficiency decreases, and the peak wavelength increases as temperature grows. Even though the temperature dependence of LEDs is well-known, few researchers have addressed the impact of thermal effects in OWC. Nonetheless, this ef-

fect is analyzed in this thesis. On the one hand, it was suggested to increase the communication channels that can be attained using a single device by taking advantage of the increase in the LED's wavelength (red-shift) along with using a multispectral camera to capture the spectral variations. Thus, this reaction, typically considered harmful to the system performance, is turned into a benefit. On the other hand, the consequences of not taking LED spectral variations in approaches that require channel compensation to diminish inter-channel interference (ICI) are examined.

In this thesis, a set of objectives has been formulated to study the use of multispectral cameras and LED thermal effects in OCC. First, it is intended to implement an OCC link based on the LED's temperature effects and a multispectral camera. Multispectral cameras possess a distinct advantage in their high-spectral resolution, which makes them suitable candidates for capturing and differentiating the spectral variations induced by thermal changes in LEDs. By implementing an OCC link that capitalizes on LED temperature effects and utilizes MS cameras, the objective is to demonstrate the feasibility of establishing multiple communication channels from a single light source.

Second, it is intended to implement nonlinear techniques for data detection in multispectral camera communication (MCC) systems with the purpose of enhancing the system performance. In this context, the primary goal lies in a comparative analysis between the performance of the OCC system employing these nonlinear methodologies and that of conventional linear methods.

Finally, the objective is to analyze thermal effects on LEDs in OCC systems' compensation stage. This objective centers on a comprehensive analysis of the thermal effects on LEDs in OCC systems using conventional RGB cameras. The goal is to quantify the impact of temperature-induced spectral variations on system performance and establish the necessity of compensating for these effects.

In order to achieve these objectives, the basic methodology followed throughout this thesis involves three main steps. First, analyze the LED behavior when its p-n junction temperature changes by developing a mechanism for controlling the temperature. Second, collect behavior characteristics from the light sources using various instrumentation equipment to characterize them and an MS camera to establish a communication link. Lastly, process data by applying several techniques to analyze them.

In this thesis, both simulations and experimental studies have been conducted. On the one hand, the thermal impact of LEDs on channel compensation in the context of OCC has been addressed. Thus, an OCC link employing an RGB LED was assessed when obsolete channel state information (CSI) in terms of temperature is used for the channel compensation, *i.e.*, when the actual p-n junction temperature of the transmitter is different from the LED temperature at optimal working conditions from which the CSI was estimated. Therefore, several temperatures were induced to the light source under test based on the Joule effect by increasing the driving current of the device. Both temperature and LED emitted signals were characterized using a thermal camera and an optical spectrometer, respectively. Then, the responses of Bayer-based and Foveon image sensors were simulated to obtain the associated CSI and perform the zero-forcing (ZF) compensation of two channel matrices at different temperatures. Finally, the system performance was evaluated, estimating signal-to-interference-plus-noise ratio (SINR) and bit error rate (BER), and demonstrating performance degradation due to LED spectral variations.

Moreover, an innovative configuration using an MS camera as a receiver in an OCC system and the thermally induced spectral changes of LEDs was carried out. The effects of temperature on LEDs, which are usually considered a detrimental factor, were used in this study to increase the number of communication channels using the same device. To achieve this result, an on-off keying (OOK) transmission was simulated to analyze

the system performance. It consisted of generating a transmitted signal (a bit stream after being affected by the channel matrix) to which noise was added. Then, a ZF equalizer was used to estimate the transmitted bit stream, applying the Moore-Penrose pseudoinverse of the channel matrix. Once the transmitted bit stream was estimated, it was compared to the sent bit stream to calculate the BER.

Finally, considering the MS camera and the effect of temperature on LEDs, a cluster-based data detection approach was performed for improving the performance of an OCC system. The balanced iterative reducing and clustering hierarchies (BIRCH) algorithm was used to generate a clustering model with the purpose of recovering the LED's signals.

This cluster analysis results in a BER enhancement with respect to linear methods, namely, ZF and minimum mean square error (MMSE). In addition, this experimental study proposed a novel approach exploring the possibility of adopting a spectral signature multiplexing based on temperature.

The success of the approach that integrates high-spectral-resolution cameras with the consideration of temperature effects on LEDs hinges on several key factors. Primarily, the spectral variations that LEDs present due to temperature fluctuations are contingent upon the materials composing the LEDs and the characteristics of the LED substrate. Typically, as temperature increases, the peak wavelength of LEDs tends to shift towards longer wavelengths, albeit at the cost of reduced efficiency. Striking a balance between accommodating this red-shift and mitigating the accompanying reduction in efficiency is of critical importance.

Concurrently, the effectiveness of this approach is intrinsically linked to the spectral resolution of the camera employed. A camera's spectral resolution dictates its sensitivity to spectral variations, and as such, cameras with a greater number of spectral bands and narrower bandpass widths are better equipped to capture and discern such variability.

Nevertheless, the adoption of this technology may encounter certain

limitations. Mainly, the high acquisition cost of high-spectral-resolution cameras, making integration into commercial off-the-shelf (COTS) devices impractical, and limited data rates due to low frame rates in most of these cameras. Despite these challenges, some models offer rolling shutter (RS) mode for increased data rates, but the non-communication-oriented design of cameras may lead to issues such as data loss or data stream merging. Additionally, addressing temperature-induced spectral changes in LEDs is crucial for maintaining reliable signal demultiplexing.

Considering the constraints and potential attributes of high-spectral-resolution cameras for communication purposes, several compelling applications can be envisioned. To mitigate the expense associated with acquiring such cameras, their primary utility should focus on enhancing existing systems equipped with cameras for communication tasks. For example, in industrial automation and quality control, these cameras can serve a dual role by detecting contaminants in food processing lines and monitoring the performance of conveyor systems, transmitting this information via OCC links. This approach facilitates real-time monitoring and maintenance in production facilities. Similarly, in precision agriculture, multispectral cameras can provide early disease detection, parasite presence, and critical data on soil nutrient levels and moisture content. Placing these cameras on fixed stands within agricultural fields offers dual benefits of crop health monitoring and data reception from field-installed sensors, facilitating informed decision-making. These applications highlight the multifaceted utility of high-spectral-resolution cameras, enhancing efficiency, monitoring, and decision-making across various domains.

La comunicación óptica inalámbrica (OWC) se perfila de manera progresiva como una tecnología crucial en las futuras redes de comunicación y se cree que está preparada para una revolución en la industria y el ámbito de la investigación. Su capacidad para ofrecer un ancho de banda amplio, una implementación rápida y un bajo consumo de energía ha atraído una atención significativa. Por lo tanto, estas características sitúan a la OWC como un candidato válido para satisfacer los requisitos de los futuros sistemas de comunicación.

Dentro de las principales tecnologías que abarcan la OWC, la comunicación óptica a través de cámaras (OCC) ha experimentado un notable crecimiento en los últimos años debido a la proliferación de dispositivos equipados con cámaras. Como resultado, la adopción generalizada de estos dispositivos, junto con los avances en los sensores de imagen, ha impulsado el interés de la OCC. Esta tecnología supera la limitación de la comunicación por luz visible (VLC) y LiFi frente a la pérdida de señal y simplifica la complejidad de la implementación en comparación con las comunicaciones ópticas por el espacio libre (FSO). Sin embargo, uno de los principales desafíos de la OCC radica en aumentar la velocidad de transmisión de datos, lo que ha llevado al desarrollo de nuevas técnicas y enfoques para mejorarla. En este contexto, se aprovecha el uso de cámaras no convencionales para mejorar el rendimiento del sistema de OCC. Dado que la velocidad de transmisión de datos está parcialmente definida por la mitad de la tasa de fotogramas de la cámara, las cámaras de alta velocidad (más de 120 fotogramas por segundo) son la elección predominante para incrementar la tasa de datos.

A pesar de esa limitación, ciertas aplicaciones priorizan factores diferentes a la velocidad de transmisión de datos, lo que las hace adecuadas para la incorporación de diferentes tipos de cámaras con el fin de mejorar el rendimiento general del sistema. Dada la escasa literatura en este ámbito, el uso de cámaras de alta resolución espectral como receptores en sistemas de OCC aún se encuentra poco explorado. Las cámaras multiespectrales (MS) e hiperespectrales (HS) proporcionan más bandas que las roja, verde y azul (RGB) convencionales mediante el uso de filtros de paso de banda estrechos. El número de bandas, así como su anchura espectral, determina la resolución espectral de la cámara. Estas características hacen que este tipo de cámaras sea una herramienta valiosa en diversas aplicaciones, como la teledetección, la agricultura y la medicina. Específicamente, las cámaras MS y HS se están convirtiendo en un factor vital en la agricultura de precisión debido a las crecientes demandas en la producción de alimentos, lo que hace necesario optimizar las prácticas agrícolas de manera sostenible. Este considerable interés y las características particulares de estos dispositivos abren una variedad de oportunidades para la comunicación. Es importante destacar que el principio de funcionamiento de este tipo de cámaras permite capturar la curva de respuesta espectral, también conocida como firma espectral, de diferentes elementos de una imagen. De esta manera, utilizando diodos emisores de luz (LEDs) con diferentes longitudes de onda máximas para transmitir ciertos datos, la cámara MS captura las señales y podría separarlas aprovechando su distintiva firma espectral para finalmente decodificar la información.

Por otro lado, el uso de LEDs ha aumentado considerablemente en la última década. Los avances en este tipo de dispositivos han llevado a mejoras en su eficiencia, lo que permite una alta intensidad luminosa con un bajo consumo de energía. Como resultado, ha aumentado la demanda de LEDs en varios sectores, como el industrial, comercial y residencial. Este aumento también ha incrementado la atención de la OWC, ya que estos

se utilizan comúnmente como fuente de luz transmisora. La característica clave que hace que estos dispositivos sean útiles para la comunicación es su capacidad de conmutación rápida que permite modular la luz.

Además, los LEDs son sensibles a las variaciones de temperatura que afectan su rendimiento y características espectrales. En general, la eficiencia luminosa disminuye y la longitud de onda máxima aumenta a medida que aumenta la temperatura. A pesar de que la dependencia de la temperatura de los LEDs es un fenómeno bien conocido, pocos investigadores han abordado el impacto de los efectos térmicos en OWC. Sin embargo, este efecto se analiza en esta tesis. Por un lado, se sugirió aumentar los canales de comunicación que se pueden obtener utilizando un solo dispositivo aprovechando el incremento en la longitud de onda de los LEDs (desplazamiento hacia el rojo) junto con el uso de una cámara multiespectral para capturar las variaciones espectrales. Así, esta reacción, que generalmente se considera perjudicial para el rendimiento del sistema, se convierte en un beneficio. Por otro lado, se examinan las consecuencias de no tener en cuenta las variaciones espectrales de los LEDs en enfoques que requieren compensación de canal para reducir la interferencia entre canales (ICI).

Las cámaras multiespectrales presentan características únicas con respecto a las cámaras convencionales. Así, se pretende explotar esas características específicas para alcanzar resultados que otros tipos de cámaras no podrían. Además, las variaciones espectrales en los LEDs debidas a cambios en la temperatura de la unión p-n, que normalmente es un efecto perjudicial para la comunicación, se considera una mejora para alcanzar nuevos canales de comunicación. Considerando estos aspectos, las hipótesis de este trabajo se enuncian a continuación.

Hipótesis 1 (H1)

La utilización de cámaras multiespectrales en sistemas de OCC mejora las capacidades de multiplexación al permitir una separación y detección eficaces de los transmisores que operan en distintas longitudes de onda.

Las cámaras multiespectrales, que cuentan con múltiples bandas centradas en diferentes longitudes de onda, proporcionan una mayor precisión espectral en comparación con las cámaras convencionales. Gracias a esta característica, los sistemas OCC pueden lograr capacidades de multiplexación mejoradas. Las distintas bandas espectrales que ofrecen las cámaras multiespectrales permiten separar los transmisores que operan a distintas longitudes de onda. Esta hipótesis sugiere que el uso de cámaras multiespectrales puede reducir la complejidad de las técnicas de multiplexación, como la multiplexación por división de longitud de onda (WDM), mejorando así el rendimiento general de los sistemas OCC.

Hipótesis 2 (H2)

Las variaciones en la longitud de onda de emisión de los dispositivos LED causadas por los efectos de la temperatura pueden detectarse y aprovecharse mediante cámaras multiespectrales para establecer nuevos canales de comunicación en sistemas de OCC.

Los LEDs presentan un desplazamiento en la longitud de onda de pico como consecuencia de las variaciones de temperatura. Las cámaras multiespectrales con alta resolución espectral pueden captar y detectar estos cambios, creando así nuevos canales de comunicación a partir de la misma fuente de luz. Esta hipótesis sugiere que, utilizando cámaras multiespectrales, los sistemas de OCC pueden beneficiarse de la información adicional que proporcionan las variaciones inducidas por la temperatura en las emisiones de los LEDs.

Los efectos de la temperatura en los LEDs, que dan lugar a desplaza-

mientos en la longitud de onda, han sido ampliamente estudiados en la literatura. Las cámaras multiespectrales ofrecen la ventaja de una alta resolución espectral, lo que les permite captar cambios sutiles en los espectros de emisión de los LEDs. Al explotar estas variaciones inducidas por la temperatura, los sistemas de OCC pueden aumentar potencialmente su capacidad de transmisión de datos. La precisión espectral de las cámaras multiespectrales facilita la separación de los transmisores que operan a distintas longitudes de onda. En consecuencia, las técnicas de multiplexación convencionales, como WDM, pueden aplicarse con mayor eficacia, simplificando la complejidad asociada a la multiplexación en los sistemas de OCC.

Los sistemas de OCC tradicionales a menudo enfrentan dificultades para separar y distinguir eficazmente las señales procedentes de varios transmisores. Las cámaras multiespectrales pueden superar esta limitación proporcionando información espectral en diferentes bandas. La mayor precisión y resolución espectral de las cámaras multiespectrales permite una separación más eficaz y precisa de los transmisores que operan a diferentes longitudes de onda. Por consiguiente, las técnicas de multiplexación pueden aplicarse con mayor facilidad y fiabilidad, lo que se traduce en un mejor rendimiento y un aumento en la capacidad de transmisión de datos en los sistemas de OCC.

Hipótesis 3 (H3)

Ignorar los efectos de la temperatura de los LEDs en la etapa de compensación de los sistemas de OCC reduce el rendimiento del sistema, afectando a la precisión y fiabilidad de la transmisión de datos.

Aunque los efectos de la temperatura en los LEDs han sido ampliamente estudiados, sus repercusiones específicas en los sistemas de OCC no se han analizado en profundidad. Esta hipótesis aborda el posible impacto de los efectos de la temperatura de los LEDs en el rendimiento de los sistemas

OCC. Si las variaciones inducidas por la temperatura en las longitudes de onda de emisión de los LEDs no se tienen en cuenta adecuadamente durante la compensación de canal, podría producirse una degradación del rendimiento del sistema. Por lo tanto, esta hipótesis enfatiza la importancia de considerar los efectos de la temperatura para garantizar una transmisión de datos precisa y fiable en los sistemas de OCC.

Las variaciones de temperatura pueden afectar significativamente al rendimiento de los LEDs, incluyendo los cambios en las longitudes de onda de emisión. La falta de consideración de estos efectos de temperatura durante la compensación del canal, puede producir imprecisiones en la detección y decodificación de señales. Las variaciones inducidas por la temperatura no compensadas pueden introducir errores y reducir el rendimiento global de los sistemas de OCC, principalmente debido a la interferencia entre canales. Por lo tanto, esta hipótesis pone de manifiesto la necesidad de técnicas adecuadas de compensación de canal que tengan en cuenta los efectos de la temperatura en los LEDs para mantener un rendimiento óptimo del sistema.

Hipótesis 4 (H4)

El uso de métodos no lineales para la detección de datos mejora el rendimiento de los sistemas de OCC, lo que resulta en tasas de error más bajas.

Para mejorar el rendimiento de los sistemas de OCC, se sugiere la aplicación de métodos no lineales para la detección de datos. Las técnicas de detección no lineales han demostrado ser prometedoras en sistemas de comunicación para mitigar deficiencias y mejorar la calidad de la señal. Esta hipótesis pretende explorar el potencial del empleo de métodos no lineales para la detección de datos en sistemas de OCC, con el objetivo de mejorar el rendimiento general del sistema en términos de capacidad de transmisión de datos, tasas de error y robustez frente al ruido y las interferencias.

Las técnicas de detección no lineales tienen la capacidad de captar relaciones complejas entre las señales transmitidas y los datos recibidos. Ex-

plorando la aplicación de estos métodos en sistemas de OCC, podemos lograr potencialmente un rendimiento de detección mejorado, especialmente en escenarios con condiciones de canal desafiantes. La investigación se centrará en adaptar y optimizar los algoritmos de detección no lineal a las características y retos únicos de los sistemas de OCC con cámaras multiespectrales. Los resultados de esta investigación pueden conducir a avances significativos en la tecnología de OCC, permitiendo menores tasas de error y una mayor fiabilidad.

Con el fin de validar las hipótesis presentadas anteriormente, se ha formulado una serie de objetivos para estudiar el uso de cámaras multiespectrales y los efectos térmicos de los LEDs en OCC. Estos objetivos se han elaborado para desarrollar el potencial de estas tecnologías y sus implicaciones para el avance de los sistemas de OCC. La consecución de estos objetivos no sólo refuerza los fundamentos teóricos de nuestras hipótesis, sino que también proporciona una comprensión global de las implicaciones prácticas y la viabilidad de aprovechar las cámaras multiespectrales, los efectos térmicos de los LEDs, las técnicas no lineales y las estrategias de compensación de temperatura en el marco de la OCC.

Objetivo 1 - (O1)

Implementar un enlace de OCC basado en los efectos de temperatura del LED y una cámara multiespectral.

Las cámaras multiespectrales poseen una clara ventaja en su alta resolución espectral, lo que las convierte en candidatas idóneas para captar y diferenciar las variaciones espectrales inducidas por los cambios térmicos en los LEDs. Mediante la implementación de un enlace de OCC que aprovecha los efectos de la temperatura de los LEDs y utiliza cámaras multiespectrales, el objetivo es demostrar la viabilidad de establecer múltiples canales de comunicación a partir de una única fuente de luz. Este objetivo engloba los siguientes subobjetivos:

1. Diseñar y construir un montaje experimental que integre cámaras multispectrales como receptores y fuentes LED como transmisores, permitiendo variaciones controladas de temperatura.
2. Caracterizar la respuesta espectral de los LEDs a distintas temperaturas. Realizar mediciones exhaustivas de los espectros de emisión de los LEDs a diferentes temperaturas para establecer un marco de referencia de los desplazamientos de longitud de onda y el ensanchamiento espectral causados por los efectos de la temperatura.
3. Diseñar esquemas de modulación de temperatura para la codificación de datos teniendo en cuenta las características de la cámara MS.
4. Desarrollar algoritmos de decodificación de datos para la cámara multispectral con el fin de decodificar los datos de manera precisa.
5. Evaluar el rendimiento del sistema utilizando métricas para validar los resultados.

Objetivo 2 - (O2)

Aplicación de técnicas no lineales para la detección de datos en sistemas de comunicación de cámaras multispectrales.

Este objetivo pretende mejorar las prestaciones de los sistemas de OCC mediante la incorporación de técnicas no lineales para la detección de datos en el marco de las cámaras multispectrales. En este contexto, el objetivo principal radica en un análisis comparativo entre el rendimiento del sistema de OCC que emplea estas metodologías no lineales y el de los métodos lineales convencionales. Los subobjetivos incluyen:

1. Evaluar y seleccionar técnicas no lineales adecuadas. Revisar técnicas de detección no lineales analizando su eficacia en el marco de OCC y elegir las técnicas más prometedoras que se ajusten a las características espectrales y operativas de las cámaras multispectrales.

2. Integrar algoritmos de detección no lineal en sistemas de OCC con cámaras MS. Adaptar e implementar los algoritmos de detección no lineal elegidos al sistema MCC, garantizando la integración para optimizar el rendimiento.
3. Establecer un enlace de comunicación utilizando cámaras multiespectrales para evaluar el rendimiento. Implementar un enlace de comunicación funcional, aprovechando las capacidades de las cámaras multiespectrales para facilitar una evaluación en profundidad del rendimiento exhibido por las técnicas no lineales integradas.
4. Realizar un análisis comparativo del rendimiento entre el sistema de OCC utilizando técnicas no lineales y métodos lineales tradicionales.

Objetivo 3 - (O3)

Analizar los efectos térmicos en los LEDs en la etapa de compensación de sistemas de OCC.

Este objetivo se centra en un análisis exhaustivo de los efectos térmicos en los LEDs en sistemas de OCC que utilizan cámaras RGB convencionales. El objetivo es cuantificar el impacto de las variaciones espectrales inducidas por la temperatura en el rendimiento del sistema y determinar la necesidad de compensar estos efectos. Los subobjetivos incluyen:

1. Establecer un entorno de temperatura controlada. Configurar un entorno experimental controlado que permita ajustar la temperatura de los LEDs manteniendo unas condiciones de ensayo constantes.
2. Medir las variaciones espectrales inducidas por la temperatura de los LEDs. Llevar a cabo una serie de experimentos para medir la respuesta espectral de los LEDs a diferentes temperaturas. Caracterizar los desplazamientos de longitud de onda y el ensanchamiento espectral causados por los cambios de temperatura.

3. Aplicar técnicas de compensación de temperatura que mitiguen los efectos negativos de las variaciones espectrales inducidas por la temperatura de los LEDs utilizando varias matrices de canal a diferentes temperaturas.
4. Evaluar el rendimiento del sistema de OCC a distintas temperaturas cuando la temperatura del LED difiere de la considerada en la etapa de compensación. Medir y analizar las métricas de rendimiento del sistema mientras se someten los LEDs a diferentes temperaturas.

Para lograr estos objetivos, la metodología básica seguida en toda esta tesis implica tres pasos principales. En primer lugar, analizar el comportamiento de los LEDs cuando cambia la temperatura de su unión p-n mediante el desarrollo de un mecanismo para controlar la temperatura. En segundo lugar, recopilar las características del comportamiento de las fuentes de luz utilizando diversos equipos de instrumentación para caracterizarlas y una cámara multiespectral para establecer un enlace de comunicación. Por último, procesar los datos aplicando diferentes técnicas para su análisis.

En esta tesis, se han llevado a cabo tanto simulaciones como estudios experimentales. Por un lado, se abordó el impacto térmico de los LEDs en la compensación de canal en el contexto de OCC. Así, se evaluó un enlace de OCC que utiliza un LED RGB cuando se emplea información del estado del canal (CSI) obsoleta en términos de temperatura para la compensación de efectos del canal, es decir, cuando la temperatura real de la unión p-n del transmisor es diferente de la temperatura del LED en condiciones óptimas de funcionamiento, a partir de la cual se estimó la CSI. Por lo tanto, se indujeron varias temperaturas en la fuente de luz sometida a prueba mediante el efecto Joule al aumentar la corriente de conducción del dispositivo. Tanto la temperatura como las señales emitidas por el LED se caracterizaron utilizando una cámara térmica y un espectrómetro óptico, respectivamente. A continuación, se simuló las respuestas de los

sensores de imagen Bayer y Foveon para obtener la CSI asociada y realizar la compensación de forzamiento a cero (ZF) de dos matrices de canal a diferentes temperaturas. Finalmente, se evaluó el rendimiento del sistema, estimando la relación señal-interferencia más ruido (SINR) y la tasa de error de bits (BER), y se demostró la degradación del rendimiento debido a las variaciones espectrales del LED.

Además, se llevó a cabo una configuración innovadora utilizando una cámara multiespectral como receptor en un sistema de OCC y se estudiaron los cambios espectrales inducidos por la temperatura en los LEDs. Los efectos de la temperatura en los LEDs, que generalmente se consideran un factor perjudicial, se utilizaron en este estudio para aumentar el número de canales de comunicación utilizando el mismo dispositivo. Para lograr este resultado, se simuló una transmisión *on-off keying* (OOK) para analizar el rendimiento del sistema. Esta consistió en generar una señal transmitida (una secuencia de bits después de ser afectada por la matriz de canal) a la cual se le agregó ruido. Luego, se utilizó un ecualizador ZF para estimar la secuencia de bits transmitida, aplicando la pseudoinversa de Moore-Penrose de la matriz de canal. Una vez estimado el flujo de bits transmitido, se comparó con la secuencia enviada para calcular la BER.

Por último, considerando la cámara MS y el efecto de la temperatura en los LEDs, se llevó a cabo un procedimiento de detección de datos basado en clústeres para mejorar el rendimiento de un sistema de OCC. Se utilizó el algoritmo de reducción iterativa equilibrada y agrupación utilizando jerarquías (BIRCH) para generar un modelo de agrupamiento con el propósito de recuperar las señales de los LEDs. Este análisis de agrupamiento da como resultado una mejora de la BER con respecto a los métodos lineales (ZF y MMSE). Además, este estudio experimental propone un enfoque novedoso que explora la posibilidad de adoptar una multiplexación de firmas espectrales basada en la temperatura.

Retomando las hipótesis planteadas, un análisis exhaustivo de las pruebas

respalda su validez. Las hipótesis H1 y H2 se demostraron en las publicaciones 2 (P2) y 3 (P3) del compendio. Para ello, se propuso una solución innovadora basada en las firmas espectrales de los LEDs y sus cambios espectrales causados por la temperatura. Gracias a la resolución espectral de las cámaras MS, se pudo obtener más de un canal por fuente de luz con una BER satisfactoria. En particular, en la P2, se realizó un primer estudio utilizando una cámara MS y explotando los efectos de la temperatura del LED. Tras caracterizar los LEDs sometidos a ensayo, se simuló un sistema de OCC asumiendo una transmisión OOK y aplicando un ecualizador ZF para obtener la señal recibida. Como resultado, se obtuvieron métricas de rendimiento como el número de condición de las matrices de canal, compuestas por las firmas espectrales de los LEDs, y la BER.

Por otro lado, en la P3 se realizó un estudio experimental aprovechando la cámara MS y las variaciones espectrales en los transmisores. Adicionalmente, este trabajo respalda la H4 ya que comparó el rendimiento del sistema utilizando métodos lineales tradicionales y *clustering* para la detección de datos, demostrando que este último obtuvo mejores resultados. Asimismo, los hallazgos de las P2 y P3 permiten alcanzar los objetivos O1 y O2 de esta tesis, esto es, la implementación de un enlace de OCC utilizando una cámara multiespectral y el efecto de la temperatura sobre los LEDs, y el uso de técnicas no lineales para la detección de datos en sistemas de OCC, respectivamente. Así, se demostró que una cámara MS podía detectar los cambios espectrales inducidos por las variaciones térmicas en los LEDs y, por tanto, explotar esta característica para conseguir más de un canal de comunicación desde el mismo dispositivo con un rendimiento satisfactorio.

Además, en la P1 se realizaron experimentos para medir el efecto de los cambios de temperatura en el proceso de compensación de canales y evaluar el rendimiento del sistema de OCC en distintas condiciones de temperatura. Se demostró que la SINR y la BER disminuían cuando había diferencias de temperatura en las matrices de canal utilizadas para la compensación.

Estas cuestiones que dificultan la consecución de una comunicación fiable validan la H3. Por lo tanto, el tercer objetivo de esta tesis (O3), consistente en examinar los efectos térmicos del LED en sistemas de OCC, se consigue también en esta publicación.

Partiendo de la base de que el uso de cámaras multispectrales para comunicación apenas se encuentra en la literatura, este trabajo ha ampliado el conocimiento actual sobre las ventajas y limitaciones de esta tecnología en OCC. Además, se ha analizado el efecto térmico del LED considerando que, aunque ha sido ampliamente investigado, sus repercusiones en OWC no han sido examinadas en profundidad. Además, este efecto, habitualmente considerado perjudicial para los sistemas, se ha aprovechado gracias a las cámaras MS para obtener más de un canal de comunicación desde un mismo dispositivo.

La mayoría de las cámaras utilizadas en OCC como receptores son cámaras convencionales debido a su omnipresencia en la mayoría de los aparatos electrónicos de consumo, por lo tanto, los resultados de esta tesis constituyen un paso inicial hacia el uso de cámaras con una alta resolución espectral para fines de comunicación. Básicamente, los dispositivos multispectrales e hiperspectrales serían beneficiosos para aquellas situaciones que hacen uso de las características espectrales de los transmisores, por ejemplo, WDM, donde se utilizan varios canales más que el RGB proporcionado por las cámaras convencionales. Así, aunque la matriz de filtros de color (CFA) presentes en el sensor de imagen de la cámara permite separar los canales RGB de un LED, el amplio ancho de banda óptico de los filtros de color provoca solapamientos entre los canales. Además, la gran anchura espectral del LED provoca interferencia entre canal (ICI). Por lo tanto, estos factores complican la obtención de canales de comunicación independientes utilizando únicamente una cámara convencional. En cambio, la riqueza espectral de las cámaras MS facilita este proceso. Asimismo, abren nuevos

enfoques, como el incremento de canales de comunicación mediante la variación espectral del LED mencionada anteriormente.

Los principales aspectos que afectan al éxito de este planteamiento que combina cámaras de alta resolución espectral y los efectos de la temperatura en los LEDs son las variaciones espectrales de los LEDs causadas por la temperatura, que, a su vez, dependen de los materiales de los LEDs, y la resolución espectral de la cámara. Por un lado, dependiendo del sustrato del LED, el comportamiento espectral del dispositivo puede variar con la temperatura, de modo que mientras que la longitud de onda pico suele aumentar al incrementarse la temperatura, la eficiencia disminuye. En este sentido, también es crucial el compromiso entre el desplazamiento al rojo y la disminución de la eficiencia. Por otro lado, la resolución de la cámara determina su sensibilidad a las variaciones. Por tanto, cuanto mayor sea el número de bandas y menor su anchura, mayor será la variabilidad captada.

No obstante, la adopción de esta tecnología puede encontrar ciertas limitaciones. Principalmente, el elevado coste de adquisición de las cámaras de alta resolución espectral, que hace inviable su integración en dispositivos comerciales salidos del estante (COTS), y la limitada velocidad de transmisión de datos debida a las bajas tasas de fotogramas de muchas de estas cámaras. A pesar de estas dificultades, algunos modelos ofrecen el modo rolling shutter (RS) que permitiría incrementar la velocidad de transmisión de datos, aunque el diseño de las cámaras, no orientado a la comunicación, puede provocar problemas como la pérdida de datos o la confusión de flujos de datos. Además, para mantener una demultiplexación fiable de la señal, es crucial abordar los cambios espectrales inducidos por la temperatura en los LEDs.

Teniendo en cuenta las limitaciones anteriores y los potenciales atributos de las cámaras de alta resolución espectral para fines de comunicación, pueden concebirse varias aplicaciones atractivas. Para mitigar el gasto asociado a la adquisición de estas cámaras, su utilidad principal debería

centrarse en mejorar los sistemas existentes que ya están equipados con estas cámaras para tareas de comunicación. Por ejemplo, en la automatización industrial y el control de calidad, estas cámaras pueden desempeñar una doble función detectando contaminantes en las líneas de procesado de alimentos y supervisando el rendimiento de los sistemas transportadores, transmitiendo esta información a través de enlaces de OCC. Este enfoque facilita la supervisión y el mantenimiento en tiempo real de las instalaciones de producción. Del mismo modo, en la agricultura de precisión, las cámaras multiespectrales pueden proporcionar detección precoz de enfermedades, presencia de parásitos y datos críticos sobre los niveles de nutrientes y el contenido de humedad del suelo. La colocación de estas cámaras en soportes fijos dentro de los campos agrícolas ofrece la doble ventaja de vigilar la salud de los cultivos y recibir datos de los sensores instalados en el campo, lo que facilita la toma de decisiones. Estas aplicaciones ponen de manifiesto la utilidad polifacética de las cámaras de alta resolución espectral en la mejora la eficiencia, la supervisión y la toma de decisiones en diversos ámbitos.

Contents

Dedication	v
Acknowledgments	vii
Abstract	ix
Resumen	xv
Contents	xxxi
Acronyms	xxxiii
1 Introduction	1
1.1 Motivation	4
1.2 Hypotheses	4
1.3 Objectives	6
1.4 Organization of the document	8
1.5 List of publications	9
1.5.1 Compendium	9
1.5.2 Other research publications	10
1.5.3 Collaborations	10
2 State of the Art	11
2.1 Optical camera communication	11
2.2 Effect of temperature on LEDs	13
2.3 High-spectral-resolution cameras	15
3 Theoretical Framework	17
3.1 Light-emitting diodes	17
3.2 Cameras	20
3.3 Processing	22
3.3.1 Channel compensation	23
4 Methodology	25
4.1 LED temperature stabilization	25
4.2 Data acquisition	26
4.2.1 Characterization	26
4.2.2 OCC link	27
4.3 Data processing	28
5 Experimental Results	33
5.1 Publication 1 (P1)	33

5.2	Publication 2 (P2)	55
5.3	Publication 3 (P3)	60
5.4	Summary	65
6	Conclusions and future research	67
6.1	Conclusions	67
6.2	Future work	70
	Bibliography	73
A	Conference proceedings.	83
B	Journal article	107
C	Supplementary scripts for OCC systems	119

Acronyms

ANN artificial neural network. 12

AWGN additive white Gaussian noise. 23, 24

BER bit error rate. 12, 29, 30, 33, 55, 60, 65, 67, 68

BIRCH balanced iterative reducing and clustering hierarchies. 24, 60, 65

CCD charge-coupled device. 20

CFA color filter array. 12, 13, 20, 68

CIE International Commission on Illumination. 12, 13

CIM color-intensity modulation. 12

CMOS complementary metal-oxide-semiconductor. 20, 27, 33

COTS commercial off-the-shelf. 1, 69

CSI channel state information. 29, 31, 33, 65

CSK color shift keying. 2, 12, 23, 33

DBSCAN density-based spatial clustering of applications with noise. 24

DC duty cycle. 25, 28

DOI digital object identifier. 9, 10

EM electromagnetic. 1

FOV field of view. 70

FSO free-space optical. 1, 2

FWHM full width at half maximum. 26, 71

GCM generalized color modulation. 12

GMM Gaussian mixture model. 24, 65

GS global shutter. 11, 20, 28, 69, 72

HS hyperspectral. 2, 4, 11, 15, 16, 68, 69, 71

ICI inter-channel interference. 3, 23, 33, 68

IDeTIC University Institute for Technological Development and Innovation in Communications. 4, 10

IEEE Institute of Electrical and Electronics Engineers. 2, 9, 11

IM intensity modulation. 2

IoT internet of things. 1

IR infrared. 1, 2, 17

ISI intersymbol interference. 12

JCR Journal Citation Reports. 8

LD laser diode. 1, 2

LED light-emitting diode. 1–8, 11–14, 16–20, 22, 23, 25–29, 31, 33, 34, 55, 60, 65, 67–71

LiFi light fidelity. 1, 2

LOS line-of-sight. 12

MCC multispectral camera communication. 7, 23, 27, 29–31, 65, 67

MDPI Multidisciplinary Digital Publishing Institute. 9

MIMO multi-input multi-output. 12, 23

MMSE minimum mean square error. 23, 60, 65, 68, 107

MS multispectral. 2–8, 11, 15–17, 20, 22, 23, 25, 27–29, 55, 60, 65, 67–72

NLOS non-line-of-sight. 12

OAM orbital angular momentum. 2

OBIA object-based image analysis. 15

OCC optical camera communication. 1–8, 11, 12, 15–17, 22, 26, 33, 55, 60, 65, 67–69, 72

OFDM orthogonal frequency division modulation. 1, 2

OOK on-off keying. 2, 27, 55, 65, 67

OWC optical wireless communication. 1–4, 11, 68

PCA principal component analysis. 71

PCB printed circuit board. 20

PD photodiode. 1, 2, 11

PET photo-electro-thermal. 14

PM pulse modulation. 2

PWM pulse-width modulation. 25

RC resistor-capacitor. 19

RF radio frequency. 1

RGB red, green, and blue. 2, 8, 12, 14, 15, 20–22, 25, 27, 29, 33, 55, 60, 65, 68

ROI region of interest. 27, 72

RS rolling shutter. 11, 20, 69, 72

SINR signal-to-interference-plus-noise ratio. 29, 33, 65, 68

SMD surface-mount device. 14

SNR signal-to-noise ratio. 23

THT through-hole technology. 19, 20, 25

UAV unmanned aerial vehicle. 69

ULPGC Universidad de Las Palmas de Gran Canaria. 4

UV ultraviolet. 1, 2, 17

VL visible light. 1, 2, 17, 23

VLC visible light communication. 1, 2, 4, 11–13, 23

VPPM variable pulse position modulation. 28, 30

WDM wavelength division multiplexing. 5, 12, 23, 33, 60, 65, 68

ZF zero-forcing. 23, 27, 29, 33, 55, 60, 65, 67, 68, 107

In the Information Age, the current 5G (and upcoming 6G) systems and internet of things (IoT) applications have caused the number of users that require access to information via the internet, and the number of wireless communication devices have grown steadily. As a consequence, it is well-known that coordinating the radio frequency (RF) spectrum has become a complex task. Hence, RF and microwave communications need complementary technologies to alleviate the shortage of their spectra due to the limited electromagnetic (EM) spectrum. Thus, it is necessary to use different ranges of the spectrum in order to benefit from higher-speed transmissions and network capacities, or enhanced spectral efficiency, among others.

In regard to this quest, optical wireless communication (OWC) is a candidate to complement RF communications. In addition to the complementarity of frequency bands, OWC is useful in situations where it is crucial to avoid interference between RF devices, such as in hospitals or airports. It includes the infrared (IR), the visible light (VL), and the ultraviolet (UV) parts of the EM spectrum, providing more frequencies for communication. Thus, OWC is increasingly becoming an essential technology in future communication networks and is foreseen to undergo a revolution in terms of industry and research. Regarding industry, it is expected that the growth in internet users and cloud computing will lead to an increase in the OWC market size from USD 18.9 billion in 2020 to USD 35.49 billion by 2028 [1]. As for research, OWC is attracting considerable interest due to its characteristics, such as huge bandwidth, rapid deployment, and low power consumption, which makes this technology a candidate to fulfill the demands of the upcoming communication systems [2].

OWC includes the following principal technologies: visible light communication (VLC), light fidelity (LiFi), free-space optical (FSO) communication, and optical camera communication (OCC) (Table 1.1) [3]. In the first place, VLC is based on using the VL spectrum to achieve communication applications with a high data rate. The main transmitters employed in VLC are light-emitting diodes (LEDs), which are usually detected by a photodiode (PD). The use of commercial off-the-shelf (COTS) LEDs permits complementing illumination with communication since light can be modulated so that the human eye would not be affected. With the purpose of providing bidirectional communication links in a high-speed wireless networking system, LiFi emerged as a high-speed light-based technology, relying mostly on orthogonal frequency division modulation (OFDM) and IR. Unlike VLC, LiFi can utilize either IR, VL, or UV [4]. However, these two technologies have the limitation of path loss that constrains long-distance links. Therefore, FSO communications can support long-range transmissions adopting a laser diode (LD) instead of an LED to overcome this constraint. Nevertheless, the drawback of this

type of technology is the sensitivity to the link conditions, for example, weather circumstances or physical obstacles.

Table 1.1: Comparison of OWC technologies. Source: [3], [5]

Technologies	VLC	LiFi	FSO	OCC
Standard	IEEE 802.15.7	IEEE 802.15.11bb, ITU G.9991	Well developed	IEEE 802.15.7a
Transmitter	LED/LD	LED/LD	LD	LED/screen
Receiver	PD	PD	PD	camera
Spectrum	VL	IR/VL/UV	IR/VL/UV	IR/VL/UV
Modulation	OOK, IM, PM, OFDM, CSK, etc	OOK, IM, OFDM, CSK, etc	OOK, IM, PM, OFDM, OAM, etc	OOK, IM, PM, OFDM, CSK, etc
Data rate	Mbps - Gbps	kbps - Gbps	Gbps	bps - Mbps
Distance	<100 m	<10 m	>1 km	up to km
Implementation complexity	moderate	moderate	high	low
Computation complexity	low	low	moderate	high
Path loss	moderate	moderate	high	low
Robustness to interference	moderate	moderate	-	high
Additional function	illumination, localization	illumination	-	imaging, localization
Limitation	illumination constraints, limited range, vulnerable to mobility	limited use in outdoor, limited range	sensitive to weather, turbulence, and physical obstructions	low data rate

On the other hand, the use of cameras in a myriad of devices has intensively grown in recent years. Besides, due to the COVID pandemic, their use for surveillance and temperature control has been fostered. Therefore, the ubiquity of these devices, as well as the advances in image sensors, has boosted the interest of OCC. This technology overcomes the limitation of VLC and LiFi against path loss and eases the complexity of the implementation with respect to FSO links. However, one of the major challenges of OCC lies in increasing the data rate, which has led to the development of new techniques and approaches to improve it. For instance, some research has focused on using machine learning strategies to overcome this problem [6], [7]. Likewise, the use of non-conventional cameras is leveraged in order to improve the OCC system performance. As the data rate is partially defined by half of the camera's frame rate, high-speed cameras (more than 120 fps) are the most common types of cameras employed to increase the data rate [8], [9].

Despite that constraint, there are applications where other factors play a more significant role than the data rate. For those cases, different types of cameras could be used to enhance the system performance. For example, Guerra *et al.* proposed employing a thermographic camera and Peltier cells as receiver and transmitters, respectively, in a system similar to OCC [10]. On the other hand, up to the author's knowledge, the use of high-spectral-resolution cameras as receivers in OCC systems has not yet been sufficiently exploited. Multispectral (MS) and hyperspectral (HS) cameras provide more bands than conventional red, green, and blue (RGB) types. In Fig. 1.1, the operating principle of this type of device is shown. It can be seen that by using LEDs with different peak wavelengths transmitting certain data, the MS camera captures the signals and could separate them taking advantage of their distinct spectral response curves, to decode the information ultimately.

Moreover, each camera band is centered at a specific wavelength and presents a width. The number of bands, as well as their spectral width, determines the camera's spectral resolution. Those characteristics make these kinds of cameras a valuable tool in several applications, such as remote sensing, agriculture, and medicine [11]–[13]. Specifically, MS and HS cameras are set to become a vital factor in precision farming due to the increasing demands in food production, making it necessary to optimize farming practices sustainably [14]. This considerable interest

and the particular features of these devices open up a variety of opportunities for communication.

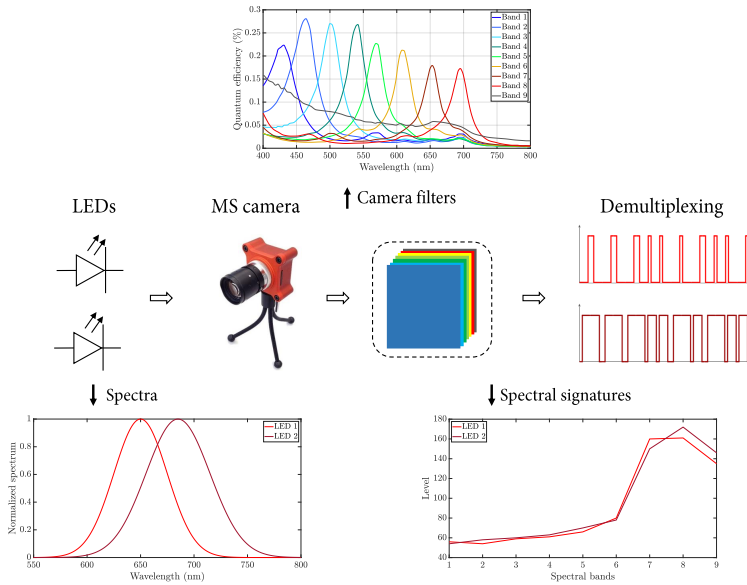


Figure 1.1: Operating principle of an MS camera in an OCC system.

Furthermore, the employment of LEDs has considerably increased in the last decade. Developments in this type of device have caused improvements in their efficiency, allowing high luminous intensity with low power consumption [15]. As a result, it has raised the LED demands in several sectors, such as industrial, commercial, and residential. This increase has also heightened the OWC attention because they are customarily used as the transmitter light source. The key feature that makes these devices helpful for communication is their rapid switching capability that allows modulating light [16].

Moreover, LEDs are sensitive to temperature variations that affect their performance and spectral features. In general, luminous efficiency decreases, and the peak wavelength increases as temperature grows [17], [18]. Even though the temperature dependence of LEDs is well-known, few researchers have addressed the impact of thermal effects in OWC [19]. Nonetheless, this effect is analyzed in this thesis. On the one hand, it was suggested to increase the communication channels that can be attained using a single device by taking advantage of the increase in the LED wavelength (red-shift) along with using a multispectral camera to capture the spectral variations. Thus, this reaction, typically considered harmful to the system performance, is turned into a benefit. On the other hand, the consequences of not taking LED spectral variations in approaches that require channel compensation to diminish inter-channel interference (ICI) are examined.

1.1 Motivation

This thesis was originated based on three principal aspects: the group's line of research and its expertise, my previous works with MS cameras, and the gap in OCC using this type of camera.

First, the foundational framework of this thesis is significantly reinforced by the presence of the University Institute for Technological Development and Innovation in Communications (IDeTIC) of the Universidad de Las Palmas de Gran Canaria (ULPGC). Notably, the Division of Photonics Technology and Communications boasts extensive experience working on VLC. In this sense, the division's active participation in numerous national and international research projects, alongside its productive collaborations with industry and academic players, such as Lightbee and the Universidad de La Laguna, exemplifies its deep-rooted engagement in the field.

Furthermore, my end-of-degree and master's thesis were founded on processing images from MS and HS cameras for remote sensing [20], [21]. They basically involved using imagery from an MS satellite sensor and an HS airborne imager, and applying computing techniques to generate land cover maps. Therefore, my prior experience with high-spectral-resolution imagery provided me with fundamental insights into the principles of this technology.

Finally, the potential characteristics provided by high-spectral-resolution cameras and their absent use in OWC inspired the emergence of this thesis. Simultaneously, the employment of LED's thermal effects collaterally arose with the purpose of exploiting the camera features. Therefore, considering those three pillars mentioned above, the aim was to broaden current knowledge of this type of camera in optical communication, as well as to find doable applications to be performed in the near future.

1.2 Hypotheses

MS cameras present unique characteristics with respect to conventional cameras. Thus, it is intended to exploit those specific features in order to reach outcomes that other types of cameras could not. Furthermore, the spectral variations on LEDs due to changes in the p-n junction temperature, which is normally a detrimental effect for communication, is considered as an improvement to reach new communication channels. Considering these aspects, the hypotheses of this work are stated as follows.

Hypothesis 1 (H1)

The utilization of multispectral cameras in OCC systems enhances the multiplexing capabilities by enabling efficient separation and detection of transmitters operating at distinct wavelengths.

Multispectral cameras, which feature multiple spectral bands centered at different wavelengths, provide enhanced spectral accuracy compared to conventional cameras. Based on this characteristic, OCC systems can achieve improved mul-

time-division multiplexing capabilities. The distinct wavelength bands offered by multispectral cameras enable the separation of transmitters operating at different wavelengths. This hypothesis suggests that utilizing multispectral cameras can alleviate the complexity of multiplexing techniques, such as wavelength division multiplexing (WDM), thereby enhancing the overall performance of OCC systems.

Traditional OCC systems often face challenges in effectively separating and distinguishing signals from multiple transmitters. Multispectral cameras can overcome this limitation by providing spectral information across different bands. The increased spectral accuracy and resolution of multispectral cameras allow for more efficient and accurate separation of transmitters operating at different wavelengths. Consequently, multiplexing techniques can be implemented with greater ease and reliability, leading to improved performance and increased data throughput in OCC systems.

Hypothesis 2 (H2)

Wavelength emission variations on LED devices caused by temperature effects can be detected and exploited using multispectral cameras to establish new communication channels in OCC systems.

LEDs exhibit a shift in peak wavelength as a result of temperature variations. Multispectral cameras with high spectral resolution can capture and detect these changes, thereby creating new communication channels from the same light source. This hypothesis suggests that by utilizing multispectral cameras, OCC systems can benefit from the additional information provided by temperature-induced variations in LED emissions.

The temperature effects on LEDs, resulting in wavelength shifts, have been extensively studied in the literature. Multispectral cameras offer the advantage of high spectral resolution, enabling them to capture subtle changes in LED emission spectra. By exploiting these temperature-induced variations, OCC systems can potentially increase their data transmission capacity. The spectral accuracy of multispectral cameras facilitates the separation of transmitters operating at distinct wavelengths. Consequently, conventional multiplexing techniques such as WDM can be applied more effectively, simplifying the complexity associated with multiplexing in OCC systems.

Hypothesis 3 (H3)

Neglecting the LED temperature effects in the compensation stage in OCC systems leads to a reduction in system performance, affecting the accuracy and reliability of data transmission.

While the temperature effects on LEDs have been extensively studied, their specific repercussions on OCC systems have not been thoroughly analyzed. This hypothesis addresses the potential impact of LED temperature effects on OCC system performance. If the temperature-induced variations in LED emission wavelengths are not adequately considered during channel compensation, it could result in a degradation of system performance. Therefore, this hypothesis emphasizes the

importance of accounting for temperature effects to ensure accurate and reliable data transmission in OCC systems.

Temperature variations can significantly affect the performance of LEDs, including changes in their emission wavelengths. Failure to consider these temperature effects during channel compensation can lead to inaccuracies in signal detection and decoding. The uncompensated temperature-induced variations may introduce errors and reduce the overall performance of OCC systems mainly because of cross-talking between channels. Thus, this hypothesis highlights the need for appropriate channel compensation techniques that account for LED temperature effects to maintain optimal system performance.

Hypothesis 4 (H4)

The use of nonlinear methods for data detection improves the performance of OCC systems, resulting in lower error rates.

To further enhance the performance of OCC systems, the application of nonlinear methods for data detection is suggested. Nonlinear detection techniques have shown promise in various communication systems for mitigating impairments and improving signal quality. This hypothesis aims to explore the potential of employing nonlinear methods for data detection in OCC systems, with the goal of enhancing the system's overall performance in terms of data throughput, error rates, and robustness against noise and interference.

Nonlinear detection techniques have the ability to capture complex relationships between transmitted signals and received data. By exploring the application of these methods in OCC systems, we can potentially achieve improved detection performance, especially in scenarios with challenging channel conditions. The investigation will focus on adapting and optimizing nonlinear detection algorithms to the unique characteristics and challenges of OCC systems. The outcomes of this research can lead to significant advancements in OCC technology, enabling lower error rates and improved reliability.

1.3 Objectives

In pursuit of validating the hypotheses presented above, a set of objectives has been formulated, each designed to shed light on specific facets of OCC using multispectral cameras and LED thermal effects. These objectives have been crafted to unravel the potential of these technologies and their implications for OCC system advancement. The achievement of these objectives not only bolsters the theoretical underpinnings of our hypotheses but also provides a comprehensive understanding of the practical implications and feasibility of leveraging multispectral cameras, LED temperature effects, nonlinear techniques, and temperature compensation strategies within the OCC framework.

Objective 1 - (O1)

Implement an OCC link based on the LED's temperature effects and a multispectral camera.

Multispectral cameras possess a distinct advantage in their high spectral resolution, which makes them suitable candidates for capturing and differentiating the spectral variations induced by thermal changes in LEDs. By implementing an OCC link that capitalizes on LED temperature effects and utilizes MS cameras, the objective is to demonstrate the feasibility of establishing multiple communication channels from a single light source. This objective encompasses the following sub-objectives:

1. Design and construct an experimental setup that integrates multispectral cameras as receivers and LED sources as transmitters, allowing controlled temperature variations.
2. Characterize LEDs' spectral response at varying temperatures. Perform comprehensive measurements of LED emission spectra at different temperatures to establish a baseline understanding of the wavelength shifts and spectral broadening caused by temperature effects.
3. Design temperature modulation schemes for data encoding considering the MS camera's characteristics.
4. Develop data decoding algorithms for the multispectral camera to decode data accurately.
5. Assess the system performance using metrics to validate the results.

Objective 2 - (O2)

Implement nonlinear techniques for data detection in multispectral camera communication systems.

This objective aims to enhance the performance of OCC systems by incorporating nonlinear techniques for data detection within the multispectral camera framework. In this context, the primary goal lies in a comparative analysis between the performance of the OCC system employing these nonlinear methodologies and that of conventional linear methods. The sub-objectives include:

1. Analyze and select suitable nonlinear techniques. Review nonlinear detection techniques analyzing their efficacy within the OCC framework and choose the most promising techniques that align with the spectral and operational characteristics of multispectral cameras.
2. Integrate nonlinear detection algorithms into OCC systems with MS cameras. Adapt and implement the chosen nonlinear detection algorithms to the MCC system.
3. Establish a communication link using multispectral cameras for performance assessment. Implement a functional communication link, exploiting the

capabilities of multispectral cameras to facilitate an in-depth evaluation of the performance exhibited by the integrated nonlinear techniques.

4. Conduct comparative performance analysis between the OCC system bolstered by the newly integrated nonlinear techniques and traditional linear methods.

Objective 3 - (O3)

Analyze thermal effects on LEDs in OCC systems' compensation stage.

This objective centers on a comprehensive analysis of the thermal effects on LEDs in OCC systems using conventional RGB cameras. The goal is to quantify the impact of temperature-induced spectral variations on system performance and establish the necessity of compensating for these effects. The sub-objectives include:

1. Establish a controlled temperature environment. Set up a controlled experimental environment that allows temperature adjustments for LEDs while maintaining consistent testing conditions.
2. Measure LED temperature-induced spectral variations. Conduct a series of experiments to measure the spectral response of LEDs at different temperatures. Characterize the wavelength shifts and spectral broadening caused by temperature changes.
3. Apply temperature compensation techniques that mitigate the negative effects of LED temperature-induced spectral variations using several channel matrices at different temperatures.
4. Evaluate OCC system performance under varying temperatures when LED temperature differs from that considered in the compensation stage. Measure and analyze the system's performance metrics while subjecting LEDs to different temperatures.

1.4 Organization of the document

This document is structured as a compendium thesis. It consists of a collection of journal publications indexed in Journal Citation Reports (JCR) that constitutes the experimental contributions of this thesis.

The organization of this document is depicted in Fig. 1.2. Chapter 1 includes the motivation, hypotheses, and objectives of the research. The remainder of the document is divided into the following chapters. First, Chapter 2 reviews the literature on OCC, LEDs, and high-spectral-resolution cameras. Next, Chapter 3 describes the fundamentals that support this work. Afterward, the methodology implemented to get the results is discussed in Chapter 4. Then, the thesis' outcomes are presented in Chapter 5 by means of the publication compendium. Finally, in Chapter 6, some conclusions are drawn, and future works from this research are proposed.

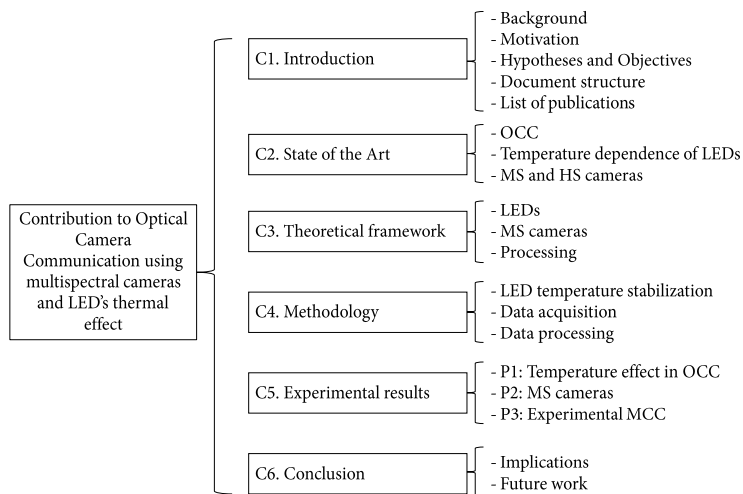


Figure 1.2: Structure of the document.

1.5 List of publications

This compendium comprises a collection of research publications that were developed during this thesis. The compendium includes a total of three papers published in indexed journals, constituting an essential part of the collection. Additionally, three additional papers have been published in conference proceedings, further contributing to the body of work presented in this compendium. Furthermore, one paper, which extends the findings of a previously published conference proceedings paper, has been published in a journal. Detailed information regarding these publications, including their respective titles, authors, and relevant bibliographic details, is presented below, ensuring comprehensive coverage of the research achievements within this thesis.

1.5.1 Compendium

The publications included in the compendium (see Chapter 5) are entitled as follows:

- D. Moreno, J. Rufo, V. Guerra, J. Rabadan, and R. Perez-Jimenez, "Effect of temperature on channel compensation in optical camera communication," *MDPI Electronics*, vol. 10, no. 3, p. 262, January 2021, DOI: 10.3390/electronics10030262.
- D. Moreno, J. Rufo, V. Guerra, J. Rabadan, and R. Perez-Jimenez, "Optical multispectral camera communications using LED spectral emission variations," *IEEE Photonics Technology Letters*, vol. 33, no. 12, pp. 591-594, June 15, 2021, DOI: 10.1109/LPT.2021.3078842.

- D. Moreno, V. Guerra, J. Rufo, J. Rabadan, and R. Perez-Jimenez, "Clustering-based data detection for spectral signature multiplexing in multispectral camera communication," *Optics Letters*, vol. 47, no. 5, pp. 1053-1056, March 2022, DOI: 10.1364/OL.449207.

1.5.2 Other research publications

In addition to the core publications within this compendium, three papers have been presented in conference proceedings (Annex A):

- D. Moreno, B. Majlesein, J. Rufo, V. Guerra, J. Rabadan and R. Perez-Jimenez, "Thermally-induced spectral variations of LED applied to optical multispectral camera communications," *2020 12th International Symposium on Communication Systems, Networks and Digital Signal Processing (CSNDSP)*, 2020, pp. 1-6, DOI: 10.1109/CSNDSP49049.2020.9249518.
- D. Moreno, B. Majlesein, V. Guerra, J. Rufo, J. Rabadan and R. Perez-Jimenez, "Comparison of clustering algorithms for data detection in Multispectral Camera Communication," *2022 4th West Asian Symposium on Optical and Millimeter-wave Wireless Communications (WASOWC)*, 2022, pp. 1-5, DOI: 10.1109/WASOWC54657.2022.9798432.
- D. Moreno, V. Guerra, J. Rufo, J. Rabadan and R. Perez-Jimenez, "Spectral Signature Multiplexing in Multispectral Camera Communication," *2022 13th International Symposium on Communication Systems, Networks and Digital Signal Processing (CSNDSP)*, 2022, pp. 515-520, DOI: 10.1109/CSNDSP54353.2022.9907907.

Furthermore, as an outcome of the findings of one of the preceding publications, an extended version of the research was subsequently published in a journal (Annex B):

- D. Moreno, V. Guerra, J. Rufo, J. Rabadan and R. Perez-Jimenez, "Multispectral Optical camera communication links based on spectral signature multiplexing," *IET Optoelectronics*, vol. 47, no. 5, pp. 91-100, 2023, DOI: 10.1049/ote2.12090.

1.5.3 Collaborations

During this thesis, the following article was developed by researchers from IDeTIC, where the author has participated as a collaborator:

- B. Majlesein, J. Rufo, D. Moreno, V. Guerra, J. Rabadan, "Underwater optical camera communications based on a multispectral camera and spectral variations of the LED emission," *Proceedings of the Workshop on Light Up the IoT*, 2020, pp. 30-35, DOI: 10.1145/3412449.3412554.

This chapter discusses the latest research in the field of the technologies used in this thesis. It also serves as a complement to the related work sections of the articles included in the compendium. It is divided into three main subsections:

- OCC technology.
- Thermal impact on LED behavior.
- Multispectral and hyperspectral camera applications.

2.1 Optical camera communication

OWC is a technology that has attracted widespread interest in recent years. Since the first developments in VLC [22], [23], where an indoor communication system using white LEDs and photodiodes was proposed, the advances in other OWC sub-parts have been boosted. Specifically, OCC is among the most commonly investigated technologies within OWC. Unlike other OWC technologies, it is based on a camera as a receiver instead of photodiodes, which provides remarkable characteristics to the system, such as ease of deployment, robustness to interference, and spatial multiplexing of the light sources, among others [3], [24], [25].

Furthermore, the fact that currently most consumer electronic devices, such as smartphones, tablets, or laptops, include a camera, as well as the advances in image sensor technology, has contributed to the increasing interest in OCC. As a result, this technology has been included in the revision of the Institute of Electrical and Electronics Engineers (IEEE) 802.15.7 standard [26].

Moreover, OCC permits both video capturing and communication, which has generated growing interest in monitoring. Typical OCC applications focus on positioning and navigation [27]–[29], vehicular communication [30]–[32], and underwater communications [33]–[35]. Regarding outdoor applications, recent works have assessed the effects of weather conditions over the optical channel, which impair the system performance due to attenuation [36]–[40]. One of the most remarkable findings of these works was the increase in the data rate of the OCC system because scattering caused by sandstorms can increase the region of interest with respect to clear atmosphere situations [39].

OCC features two communication modes depending on the sensor's scanning method. Sensors presenting global shutter (GS) acquisition simultaneously expose every pixel per frame and can only detect waveforms with bandwidths below half the frame rate. On the other hand, image sensors with rolling shutter (RS) scanning scan the image sequentially and permit higher speed communication since several changes in the optical source's waveform can be captured within a single frame. Nonetheless, since OCC is based on image-forming optics, the

maximum achievable speed depends on the projected size of the light source [41]. Some authors propose the use of non-line-of-sight (NLOS) OCC links in order to maximize the optical source's size (which is, in this case, formed by wall or floor reflections). Bani-Hassan *et al.* carried out an experiment comprising an array of ceiling-mounted transmitters and a camera pointing slightly downwards [42]. The obtained results suggested that MIMO-based communication using NLOS links is feasible in OCC, thanks to the receiver's sensitivity. However, performance metrics such as BER are significantly reduced with respect to the line-of-sight (LOS) cases.

On the other hand, since these cameras are designed for photography, OCC's maximum achievable data rate is limited by the device's pixel clock and scanning method, allowing only low data rate transmissions [25]. Hence, addressing the challenge of enhancing data rates has been a central focus in OCC, leading to the proposal of various schemes and techniques. In an effort to mitigate intersymbol interference (ISI) and improve the data rate, Younus *et al.* introduced an artificial neural network (ANN) equalizer. The authors trained the ANN once for multiple exposure times and stored the resulting model in a look-up table [43]. However, their approach lacked robustness when dealing with high exposure times, thereby limiting its applicability in scenarios that require visualization and data collection. This limitation was addressed in a subsequent study [6], where a convolutional autoencoder was employed to enhance signal quality. This approach allowed for exposure times up to seven times longer than the symbol period while employing a more computationally efficient architecture compared to the method proposed in [43]. Another notable advancement was made by Huang *et al.*, who proposed a real-time OCC system based on color-intensity modulation multi-input multi-output (CIM-MIMO). Their approach involved the creation of a high-dimensional signal constellation and parallel communication channels utilizing spatial, color, and intensity dimensions. This strategy aimed to increase the data rate and enhance the performance in terms of BER [44].

Additionally, the color filter array (CFA) located over most camera sensors allows increasing the data rate by using LEDs of different wavelengths and WDM, getting independent signals for each light source (Fig. 2.1). Several studies, for instance, [45], [46], and [47], have been conducted on WDM techniques to enhance the system performance. Furthermore, a number of works have taken advantage of this image sensor's ability to separate colors of the RGB LEDs and obtain parallel OCC systems using color shift keying (CSK). This technology inherited from VLC permits increasing throughput and reducing ISI by modulating the light signals modifying the RGB colors' intensity after mapping data onto the constellation symbol from the International Commission on Illumination (CIE) 1931 color space (Fig. 2.2) [48]–[50]. A chromaticity diagram is also employed in generalized color modulation (GCM), in which the intensities of the optical signals are modulated from multiple LEDs, regardless of the target color [51], [52].

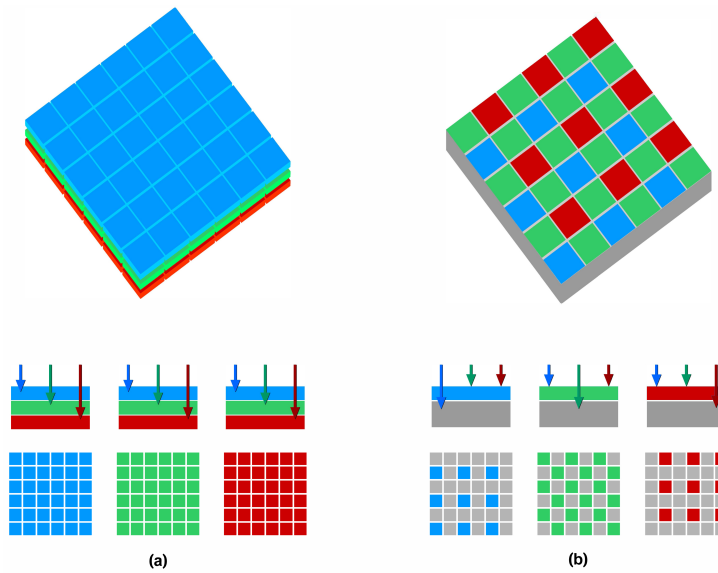


Figure 2.1: CFAs of (a) Foveon-based sensor, and (b) Bayer filter sensor. Bayer mosaic contains 25%, 50%, and 25% of red, green, and blue regions, respectively, while Foveon mosaic presents 100% of the color.

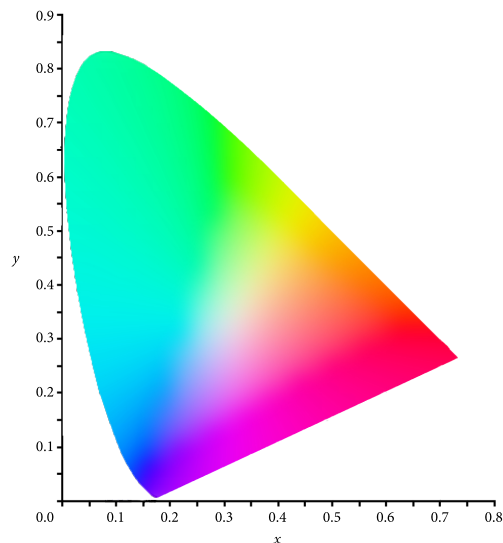


Figure 2.2: CIE 1931 color space chromaticity diagram.

2.2 Effect of temperature on LEDs

Turning now to the light sources employed to transmit the data streams, LED-based lamps are the preferred transmitter for VLC communication mainly because of their fast switching capability, although other devices, such as digital displays, have been used to send the information [53]. In addition, these devices have been

thoroughly studied in the literature, and it is well-known how sensitive they are to temperature.

Thermal modeling of LED sources has been considered on the luminaire design in order to improve its performance and reliability. In this regard, photo-electro-thermal (PET) modeling has received much attention in terms of research [54]–[57].

As to the effects of temperature on the LED's emitted spectrum, numerous studies analyzed the peak wavelength variation and the consequences in the emitted color and light intensity. For example, in [58], surface-mount device (SMD) LED's optical parameters were measured at various temperature conditions. It revealed that the peak wavelengths were expectedly red-shifted as temperature increased. Besides, intensity, spectral width, and color-coordinates shift were affected. In addition, luminous flux and efficacy on LEDs were analyzed at different operating conditions in [59]. Based on the fact that luminous flux and efficacy decrease as junction temperature grows, the authors determined the optimized conditions of the LEDs.

Regarding the color variation due to thermal changes, Muthu *et al.* measured the color change in RGB LEDs depending on temperature. They concluded that the highest color point variation was found on the blue LED [60]. Another work performed by Spagnolo *et al.* concentrated on using commercial LEDs to be employed in railway and traffic light signals respecting limits imposed by the norms. Therefore, they examined the LED's thermal behavior and proposed a system that compensates intensity and chromaticity in order to comply with the specifications [61]. In [62]–[64], the impact of the junction temperature increase on LED features was addressed. Narendran *et al.* analyzed the degradation of white LEDs caused by the yellowing of the epoxy, evaluating the main factors that affect them (p-n junction temperature, short-wavelength radiation, and the position of the phosphor layer). Their findings suggested that the junction temperature had a more significant impact than the short-wavelength amplitude [62]. Next, Muslu *et al.* examined the electrical, optical, and thermal behaviors of RGB LEDs. The authors estimated the junction temperature using the forward voltage method. Besides, the largest slope of the calibration equation was found for the green LED, suggesting a higher sensitivity to temperature variation in that LED than in the others [63]. Finally, Lu *et al.* studied the spectrum shift, and the color difference at room temperature of a flexible GaN-based LED array to test its behavior for display applications. In their experiment, the spectral behavior remained stable with minor color differences and slight temperature variation [64].

On the other hand, many studies have researched LED lifetime by accelerated aging test. These tests stressed the LED with the two leading causes that affect them, the temperature and the current through the LED. Most recent evidence shows that luminous flux, color changes, and lifetime are sensitive to thermal effects, as well as current stress degrades the LEDs more than thermal stress [65]–[68].

2.3 High-spectral-resolution cameras

As mentioned above, high-spectral-resolution cameras have not been used in optical communication. Instead, RGB cameras are the most common ones that have been employed as receivers in OCC schemes. This is mainly because the widespread use of those image sensors in the majority of conventional devices, such as smartphones or surveillance systems. Nonetheless, high-spectral-resolution sensors provides a greater range of spectral detail since they have more bands than conventional RGB. Fig. 2.3 depicts a comparison between the types of cameras mentioned above.

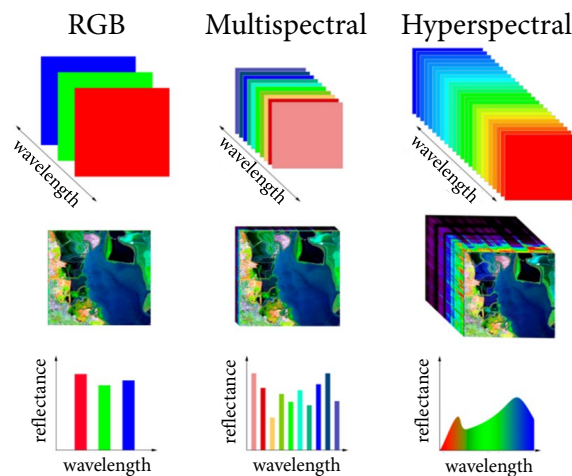


Figure 2.3: RGB, multispectral, and hyperspectral camera's characteristic comparison.

Due to the higher level of information that multispectral and hyperspectral devices provide, these types of cameras have been usually employed in several sectors, such as remote sensing, healthcare, industry, biotechnology, agriculture, *etcetera* [69], [70]. Initial studies utilized multispectral cameras for space-based imaging and remote sensing to analyze the environment since it provides more information than aerial photography. By capturing data across multiple spectral bands, these cameras enable the identification and characterization of specific materials, vegetation health, water quality, land-use classification, environmental monitoring, and archaeological sites. The ability to obtain comprehensive spectral data allows researchers and environmental agencies to study and monitor various ecosystems, track changes over time, and make informed decisions regarding land management, resource allocation, and conservation efforts [71]–[73]. One of the main applications in remote sensing is image classification. Hence, many studies applied classification techniques, such as unsupervised, semi-supervised, and supervised image classification (pixel-based techniques), and, more recently, due to the improvement of spatial resolution, object-based image analysis (OBIA) to assign land cover classes to pixels [73]–[76].

Another common use of high-spectral-resolution cameras has been medical imaging to diagnose health issues. These cameras can capture spectral data beyond what is visible to the naked eye, providing detailed information about the biochemical composition and physiological properties of tissues and organs. With this information, medical professionals can improve the accuracy of diagnoses, monitor treatment effectiveness, and identify early markers of diseases. From early studies on magnetic resonance [77], [78] to new approaches in pathological diagnosis, non-contact detection, telepathology support systems, among others [13], [79], [80], clinical medicine has benefited from multispectral/hyperspectral imaging, especially as it enables noninvasive monitoring of human parameters.

Within the industrial sector, multispectral and hyperspectral cameras contribute to quality control, product inspection, process optimization, and military applications. These cameras can analyze the spectral signatures of materials, detect defects or inconsistencies, and ensure adherence to specific standards or specifications. Industries such as food processing, pharmaceuticals, textiles, and electronics benefit from the ability to identify contaminants, assess product quality, and enhance production efficiency. By integrating multispectral and hyperspectral imaging technologies into industrial processes, companies can minimize waste, reduce costs, and improve overall product reliability and safety [81]–[83].

In agriculture, multispectral and hyperspectral cameras have revolutionized crop monitoring, precision farming, and yield optimization. By capturing spectral data from agricultural fields, these cameras allow farmers to assess crop health, detect nutrient deficiencies, identify disease or pest infestations, and determine optimal harvesting times [84]–[86].

Furthermore, for many years the field of multispectral/hyperspectral imaging has been bound to machine learning techniques in order to carry out classification analysis. In this regard, the last years have witnessed enormous growth in deep learning methods in different applications [71], [87]–[89], improving classification accuracy and providing helpful characteristics for prediction.

Overall, the utilization of multispectral and hyperspectral cameras across these sectors demonstrates their significance in providing detailed information for a wide range of applications. However, to the best of my knowledge, no use of this kind of cameras has been performed in optical communication.

Therefore, the high level of spectral detail provided by multispectral cameras opens up new possibilities in the OCC field. In fact, the number of filters presented on MS/HS cameras allows a new approach for multiplexing signals of different wavelengths based on the spectral signature of the light source. Likewise, considering the temperature effects mentioned above, a high-spectral-resolution camera could be used to capture the variation of the LED's spectral emission. Hence, by inducing a controlled temperature to the LED, it would be possible to have the same light source with a different spectral signature. Consequently, this spectral variation could be used to implement several communication channels in an OCC link with a multispectral camera as a receiver. This last proposal is one of the main hypotheses of this work, as aforementioned.

This chapter describes the basic technologies employed in this thesis and the fundamental aspects of the OCC systems. First, the LED spectral behavior with temperature is analyzed. Furthermore, a comparison between a conventional camera and an MS camera is examined. Finally, the processing techniques used in this thesis are described.

3.1 Light-emitting diodes

In recent years, LED-based lamps have been intensively used for lighting purposes due to their advantages against old incandescent and fluorescent luminaires, such as efficiency, long lifetime, and lower power consumption. Moreover, a valuable feature of LEDs lies in their fast switching capability, which makes this technology suitable for communication. Thus, the light can be modulated with a rapid on-off switching speed, transmitting the data that a photodetector or a camera receives [90].

Furthermore, the semiconductor material of the LED determines its wavelength emission, allowing infrared, visible light, and ultraviolet radiation. Table 3.1 lists the most common materials employed for different emission colors.

Table 3.1: LED emission colors by material. Source: [91]

Material	Wavelength (nm)	Color
GaAs	885	Infrared
GaP	549 to 700	Green to red
InGaAlP	539 to 653	
InGaN	388 to 590	Ultraviolet to green
GaN	365	Ultraviolet to blue

On the other hand, as discussed in previous chapters, temperature affects LED characteristics. Therefore, one of the most relevant LED aspects to consider in optical communications is the temperature dependence on the LED spectrum. The principle of this phenomenon is defined as follows (Fig. 3.1). First, LEDs emit light based on a recombination of electrons and holes in a p-n junction; that is when an electron achieves sufficient energy to cross the forbidden energy gap and reaches a higher energy level (conduction band). Afterward, once that electron returns to a lower energy level (valence band), a photon is emitted with a particular wavelength. The Planck-Einstein relation relates the wavelength and the energy gap (Equation 3.1). In turn, the energy gap depends on the p-n junction temperature as a function of the LED substrate, which is usually modeled by Equation 3.2. Therefore, in most

semiconductor materials, the energy gap decreases as temperature increases [92], and thereby the peak wavelength of the LED grows (joining Equations 3.1 and 3.2).

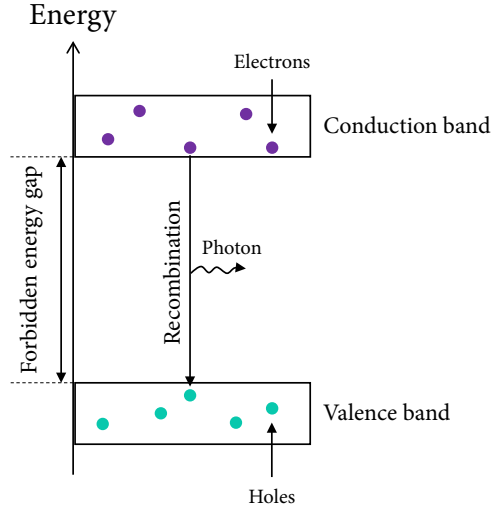


Figure 3.1: Photon emission after the recombination of charge carriers (electrons and electron holes) in a semiconductor.

$$E_g = hf = \frac{hc}{\lambda}, \quad (3.1)$$

where h is Planck's constant, f is frequency, c is the speed of light in vacuum and λ is wavelength.

$$E_g = E_0 - \frac{\alpha T^2}{T + \beta}, \quad (3.2)$$

where T is temperature, E_0 is energy gap at 0K temperature condition, and α and β are semiconductor-dependent constants, which are empirically determined.

In addition, LED's junction temperature is affected by the forward current, as well as the ambient temperature and the heat sink material [93]. In this sense, the p-n junction temperature can be measured for a constant current due to the voltage-temperature relation [94]. However, in this thesis, the LED temperature was estimated employing a thermographic camera. Further details can be found in the compendium articles.

Moreover, the relationship between current and temperature on an LED is of significant interest. Temperature tends to increase with current, a phenomenon attributed to the Joule heating effect. On the contrary, the voltage-temperature relationship is inversely proportional because the semiconductor temperature coefficient of resistance is usually negative. Thus, as temperature grows, resistance decreases what, in turn, increases the number of charge carriers available for recombination [95].

Furthermore, LED thermal behavior is often analyzed using a Cauer network, which serves as an equivalent thermal model [96]. The Cauer network employs

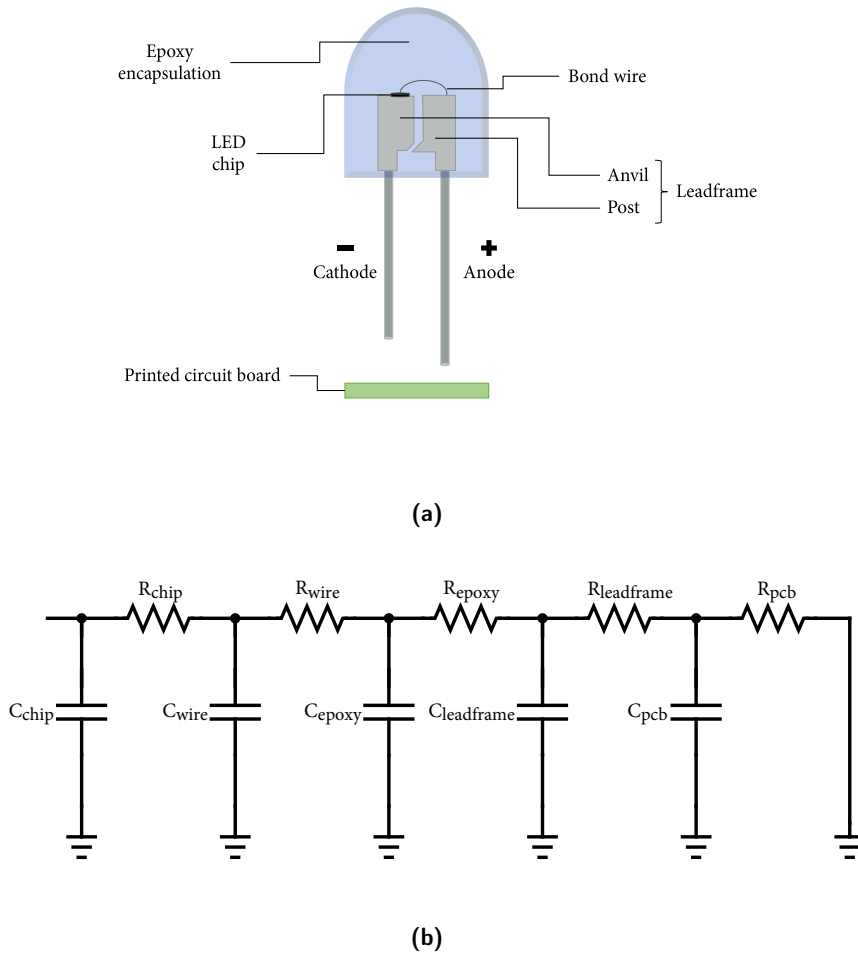


Figure 3.2: (a) Typical structure of THT LED. (b) Cauer RC network of THT LED.

a combination of thermal resistances and thermal capacitances to represent the pathways of heat flow within the LED structure, similar to electrical resistances and capacitances (resistor-capacitor (RC) circuit). Fig. 3.2 shows the typical structure of through-hole technology (THT) LED and its corresponding Cauer network.

To comprehend the temperature distribution within a typical THT LED, several key materials are considered and integrated into the Cauer network. First, the LED chip, which is the semiconducting material, also known as the die material, plays a vital role as it emits light when an electric current is applied. This material is responsible for generating heat in the initial stages.

Second, the bond wire is another crucial component that bonds the die to the leadframe. By facilitating the transfer of heat from the die to the leadframe, the thermal properties of the bond wire significantly influence the efficiency of heat dissipation from the LED chip. In addition, the leadframe, typically made of metal, serves a dual purpose of supporting the die and providing electrical connections

to the external environment. Moreover, the leadframe can function as a heatsink, aiding in the extraction of heat from the die and its dispersion.

On the other hand, the epoxy encapsulation encompasses the LED chip and inner parts of the leadframe within a protective plastic shell. In addition to providing physical protection, the epoxy encapsulation also offers some level of electrical insulation. However, it can also contribute to heat entrapment, potentially leading to an increase in temperature within the die and leadframe.

Finally, if the THT LED is mounted on a printed circuit board (PCB), the board itself and its properties can significantly impact the thermal behavior of the LED. Especially when the PCB is designed to act as a heat sink, it influences the dissipation of heat from the LED structure.

Each of these materials mentioned above can be represented within the Cauer network as a combination of thermal resistance (reflecting the resistance to heat flow) and thermal capacitance (indicating the capacity to store heat). By analyzing this network, it becomes feasible to comprehend the heat generation, spread, and dissipation mechanisms within the THT LED. Moreover, modifications in the properties or arrangement of these materials can potentially affect the LED's performance and lifespan.

3.2 Cameras

Most digital cameras possess a complementary metal-oxide-semiconductor (CMOS) image sensor, which is less costly and physically smaller than charge-coupled device (CCD) sensors [25]. In addition, CMOS-based cameras feature two acquisition modes (GS and RS), as mentioned in Section 2. Fig. 3.3 depicts both modes' basic principles of operation. GS mode offers benefits when recording moving subjects, as RS cameras can create distortions due to the delay between scanning the first row of the image and the last row. However, GS operation has a limitation in data rate, whereas RS mode permits capturing numerous LED states in a single frame. Nonetheless, the link distance must be considered so as not to degrade performance in RS mode [53].

Furthermore, general-purpose CMOS cameras typically present a CFA on top of the sensor that is responsible for color imaging. These filters present the three primary colors (RGB), usually arranged in a Bayer pattern. However, there exist alternatives, such as the Foveon X3 sensor, in which the RGB layers are vertically stacked instead of using a mosaic [3].

On the other hand, MS cameras extend this approach one step further by capturing images with numerous color bands and narrow band-pass filters [97]. Fig. 3.4 shows the filter responses of a conventional Bayer-based camera and an MS camera. It can be seen that the multiple MS bands enrich the spectral information; for example, red wavelengths are covered by three bands in the MS camera, whereas the RGB camera has only one band with a large width for this color.

Based on these MS bands, elements presented on the images captured by the camera present a specific spectral response curve called a spectral signature. Similar to how different surfaces of an image can be distinguished in remote sensing

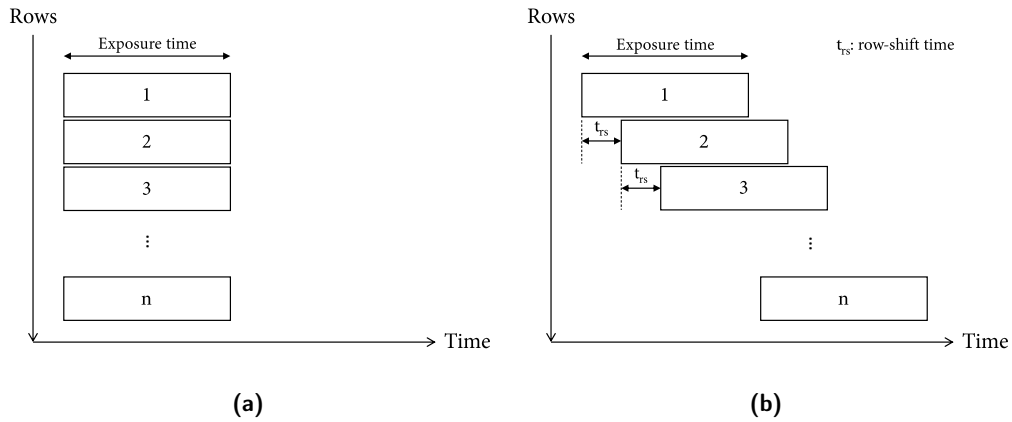
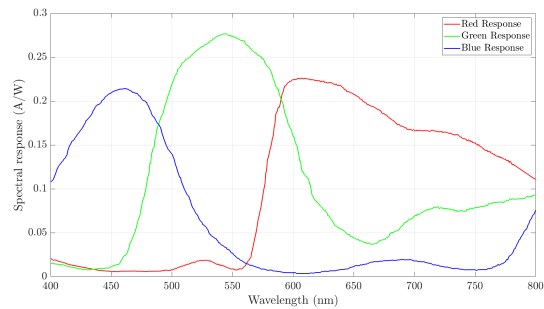
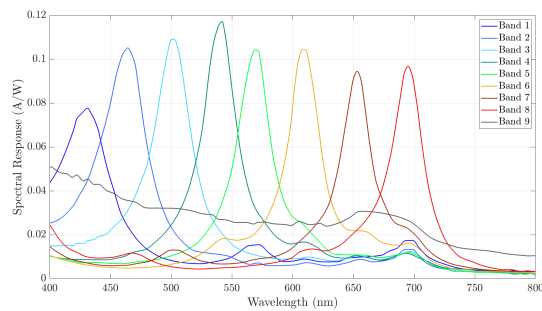


Figure 3.3: Camera's acquisition modes: **(a)** Global shutter: all the sensor's pixels are exposed simultaneously. **(b)** Rolling shutter: the pixels are exposed row by row with a t_{rs} period between the start of exposure of each row.



(a)



(b)

Figure 3.4: Camera filter responses: **(a)** RGB camera. **(b)** Multispectral camera.

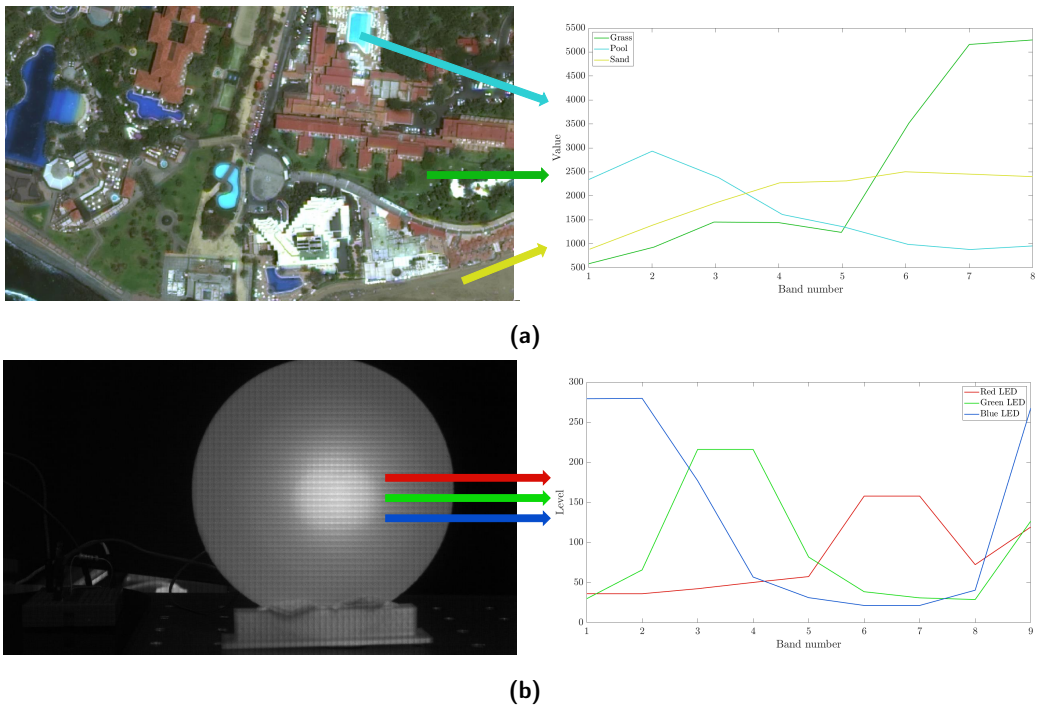


Figure 3.5: (a) A satellite image showing different elements of a surface that present distinct spectral signatures. Grass, sand, and pools can be discriminated by their different levels of reflectance. (b) LEDs with different wavelengths can also be distinguished by their spectral signature. A simple example can be seen using three RGB LEDs.

applications because of their distinct spectral signature, the light beams of LEDs with different wavelengths can be differentiated in OCC (Fig. 3.5). Therefore, novel approaches in OCC can be developed exploiting this feature.

3.3 Processing

Considering the aforementioned LED spectral variation by temperature and the characteristics of multispectral cameras, a new approach based on the spectral signatures of the transmitters for multiplexing different signals is proposed in this thesis.

It consists of an LED-to-camera communication using a multispectral camera as a receiver, which allows taking advantage of the numerous device bands to distinguish signals of different wavelengths. Furthermore, the LED spectral variation due to temperature is leveraged. Since the LED spectral response curve varies with thermal changes, those modifications can be grasped by a high-spectral-resolution camera. Therefore, new communication channels can be achieved utilizing the same transmitter device, as the LED spectral signature modifies with temperature.

With this in mind, the camera’s response upon receiving an LED signal could be modeled by Equation 3.3.

$$r_{ij} = \sum_k F_i(\lambda_k) \cdot S_j(\lambda_k, T) \cdot R(\lambda_k) \quad (3.3)$$

where k is the visible light spectral range, i is the band number of the multispectral camera, j is the current supplied to the LED, λ is the wavelength, $F(\lambda)$ is the filter transmission, $S(\lambda, T)$ is LED's emission spectrum, T is temperature, and $R(\lambda)$ is the silicon responsivity.

By examining Equation 3.3, it becomes evident that the camera's response (r_{ij}) is determined by a combination of factors, such as, the filter transmission, which accounts for the camera's optical characteristics at each wavelength, the LED's emission spectrum, which incorporates the LED's varying spectral response due to temperature changes, and the silicon responsivity, which characterizes the camera's sensitivity to different wavelengths.

Theoretically, as many communication channels as camera's spectral bands could be achieved. However, it is crucial that the spectrum of the transmitters is distinguishable by the camera, which depends on the receiver's resolution.

3.3.1 Channel compensation

Channel compensation is critical in any system subject to ICI. Several techniques aim to alleviate ICI, such as MIMO, CSK and WDM, which require an equalization stage to minimize the interference in VLC systems. Zero-forcing (ZF) and minimum mean square error (MMSE) equalizers are the usual algorithms applied to equalize [98]–[100]. Furthermore, recently nonlinear methods, such as cluster analysis, have been used in order to improve the system performance with respect to traditional linear methods.

First, the received signal y can be represented as:

$$y = \mathbf{H} \cdot x + n, \quad (3.4)$$

where \mathbf{H} is the channel matrix, x is the transmitted signal, and n is additive white Gaussian noise (AWGN).

ZF equalizer is a linear algorithm that reduces ICI to zero in a noiseless scenario. In multispectral camera communication (MCC), the channel matrix is formed by the responses of each camera band, i.e., the spectral signature. In most cases, this matrix could be non-square if the number of transmitters is different from the number of bands. For those cases, the Moore-Penrose pseudo-inverse (\mathbf{W}) can be used to get the inverse channel matrix (Equation 3.5), which is applied to the received signal.

$$\mathbf{W}_{ZF} = \mathbf{H}^T (\mathbf{H} \cdot \mathbf{H}^T)^{-1}, \quad (3.5)$$

where T indicates transposition.

On the other hand, MMSE equalizers are typically employed in communication systems instead of ZF ones since they consider the system's noise to optimize the output signal-to-noise ratio (SNR). Equation 3.6 reveals the calculation of the matrix that is used to make the received signal close to the transmitted signal.

$$\mathbf{W}_{MMSE} = \mathbf{H}^T \left(\mathbf{H} \cdot \mathbf{H}^T + \frac{1}{SNR} \cdot \mathbf{I} \right)^{-1}, \quad (3.6)$$

where \mathbf{I} is the identity matrix. It can be noted from Equation 3.6 that for high SNR values, the Moore-Penrose inverse used in ZF equalization (Equation 3.5) and the matrix used in MMSE are equivalent.

Once the compensation matrix \mathbf{W} is calculated, introducing the linear compensation in Equation 3.4 yields an estimation of the transmitted signal (Equation 3.7).

$$\hat{x} = \mathbf{W} \cdot y = \mathbf{W} \cdot (\mathbf{H} \cdot x + n) \quad (3.7)$$

It must be considered that regardless of the estimation mechanism of \mathbf{W} , its components will be subject to AWGN. Therefore, the compensation mechanism will not be ideal, and an estimation of the compensation performance is needed. In this regard, the condition number of the channel matrix can be used as this performance metric (Equation 3.8) [101]. Well-conditioned matrices (values close to one) better estimate the transmitted signal than ill-conditioned ones (values much higher than one).

$$\text{cond}(\mathbf{H}) = \|\mathbf{H}\| \cdot \|\mathbf{H}^{-1}\| \quad (3.8)$$

On the other hand, machine learning approaches, such clustering, can be used for data detection. Cluster analysis is an unsupervised learning method that uses datasets made up of unlabeled data to identify a logical structure by grouping similar data points in the same cluster. There are various clustering algorithms that can be classified into different categories depending on how they work [102]. For instance, some of the most common types of clustering algorithms are hierarchy-, partition-, density-, and distribution-based clustering. Table 3.2 summarizes those categories. Hence, hierarchical and partitioning clustering are based on proximity (distance or similarity), density-based clustering on composition, and distribution-based clustering on probability.

Table 3.2: Types of clustering algorithms. Source: [102]

Category	Typical algorithm	Principle
Hierarchical clustering	BIRCH	Constructs a tree of clusters
Partitioning clustering	K-means	Represents each cluster by its cluster center (centroid)
Density-based clustering	DBSCAN	Defines regions of high data density as clusters
Distribution-based clustering	GMM	Creates clusters based on the likelihood of data belonging to the same distribution

First, it is necessary to use some received signals to train the clustering model. This is a critical part since the system performance is considerably affected by it. Moreover, depending on the algorithm employed, different parameters can be set to fine-tune the model. Once the model is fitted, the clusters are assigned to a corresponding symbol to recover the transmitted signals. Having obtained the transmitted bit streams, either by traditional linear methods or by clustering techniques, a correlation function can be applied to determine the received data, which is afterward decoded.

This chapter includes the materials and methods employed in this thesis. However, since this thesis consists of a compendium of publications and each article followed a different approach, the common procedures are described in this chapter, whereas a thorough explanation is provided in each paper discussed in Chapter 5.

Therefore, the basic methodology of this thesis could be organized as shown in Fig. 4.1. First, the LEDs' spectral features were modified by inducing thermal changes in their p-n junction temperature. For this reason, and because no external sources were employed to heat the devices, the LEDs were powered at different currents for a period of time until they reached their thermal steady state. Second, behavior characteristics from the light sources were collected using various instrumentation equipment to characterize them and an MS camera to establish a communication link. Lastly, data were processed by applying several techniques to analyze them.

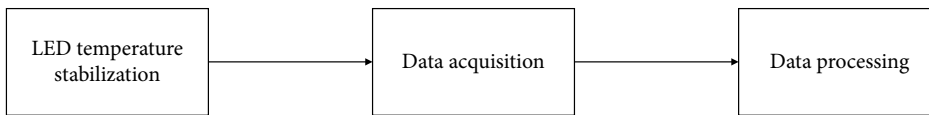


Figure 4.1: Common methods followed throughout this thesis.

4.1 LED temperature stabilization

Since one of the objectives of this thesis was to analyze the LED behavior when its p-n junction temperature changes, a mechanism for controlling the temperature with sufficient accuracy has been developed. In particular, the temperature of several LEDs was modified by applying different bias currents (Joule effect). Thus, the higher the bias current, the higher the p-n junction temperature. Throughout this thesis, only 5-mm THT LEDs were used in the experimental setups—specifically, red, and common cathode RGB LEDs.

The driving currents were supplied using two different circuits (Fig. 4.2). In the one case, a current source fed directly to the LED; in the other case, the current was controlled by a circuit powered by a voltage source. This current could be set by selecting R1 (Equation 4.1). Moreover, in the latter case, a microcontroller was utilized to configure each LED with a different pulse-width modulation (PWM) duty cycle (DC) in order to set a target temperature.

$$R1 = \frac{V_{DD} - (V_{LED} + V_{DS})}{I}, \quad (4.1)$$

obtaining information such as the time it takes to stabilize their temperature and the maximum achievable value.

Lastly, once the spectra and temperature were measured, an MS camera (SILIOS Technologies CMS-C1-C-EVR1M-GigE) was used to get the spectral signatures and examine whether they were distinguishable by it or not. This camera possesses a modified Bayer matrix consisting of a group of 3x3 pixels, referred to as macro-pixel, which serves as a spectral band filter (Fig. 4.3). The construction of this macro-pixel is uniform across the entire CMOS sensor area, ensuring its replication throughout.

Band 8	Band 7	Band 6
Band 1	Band 9	Band 5
Band 2	Band 3	Band 4

Figure 4.3: Macro-pixel presented in the MS camera used in this thesis.

Table 4.1 details the critical parameters of the devices mentioned above. Moreover, various tools were employed to not saturate the devices due to the high intensity of the LED beams, such as an integrated sphere and a diffuser.

4.2.2 OCC link

The experiments carried out in this thesis were simulated and experimentally performed. Regarding the simulations, two schemes were followed (Fig. 4.4): one simulating the response of a conventional camera and analyzing the impact of temperature on channel compensation; the other using an MS camera to assess its performance in a communication link. As seen in Fig. 4.4 (a), the spectra of RGB LEDs at different temperatures were used to simulate the response of Foveon and Bayer-based cameras. Then, from this information, the channel matrix was calculated to be compensated (using a ZF equalizer). Finally, the impact of temperature on the compensation was addressed. Besides, Fig. 4.4 (b) shows the diagram with the steps to simulate a communication link with an MS camera as a receiver (MCC) assuming an OOK transmission. First, the channel matrix was formed using the LED's spectral signatures, and a list of bit streams was generated. After that, a ZF equalizer was employed to obtain the estimated bit streams. Lastly, the system performance could be assessed using various metrics.

On the other hand, the experimental research followed the scheme shown in Fig. 4.5. It began with the region of interest (ROI) selection, in this case, where the LED's light beams were mixed. Afterward, each transmitter's spectral signatures

Table 4.1: Devices specifications. Sources: [103]–[106]

Device	Characteristics	
Spectrometer <i>Spectral Products SM442</i>	Image sensor	Toshiba TCD 1304
	Pixels	3648
	Spectral resolution (nm)	0.15 to 10 depending on the slit and grating choices
	Spectral range (nm)	200 - 1050
	Aperture	f/2.7
Light meter <i>Gigahertz BTS256</i>	Slit options (μm)	5, 10, 25, 50, 100, 200, 400
	Spectral range (nm)	360 - 830
	Bandwidth (nm)	5
	Data resolution (nm)	1
	Integration time (ms)	5.2 - 30000
Thermographic camera <i>FLIR A645</i>	Resolution (pixels)	640 \times 480
	Object temperature range ($^{\circ}\text{C}$)	-20 - 650
	Thermal sensitivity ($^{\circ}\text{C}$)	<0.05 at +30 $^{\circ}\text{C}$
	Aperture	f/1.0
	Maximum frame rate (fps)	25
Multispectral camera <i>SILIOS Technologies CMS-C1-C-EVR1M-GigE</i>	Resolution (pixels)	1280 \times 1024 (raw image) 426 \times 339 (multispectral images)
	Bands' center wavelength (nm)	B1: 424
		B2: 464
		B3: 504
		B4: 544
		B5: 573
		B6: 614
		B7: 656
		B8: 699
		B9: 400 - 800
Exposure time (s)	10 μ to 2	
Maximum frame rate (fps)	60	

were stored and used for channel separability analysis and equalization. The next step consisted of transmitting bit sequences, 8b/10b encoded, in a microcontroller. Furthermore, the microcontroller generated variable pulse position modulation (VPPM) signals that permit inducing the desired temperature in the LED. Fig. 4.6 illustrates an example of two transmissions using the encoding mentioned earlier. Transmitter 1 was set with 70% DC, whereas transmitter 2 with 30% DC. In addition, a header and a footer were added to the transmission frame to improve the data detection process. Likewise, avoiding long sequences of "1" or "0" was indispensable to prevent modifications in the spectral signatures owing to their high thermal sensitivity. In this sense, this encoding allowed bit streams with non-consecutive zeros and ones.

Regarding the reception, the MS camera took the images in GS mode to eventually estimate the received data and assess the system performance.

Furthermore, in this thesis, the experiments were performed under controlled conditions in a dark chamber. No different channel models were considered since the main aim of this research was to conduct a preliminary study exploiting the temperature effect on LEDs and MS cameras, and different conditions would not affect them. Fig. 4.7 shows a representation of the experimental setup followed in this thesis.

4.3 Data processing

In this section, the processing techniques performed in this thesis are discussed. As reported previously, two main approaches were conducted in order to evaluate the system performance in distinct scenarios.

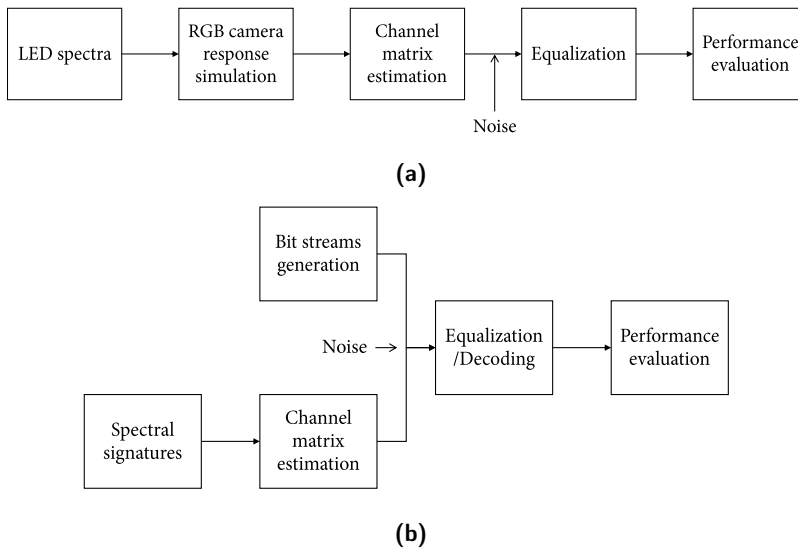


Figure 4.4: Flow diagrams of the simulation experiments: (a) RGB camera scheme. (b) MS camera scheme.

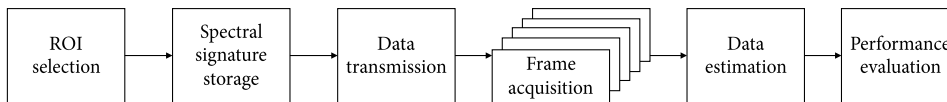


Figure 4.5: Flow diagram of the experimental work.

In the first place, the processes involved in the analysis of the temperature effect on channel compensation are illustrated in Fig. 4.8. Once the channel matrix was estimated, it was compensated using a ZF equalizer and an obsolete channel state information (CSI), distinct from the one measured corresponding to the new stationary temperature regime of the LED. Owing to the difference between the reference CSI and the instantaneous CSI, which is at a different temperature, the signal-to-interference-plus-noise ratio (SINR) and, eventually, the BER were worsened. Therefore, those two metrics were examined in this work.

In the second place, the typical workflow followed in this research for the MCC links is depicted in Fig. 4.9:

1. The received signal S , containing several mixed LED light beams corresponding to various transmissions, was divided into n individual signals by applying either a linear equalization approach or a cluster analysis.
2. Because the packet structure was known in advance, those signals were correlated with a matrix comprising all the available transmitted bit streams (2^{bits}).
3. The maximum coefficient was obtained, providing the highest match, which eventually permitted obtaining the decoded bit stream.

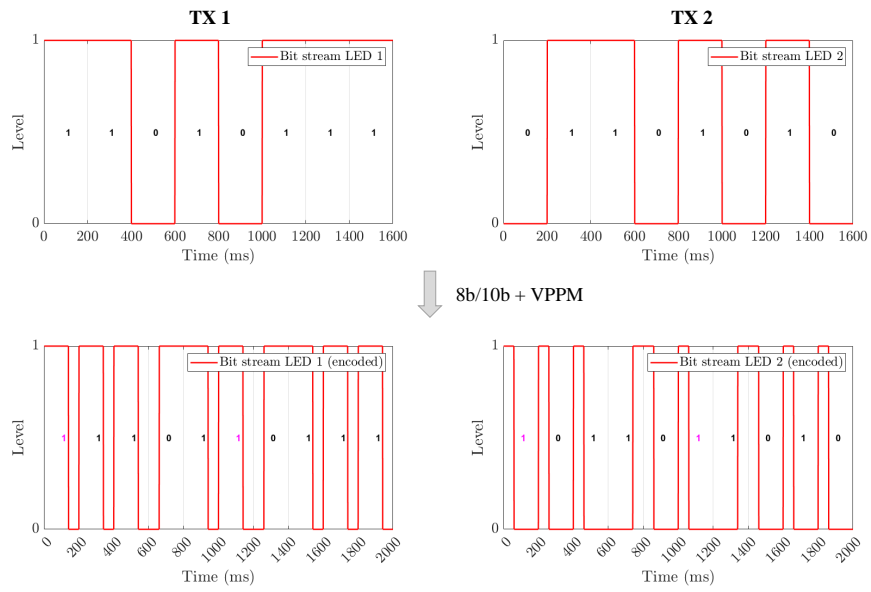


Figure 4.6: Examples of signals encoded using 8b/10b and VPPM. The first column represents the bit stream of transmitter 1 and the second column of transmitter 2. The first row represents the bit streams before encoding and modulation, and the second row represents the bit streams after these processes.

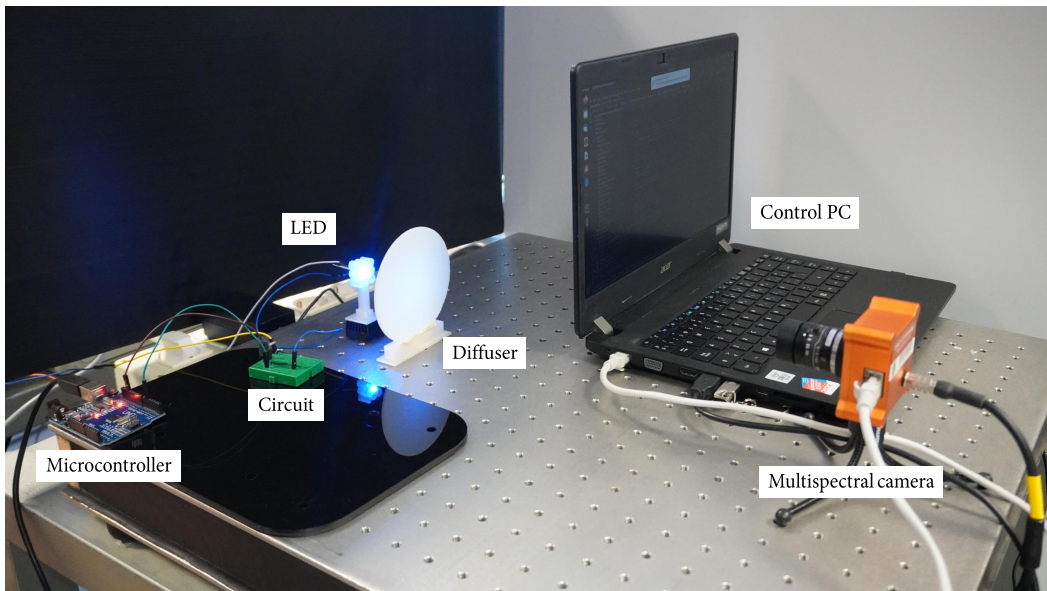


Figure 4.7: Experimental setup used to the MCC link.

4. The transmitted and estimated bit streams were compared to calculate the BER.

Alternatively, the condition number of the channel matrix was calculated to obtain a metric of how separable the signals are and how it affects the system performance. Typically, matrices comprising spectral signatures of the same color

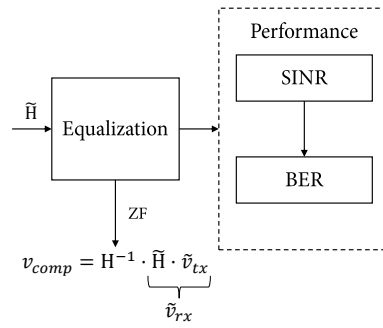


Figure 4.8: Diagram of the processing performed to analyze the temperature effect on LEDs in channel compensation. \tilde{H} represents the current CSI, \tilde{v}_{tx} the transmitted symbol, \tilde{v}_{rx} the received symbol, and v_{comp} the CSI-compensated symbol.

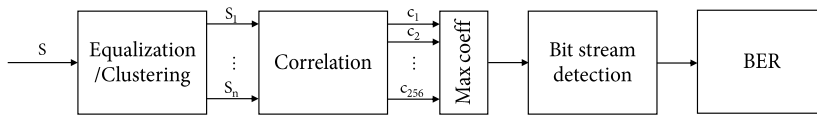


Figure 4.9: Workflow followed for data processing in an MCC scheme. s represents the received signal, S_n the individual signals, n the number of transmitters, and $c_1 \dots c_{256}$ the correlation coefficients.

at a different current are worse conditioned than a matrix formed by the spectral signatures of different colors (more differences between signatures than in the former case). It is mathematically explained because if a spectral signature is close to being a linear combination of others, the condition number tends to infinity.

The publications of the compendium are presented in this chapter. Before each article, a brief explanation is given, introducing the main topic, describing the methodology applied, and the results obtained. Lastly, an overview of each publication's contribution is provided. In addition, a summary of the articles resulting from this research but not included in the compendium is added at the end of this chapter.

5.1 Publication 1 (P1)

The first work included in this compendium, entitled "*Effect of Temperature on Channel Compensation in Optical Camera Communication*" [107], addresses the thermal impact of LEDs on channel compensation in the context of OCC, aligning with the pursuit of Objective 3 (O3). CMOS cameras usually possess three channels (RGB) resulting from Foveon or Bayer-based image sensor filters. This feature permits using modulation schemes, such as WDM and CSK, to improve the OCC system's data rate. However, the use of these techniques typically involves including a compensation stage in order to attenuate the inter-channel interference caused by the overlap of the color filters. In this work, a CSI is estimated, and a ZF equalizer is applied for the channel compensation. Nonetheless, the spectral changes in LEDs induced by temperature variations on the p-n junction should be considered in the compensation stage as it could diminish the system performance.

In this work, an OCC link employing an RGB LED was assessed when obsolete CSI in terms of temperature is used for the channel effects compensation, i.e., when the actual p-n junction temperature of the transmitter is different from the LED temperature at optimal working conditions from which the CSI was estimated. Therefore, several temperatures were induced to the light source under test based on the Joule effect by increasing the driving current of the device. Both temperature and LED emitted signals were characterized using a thermal camera and an optical spectrometer, respectively. Then, the responses of Bayer-based and Foveon image sensors were simulated to obtain the associated CSI and perform the ZF compensation of two channel matrices at different temperatures. Finally, the system performance was evaluated, estimating SINR and BER.

One of the strong points of this study lies in considering the LEDs' spectral variation produced by temperature in the compensation stage of an OCC system for the first time, up to the authors' knowledge. The findings revealed that SINR and BER are affected as the difference in temperature between the reference CSI and the current CSI increases. Furthermore, this paper indicated that the Bayer-based sensor was less penalized than the Foveon sensor as the overlap between the RGB filters in the latter is higher. Lastly, the blue color was the most affected LED due to its red-shifted spectrum and the characteristics of the sensor's filtering

scheme. However, the performance of these devices depends on the composition and operating conditions of the LED that determine its spectral variation with temperature.

Article

Effect of Temperature on Channel Compensation in Optical Camera Communication

 Daniel Moreno , Julio Rufo , Victor Guerra * , Jose Rabadan  and Rafael Perez-Jimenez 

Institute for Technological Development and Innovation in Communications (IDeTIC), Parque Científico Tecnológico de la ULPGC, Polivalente II, Planta 2, 35017 Las Palmas de Gran Canaria, Spain; dmoreno@idetec.eu (D.M.); jrufo@idetec.eu (J.R.); jrabadan@idetec.eu (J.R.); rperez@idetec.eu (R.P.-J.)

* Correspondence: vguerra@idetec.eu

Abstract: General-purpose Complementary Metal Oxide Semiconductor (CMOS) sensors perform the image desegregation in three channels (red, green, and blue) as a result of a band-pass wavelength filtering carried out using Foveon or Bayer filters. This characteristic can be used in Optical Camera Communication (OCC) systems for increasing the links' data rate by introducing Wavelength Division Multiplexing (WDM) or Color Shift Keying (CSK) modulation schemes. However, these techniques need a compensation stage to mitigate the cross-talk between channels introduced by the filters. This compensation is performed by a Channel State Information (CSI) estimation and a zero-forcing compensation scheme. The impact of the temperature effects of light-emitting diode (LED) emissions on the zero-forcing compensation scheme's performance has not been analyzed in depth. This work presents a comprehensive methodology and experimental characterization of this impact for Foveon and Bayer-based image sensors, assuming that the CSI is estimated under temperature conditions different from the LED's stationary temperature regime. Besides, Signal-to-Interference-plus-Noise Ratio (SINR) and Bit Error Rate (BER) performance metrics are presented in order to estimate the repercussion in an OCC link. The results reveal that the Foveon sensor obtains more unsatisfactory performance than the Bayer-based sensor. On the other hand, the blue band is the most penalized by the thermal effect.

Keywords: LED; Optical Camera Communication; temperature effects; spectrum; channel compensation



check for updates

Citation: Moreno, D.; Rufo, J.; Guerra, V.; Rabadan, J.; Perez-Jimenez, R. Effect of Temperature on Channel Compensation in Optical Camera Communication. *Electronics* **2021**, *10*, 262. <https://doi.org/10.3390/electronics10030262>

Academic Editor: Imran Ansari
Received: 24 November 2020
Accepted: 20 January 2021
Published: 22 January 2021

Publisher's Note: MDPI stays neutral with regard to jurisdictional claims in published maps and institutional affiliations.



Copyright: © 2021 by the authors. Licensee MDPI, Basel, Switzerland. This article is an open access article distributed under the terms and conditions of the Creative Commons Attribution (CC BY) license (<https://creativecommons.org/licenses/by/4.0/>).

1. Introduction

Optical Camera Communication (OCC) is an Optical Wireless Communication (OWC) technology based on the use of general-purpose cameras for gathering data from optical sources. This technology was included in the last revision of the IEEE 802.15.7 standard on Visible Light Communication (VLC) [1], where several physical layer (PHY) transmission modes were defined. The most remarkable advantage of OCC with respect to traditional VLC is the ubiquity of cameras embedded into smartphones, tablets and laptops. Therefore, the likelihood of a massive adoption of OCC by the market is higher than in the case of other VLC technologies, which would require a costly adaptation of the device's interfaces. Furthermore, although OCC is intended to provide low-speed capabilities, the inherent spatial multiplexing capacity of cameras allows an easy integration of Multiple-Input Multiple-Output (MIMO) schemes [2].

Currently, OCC is being proposed as an enabling technology in Smart Cities [3], Intelligent Transportation Systems (ITS) [4], and e-Health [5]. Moreover, OCC has led to several theoretical and experimental works related to Visible Light Positioning (VLP) [6,7], which may lead to a location-aware system feasible for marketing applications. Nevertheless, the use of OCC in the environments mentioned above is limited by the link geometry and the camera's optical system since the maximum achievable data rate in OCC is directly related to the projected size of the light source on the image sensor [8].

General-purpose Complementary Metal Oxide Semiconductor (CMOS) cameras usually present three color channels (red, green, and blue) comprising the typical RGB scheme. Each channel results from a band-pass wavelength filtering carried out typically using Foveon or Bayer-based image sensors [9]. These color-filter mosaics present a considerable overlap between their transmission spectra (Figure 1). Wavelength Division Multiplexing (WDM) or Color Shift Keying (CSK) communication schemes need to compensate the induced inter-channel interference in order to improve the Signal-to-Interference Ratio (SIR) and thus the Bit Error Rate (BER) performance [10]. This compensation is typically carried out by obtaining the Channel State Information (CSI) in the form of a deterministic channel matrix and performing a matrix multiplication by its inverse, constituting a Zero-Forcing (ZF) scheme. Many other approaches are currently being used in massive MIMO systems [11], but their higher complexity and computational cost are generally not justified in 3-channel OCC systems.

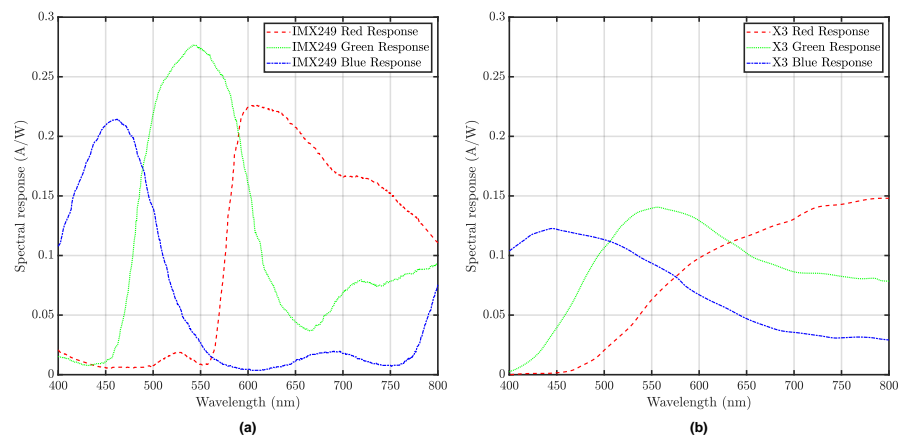


Figure 1. Image sensor filter responses. These graphs illustrate the product between filter transmissivity and silicon sensor responsivity. (a) Sony IMX249. (b) Foveon X3. Dashed line, dotted line, and dash-dot line correspond to red, green, and blue, respectively.

On the other hand, Light-Emitting Diode (LED) devices increase their temperature with respect to their driving current due to the Joule effect. In addition, the p-n junctions' response is very sensitive to these temperature variations, producing significant modifications on the emitted spectrum and the energy efficiency of the light source. As a general rule of thumb, the band gap energy of the substrate is reduced as temperature increases [12], and therefore its peak wavelength red-shifts. Furthermore, an increment in the vibrational energy due to temperature leads to a reduction of the quantum efficiency (electron-to-photon conversion rate) [13].

The effects of temperature on both light sources and optical camera receivers are well documented in the literature separately. Nonetheless, the impact of the aforementioned temperature effects of LED emissions on the performance of the zero-forcing compensation scheme has not been analyzed in depth. This work provides a comprehensive methodology and experimental characterization of this impact using commercially available devices. It has been assumed that the CSI is acquired subject to an initial temperature condition, different from the stationary temperature regime of the LED. Therefore, the product between the obsolete inverted CSI matrix and the actual channel matrix will not be the identity, resulting in an SIR penalty. LED lamps located outside buildings directly exposed to solar radiation, vehicle headlights, or any LED-based source subject to critical heat conditions in industrial environments can suffer from the aforementioned effects. Large time-dependent temperature gradients can occur (in both directions), and the link quality must comply with the system's requirements regardless of the environmental conditions. This work

provides experimental evidence about the necessity of consistent channel compensation mechanisms in these scenarios.

This paper is structured as follows. Section 2 performs an in-depth analysis of the related works available in the literature, Section 3 discusses the details of the OCC link, Section 4 describes the channel compensation procedure, and Section 5 introduces the methodology and the experimental setup implemented to obtain the results, which are presented in Section 6. Finally, these results are discussed in Section 7.

2. Related Work

This work underlines the importance of considering the effect of temperature on LEDs when compensating the channel in OCC. Temperature effects on those light sources have thoroughly been studied in the literature. A number of studies have found that the efficiency and the spectral features of the LEDs are very sensitive to thermal changes. Furthermore, several approaches have been proposed to perform channel compensation in VLC and OCC systems, but none have dealt with the mentioned temperature effects.

Photo-Electro-Thermal (PET) modeling of LED sources has a significant impact on luminaire design and optimization. These three domains are usually tightly coupled, and the design of illumination fixtures must take into account the interactions between them. Commercial LED lamps are customarily manufactured using arrays of LED. Due to the manufacturing process, each device presents slightly different characteristics that could affect the performance (and ultimately the reliability) of the LED system. Chen et al. proposed a 3D PET model for predicting the behavior of lamps built with non-identical LED parts [14]. The model, based on the use of a grid-like partition of the domain of interest combined with coupling equations, presented high accuracy compared to the experimental results. Almeida et al. proposed a PET model that included transient analysis for predicting the impact of driving current ripple effects on both the thermal and the photometric outputs of an LED. The authors obtained experimental evidence about the benefits of driving LED devices with rippled inputs (DC current plus a sine-like signal) for improving the lifespan of these devices without affecting the human perception [15]. This type of input enables smaller capacitance filter values, which allow the use of more reliable technologies compared to electrolytic capacitors (such as film capacitors). In addition to these models, Shen et al. included the effects of phosphor temperature in a PET model, showing that a good thermal design considering this aspect is capital to maintain performance in White LED (WLED) devices [16]. Unlike Shen et al., a dynamic PET analysis was carried out by Hui, Lee, and Tan in [17]. The authors proposed a modification of the steady-state PET equations from Chen et al. [14], including the coupling effect of phosphor-to-LED (and vice versa) in the thermo-electric domain, as well as the electro-optic efficiency reduction on phosphor due to temperature. All these models were focused on the lighting industry and aimed to develop models suitable for manufacturers and designers. Nonetheless, communication metrics have not been included in PET models yet (up to the authors' knowledge).

Regarding the emitted spectrum variation due to the p-n junction temperature, Ray-pah et al. carried out an investigation measuring the spectrum of a Surface Mount Device (SMD) LED at ambient and high-temperature conditions that demonstrated a red-shift in the peak wavelength and a decrease in intensity as temperature grew [18]. Some studies related to thermal effects on LED focused on the emitted color variation. Muthu et al. performed experimental measurements of color variation in RGB LEDs as a function of temperature, concluding that the blue LED has the highest color point variation [19]. Spagnolo et al. discussed LED applications in railway and traffic light signals proposing a system that compensate intensity and color stability in order to respect limits imposed by the norms [20]. Lu et al. established a relationship between color difference and temperature using a blue transparent flexible mini-LED array [21].

Furthermore, the LED luminous efficiency has been enhanced over the past few years owing to different techniques. Lee et al. investigated the thermal and optical characteristics

of a warm white LED, studying both the effects of thermal interface materials (TIM) and the impact of the driving current on the LED performance. The authors remarked the importance of a comprehensive design of the internal thermal structure and the appropriate selection of the packaging material to extend the lifetime and preserve the performance of the LED [22]. Regarding the effect of the driving current, Raypah et al. analyzed the optimal working conditions of a low-power SMD LED concerning the luminous flux and its efficacy [23]. The authors compared how those properties were affected by the injection current and the ambient temperature, concluding that the latter affected more that LED's substrate. Chen et al. carried out a study analyzing the effect of rapid thermal cycling on luminous flux and luminous efficiency of high-power LED, demonstrating that the effect could significantly impair the LED properties and interface microstructures [24].

Channel compensation is a capital processing stage in any system in which there is inter-channel interference. In VLC-based systems, MIMO and CSK (and WDM) are the two main techniques that can require compensation. MIMO VLC systems have attracted the attention of the scientific and industrial communities in recent years due to their potential use in real environments using multi-LED lamps and the current industrial trend based on the application of Orthogonal Frequency Division Multiplexing (OFDM) [25,26]. According to this trend, Hong et al. studied adaptive bit-loading and power-allocation schemes for indoor MIMO-VLC systems [27]. The authors proposed the use of 2×2 receiver arrays with angular diversity. The simulation results, which included a realistic estimation of the impulse responses, show that elevation angles close to 45° can optimize the BER performance after channel compensation. However, the transmission-side setup included four independent LED lamps separated by a large distance, and no jitter or synchronization issues were mentioned in the paper. This last aspect is essential when the spatial diversity emitter covers a significant deployment area, as highlighted by Ramirez-Aguilera et al. in [28]. A similar work based on the same angular diversity concept was presented by Wei, Zhang, and Song in [29]. In this case, the authors validated a cubic receiver under laboratory conditions, demonstrating the feasibility of the $\pi/2$ -diversity. Akande and Popoola in [30] performed a comprehensive comparison between spatial multiplexing and repetitive coding MIMO techniques for Carrierless Amplitude and Phase (CAP) modulation. The authors demonstrated that repetitive coding is a better option for highly-correlated channels due to the ill-conditioned nature of the channel matrix (similar channel gains for each channel). However, this depends on the input SNR. Luo et al. proposed the use of an RGB OCC link in [31]. The authors demonstrated spectral efficiencies up to 3 bits/s/Hz in a 60 m link in their work. Although the paper states that MIMO techniques were employed, a single-LED link was essayed. Regarding RGB channel compensation, a ZF scheme (as in [10]) was used with no output SNR penalty (typical issue of ZF) thanks to the use of imaging optics at the receiver side.

Anusree and Jeyachitra studied different compensation techniques for MIMO-VLC systems [32]. The authors analyzed the performance of ZF, ZF with successive interference cancellation (ZF-SIC), and Minimum Mean Squared Error (MMSE) equalizers. As expected, the best performance was obtained for the MMSE equalizer, which considers the channel matrix's noisy nature. Nonetheless, the covariance matrix must be known a priori or estimated before the compensation stage. In order to overcome this limitation, Gao et al. proposed using a convolutional autoencoder to denoise the channel matrix [33]. Nevertheless, this proposal was based only on simulation results and no experimental outcomes were provided.

3. Optical Camera Communication Link Model

Complementary Metal Oxide Semiconductor (CMOS) cameras usually employ Rolling Shutter (RS) scanning. This type of scanning is based on exposing the sensor to the incoming light on a row basis. The row shift time is normally grasped to perform a time-to-space conversion, capturing the light source variations along the sensor's scanning dimension. This effect is one of the most important aspects of OCC and has enabled a multitude of

communications techniques, such as Undersampled Frequency Shift On and Off Keying (UFSOOK), WDM and MIMO [31], CSK [34], and 2D-OFDM [35].

Generally, most cameras possess a Color Filter Array (CFA) that is usually located over the image sensor. This allows the camera to split signals from light sources depending on wavelengths. Figure 2 shows both Bayer and Foveon RGB filter pattern. Bayer mosaic contains 25%, 50%, and 25% of red, green, and blue regions, respectively, while Foveon mosaic presents 100% of the color. Consequently, Foveon abolishes the de-mosaicing process, and its spectral response is based on the light absorption behavior of silicon [36]. These characteristics have prompted the use of cameras to carry out WDM, CSK, and MIMO systems by using RGB LEDs as a light source. Nevertheless, as mentioned above, those filters present an overlap between their RGB channels, causing channel cross-talk. Thus, an approach to compensate this interference between channels is needed.

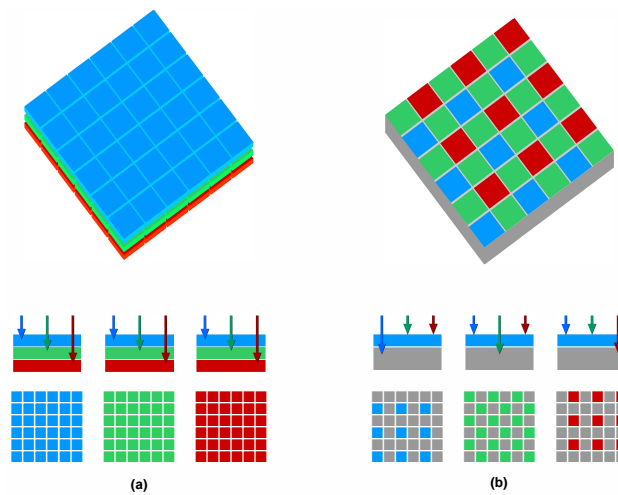


Figure 2. Filter patterns for the spectral information acquisition. (a) Foveon-based sensor. (b) Bayer filter sensor.

3.1. Link Budget

According to the typical formulation of an OWC link budget, the optical power impinging the main lens of a camera can be expressed as shown in Equation (1).

$$P_{rx} = P_{tx}R(\theta, \phi) \frac{A_{lens}}{d^2} \cos(\Psi) \tag{1}$$

where P_{rx} is the received power, P_{tx} is the optical source’s radiant power, $R(\theta, \phi)$ is the source’s radiation pattern at elevation θ and azimuth ϕ , A_{lens} is the main lens’ cross section, d is the link range, and Ψ is the impact angle. Furthermore, thanks to the use of image-forming optics, in a perfectly focused situation the received optical power would be divided among the projected size of the light source (Equation (2) [8]).

$$A_{proj} = \frac{N_x N_y}{FOV_x FOV_y} \frac{A_{tx}}{d^2} \tag{2}$$

A_{proj} is the projected size of the light source on the sensor (expressed in pixels); N_x and N_y define the sensor’s pixel resolution; FOV_x and FOV_y are the camera’s horizontal and vertical fields of view, respectively; and A_{tx} is the transmitter’s effective area (from the

receiver’s viewpoint). Joining Equations (1) and (2) it yields the received optical power at each pixel (Equation (3)).

$$P_{px} = P_{tx}R(\theta, \phi) \frac{A_{lens}}{A_{tx}} \frac{FOV_x FOV_y}{N_x N_y} A_{px} \cos(\Psi) \tag{3}$$

P_{px} is the pixel power (in watts) and A_{px} is the pixel area. This last equation is valid for scenarios in which A_{proj} is strictly greater than one pixel. Finally, the electron yield $S_{px}^{(i,j)}$ of the i -th emitter on the j -th sub-pixel (color) after the optoelectronic conversion takes into account the filter response $F_j(\lambda)$ (from the Bayer filter or the Foveon architecture); the emission spectrum $\tilde{S}^{(i)}(\lambda, T)$, which depends on wavelength (λ) and temperature (T); and silicon quantum efficiency, as Equation (4) describes.

$$S_{px}^{(i,j)} = P_{px} \int_{\lambda} \tilde{S}^{(i)}(\lambda, T) F_j(\lambda) \mathfrak{R}(\lambda) \frac{E_{ph}(\lambda)}{q} d\lambda \tag{4}$$

Silicon quantum efficiency is described by the responsivity curve of the material $\mathfrak{R}(\lambda)$, the photon energy $E_{ph}(\lambda)$, and the electron charge q . As it can be observed, the link budget depends on two separate phenomena. The link’s geometry defines the amount of energy that arrives at the main lens of the receiver, which is wavelength-independent at least in Line-Of-Sight (LOS) scenarios, which is the case under study. On the other hand, the emission spectrum, which is affected by the device’s p-n junction temperature, and the wavelength-dependent behavior of the receiver define the final electron yield.

3.2. Noise Sources

The most important noise sources in OCC are shot noise, Johnson noise, and Fixed-Pattern Noise (FPN). Shot noise has a quantum nature and is related to the fluctuations that occur during optoelectronic conversion. This kind of noise comprises photo-generated noise (N_{px}), whose variance linearly increases with the photo-generated current, readout noise (N_{ro}), and dark current noise (N_d). Readout noise occurs when the pixel value is delivered by the CMOS circuitry and does not depend on the input signal level. Although shot noise is Poisson distributed, it is usually approximated by a Gaussian assuming sufficient input power (high number of incident photons). Johnson noise (N_{th}) occurs due to the thermal agitation of the receiver’s molecules and is dominant under low-light conditions. Finally, FPN is related to the nonuniformity of the sensor’s pixel response, although it has a residual impact on communications systems. As it can be observed in Equation (5), all the noise contributions can be summed up into an overall noise variance σ_N^2 .

$$\sigma_N^2 = (N_d + N_{px}) \cdot T_{exp} + N_{ro}^2 + N_{th}^2 \tag{5}$$

N_{px} (photo-generated shot noise variance) is equal to $S_{px}^{(i,j)}$, according to the Poisson nature of shot noise. All the above terms are referred to Root Mean Square (RMS) electrons. Combining Equation (3) with Equation (5) and considering several interfering contributions (other channels), the Signal-to-Interference-plus-Noise Ratio (SINR) formula can be easily obtained (Equation (6)). $S_{px}^{(i,j)}$ defines the rate at which electrons are converted into the device (i -th emitter to j -th receiver). Therefore, the amount of electrons in a given time window (after a row scanning in the CMOS sensor) is obtained by integrating this rate during the camera’s exposure time T_{exp} .

$$SINR_j = \frac{\left(S_{px}^{(j,j)} T_{exp} \right)^2}{\left(N_d + \sum_{j=1}^n S_{px}^{(i,j)} \right) \cdot T_{exp} + N_{ro}^2 + N_{th}^2 + \sum_{j \neq i} \left(S_{px}^{(i,j)} T_{exp} \right)^2} \tag{6}$$

3.3. Emitted Spectrum versus Temperature

The photons emitted by an LED present a wavelength that is related to the energy gap of the semiconductor substrate. In addition, the energy gap is affected by the p-n junction temperature, which is usually modeled using Equation (7). According to the authors of [37], in most semiconductor materials, the energy gap diminishes as temperature increases. Therefore, as the wavelength is inversely proportional to this gap, the LED's peak wavelength increases with temperature.

$$E_g = E_0 - \frac{\alpha T^2}{T + \beta} \tag{7}$$

where T is temperature, E_0 is energy gap at 0 K temperature condition, and α and β are semiconductor-dependent constants, which are empirically determined.

Nonetheless, the LED substrate must be taken into consideration. In [12], the authors demonstrated that depending on the Indium (In) content in InGaN alloys (green and blue LEDs), the band gap may not decrease with temperature as many materials do, but can even increase with temperature. Furthermore, junction temperature affects both spectral width and luminous efficiency. In general, as temperature increases, the conversion efficiency decreases and the spectral width increases [13].

As has been already mentioned, temperature produces spectral changes on the LED emission. In this study, these variations would affect $S_{px}^{(i,j)}$ from Equation (4) as the terms $\tilde{S}^{(i)}(\lambda, T)$ are temperature-dependent. Consequently, the SINR will also be affected.

4. Channel Compensation in Optical Camera Communication

Channel compensation is usually a two-stage procedure. During the first stage, the CSI of the OCC channel is obtained in order to form the channel matrix. In this work, the CSI is derived from the contributions of each emitted spectrum to the three wavelength-divided receivers ($S_{px}^{(i,j)}$ terms). It has been assumed that the link establishment procedure includes a training sequence in which each emitter is turned on sequentially in a Time-Division-Multiple-Access (TDMA) scheme (as in [10]). The elements of this matrix, named \mathbf{H} hereinafter, respond to Equation (8).

$$h_{ij} = \begin{cases} K_{cam} (S_{px}^{(i,j)} T_{exp} + N) & \text{if } S_{px}^{(i,j)} T_{exp} + N < h_{max} \\ K_{cam}(h_{max}) & \text{otherwise} \end{cases} \tag{8}$$

where h_{ij} is the response of the camera's j -th receiver to the i -th emitter and K_{cam} is a function comprising the effects introduced by the camera's analog gain, the analog-to-digital conversion, and the nonlinear gamma correction. h_{max} is the full-well-capacity of the image sensor, measured in electrons. It must be noted that \mathbf{H} is subject to noise-induced errors, as the noise term N suggests (which presents the variance of Equation (5)). In addition, it has been assumed without loss of generality that the impulse response of the optical channel can be modeled as a Dirac's delta as the frequency response of the camera system is significantly smaller (bounded by T_{exp}) than the channel bandwidth of any OWC indoor scenario. Regarding the optical system's spatial response, it has been assumed that the light source presents uniform radiance.

Furthermore, the second stage of the compensation is based on calculating the inverse of the obtained matrix and multiplying it by the received vector (Equation (9)). This vector implicitly includes the current CSI $\hat{\mathbf{H}}$, and this multiplication aims to mitigate the inter-channel interference. In an ideally compensated scenario, the interference term of

Equation (6) (right term of the denominator) would vanish, but the shot noise contribution of each channel would remain.

$$v_{comp} = \overbrace{\mathbf{H}^{-1}}^{\mathbf{I}_H} \cdot \underbrace{\tilde{\mathbf{H}} \cdot \tilde{v}_{tx}}_{\tilde{v}_{rx}} \quad (9)$$

\tilde{v}_{tx} is the transmitted symbol, \tilde{v}_{rx} is the received symbol and v_{comp} is the CSI-compensated symbol. The performance of the channel compensation depends on several parameters, such as the condition number of \mathbf{H} [38] and the similarity between the latter and $\tilde{\mathbf{H}}$. If both matrices are identical, the compensation results in $\mathbf{I}_H = \mathbf{I}$, where \mathbf{I} is the identity matrix. Static links (or under slow movement regimes) are generally assumed to work in a stationary condition. Nonetheless, as will be demonstrated in the following sections, this assumption does not hold anymore if temperature effects are included in the model.

5. Methodology

The main objective of this paper is to evaluate the effect of compensating an RGB OCC channel by using obsolete CSI in terms of temperature. As was aforementioned, the emission spectrum of an LED is highly dependent on temperature, usually displacing the peak wavelength to lower energies, decreasing the coherence (spectrum broadening) and lowering the light source's efficiency. These effects cause significant variations between the CSI of an LED at ambient temperature with respect to the same LED at its stationary temperature. In a real OCC link in which the transmitter was subject to significant temperature variations due to the environment (e.g., extreme weather conditions or industrial environments), the channel compensation procedure would result in an SINR penalty due to the difference between the reference CSI and the instantaneous CSI.

5.1. Experimental Setup

The spectra of several LEDs (from a common cathode RGB LED) were measured at different driving currents (and hence different p-n junction temperatures) using a programmable current source and a spectrometer. The LED under test was mounted on an adapter for an integrating sphere's input, and it was directly connected to the current source. The temperature of the LED was estimated using a thermographic camera pointing to the LED's back, as it is the best position to estimate the p-n junction temperature. The LED device under test was driven at different DC currents in order to induce temperature variation due to the Joule effect. No heat sink was applied to the device to allow the thermography-based measurement and avoid heat loss in the p-n junction. The experimental setup is illustrated in Figure 3. All the devices were connected to the control PC through an Ethernet switch, except the spectrometer, which used USB. An automation script was developed in order to ease the characterization procedure.

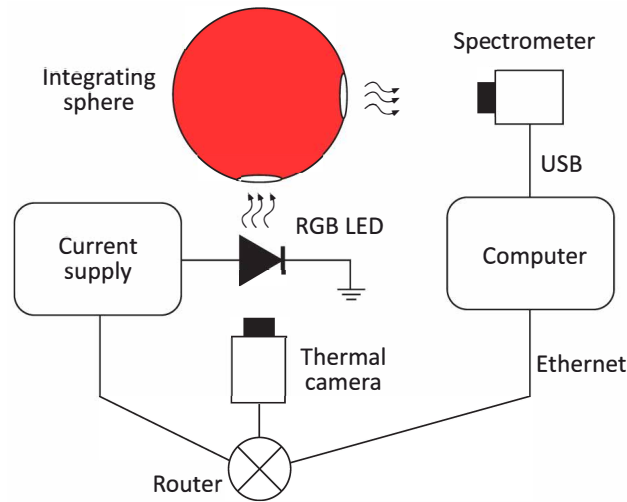


Figure 3. Diagram of the experimental setup.

5.2. Description of the Experiment

The experiment was designed as a two-stage procedure. During the first part, the spectra of the LED under test were acquired, while during the second part, these data were used to obtain different communications metrics for OCC. As was commented, a script was developed in order to automate the spectrum acquisition procedure. Figure 4 depicts the flow diagram of the whole experiment. The LED was driven from 10 mA to 150 mA in steps of 10 mA. Before starting the spectrum acquisition, a waiting time of 3 min was applied to ensure temperature stabilization in the p-n junction.

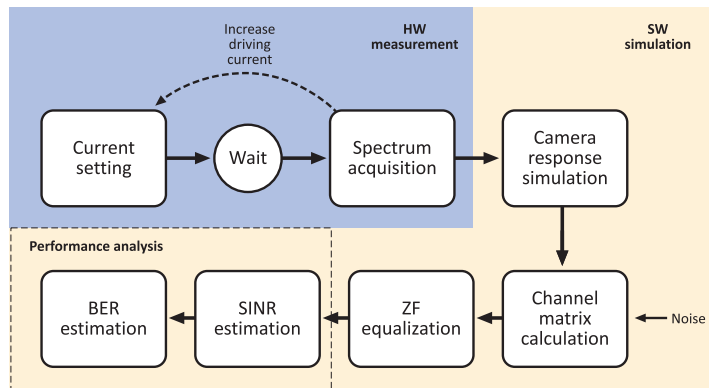


Figure 4. Flow diagram of the experimental procedure.

All the acquired spectra were energy-normalized to enable their use in the following estimation stages. This preprocessing step was needed because of the selected heating method based on the Joule effect. As temperature increased with the driving current, the total emitted power of the LED also increased. The response of a CMOS optical camera was estimated using the equations of Section 6 and the parameters of Table 1. Although the temperature effect of the CMOS image sensors is relevant and increases noise in cameras [39], it was not considered in this scheme because the cameras were assumed to be subject to normal temperature conditions. In addition, this experiment was focused on the temperature effect on the LED and not on evaluating thermal noise effects on the receiver side.

Table 1. Parameters of the experimental setup.

Parameter	Value
Current source	Yokogawa GS820
Spectrometer	Spectral Products SM442
Integrating sphere	Gigahertz ϕ 32 cm
Thermal camera	FLIR A640
CMOS sensors	Sony IMX249 and Foveon X3
RGB LED under test	Kingbright L-154A4SUREQBFZGEW
Temperature range	27 °C to 80 °C
Driving current	10 mA to 150 mA
Red peak wavelength	676 nm @ 10 mA
Green peak wavelength	563 nm @ 10 mA
Blue peak wavelength	460 nm @ 10 mA
Input SNR	30 dB, 20 dB, 10 dB
Spectrometer's integration time	25 ms

The channel matrices at different temperatures were formed by stacking the individual contributions of each LED on the three RGB bands plus the camera noise. Each row was then normalized respect to the matrix's diagonal term to avoid affecting the signal's energy during the compensation procedure. In this work, both Foveon and Bayer-based sensors were considered to compare the resulting performances. The effect of the input SNR level due to the noise signal introduced by the camera (Equation (5)) was also taken into account. This SNR level was estimated comparing the diagonal terms of the channel matrix respect to the corresponding noise power.

Finally, the impact of compensating the channel using ZF and obsolete CSI on the SINR was evaluated. The SINR resulting from the ZF compensation of two matrices at different temperatures was obtained (Equation (10)). The SINR of each wavelength band was calculated as the ratio between the target band's power respect to the addition of the interfering bands' powers (Equation (10)). This assumes that all considered LEDs emit the same power, which is not unrealistic as the light sources were driven by the same currents, presented approximately 1 mW/mA efficiency, and had the same radiation pattern. Taking into account the random nature of the input, this calculation was repeated 10,000 times to provide an average estimation.

$$SINR_i(\text{dB}) \approx 20 \log(\mathbf{I}_{H,ii}) - 10 \log\left(\sum_{j \neq i} \mathbf{I}_{H,jj}^2\right) \quad (10)$$

Using this metric, it could be possible to estimate BER of an OOK-based OOC link according to Equation (11), where $Q(\cdot)$ is the cumulative tail distribution of a standard normal (Q-function). This equation holds for both Global Shutter and Rolling Shutter schemes.

$$BER = Q\left(\sqrt{SINR}\right) \quad (11)$$

6. Results

Figure 5 depicts the measured spectra of the different RGB LEDs at various temperatures. It can be observed how the spectra change as the p-n junction temperature increases, causing peak-wavelength shifts, spectral broadening, and spectral shape distortions. It must be noted that the responses are normalized by the maximum value in order to ease the visualization of the aforementioned phenomena, so changes in LED efficiency caused by temperature are not appreciated.

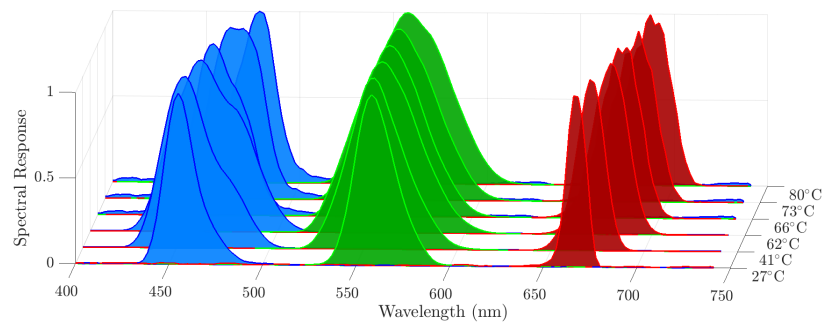


Figure 5. Emission spectra at different p-n junction temperatures.

In order to illustrate the potentially harmful effects of compensating the RGB channel with obsolete CSI, the SINR at different p-n junction temperatures was obtained using the CSI corresponding to 27 °C and 60 °C. Some exemplary thermographic images are presented in Figure 6, illustrating the p-n junction temperature estimation procedure.

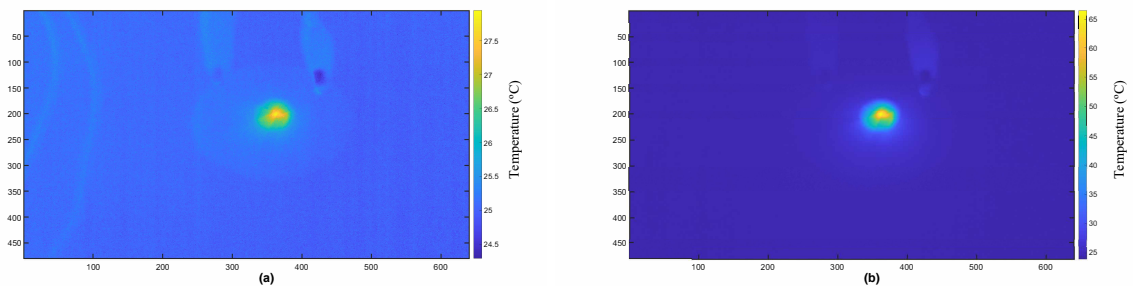


Figure 6. Examples of images of the blue light-emitting diode (LED) driven at different currents, taken by a thermographic camera. (a) LED at 10 mA and (b) LED at 100 mA. Both X and Y axes correspond to pixels.

The results section has been divided into three cases depending on the input SNR. High, medium, and low SNR values are associated with 30 dB, 20 dB, and 10 dB, respectively. This distinction has been carried out to analyze the input SNR's combined effect and the emitter's temperature variations on the system performance. Each subsection includes the effect of compensating the RGB OCC link using channel matrices at two different temperatures, as described above. Furthermore, this effect is evaluated on the two considered CMOS sensors, obtaining the SINR after the ZF compensation and, ultimately, the expected BER assuming an OOK transmission.

6.1. High SNR Case

Figures 7 and 8 show the SINR for an input SNR of 30 dB, which is labeled as high. For both IMX249 and X3 sensors, the penalty of compensating the channel with obsolete CSI affected the blue band reducing its SINR to unpractical values (below ~ 10 dB) regarding the reference temperature. The red and green bands were also affected, especially in the X3 device.

From Figure 9b, it can be noted a step step beginning approximately at 62 °C. Two reasons mainly caused this for the X3 sensor: first, the blue receiver's spectral response is noticeably wider in X3 than in IMX249 (Figure 1). Second, above 62 °C, the blue LED spectra are broadened (Figure 5). Therefore, the combination of both phenomena leads to greater interference and, consequently, to an abrupt decrease in the SINR from 62 °C. Moreover, in Figure 8a, the blue LED showed a band-pass characteristic because of the compensation at 60 °C. The SINR level is theoretically at its maximum when the CSI

employed for compensation corresponds to an LED at a temperature equal to the LED's stationary temperature regime. Thus, when the LED temperature of the CSIs deviates from the CSI reference temperature, the SINR decreases. The same effect can be seen in Figure 7, in which the maximum level is at 27 °C (the corresponding temperature of the CSI used to compensate).

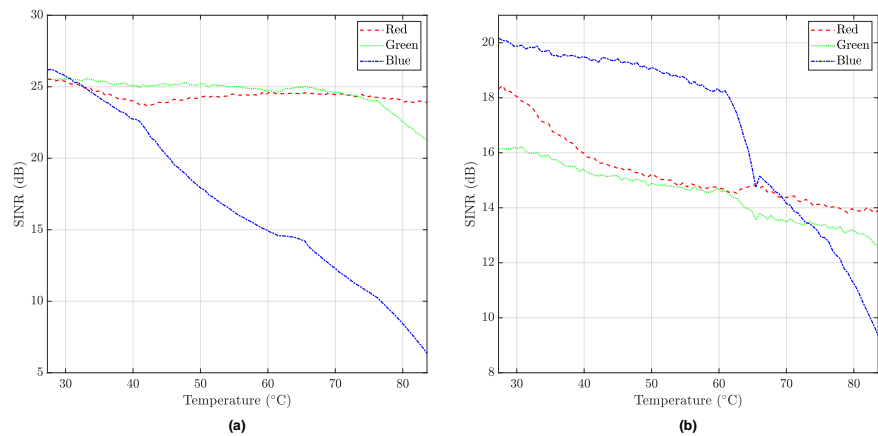


Figure 7. Signal-to-Interference-plus-Noise Ratio (SINR) at different temperatures, compensating the channel using the Channel State Information (CSI) corresponding to 27 °C and with a high SNR value (30 dB). (a) Sony IMX249 and (b) Foveon X3. Dashed line, dotted line, and dash-dot line correspond to red, green, and blue, respectively.

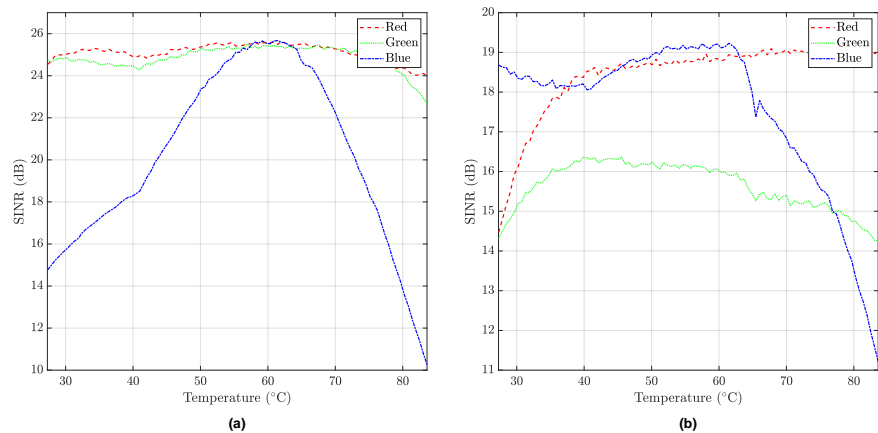


Figure 8. SINR at different temperatures, compensating the channel using the CSI corresponding to 60 °C and with a high SNR value (30 dB). (a) Sony IMX249 and (b) Foveon X3. Dashed line, dotted line, and dash-dot line correspond to red, green, and blue, respectively.

It can be observed from Figure 5 that as temperature increased, the blue spectrum was significantly red-shifted, intensifying its intersection with the green component of the Bayer and Foveon filters. Although the red and the green LED emission presented a similar behavior with respect to temperature increments, its contributions to the other components of the filters remained at low levels in the case of the IMX249. These effects were translated into a rapid decrease in the SINR at the blue wavelength, while both red and green components remained more stable. For the X3, due to the overlapping of its filters, red and green presented a higher decrease in SINR.

Figures 9 and 10 depict the BER performance. For a high input SNR, the BER was below the Forward Error Correction (FEC) limit [40] for most temperature differences. Although the BER increased with the temperature difference, there were values above this limit only while using the CSI corresponding to 27 °C to compensate CSIs corresponding to temperatures higher than roughly 80 °C. In Figures 9a and 10a, the BER performance of the red and green bands were well under 10^{-10} . As expected, the BER was worse in the blue band than in the red and green due to the spectra red-shifting and the RGB filters overlapping, as seen in the SINR cases. These results suggest that in those links that require high SNR levels to reach higher data rates, the temperature effect would be more significant and must be taken into consideration.

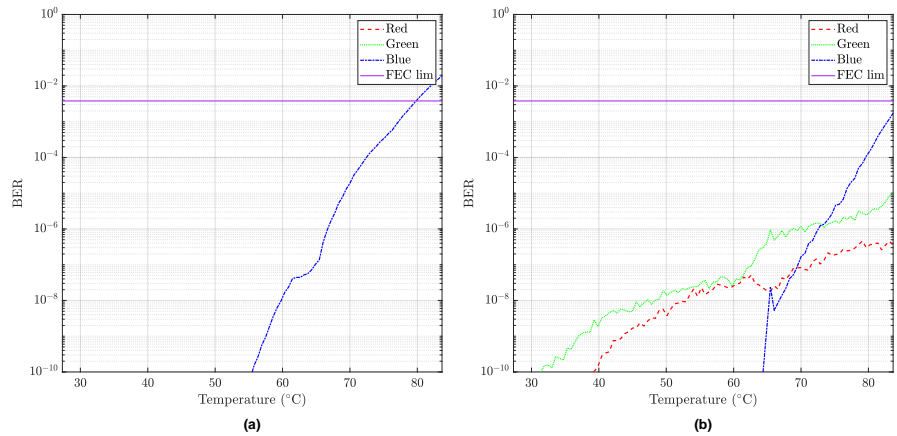


Figure 9. Bit error rate (BER) at different temperatures, compensating the channel using the CSI corresponding to 27 °C and with a high SNR value (30 dB). (a) Sony IMX249 and (b) Foveon X3. Dashed line, dotted line, and dash-dot line correspond to red, green, and blue, respectively.

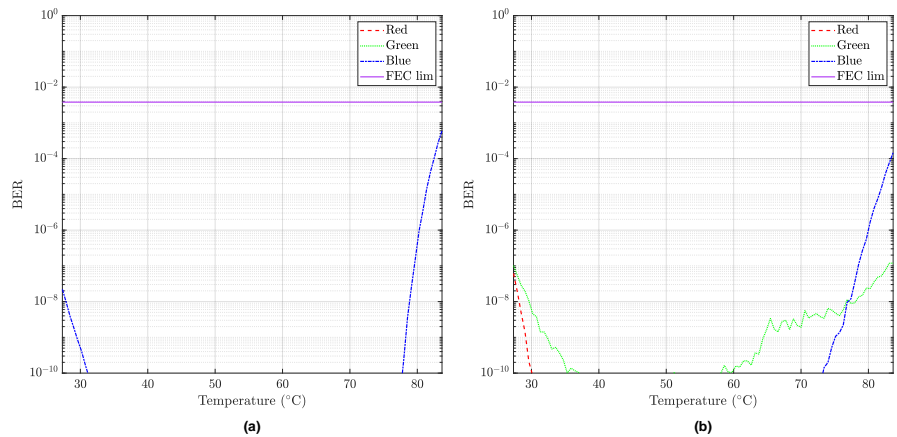


Figure 10. BER at different temperatures, compensating the channel using the CSI corresponding to 60 °C and with a high SNR value (30 dB). (a) Sony IMX249 and (b) Foveon X3. Dashed line, dotted line, and dash-dot line correspond to red, green, and blue, respectively.

6.2. Medium SNR Case

Figures 11 and 12 show the SINR for a SNR of 20 dB. In this case, the penalty was still evident in the blue band. However, in the X3 sensor, the higher noise level started hiding the temperature effect on its performance. In the X3, the red and green channels still

decreased in SINR when compensated with an obsolete CSI in temperature, although it was less noticeable in the IMX249.

Figures 13 and 14 depict the BER performance. In this case, most values were below the FEC limit in the IMX249, while in the X3, most values were above the limit. As in the last case, BER values were only above the limit using the CSI corresponding to 27 °C compensating CSIs corresponding to temperatures higher than roughly 80 °C in the Sony device. On the other hand, the BER was above the FEC limit using the CSI corresponding to 27 °C to compensate CSIs corresponding to temperatures higher than roughly 32 °C in the Foveon device. For those cases where the CSI was at a temperature near the operating LED, temperature was used as a reference for compensating, all the values were below the FEC limit using the Bayer-based sensor, while the vast majority of them were above $3.8 \cdot 10^{-3}$ using the Foveon sensor. Likewise, the blue band was again the most affected by temperature.

These results showed that Bayer-based sensors have an advantage over Foveon sensors, in which RGB spectral responses are considerably overlapped.

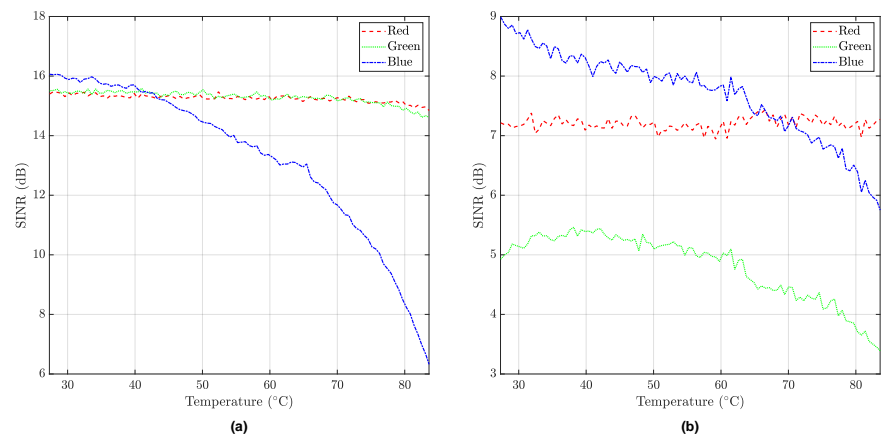


Figure 11. SINR at different temperatures, compensating the channel using the CSI corresponding to 27 °C and with a medium SNR value (20 dB). (a) Sony IMX249 and (b) Foveon X3. Dashed line, dotted line, and dash-dot line correspond to red, green, and blue, respectively.

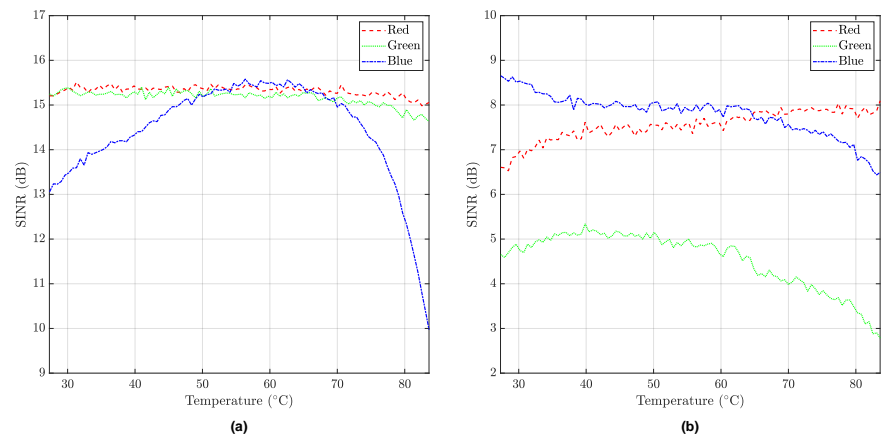


Figure 12. SINR at different temperatures, compensating the channel using the CSI corresponding to 60 °C and with a medium SNR value (20 dB). (a) Sony IMX249 and (b) Foveon X3. Dashed line, dotted line, and dash-dot line correspond to red, green, and blue, respectively.

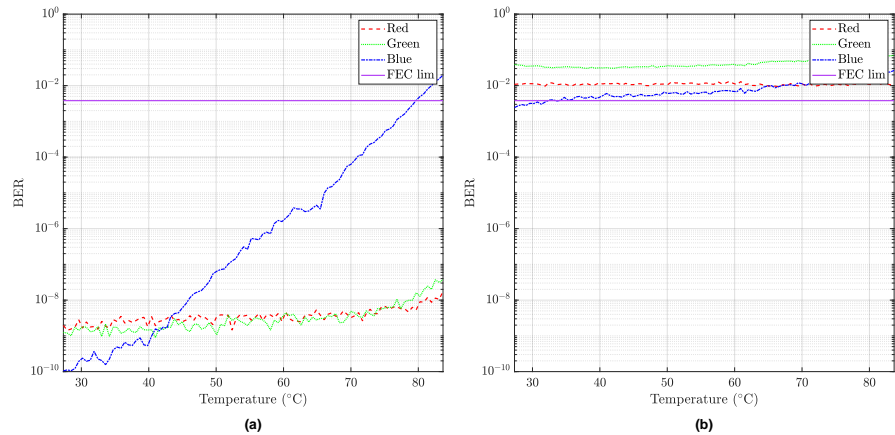


Figure 13. BER at different temperatures, compensating the channel using the CSI corresponding to 27 °C and with a medium SNR value (20 dB). (a) Sony IMX249 and (b) Foveon X3. Dashed line, dotted line, and dash-dot line correspond to red, green, and blue, respectively.

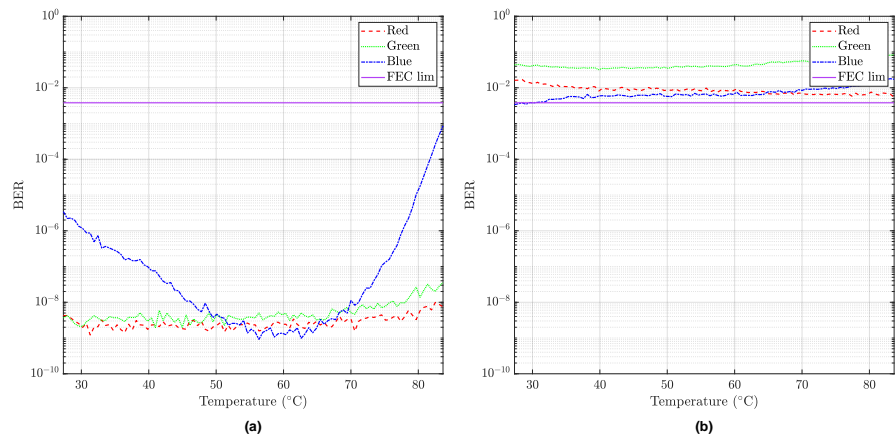


Figure 14. BER at different temperatures, compensating the channel using the CSI corresponding to 60 °C and with a medium SNR value (20 dB). (a) Sony IMX249 and (b) Foveon X3. Dashed line, dotted line, and dash-dot line correspond to red, green, and blue, respectively.

6.3. Low SNR Case

Figures 15 and 16 show the SINR for a SNR of 10 dB. As the noise level was high, the observed decrease in SINR in the other cases caused by compensating the channel with an obsolete CSI was not appreciated in the X3 sensor. In the IMX249, the temperature effect was still appreciable, but much less than in the previous cases. Therefore, considering the temperature effect is significant only at medium–high SNR levels.

Figures 17 and 18 depict the BER performance. Because of a low input SNR, the BER increased as the temperature increased. This effect was slightly appreciable in both devices. However, there were no BER values below the FEC limit in any case. This poor outcome occurred as a result of the ZF method, which highly penalized the BER performance in those cases when the noise level was considerably high.

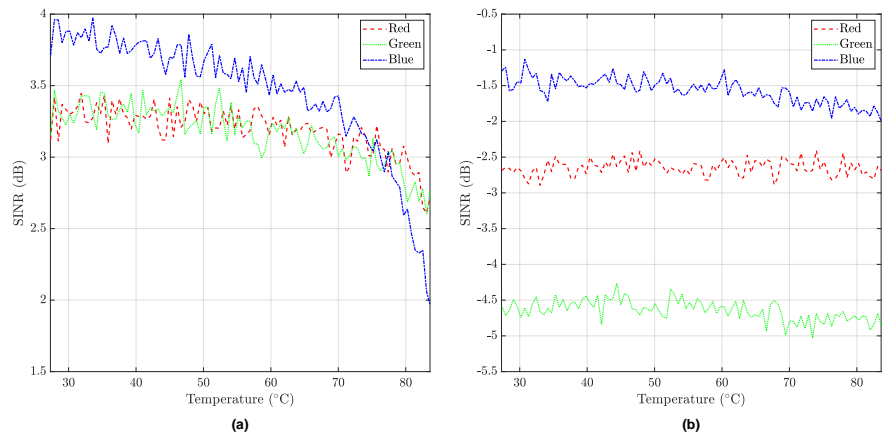


Figure 15. SINR at different temperatures, compensating the channel using the CSI corresponding to 27 °C and with a low SNR value (10 dB). (a) Sony IMX249 and (b) Foveon X3. Dashed line, dotted line, and dash-dot line correspond to red, green, and blue, respectively.

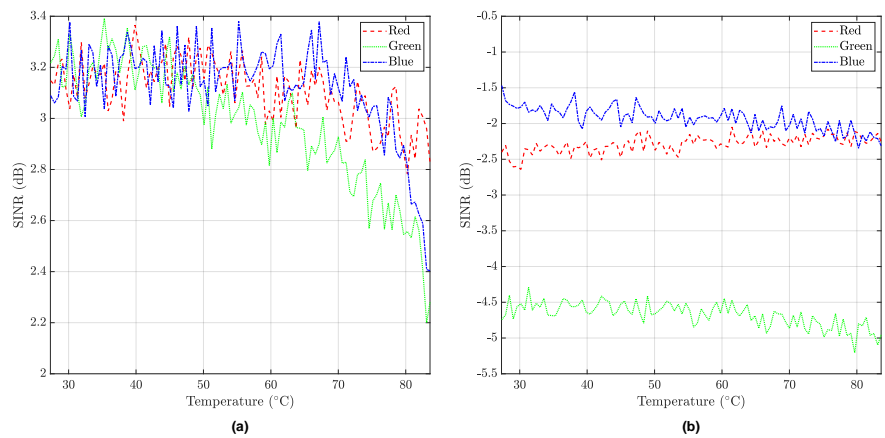


Figure 16. SINR at different temperatures, compensating the channel using the CSI corresponding to 60 °C and with a low SNR value (10 dB). (a) Sony IMX249 and (b) Foveon X3. Dashed line, dotted line, and dash-dot line correspond to red, green, and blue, respectively.

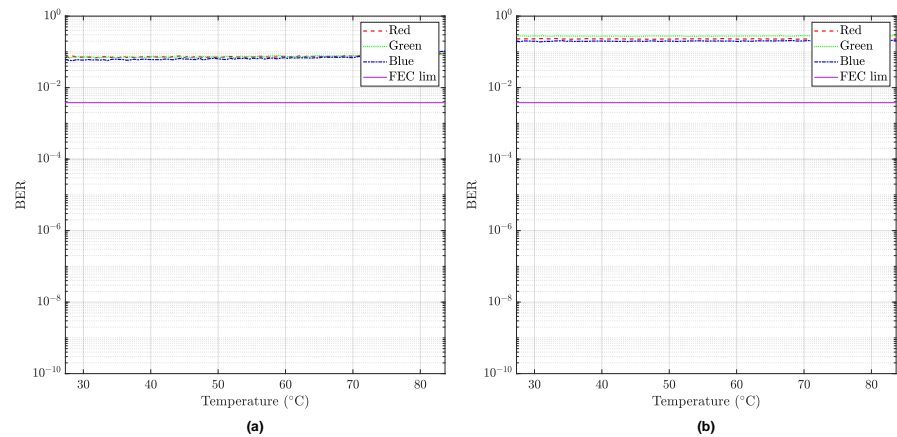


Figure 17. BER at different temperatures, compensating the channel using the CSI corresponding to 27 °C and with a low SNR value (10 dB). (a) Sony IMX249 and (b) Foveon X3. Dashed line, dotted line, and dash-dot line correspond to red, green, and blue, respectively.

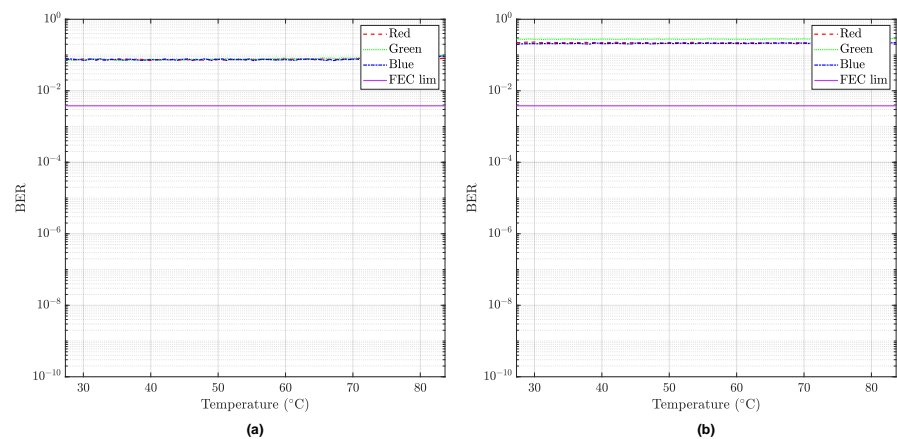


Figure 18. BER at different temperatures, compensating the channel using the CSI corresponding to 60 °C and with a low SNR value (10 dB). (a) Sony IMX249 and (b) Foveon X3. Dashed line, dotted line, and dash-dot line correspond to red, green, and blue, respectively.

7. Conclusions

The effects of temperature on light sources are well studied, showing a direct relationship between peak wavelength and spectral width concerning the p-n junction temperature. Nonetheless, these spectral variations are not usually considered when designing multi-wavelength links based on WDM or CSK, for instance. At least under reduced mobility conditions, these kinds of systems rely on the assumption that CSI does not change as the link geometry does not vary. Nevertheless, as has been demonstrated in this paper, CSI changes due to temperature effects.

The experimental part of this work was based on obtaining the emission spectra of an RGB LED at different temperatures. An experimental setup comprising a thermal camera for measuring the p-n junction temperature, an integrating sphere, and a spectrometer was implemented. The LED's stabilized p-n junction temperature was obtained after a settling period because the devices were under normal ambient conditions, and only the driving current affected the LED to produce significant changes in its temperature. However, in some scenarios where the light source would be exposed to high temperatures,

the operating LED temperature can change rapidly, causing undesired and unforeseen outcomes. No heat sink was employed in this experiment as the main objective was to analyze the temperature effect on the LEDs, and the use of such a device would have reduced the consequence caused by high temperature. The LEDs performance adding a heat sink to the test condition would improve since the LED spectral features would have been less affected.

In this work, the harmful effect of compensating an OCC RGB channel using obsolete CSI in terms of temperature has been explored. After a comprehensive characterization of the light sources at different measured p-n junction temperatures, the associated CSI were obtained by simulating the response of Commercial-Off-The-Shelf (COTS) CMOS cameras. The resulting SINR after the zero-forcing compensation was calculated. It was observed that as the temperature difference between the reference and current CSIs increased, the resulting SINR penalty was higher (lower SINR values). Specifically, the blue channel was profoundly affected, reaching unpractical SINR values below 10 dB. Red and green channels presented small sensitivity to temperature-induced spectral variations in the IMX249, while in the X3 the decrease in SINR was higher. The reason for this is that the blue spectrum was significantly red-shifted, intensifying its intersection with the green component of the Bayer and Foveon filters. The decrease in the blue signal is also caused by the lower response of the blue component in both filters due to the use of a silicon-based CMOS device. Although the red and green spectra were also distorted by temperature, the SINR was not impaired in those bands in the IMX249. However, the decrease mentioned above in SINR on red and green channels might be interpreted as a result of the overlapping between the RGB filters in the X3 sensor. On the other hand, it was clearly observed that the temperature effect was masked as the input SNR level decreased. Besides, the noise affected more the X3 sensor than IMX249 due to the greater overlapping of the first one's spectral responses (Figure 1). The cross-talk between components makes the Foveon X3's associated channel matrix less robust to noisy inputs than the Bayer-based image sensors, which are better conditioned.

Regarding the BER performance, first, it was observed that for high input SNR values, the BER was below $3.8 \cdot 10^{-3}$ (FEC limit) for the majority of temperature differences between the reference CSI employed for compensating and the current CSIs. As the BER increased with temperature difference, approaches that are more sensitive to SINR variations than OOK transmissions would be strongly affected by the thermal impact during the compensation procedure. Second, for a medium input SNR, the results reinforced the usefulness of a Bayer-based image sensor over a Foveon device. While the BER was below the FEC limit for almost all the temperature difference in the IMX249 sensor, most of the values were above the limit in the X3. Finally, for a low-input SNR, this poor performance was not unexpected. In fact, the ZF scheme inevitably penalizes the BER in these low SNR cases. As in the SINR analysis, the blue LED was the most thermal-affected device in the BER performance.

These results suggest that it would be recommended to not using blue LEDs when the transmitter is subject to high-temperature gradients that can cause variations in the emitted spectra. Nonetheless, those spectral changes on GaN and InGaN LED depend on the specific compositions and should be further characterized.

It must be remarked that these results are limited by the use of Bayer and Foveon filtering schemes (with severely overlapped sub-filters) and by the essayed devices. Nevertheless, the results obtained in this work demonstrate that temperature effects must be taken into account when designing multi-wavelength links.

To conclude, future research should consider the temperature effect during the channel compensation process. Besides, further work based on this topic needs to be performed to provide techniques that mitigate this effect, such as more robust compensation techniques than ZF equalization (e.g., using a minimum mean square error (MMSE) estimator) or temperature stabilization stages in the emitting system. Finally, a more comprehensive

study linking the temperature-induced spectral variations of the optical sources and the design of the filter arrays is needed to provide more insight about this topic.

Author Contributions: Conceptualization, J.R. (Julio Rufo); Formal analysis, J.R. (Julio Rufo) and V.G.; Funding acquisition, R.P.-J.; Investigation, D.M.; Methodology, D.M.; Resources, J.R. (Jose Rabadan); Software, V.G.; Supervision, J.R. (Jose Rabadan) and R.P.-J.; Writing—original draft, D.M. and V.G.; Writing—review and editing, J.R. (Julio Rufo), J.R. (Jose Rabadan), and R.P.-J. All authors have read and agreed to the published version of the manuscript.

Funding: This research was funded by the Spanish Research Administration (MICINN project: OSCAR, ref.: TEC 2017-84065-C3-1-R) and was made possible from the Trainee Predoctoral Research Staff Program (2019) of the Universidad de Las Palmas de Gran Canaria.

Conflicts of Interest: The authors declare no conflict of interest.

References

1. IEEE 802.15 Work Group. *IEEE Standard for Local and Metropolitan Area Networks—Part 15.7: Short-Range Optical Wireless Communications*; IEEE Std 802.15.7-2018 (Revision of IEEE Std 802.15.7-2011); IEEE: Piscataway, NJ, USA, 2019; pp. 1–407. [\[CrossRef\]](#)
2. Bani Hassan, N.; Ghassemlooy, Z.; Zvanovec, S.; Biagi, M.; Vegni, A.M.; Zhang, M.; Luo, P. Non-Line-of-Sight MIMO Space-Time Division Multiplexing Visible Light Optical Camera Communications. *J. Light. Technol.* **2019**, *37*, 2409–2417. [\[CrossRef\]](#)
3. Chavez-Burbano, P.; Guerra, V.; Rabadan, J.; Perez-Jimenez, R. Optical camera communication for smart cities. In Proceedings of the 2017 IEEE/CIC International Conference on Communications in China (ICCC Workshops), Qingdao, China, 22–24 October 2017; pp. 1–4.
4. Do, T.; Yoo, M. A Multi-Feature LED Bit Detection Algorithm in Vehicular Optical Camera Communication. *IEEE Access* **2019**, *7*, 95797–95811. [\[CrossRef\]](#)
5. Hasan, M.K.; Shahjalal, M.; Chowdhury, M.Z.; Jang, Y.M. Access Point Selection in Hybrid OCC/RF eHealth Architecture for Real-Time Remote Patient Monitoring. In Proceedings of the 2018 International Conference on Information and Communication Technology Convergence (ICTC), Jeju, Korea, 17–19 October 2018; pp. 716–719.
6. Liu, X.; Wei, X.; Guo, L. DIMLOC: Enabling High-Precision Visible Light Localization Under Dimmable LEDs in Smart Buildings. *IEEE Internet Things J.* **2019**, *6*, 3912–3924. [\[CrossRef\]](#)
7. Lin, X.; Zhang, L. Intelligent and Practical Deep Learning Aided Positioning Design for Visible Light Communication Receivers. *IEEE Commun. Lett.* **2020**, *24*, 577–580. [\[CrossRef\]](#)
8. Chavez-Burbano, P.; Guerra, V.; Rabadan, J.; Rodríguez-Esparragón, D.; Perez-Jimenez, R. Experimental Characterization of Close-Emitter Interference in an Optical Camera Communication System. *Sensors* **2017**, *17*, 1561. [\[CrossRef\]](#) [\[PubMed\]](#)
9. Liu, W.; Xu, Z. Some practical constraints and solutions for optical camera communication. *Philos. Trans. R. Soc. A Math. Phys. Eng. Sci.* **2020**, *378*. [\[CrossRef\]](#)
10. Jurado-Verdu, C.; Matus, V.; Rabadan, J.; Guerra, V.; Perez-Jimenez, R. Correlation-based receiver for optical camera communications. *Opt. Express* **2019**, *27*, 19150–19155. [\[CrossRef\]](#)
11. Jee, J.; Kwon, G.; Park, H. A Comparative Study on the Compensation Schemes for Transceiver I/Q Imbalances of Massive MIMO System. In Proceedings of the 2019 25th Asia-Pacific Conference on Communications (APCC), Ho Chi Minh City, Vietnam, 6–8 November 2019; pp. 292–296.
12. Zhao, C.; Zhang, R.; Liu, B.; Fu, D.; Chen, H.; Li, M.; Xie, Z.; Xiu, X.; Gu, S.; Zheng, Y. The temperature dependence of optical properties of InGaN alloys. *Sci. China Phys. Mech. Astron.* **2012**, *55*, 396–399. [\[CrossRef\]](#)
13. Park, J.; Lee, C.C. An electrical model with junction temperature for light-emitting diodes and the impact on conversion efficiency. *IEEE Electron Device Lett.* **2005**, *26*, 308–310. [\[CrossRef\]](#)
14. Chen, H.; Lin, D.; Tan, S.; Hui, S.Y. Chromatic, Photometric and Thermal Modeling of LED Systems With Nonidentical LED Devices. *IEEE Trans. Power Electron.* **2014**, *29*, 6636–6647. [\[CrossRef\]](#)
15. Almeida, P.S.; Bender, V.C.; Braga, H.A.C.; Dalla Costa, M.A.; Marchesan, T.B.; Alonso, J.M. Static and Dynamic Photoelectrothermal Modeling of LED Lamps Including Low-Frequency Current Ripple Effects. *IEEE Trans. Power Electron.* **2015**, *30*, 3841–3851. [\[CrossRef\]](#)
16. Shen, X.; Chen, H.; Lin, J.; Li, Y.; Lin, H.; Chen, J.; Chen, C. Analysis and Modeling of Optical and Thermal Properties of Phosphor Converted White Light Emitting Diode. *IEEE Access* **2019**, *7*, 118679–118689. [\[CrossRef\]](#)
17. Hui, S.Y.; Lee, A.T.L.; Tan, S. New Dynamic Photo-Electro-Thermal Modeling of Light-Emitting Diodes With Phosphor Coating as Light Converter Part I: Theory, Analysis, and Modeling. *IEEE J. Emerg. Sel. Top. Power Electron.* **2020**, *8*, 771–779. [\[CrossRef\]](#)
18. Raypah, M.E.; Devarajan, M.; Sulaiman, F. Influence of injection current and ambient temperature on intensity and wavelength of low-power SMD LED. In Proceedings of the 2016 IEEE 37th International Electronics Manufacturing Technology (IEMT) & 18th Electronics Materials and Packaging (EMAP) Conference, George Town, Malaysia, 20–22 September 2016; Institute of Electrical and Electronics Engineers Inc.: Piscataway, NJ, USA 2016. [\[CrossRef\]](#)

19. Muthu, S.; Schuurmans, F.J.; Pashley, M.D. Red, green, and blue LED based white light generation: Issues and control. In Proceedings of the Conference Record of the 2002 IEEE Industry Applications Conference. 37th IAS Annual Meeting (Cat. No.02CH37344), Pittsburgh, PA, USA, 13–18 October 2002; Volume 1, pp. 327–333. [\[CrossRef\]](#)
20. Spagnolo, G.S.; Papalillo, D.; Martocchia, A. LED Applications in Railway Signals: Wavelength and Intensity vs. Temperature Variation. *J. Transp. Technol.* **2012**, *2*, 78–83. [\[CrossRef\]](#)
21. Lu, B.; Wang, Y.; Hyun, B.R.; Kuo, H.C.; Liu, Z. Color Difference and Thermal Stability of Flexible Transparent InGaN/GaN Multiple Quantum Wells Mini-LED Arrays. *IEEE Electron Device Lett.* **2020**, *41*, 1040–1043. [\[CrossRef\]](#)
22. Lee, Z.Y.; Devarajan, M. Simultaneous study of thermal and optical characteristics of light-emitting diode. In Proceedings of the 2012 10th IEEE International Conference on Semiconductor Electronics (ICSE), Kuala Lumpur, Malaysia, 19–21 September 2012; pp. 115–118. [\[CrossRef\]](#)
23. Raypah, M.E.; Sodipo, B.K.; Devarajan, M.; Sulaiman, F. Estimation of Luminous Flux and Luminous Efficacy of Low-Power SMD LED as a Function of Injection Current and Ambient Temperature. *IEEE Trans. Electron Devices* **2016**, *63*, 2790–2795. [\[CrossRef\]](#)
24. Chen, J.; Wan, N.; Li, J.; He, Z.; Wu, Y. A comparative study of properties and microstructures on thermal fatigue testing of a high-power LED. In Proceedings of the 2016 17th International Conference on Electronic Packaging Technology (ICEPT), Wuhan, China, 16–19 August 2016; Institute of Electrical and Electronics Engineers Inc.: Piscataway, NJ, USA 2016; pp. 576–579. [\[CrossRef\]](#)
25. Azhar, A.H.; Tran, T.; O'Brien, D. A Gigabit/s Indoor Wireless Transmission Using MIMO-OFDM Visible-Light Communications. *IEEE Photonics Technol. Lett.* **2013**, *25*, 171–174. [\[CrossRef\]](#)
26. Zhong, W.; Chen, C.; Wu, D.; Ghassemlooy, Z. MIMO visible light communications system using imaging receiver with angle diversity detectors. In Proceedings of the 2016 15th International Conference on Optical Communications and Networks (ICOON), Hangzhou, China, 24–27 September 2016; pp. 1–3. [\[CrossRef\]](#)
27. Hong, Y.; Wu, T.; Chen, L. On the Performance of Adaptive MIMO-OFDM Indoor Visible Light Communications. *IEEE Photonics Technol. Lett.* **2016**, *28*, 907–910. [\[CrossRef\]](#)
28. Ramirez-Aguilera, A.M.; Luna-Rivera, J.M.; Perez-Jimenez, R.; Rabadan-Borges, J.; Guerra, V.; Suarez-Rodriguez, C. Visible Light Communication Constraints in Practical Indoor Lighting Systems. In Proceedings of the European Wireless 2016; 22th European Wireless Conference, Oulu, Finland, 18–20 May 2016; pp. 1–5.
29. Wei, L.; Zhang, H.; Song, J. Experimental Demonstration of a Cubic-Receiver-Based MIMO Visible Light Communication System. *IEEE Photonics J.* **2017**, *9*, 1–7. [\[CrossRef\]](#)
30. Akande, K.O.; Popoola, W.O. MIMO Techniques for Carrierless Amplitude and Phase Modulation in Visible Light Communication. *IEEE Commun. Lett.* **2018**, *22*, 974–977. [\[CrossRef\]](#)
31. Luo, P.; Zhang, M.; Ghassemlooy, Z.; Minh, H.L.; Tsai, H.M.; Tang, X.; Png, L.C.; Han, D. Experimental Demonstration of RGB LED-Based Optical Camera Communications. *IEEE Photonics J.* **2015**, *7*. [\[CrossRef\]](#)
32. Anusree, A.; Jeyachitra, R.K. Performance analysis of a MIMO VLC (Visible Light Communication) using different equalizers. In Proceedings of the 2016 International Conference on Wireless Communications, Signal Processing and Networking (WiSPNET), Chennai, India, 23–25 March, 2016; pp. 43–46. [\[CrossRef\]](#)
33. Gao, Z.; Wang, Y.; Liu, X.; Zhou, F.; Wong, K. FFDNet-Based Channel Estimation for Massive MIMO Visible Light Communication Systems. *IEEE Wirel. Commun. Lett.* **2020**, *9*, 340–343. [\[CrossRef\]](#)
34. Chen, H.W.; Wen, S.S.; Wang, X.L.; Liang, M.Z.; Li, M.Y.; Li, Q.C.; Liu, Y. Color-Shift Keying for Optical Camera Communication Using a Rolling Shutter Mode. *IEEE Photonics J.* **2019**, *11*. [\[CrossRef\]](#)
35. Nguyen, T.; Thieu, M.D.; Jang, Y.M. 2D-OFDM for Optical Camera Communication: Principle and Implementation. *IEEE Access* **2019**, *7*, 29405–29424. [\[CrossRef\]](#)
36. Rush, A.; Hubel, P. X3 Sensor Characteristics. *J. Soc. Photogr. Sci. Technol. Jpn.* **2003**, *66*, 57–60.
37. Varshni, Y.P. Temperature dependence of the energy gap in semiconductors. *Physica* **1967**, *34*, 149–154. [\[CrossRef\]](#)
38. Foschini, G.; Gans, M. On Limits of Wireless Communications in a Fading Environment when Using Multiple Antennas. *Wirel. Pers. Commun.* **1998**, *6*, 311–335. [\[CrossRef\]](#)
39. Lin, D.L.; Wang, C.C.; Wei, C.L. Quantified temperature effect in a CMOS image sensor. *IEEE Trans. Electron Devices* **2010**, *57*, 422–428. [\[CrossRef\]](#)
40. Leven, A.; Vacondio, F.; Schmalen, L.; ten Brink, S.; Idler, W. Estimation of Soft FEC Performance in Optical Transmission Experiments. *IEEE Photonics Technol. Lett.* **2011**, *23*, 1547–1549. [\[CrossRef\]](#)

5.2 Publication 2 (P2)

In the publication entitled “*Optical Multispectral Camera Communications Using LED Spectral Emission Variations*” [108], a pivotal step was taken by employing an MS camera as a receiver in an OCC system. This innovative configuration capitalizes on the thermally induced spectral variations of LEDs, constituting a direct stride towards the realization of Objective 1 (O1). The effects of temperature on LEDs, which are usually considered a detrimental factor, were used in this study to increase the number of communication channels using the same device. It was made possible by the MS camera that presents the appropriated spectral resolution to distinguish the subtle changes in the LED spectra.

First, an RGB LED was characterized by measuring the junction temperature, the emitted spectrum and each color’s spectral signature at different driving currents to induce the spectral variations by the Joule effect. A thermal camera, a spectrometer, and an MS camera were used for those measurements, respectively.

Second, different matrices (one for each LED color) were formed using the LED spectral response curves. Those matrices were mentioned in the paper as channel matrices. In turn, the condition number was calculated in order to have a metric for the channel separability of the LEDs at different temperatures. It provides a metric in such a way that the closer to one, the more separable the channels available for independent data transmissions.

Lastly, an OOK transmission was simulated to analyze the system performance. It consisted of generating a transmitted signal (a bit stream after being affected by the channel matrix) to which noise was added. Then, a ZF equalizer was used to estimate the transmitted bit stream, applying a Moore-Penrose pseudoinverse of the channel matrix. Once the transmitted bit stream was estimated, it was compared to the sent bit stream to calculate the BER.

The use of a high-spectral-resolution camera in an OCC link in order to capture the changes induced by variation in the LED’s p-n junction temperature highlights among the contribution of this work. Moreover, the condition number provided an indication to quantify the separability between distinct spectral signatures and predict the success of the system performance. Thus, well-conditioned matrices got more satisfactory results than ill-conditioned ones. Another notable result emerging from this work is the new channels attained from the same physical device due to the changes induced by temperature and captured by the MS camera.

Optical Multispectral Camera Communications Using LED Spectral Emission Variations

Daniel Moreno¹, Julio Rufo¹, Victor Guerra¹, Jose Rabadan, and Rafael Perez-Jimenez

Abstract—This work proposes using the changes in the LEDs' spectral emission induced by temperature variations to implement emitters for new communication channels in Optical Camera Communication (OCC) systems. If a camera can discriminate the shift in LEDs' spectral response, these modifications can be contemplated as a new data channel. The main advantage is that new channels can be obtained from the same physical optical emitter device, only temperature changes are needed. Thus, in this work, the use of multispectral or hyperspectral cameras as OCC receivers is proposed to increase the number of available communication channels, taking advantage of the high spectral resolutions of the camera devices.

Index Terms—OCC, multispectral, hyperspectral, LED, temperature dependence, peak wavelength.

I. INTRODUCTION

OPTICAL Camera Communication (OCC) has gained momentum in the last few years. The ubiquity of embedded optical cameras into consumer electronic devices such as Smart Phones, Tablets or laptops is expected to facilitate the mass adoption of this technology in the near future. In this sense, it is worth highlighting that this technology has been included in the revision of the IEEE 802.15.7 standard on Visible Light Communications [1], occupying a significant part of the document. Most recent OCC CMOS-based sensors allow high-speed communication due to the rolling shutter scanning mode; however, since OCC is based on image-forming optics, the maximum achievable speed depends on the light source's projected size [2].

On the other hand, multispectral cameras (and hyperspectral cameras) have been intensively used in several sectors such as agriculture [3], failure inspection in industry [4], and biotechnology [5]. Multispectral and hyperspectral cameras provide a higher number of communication bands, much more numerous than the three RGB channels available in conventional cameras. In this way, Optical Multispectral Camera

Manuscript received March 29, 2021; revised May 3, 2021; accepted May 6, 2021. Date of publication May 10, 2021; date of current version May 14, 2021. This work was supported in part by the Trainee Predoctoral Research Staff Program (2019) of the Universidad de Las Palmas de Gran Canaria, in part by the Canary Islands Regional Government under Project ATICCuA ProID2017010053, and in part by the Spanish Research Administration through the Ministerio de Ciencia e Innovación (MICINN) Project: Arquitecturas Ópticas Híbridas Para Ciudades Inteligentes (OSCAR) under Grant TEC 2017-84065-C3-1-R. (Corresponding author: Daniel Moreno.)

The authors are with the Institute for Technological Development and Innovation in Communications, Universidad de las Palmas de Gran Canaria, 35017 Las Palmas de Gran Canaria, Spain (e-mail: dmoreno@idetec.eu).

Color versions of one or more figures in this letter are available at <https://doi.org/10.1109/LPT.2021.3078842>.

Digital Object Identifier 10.1109/LPT.2021.3078842

Communication (OMCC) opens up a range of possibilities in this area. Nevertheless, in order to carry out Wavelength Division Multiplexing (WDM), several devices presenting different peak wavelengths are usually needed. This leads to a channel-crosstalk compensation problem similar to the channel matrix estimation and inversion problem of Multiple Input Multiple Output (MIMO) systems.

Moreover, LED devices are affected by temperature. The most important effects are a variation on the emitted spectrum and a reduction of the luminous efficiency. The LED spectral changes induced by temperature variations are analyzed as a potentially positive phenomenon in this work. Taking advantage of the spectral richness of LED emissions and the significant number of bands that a multispectral (or hyperspectral) camera may present, several separable communication channels can be established using the same kind of device, reducing the system's complexity and cost.

In this letter, Section II presents the theoretical framework that supports the work. Sections III and IV present both the characterization methodology and results regarding the effects of temperature on the used LED devices. Furthermore, the application of this characterization is presented in Section V using a CMOS-based multispectral camera. Finally, several conclusions are extracted in Section VI.

II. EFFECT OF TEMPERATURE ON LED

The photons emitted by an LED present a wavelength that is related to the energy gap of the semiconductor substrate. In addition, the energy gap is affected by the p-n junction temperature, which is usually modeled using Equation 1. According to [6], in most semiconductor materials the energy gap diminishes as temperature increases. Therefore, as wavelength is inversely proportional to this gap, the peak wavelength of the LED increases with temperature.

$$E_g = E_0 - \frac{\alpha T^2}{T + \beta} \quad (1)$$

where T is temperature, E_0 is energy gap at 0 K temperature condition, and α and β are semiconductor-dependent constants, which are empirically determined.

Nonetheless, the metallic content in the LED material must be taken into consideration. In [7], the authors demonstrated that depending on the Indium (In) content in InGaN alloys (green and blue LEDs), the band gap may increase with temperature.

Furthermore, in general, the conversion efficiency decreases and the spectral width grows as temperature increases [8]. In this work, these generally undesired changes on the LED emission are grasped to improve communications by increasing the number of communication channels. Although these spectral variations may be subtle, the use of high spectral resolution cameras (such as multispectral cameras) is proposed as suitable and commercially-available receivers.

III. METHODOLOGY

The main objective of this letter is to take advantage of the spectral changes of the LED caused when its temperature increases, in the sense that the wavelength variation could be captured by a multispectral camera and then find an OCC application. This goal is achieved by carrying out the characterization of some LEDs to determine how the temperature affects their spectrum. In addition, those LEDs have been used in combination with a multispectral camera to form a communication link. Finally, some performance metrics regarding channel separability have been obtained to assess the feasibility of Optical Multispectral Camera Communications (OMCC), taking advantage of temperature-induced variations on the LEDs.

In order to induce different junction temperatures, the LEDs (common cathode RGB LED) were driven using currents ranging from 10 mA to 130 mA. For each current, the junction temperature, the emitted spectrum, and the multispectral signature were obtained. Due to temperature diffusion effects, the system was stabilized for 5 minutes before acquiring the measurements mentioned above, in spite of the fact that the LEDs under test reached their thermally stable state after about 3 minutes. The devices were under ambient conditions, no external sources were employed to increase the LED's temperature and they were not externally thermally stabilized. Just their driving current was used to induce thermal variations owing to the Joule effect.

The experiments were carried out using the setups depicted in Figs. 1a and 1b. The devices under test were driven using an Ethernet-controlled current source (Yokogawa GS820). The LED junction temperature was measured using a thermographic camera (FLIR A645), while the emission spectra were obtained using a spectrometer (Spectral Products SM442). In order to complement this spectral measurement, the radiant power of each LED at the different tested currents was measured using an integrating sphere and an LED tester (Gigahertz BTS256).

Once the LEDs were characterized, a multispectral camera (SILIOS Technologies CMS-C1-C-EVR1M-GigE) was used to capture the wavelength variation. This 9-bands camera (8 color narrow bands and 1 panchromatic band) covers the wavelength range from 400 to 1000 nm. Those bands are the result of eight band-pass filters (narrow bands) and a filter sensitive to the entire wavelength range (panchromatic band). It has a CMOS sensor and a resolution of 1280 (H) \times 1024 (V) in the raw picture and 426 (H) \times 339 (V) for multispectral images. Furthermore, it was ensured that the images were not saturated, and the spectral signatures at several temperatures were extracted from them.

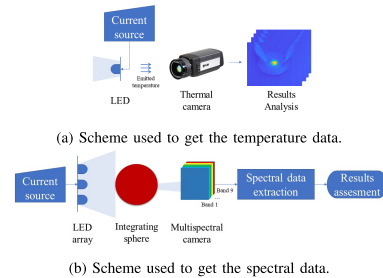


Fig. 1. System setup schemes.

Since the main objective of this work is to demonstrate the feasibility of grasping the spectral variation of LEDs with temperature, the channel separability of a combined emission using an arbitrary number of devices was evaluated using the condition number (Equation 2). This number is an algebraic metric that shows how small variations on a matrix may produce great variations on its inverse. In other words, this metric provides an indication as to whether several emissions can be separated as different channels. Well-conditioned matrices present condition numbers close to one, while ill-conditioned ones have high-value metrics.

$$\text{cond}(S) = \|S\| \cdot \|S^{-1}\| \quad (2)$$

S is the matrix comprising the spectral signatures. The spectral responses are added to the matrix S so that it has one signature per column. Thus, the matrix dimension is $sb \times sr$, where sb is the number of spectral bands (in this case, 9) and sr is the number of signatures appended. This strategy has been proposed in VLC MIMO systems [9], and also in traditional RF MIMO works as a suitable mathematical tool. Additionally, condition number penalizes the signal-to-noise ratio (SNR) depending on the required spectral efficiency [10].

After obtaining the spectral signatures and the corresponding S matrix, the OCC system performance was simulated assuming an On-Off Keying (OOK) transmission. This simulation involved a transmission signal composed of a bit stream b (generated as a uniformly distributed pseudo-random sequence) and a normally distributed noise signal n , whose level depends on the selected SNR and the reference power (estimated from the relative maximum power inside S). Then, a reception process based on a zero-forcing (ZF) equalization (Equation 3) is applied to the transmitted signal for obtaining the received bit stream \hat{b} . Finally, the system's BER performance is evaluated for the considered SNR values (from 10 dB to 40 dB). Sequences of 10^6 bits per simulation were used, limiting the maximum accuracy to 10^{-6} , and matrices S with all the 2-channel combinations were assessed in order to analyze channel separability.

No different channel models have been considered in the simulation because the targeted-effect of temperature variations in a Tx-Rx link would not be affected by them.

$$\hat{b} = (b \cdot S + n) \cdot S^+ \quad (3)$$

where S^+ is the Moore-Penrose pseudoinverse of channel matrix S .

TABLE I
SPECTRAL INFORMATION AT DIFFERENT TEMPERATURES

LED	Red			
Current (mA)	10 (27 °C)	50 (38 °C)	100 (56 °C)	130 (65 °C)
Peak wavelength (nm)	659.6	663.6	672.5	680.7
FWHM (nm)	8.73	14.97	22.33	24.15
Peak spectral radiant power (μW/nm)	2.75	10.53	12.33	8.29

LED	Green			
Current (mA)	10 (27 °C)	50 (42 °C)	100 (65 °C)	130 (76 °C)
Peak wavelength (nm)	547.2	544.9	545.1	546.8
FWHM (nm)	23.73	31.80	40.92	43.18
Peak spectral radiant power (μW/nm)	6.76	16.57	18.75	15.94

LED	Blue			
Current (mA)	10 (28 °C)	50 (43 °C)	100 (66 °C)	130 (78 °C)
Peak wavelength (nm)	486.1	486.1	490.5	499.6
FWHM (nm)	16.68	29.62	45.85	32.10
Peak spectral radiant power (μW/nm)	11.32	24.65	26.23	25.91

IV. CHARACTERIZATION RESULTS

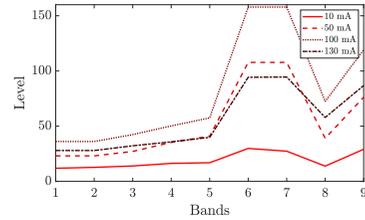
Table I summarizes the temperature-induced effects on the LED emission. The peak wavelength, the Full Width at Half Maximum (FWHM) and the peak spectral radiant power values of each spectrum are shown. It can be observed that, in most cases, the emitted peak wavelength grew (the energy band gap decreases) as the junction temperature increased. The largest shift was obtained for the red LED with a difference of 21.1 nm for a temperature span of 38 °C. The blue LED presented a 13.5 nm shift for a temperature variation of 50 °C. Finally, the measurements on the green LED showed that the peak wavelength slightly decreased with temperature. In this case, the highest peak wavelength was found at the minimum temperature. This behavior differs from the other colors' because of the metallic content in the green LED, as discussed in Section II.

Furthermore, it must be noted that the spectral width changed with temperature. The most remarkable variation was obtained in blue, in which the dissimilarity between the width at 28 °C and 66 °C was approximately 30 nm (Table I).

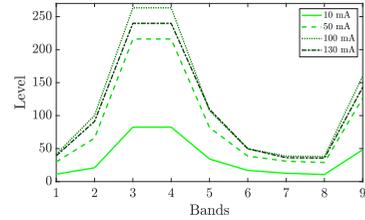
Finally, concerning the spectral radiant power, the highest levels were obtained for the blue LED, followed by green and red. Note that this measurement did not take into account the electrical power, which would have shown that the red LED presents the highest quantum efficiency. Moreover, it can be noted that at the maximum temperature (driving current 130 mA), the power decreases with respect to the second maximum. Therefore, temperature affected the LED efficiency as expected.

V. MULTISPECTRAL CAMERA RESULTS

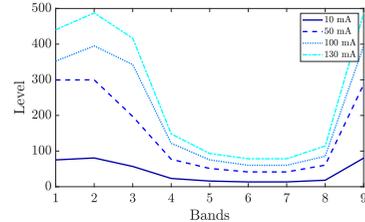
From the pictures taken by the camera, it can be seen how the wavelength changed when the temperature of the LED was modified. This effect is observed in the spectral signature of the LEDs (Fig. 2). As an example, Fig. 2c depicts the energy captured by each band of the multispectral camera for the blue LED. Focusing on bands 1, 2 and 3 (centered in 427, 461 and 501 nm, respectively), the wavelength shift can be slightly noticed. In the first place, as temperature increased, part of the emission captured in band 1 was displaced to band 2, which caused growth on its level. While the blue LED was at 10 mA and 50 mA, the level of bands 1 and 2 barely varied, keeping their levels near 75 and 300, respectively. However, when this LED was at 100 mA and 130 mA, the level from band 1 to



(a) Red LED.



(b) Green LED.



(c) Blue LED.

Fig. 2. Spectral signatures of the RGB LED at different temperatures. Solid line, dashed line, dotted line and dash-dot line correspond to 10 mA, 50 mA, 100 mA and 130 mA, respectively.

TABLE II
CONDITION NUMBER OF THE MATRICES OF SPECTRAL SIGNATURES

# channels	Best combination (current supplied in mA)			Condition number (dB)		
	R	G	B	R	G	B
2	50, 130	50, 130	50, 100	21.9	29.9	24.5
3	10, 50, 130	10, 100, 130	50, 100, 130	28.9	36.2	45.4
4	10, 50, 100, 130	10, 50, 100, 130	10, 50, 100, 130	47.9	52.3	50.7

band 2 increased roughly 100 times (see the slope from band 1 to band 2 in Fig. 2c). The same occurred with bands 2 and 3. This happened noticeably not only due to the red-shifting of the peak wavelength but also to the increment of the FWHM. Apart from the wavelength variation, an evident increment on these bands' level was observed since the temperature was modified by varying the driving current. Besides, the band 9 (panchromatic) increased with current as well, since this band capture data from the entire visible spectrum, being more sensitive in the blue wavelengths. Thus, it can be understood as a power averaging due to the almost flat response of its filter. Similar effects are noted in the spectral signatures of the other tested devices (Figs. 2a and 2b).

The condition number was applied to the matrix of spectral signatures (channel matrix) to mathematically prove that a combined emission of identical devices subject to different temperatures can form separable channels. With the information obtained during the characterization mentioned above, all the available combinations of channel matrices were analyzed.

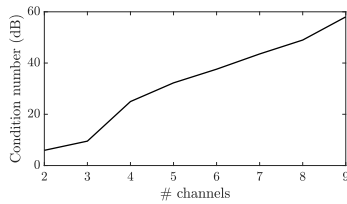


Fig. 3. Minimum condition number obtained for each combination of RGB colors depending on the channels added.

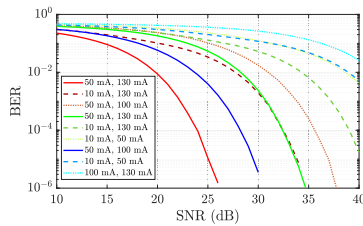


Fig. 4. BER performance of each RGB LED combining two spectral responses at different temperatures. The line color represent the LED color (red, green and blue) and the current values presented in the box are the LEDs driving current for the channel matrix generation. Solid line, dotted line and dashed line correspond to best, worst and average condition number cases, respectively.

Table II highlights the best results depending on the number of target-independent channels. It was observed that the more signatures are added, the more the condition number increases. A striking result that emerged from these data is that the lowest condition numbers were obtained for the red LED. On the other hand, the green LED presented the worst condition number combining four channels. Finally, the blue LED's condition number had a steep growth from two to three channels. This result was obtained for the matrix that included the LED responses at 50 mA and 100 mA, even though the largest wavelength variation was obtained between 10 mA (and 50 mA) and 130 mA. These values were obtained only by combining spectral signatures of a single color at different temperatures.

Moreover, the best combination of channels in terms of condition number (using the three RGB devices) can be observed in Fig. 3, ranging from 2 to 9 channels (theoretical maximum). As was expected, lower condition numbers were obtained when a combination of different colors was possible, i.e., for 2 and 3 channels. Not surprisingly, as the number of channels increases, so does the condition number. These results offer compelling evidence about the feasibility of providing additional communication channels from a single type of device.

Lastly, the BER performance results are compared in Fig. 4. They correspond to several examples of each RGB color while combining two channels at different currents. These examples show the best, the worst and the average cases regarding the condition number of the matrix S . As can be seen, the best results were expectedly obtained for those well-conditioned matrices (21.9 dB, 29.9 dB and 24.5 dB for red, green and

blue, respectively). On the contrary, in the ill-conditioned matrices (47.9 dB, 52.3 dB and 50.7 dB for red, green and blue, respectively), the added noise significantly affected their BER performance, even at high SNR levels.

VI. CONCLUSION

In this work, the effect of the junction temperature on an LED's emitted spectrum has been experimentally characterized. Furthermore, the spectral variation has been recorded using a multispectral camera. The measurements showed a significant difference between the spectral signature of each LED at different temperatures.

The main objective of this letter was to demonstrate that the aforementioned differences could be used to establish independent communication channels in an OMCC application. In order to assess this, the condition number of the resulting channel matrix was evaluated. It was observed that it is feasible to multiplex several data channels using the same kind of device driven at different average currents (and hence, different temperatures). Additionally, a simulation was developed assuming an OOK transmission to evaluate the OCC system performance. From the BER curves, it could be noted that the better conditioned were the channel matrices, the better the BER performance.

Traditionally, the number of available independent channels using RGB emitters has been assumed to be three (generally, one per device). Nonetheless, this work has demonstrated that using the combination of wavelength-shifted emitters, grasping temperature effects, this limitation that usually damages the transmitted signal can be exceeded, allowing reach up to the number of the receiver's available bands.

REFERENCES

- [1] *Short-Range Optical Wireless Communications (802.15.7-2018)*, Standard 802.15.7-2011, Apr. 2019.
- [2] C. Jurado-Verdu, V. Matus, J. Rabadan, V. Guerra, and R. Perez-Jimenez, "Correlation-based receiver for optical camera communications," *Opt. Exp.*, vol. 27, no. 14, pp. 19150–19155, Jul. 2019. [Online]. Available: <https://www.opticsexpress.org/abstract.cfm?URI=oe-27-14-19150>
- [3] H. Liu, S.-H. Lee, and J. S. Chahl, "A multispectral 3-D vision system for invertebrate detection on crops," *IEEE Sensors J.*, vol. 17, no. 22, pp. 7502–7515, Nov. 2017.
- [4] M. Rosenberger, "Multispectral edge detection algorithms for industrial inspection tasks," in *Proc. IEEE Int. Conf. Imag. Syst. Techn. (IST)*, Oct. 2014, pp. 232–236.
- [5] F. Meriaudeau, V. Paquit, N. Walter, J. Price, and K. Tobin, "3D and multispectral imaging for subcutaneous veins detection," in *Proc. 16th IEEE Int. Conf. Image Process. (ICIP)*, Nov. 2009, pp. 2857–2860.
- [6] Y. P. Varshni, "Temperature dependence of the energy gap in semiconductors," *Physica*, vol. 34, no. 1, pp. 149–154, Jan. 1967.
- [7] C. Zhao *et al.*, "The temperature dependence of optical properties of InGaN alloys," *Sci. China Phys., Mech. Astron.*, vol. 55, no. 3, pp. 396–399, Mar. 2012.
- [8] J. Park and C. C. Lee, "An electrical model with junction temperature for light-emitting diodes and the impact on conversion efficiency," *IEEE Electron Device Lett.*, vol. 26, no. 5, pp. 308–310, May 2005.
- [9] T.-A. Tran and D. C. O'Brien, "Performance metrics for multi-input multi-output (MIMO) visible light communications," in *Proc. Int. Workshop Opt. Wireless Commun. (IWOW)*, Oct. 2012, pp. 1–3.
- [10] G. J. Foschini and M. J. Gans, "On limits of wireless communications in a fading environment when using multiple antennas," *Wireless Pers. Commun.*, vol. 6, no. 3, pp. 311–335, Mar. 1998.

5.3 Publication 3 (P3)

The last publication in the compendium, entitled “*Clustering-based data detection for spectral signature multiplexing in multispectral camera communication*” [109], presented a cluster-based data detection approach to enhance the performance of an OCC system. As an extension work of [108], the MS camera and the effect of temperature on LEDs were leveraged. Thus, it experimentally examined the results using a linear method versus the clustering technique, thereby engaging with the pursuit of Objectives O1 and O2.

In this article, three pairs of LEDs of different colors (RGB) were employed (two red, two green, and two blue LEDs), in which their p-n junction temperature was altered by the Joule effect to attain distinct spectral signatures that the MS camera captured afterward. Then, a clustering model was generated using a BIRCH algorithm. Thus, once the clusters of the received signal were assigned to a corresponding symbol, the two LED signals were recovered. Subsequently, the BER performance of each signal was estimated.

On the other hand, a comparison of the cluster analysis with traditional linear methods was performed. In this case, ZF and MMSE equalizers were used to compensate the channel matrix composed of the spectral signatures of each LED and achieve the separate LED signals. Finally, the BER performance obtained from the two procedures was compared.

The BER enhancement achieved with cluster analysis with respect to linear methods was the most remarkable contribution. Moreover, a novel approach was proposed exploring the possibility of adopting a spectral signature multiplexing based on temperature. It is an innovative method as an alternative to WDM. Consequently, in this study, this new proposal’s performance was assessed by using the characteristics of multispectral cameras that allow discriminating the spectral responses of LEDs at different temperatures. Besides, it was demonstrated that a satisfactory transmission using this procedure relies on the variation achieved by temperature on the LEDs, as well as in the resolution of the MS camera.

Clustering-based data detection for spectral signature multiplexing in multispectral camera communication

DANIEL MORENO,^{1,*}  VICTOR GUERRA,²  JULIO RUFO,³  JOSE RABADAN,¹  AND RAFAEL PEREZ-JIMENEZ¹ 

¹Institute for Technological Development and Innovation in Communications (IDeTIC), Universidad de las Palmas de Gran Canaria (ULPGC), 35017 Las Palmas de Gran Canaria, Las Palmas, Spain

²Pi Lighting Sarl, 1950 Sion, Valais, Switzerland

³Ramon y Cajal Researcher, Universidad de La Laguna (ULL), 38208 San Cristobal de La Laguna, Santa Cruz de Tenerife, Spain

*Corresponding author: daniel.moreno@ulpgc.es

Received 22 November 2021; revised 14 January 2022; accepted 14 January 2022; posted 19 January 2022; published 17 February 2022

Optical camera communication (OCC) is a promising technology to be used in future wireless communication systems. In this work, a cluster-based data detection procedure is applied to enhance the performance of an OCC system. A multispectral camera is employed to capture the spectral variations in light-emitting diodes (LEDs) caused by temperature. This strategy's system performance is compared with a system that uses traditional linear methods, such as zero-forcing (ZF) and minimum mean square error (MMSE) equalizers. The findings of this study indicate that an improvement in the bit error rate (BER) can be achieved by applying a clustering approach. © 2022 Optica Publishing Group

<https://doi.org/10.1364/OL.449207>

Optical wireless communications (OWCs) are widely considered to be a key technology in future wireless communication systems. Furthermore, within OWC, optical camera communication (OCC) has received significant attention in recent years mainly because of the development of cameras and image sensors, and their pervasiveness in consumer electronics devices, such as smartphones, tablets, automobiles, etc. [1].

There has been a rapid rise in the use of OCC in the last few years. Most research has focused on improving the data rate since it is a crucial issue of OCC systems due to the limitation of the camera's scanning method. For instance, Arai *et al.* developed an image sensor communication (ISC) system using a rotary light-emitting diode (LED) transmitter based on the generation of afterimages by rotating the blinking LEDs. It permitted the camera to capture more bits per image, increasing the data rate 60 times more than using a conventional ISC system [2].

However, machine-learning-based approaches are generating considerable traction in the field of communication systems. Recent findings regarding unsupervised learning have led to an improvement in the performance of OWC systems. Wu and Chi increased the data rate of an underwater visible light communication (VLC) system using a k-means algorithm to correct the phase deviation of 8-quadrature amplitude modulation (QAM)

[3], which improved the data rate up to 75 Mbps. A k-medoids algorithm was employed by Wang *et al.* in a VLC system based on direct current biased optical orthogonal frequency-division multiplexing (DCO-OFDM). The clustering algorithm was applied in the post-equalization stage to reduce the noise and determine the constellation points that were distorted, which enhanced the system's bit error rate (BER) [4].

In this work, the use of a clustering algorithm is proposed for compensating signals from thermally induced LED spectral variations in a multispectral camera communication (MCC) system. The multispectral camera provides the spectral resolution needed to detect the changes of the LED's spectral response evoked by temperature. Thus, several communication channels are obtained by employing the same transmitter device because each light source has a distinct spectral signature at different temperatures. Therefore, a multispectral camera that can discriminate signals with different spectral characteristics enables implementation of a temperature-based spectral signature multiplexing approach. Finally, the cluster analysis allows for recovering the individual transmitted signals and carrying out the decoding process.

The principal elements on which the proposed system is based are on the one hand, the impact of temperature on LED devices; on the other hand, clustering techniques implemented in OWC systems.

It is common knowledge that LED devices are affected by temperature. In the literature, many works have studied the thermal impact on those light sources due to changes in the p-n junction temperature of the LED [5,6]. Spectral emission variation is one of the effects to consider in OWC. In general, the peak wavelength increases with temperature, demonstrated by joining the Varshni and Planck–Einstein relations. Few studies have taken this effect into account, proving that it reduces the system performance [7,8].

Nevertheless, recent developments, including this Letter, have concentrated on taking advantage of this *a priori* detrimental effect to increase the number of communication channels [9]. This improvement could be achieved using a multispectral camera, as this type of device presents enough spectral resolution to

distinguish the components of the spectral response of LEDs at different temperatures.

Cluster analysis is an unsupervised learning method that uses datasets made up of unlabeled data to identify a logical structure by grouping similar data points in the same cluster. This method has been recently used in OWC. For example, Ma *et al.* employed a k-means clustering algorithm to reduce the nonlinear distortion effects in a VLC system with Nyquist pulse-amplitude modulation (PAM), improving the BER performance with respect to previous works [10]. In [11], Shi *et al.* applied an algorithm based on density-based spatial clustering of applications with noise (DBSCAN) in a PAM-7 multiple-input single-output (MISO) underwater VLC system. Their proposal used DBSCAN to solve the wrong assignment problem caused by the mismatch between the two LEDs employed in the transmission. Furthermore, some studies have used machine learning schemes based on neural networks (NN) to reduce inter-symbol interference (ISI) caused by the pixel-row exposure delay in rolling shutter image sensors [12,13].

In this study, a hierarchical method is used. Balanced iterative reducing and clustering hierarchies (BIRCH) is a clustering algorithm that builds a height-balanced tree data structure, called the clustering feature (CF) tree. The CF tree compacts the dataset into a set of CF nodes containing a number of CF sub-clusters. Each non-leaf node represents a sub-cluster consisting of all the sub-clusters represented by its entries. In turn, each leaf node is a summary, where all its entries are a CF sub-cluster. The CF tree has two parameters: the branching factor defines the maximum number of sub-clusters in a node and the threshold defines the maximum number of data points a sub-cluster in a leaf node can have. The CF entry of a cluster is defined as follows [14]:

$$CF = \{N, \vec{LS}, SS\}, \quad (1)$$

where N is the number of data points in the cluster, \vec{LS} is the linear sum of N data points, and SS is the square sum of N data points.

The main objective of this work is to enhance the performance of a multispectral (MS) camera in a communication link using a clustering algorithm. We propose using LEDs at different temperatures to get distinct spectral signatures that the MS camera can detect. Thus, the same light source can provide more than one channel when it is induced at a different temperature. Furthermore, to assess the system performance, two approaches are compared. First, the channel matrix was compensated by applying zero-forcing (ZF) and minimum mean square error (MMSE) equalizers, which enables attaining those new channels. Second, a clustering algorithm is employed to obtain the individual signals of each LED.

The experimental setup employed in this research is depicted in Fig. 1. It consisted of different types of LEDs as transmitters, where the driving current of each light source was controlled by a circuit powered by a voltage source. Furthermore, a micro-controller connected to each LED circuit generated a variable pulse position modulation (VPPM) signal determined by the target temperature induced in the LED due to the Joule effect. Lastly, the micro-controllers were connected through the serial port to the control PC responsible for sending the data.

The MS camera was connected to the PC via Ethernet, managing the image capture process. In addition, a diffuser placed between the transmitters and the camera aimed to mix the light beams and prevent saturation of the levels in the camera.

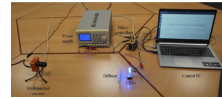


Fig. 1. Representation of the experimental setup. A dark chamber was used to place the actual experiment.

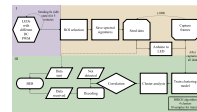


Fig. 2. Flowchart of the experimental procedures. It is split into three phases: Phase I, LED temperature stabilization; Phase II, transmission and reception; Phase III, clustering and performance assessment.

Moreover, the setup was situated in a dark chamber to reduce the background-light interference. Finally, all the processes were orchestrated by a Python-based automation script.

This experiment consisted of three phases, as shown in Fig. 2. First, in Phase I, pairs of LEDs of the same model were employed (two red, two green, and two blue LEDs), modifying their p-n junction temperature by the Joule effect to obtain distinct spectral signatures that the MS camera could capture. To reach various spectral responses, each LED was configured with a different pulse-width modulation (PWM) duty cycle (DC) value. No heat sink was used because it was required to obtain the maximum possible temperature variation in the LEDs. The LED thermal steady-state was achieved by keeping the LEDs in an idle state for five minutes, setting the DC for each LED at 30% and 70%.

Second, Phase II involved the data transmission and camera reception. Once the region of interest (ROI) was selected, a list of 1000 8-bit data was sent by each LED. It employed an 8B/10B encoding to allow for the use of a header consisting of non-consecutive zeros and ones, which would affect the spectral signature due to its high sensitivity to temperature.

Finally, in Phase III, cluster analysis was carried out, and system performance was assessed. First, multiple groups of ten bit streams from the received frames were used to train the clustering model. A preliminary heuristic search was performed to select the model's parameters. Then, the best training set was chosen after evaluating the BER performance using each set. When the model learned the clusters, those were assigned to a corresponding symbol (00, 01, 10, or 11). Each symbol was interpreted as listed in Table 1, recovering the two LED signals. Next, the resulting signals were correlated (Pearson correlation function) with a matrix comprising all available transmitted signals (a total of 2^{bits}). As soon as the correlation was performed, the maximum value was taken and compared to thresholds from 0 to 0.95 in steps of 0.05. If the maximum value was less than the threshold, the bit stream was considered as not detected. Otherwise, the received signal was decoded, and its BER was estimated. To compare the clustering results to traditional linear methods, instead of performing the cluster analysis in Phase III, the LED's spectral responses were used to comprise a channel matrix. Then, an equalizer was employed to obtain the separate LED's received bit streams. These phases were repeated for each LED color. Table 2 details the key parameters of the experiment.

Table 1. Cluster Interpretation

Symbol	LED State
00	Both LEDs OFF
01	One LED ON, one LED OFF
10	One LED ON, one LED OFF
11	Both LEDs ON

Table 2. Experiment Key Parameters

Parameter	Value
Transmitter	
Light sources	Kingbright L-53SRC-C (Red) Kingbright L-154A4SUREQBFZGEW (Green, Blue)
Dominant wavelengths/nm	660 (Red), 520 (Green), 460 (Blue)
Control device	Arduino UNO
Receiver	
Camera	SILIOS Technologies CMS-C1-C-EVR1M-GigE 1280 × 1024 (raw image)
Resolution/px	426 × 339 (multispectral images)
Band's center wavelength/nm	B1, 424; B2, 464; B3, 504; B4, 544; B5, 573; B6, 614; B7, 656; B8, 699; B9, 400–800 (pan)
Exposure time/ms	20 (Red), 6.5 (Green), 0.25 (Blue)
Aperture	f/2.4
Frame rate/fps	50
Shutter mode	Global shutter
Bit Stream	
Coding	8B/10B
Modulation	VPPM
Bit time/ms	200
Duty cycle	30%, 70%
Bits	Header, 10; Payload, 8; Footer, 10
Clustering	
Algorithm	BIRCH
Number of clusters	4
Threshold	0.01
Branching factor	50

The spectral signatures of the LEDs employed in this work are shown in Fig. 3. It can be noted that the responses of red and green LEDs presented more variation than the blue LEDs. Figure 4 shows an example of the clusters obtained for a bit stream of the red LEDs. Four groups of data assigned to the corresponding symbols can be seen. The x - and y -axis represent the camera levels (0–255) of bands 1 and 7, respectively. The range of levels is different in each spectral band depending on the spectral signature of the LEDs. Note that the most energetic clusters were assigned to the symbol "11", while the least energetic to "00".

The system performance is shown in Fig. 5. The BER and the not detected bit streams are depicted. The best results were achieved for the red and the green LEDs. However, the blue LEDs did not show a satisfactory performance. It can be noted from Fig. 5(a) that the BER of the red LEDs was approximately

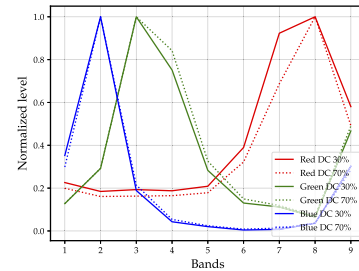


Fig. 3. Spectral signatures of the red (right dotted and solid curves), green (middle dotted and solid curves), and blue (left dotted and solid curves) LEDs at different temperatures. Solid and dotted lines correspond to the LEDs working at 30% and 70% DC values, respectively.

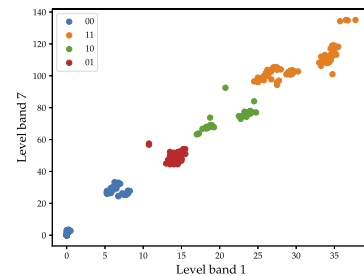


Fig. 4. Scatter plot showing an example of the clusters obtained for bit streams of the red LEDs using bands 1 and 7. From left to right, 00, 01, 10, 11.

Table 3. Clustering and Equalization Stage Comparison

Duty Cycle	Color	BER Below FEC Limit (Non-Detected Bitstreams)		Minimum BER (Non-Detected Bitstreams)	
		CA	EQ	CA	EQ
30%	Red	3.5×10^{-3} (0.5%)	3.7×10^{-3} (3.1%)	0 (3.4%)	0 (65%)
	Green	3.4×10^{-3} (14.1%)	2.5×10^{-3} (16.5%)	0 (39%)	0 (16.5%)
	Blue	6.5×10^{-4} (95%)	3.7×10^{-3} (43.1%)	6.5×10^{-4} (95%)	0 (83%)
70%	Red	3.5×10^{-3} (0.4%)	3.7×10^{-3} (3.3%)	0 (40%)	0 (16%)
	Green	2.6×10^{-3} (5%)	3.8×10^{-3} (10.5%)	0 (9%)	0 (14.5%)
	Blue	3.7×10^{-3} (90%)	1.4×10^{-3} (97.5%)	7.7×10^{-4} (98%)	1.4×10^{-4} (97.5%)

6×10^{-3} for the LEDs at 30% and 70% from thresholds of 0 to 0.4. At a threshold of 0.5, both LEDs achieved a BER below the forward error correction (FEC) limit (3.8×10^{-3}), not detecting less than 1% of the bit streams.

The performance of the green LEDs is presented in Fig. 5(b). From thresholds of 0 to 0.4, the BER was near 2×10^{-2} for the

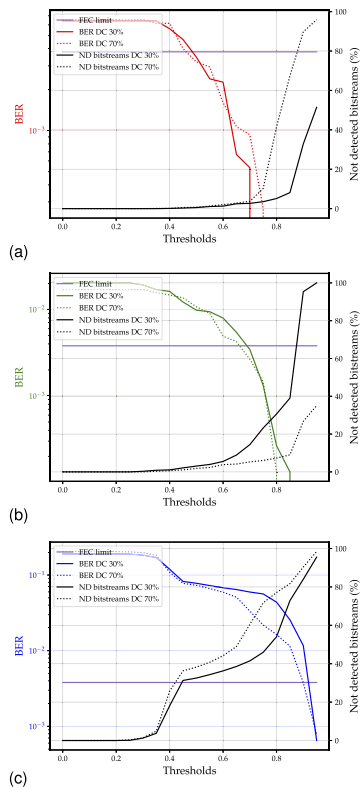


Fig. 5. BER and not detected bit streams at different correlation thresholds corresponding to the pairs of (a) red (left dotted and solid curves), (b) green (left dotted and solid curves), and (c) blue (right dotted and solid curves) LEDs. Solid and dotted lines correspond to the LEDs working at 30% and 70% DC values, respectively. FEC limit is represented by the horizontal line in (a), (b), and (c).

LEDs at 30% and 70%. From thresholds greater than 0.7, both LEDs reached a BER below the FEC limit, but 14% and 5% of the bit streams were not detected for the LEDs at 30% and 70%, respectively.

Finally, as illustrated in Fig. 5(c), the blue LEDs only achieved a successful BER at the cost of missing most of the bit streams. This poor performance was not surprising. In fact, the slight changes in its spectral response due to thermal variation in the LED's p-n junction did not permit the camera to distinguish signals at different temperatures.

Table 3 compares the system performance applying an equalizer for the channel compensation (EQ) and the cluster analysis (CA) used in this study. It reports the BER when the FEC limit was reached and the minimum value was achieved, as well as the percentage of non-detected bit streams. The most striking result to emerge from the data comparison was the improvement in the red LEDs' performance while using the clustering algorithm, especially concerning the missed bit streams. The green LEDs also slightly enhanced their performance with the cluster-based detection. However, the blue LEDs could not benefit from the clustering, as mentioned above.

In this Letter, a cluster-based data detection technique has been employed in an MCC system. The LEDs' temperature effects have been exploited to achieve more than one communication channel from the same device. Hence, distinct spectral signatures are obtained from a light source at different temperatures so that an MS camera can capture the spectral variation. Furthermore, an improvement of the system performance by using a clustering algorithm to detect the signals from each LED was expected.

This work provides a powerful methodology for detecting data in any system involving several communication channels. It has been demonstrated that up to two channels can be achieved from the same LED employing temperature and the MS camera. However, the number of channels could be increased by using a higher spectral-resolution camera featuring more spectral bands and different LEDs that present more variations in their spectrum. In addition, it has been seen that the cluster-based approach enhanced the system performance of the red and green LEDs to linear methods, such as ZF and MMSE equalizers.

However, the present study could not improve the performance of the blue LEDs. This unsatisfactory result occurred because there was no significant difference between the spectral response of both devices at different temperatures.

Future work could be focused on testing various clustering algorithms for data detection. Then, the algorithm parameters can be fine-tuned with the purpose of getting the best model.

Funding. Agencia Estatal de Investigación (PID2020-114561RB-I00); Universidad de Las Palmas de Gran Canaria (2019, Trainee Predoctoral Research Staff Program).

Disclosures. The authors declare no conflicts of interest.

Data availability. Data underlying the results presented in this paper are not publicly available at this time but may be obtained from the authors upon reasonable request.

REFERENCES

1. M. Z. Chowdhury, M. K. Hasan, M. Shahjalal, M. T. Hossain, and Y. M. Jang, *IEEE Commun. Surv. Tutor.* **22**, 930 (2020).
2. S. Arai, Z. Tang, A. Nakayama, H. Takata, and T. Yendo, *IEEE Photonics J.* **13**, 7300611 (2021).
3. X. Wu and N. Chi, *Opt. Commun.* **444**, 147 (2019).
4. Y. Wang, M. Zhang, H. Zhou, X. Wang, C. Qin, W. He, and X. Ren, *2021 2nd Information Communication Technologies Conference (ICTC)*, Nanjing, China (May 7, 2021), pp. 107–111.
5. M. E. Raypah, B. K. Sodipo, M. Devarajan, and F. Sulaiman, *IEEE Trans. Electron Devices* **63**, 2790 (2016).
6. R. O. Ocaya, *Measurement* **162**, 107910 (2020).
7. E. Tugcu, A. Yazgan, C. Albayrak, and K. Turk, *Opt. Commun.* **463**, 125451 (2020).
8. D. Moreno, J. Rufo, V. Guerra, J. Rabadan, and R. Perez-Jimenez, *Electronics* **10**, 262 (2021).
9. D. Moreno, J. Rufo, V. Guerra, J. Rabadan, and R. Perez-Jimenez, *IEEE Photonics Technol. Lett.* **33**, 591 (2021).
10. J. Ma, J. He, J. Shi, J. He, Z. Zhou, and R. Deng, *IEEE Photonics Technol. Lett.* **31**, 935 (2019).
11. M. Shi, Y. Zhao, W. Yu, Y. Chen, and N. Chi, *IEEE Photonics J.* **11**, 7905013 (2019).
12. K.-L. Hsu, C.-W. Chow, Y. Liu, Y.-C. Wu, C.-Y. Hong, X.-L. Liao, K.-H. Lin, and Y.-Y. Chen, *Opt. Express* **28**, 39956 (2020).
13. Y.-S. Lin, C.-W. Chow, Y. Liu, Y.-H. Chang, K.-H. Lin, Y.-C. Wang, and Y.-Y. Chen, *Opt. Express* **29**, 31680 (2021).
14. T. Zhang, R. Ramakrishnan, and M. Livny, *SIGMOD Rec.* **25**, 103 (1996).

5.4 Summary

Table 5.1 outlines the main contributions of each publication in the compendium. First, P1 provides further evidence that spectral variation of LEDs should be taken into account in the compensation stage of an OCC system since it degrades its performance. Second, the findings in P2 suggests that more than one communication channel can be obtained from the same device if its spectral features are modified by temperature and detected by a high-spectral-resolution camera. Lastly, P3 underlines the benefits in BER of clustering techniques against linear methods such as ZF or MMSE.

Table 5.1: Summary of the key contributions on methodology and results of the publications of the compendium.

	Design	Processes	Metrics	Findings
P1	RGB OCC channel compensation with CSI at different temperatures	Thermally induced LED variations ZF equalization Foveon and Bayer-based sensors estimation	SINR BER	Performance degradation due to LED's spectral variations
P2	OOK simulation of an MCC system after LED experimental characterization	Thermally induced LED variations ZF equalization Spectral signature multiplexing	Condition number BER	Increase in the number of communication channels from the same device
P3	Cluster-based data detection approach in an MCC system	Thermally induced LED variations BIRCH algorithm Spectral signature multiplexing	BER	BER improvement with respect to traditional linear methods

In addition, the articles that comprised this study resulted in various works published in conference proceedings, compiled in Annex A. All of them were grounded on the thermal influences on the spectral properties of LEDs and the employment of a high-spectral-resolution camera to benefit from the temperature impact.

In the first place, a characterization of different LEDs was performed to analyze their spectral behavior at several temperatures in [110]. Moreover, the use of a multispectral camera was proposed to take advantage of temperature variations and apply a WDM system using the distinct LED spectral signatures.

Then, in [111], different clustering algorithms were applied following the methodology of [109]. In this case, four typical algorithms were used for data detection: BIRCH (hierarchy-based clustering), k-means and mini-batch k-means (centroid-based clustering), and Gaussian mixture model (distribution-based clustering). The BER for each algorithm applied was estimated, and the results were compared.

Finally, in [112], an MCC system was implemented using equalization techniques to the channel matrix to extract the estimated transmitted signals. Likewise, the system performance was assessed by calculating the BER.

The performance of a high-spectral-resolution camera in an OCC system, along with the consequences of temperature variations in LEDs, has been discussed throughout this thesis. The results and the possible future studies that can be inferred from this research are outlined in this chapter.

6.1 Conclusions

Returning to the hypotheses posed in Chapter 1, a thorough exploration of the evidence substantiates their validity. As a reminder, H1 proposed that leveraging multispectral cameras in OCC systems amplifies multiplexing capabilities, allowing the efficient separation and detection of transmitters operating at distinct wavelengths. In alignment with H2, it was suggested that wavelength emission variations in LED devices, stemming from temperature effects, can indeed be harnessed through multispectral cameras, effectively establishing additional communication channels within OCC systems. Furthermore, H3 regarding the criticality of considering LED temperature effects in the compensation stage was firmly validated, underscoring the pivotal role of this consideration in preserving the accuracy and reliability of data transmission. Lastly, H4 introduced the application of nonlinear methods, and the subsequent exploration underscored their potential in refining OCC system performance, leading to lower error rates.

Hypotheses H1 and H2 were proven in publications 2 (P2) and 3 (P3) of the compendium [108], [109]. As described in Chapter 5, an innovative solution based on the LEDs' spectral signatures and their spectral changes caused by temperature was proposed. Owing to the MS cameras' spectral resolution, more than one channel per light source could be obtained with satisfactory BER.

In particular, in P2, a first study using an MS camera and exploiting the LED's temperature effects was carried out. After characterizing the LEDs under test, an OCC system was simulated assuming an OOK transmission and applying a ZF equalizer to obtain the received signal. As a result, performance metrics such as the condition number of the channel matrices comprised by the LED's spectral signatures and the BER were obtained.

On the other hand, an experimental study taking advantage of the MS camera and the spectral variations on the transmitters was conducted in P3. Additionally, this work supports H4 as it compared the system performance using traditional linear methods and clustering for data detection, showing that the latter obtained better results. Likewise, the findings of P2 and P3 allow the achievement of the objectives O1 and O2 of this thesis, namely the implementation of an OCC link using a MS camera and the effect of temperature on LEDs, and the use of nonlinear techniques for data detection in MCC systems, respectively. Thus, it was proven that an MS camera could detect the spectral changes induced by thermal

variations on LEDs and, therefore, exploit this feature to achieve more than one communication channel from the same device with successful performance.

Moreover, experiments to measure the effect of temperature changes on the channel compensation process and evaluate the performance of the OCC system under various temperature conditions were conducted in P1 [107]. It showed that SINR and BER decreased when there were temperature differences in the channel matrices used for compensation. These issues that difficult to achieve reliable communication validate H3. Therefore, the third objective of this thesis (O3), consisting of examining the LED's thermal effects in OCC systems, is achieved in this publication as well.

Based on the fact that the use of multispectral cameras for communication is hardly found in the literature, this work has widened current knowledge of the benefits and limitations of this technology in OCC. Furthermore, the LED's thermal effect has been analyzed considering that, even though it has been widely investigated, its repercussions in OWC have not been thoroughly examined. Moreover, this effect, usually deemed to detriment systems, has been exploited thanks to MS cameras to obtain more than one communication channel from the same device. In summary, these have derived the achievement of the following objectives and sub-objectives:

- First utilization of an MS camera in a simulated and experimental OCC system.
- Leveraging the spectral changes caused by temperature on LEDs to obtain new communication channels.
- Evaluation of the consequences of not taking into account the thermally induced variations on LEDs in the channel compensation stage.
- Implementation of a novel spectral signature multiplexing approach.
- System performance comparison between traditional linear methods (ZF and MMSE) and clustering approaches.

It was declared in Chapter 2 that most of the cameras used in OCC as receivers were conventional ones due to their pervasiveness in the majority of consumer electronics. Therefore, these thesis' results constitute an initial step toward the use of cameras with a high spectral resolution for communication purposes. Basically, MS and HS devices would be beneficial for those situations that make use of spectral features of the transmitters, for example, WDM, where several channels more than the RGB provided by conventional cameras are used. Thus, although the CFA presented on the camera's image sensor permits to separate RGB channels from an LED, the wide optical bandwidth of the color filters causes overlap between the channels. Besides, wide LED's spectral width brings about ICI. Therefore, those factors complicate obtaining independent communication channels using only a conventional camera. Instead, the spectral richness of MS cameras facilitates this process. Additionally, they open up new approaches, namely, the increase of communication channel by means of the LED spectral variation mentioned above.

The main aspects that affect the success of this approach that combines high-spectral-resolution cameras and the temperature effects on LEDs are the LEDs' spectral variations caused by temperature, which, in turn, depend on the LED materials, and the camera's spectral resolution. On the one hand, relying on the LEDs substrate, the LED's spectral behavior with temperature may differ so that while peak wavelength usually increases as temperature grows, the efficiency diminishes. In this sense, it is also crucial to have a trade-off between the red-shift and the decrease in efficiency. On the other hand, the camera resolution determines how sensitive to variation it is. Hence, the greater the number of bands and the narrower their width, the more variability would capture.

Nonetheless, a few aspects could limit the utilization of this technology. First, the acquisition cost of high-spectral-resolution cameras is clearly a constraint. Typically employed in professional sectors, MS and HS cameras are expensive compared to conventional cameras, so their presence in COTS devices is non-existent. Second, as in OCC, the low data rate is a limitation. It is common for these cameras to have a low frame rate, which restricts the transmission speed in those cases where GS mode is employed. However, some models allow capturing with RS mode, increasing the data rate. Moreover, since cameras are not designed for communication, frame rate instability could result in difficulties, for example, missing part of the transmission or mixing two distinct bit streams. On the other hand, regarding the LED spectral changes induced by temperature, potential problems rely on keeping stable the p-n junction temperature of the LEDs so as not to vary their spectral signatures and be able to demultiplex the signals.

Having considered the limitations and the potential characteristics of high-spectral-resolution cameras for communication purposes, several possible applications can be developed. The main areas of deployment of MS and HS cameras were described in Chapter 2. In order to avoid the expense of acquiring such cameras, the principal uses of these cameras should concentrate on complementing the primary goal of systems that already have cameras installed with communication. For example, in production lines where the cameras are employed to identify contaminated food and feed, they can be used to indicate if there is a problem with the conveyor belt by means of a sensor connected to the LED that detects instances where food is present, as well as if there is an issue with the roller and transmit the information by an OCC link where the MS camera is involved as a receiver (Fig. 6.1).

Another conceivable application could be developed in farming. Over the past few years, it has become more common to employ multispectral cameras for assessing soil production and monitoring plant development. In fact, the expected increase in world population by the end of this century (about 10 billion inhabitants by 2100) suggests that the methods used in traditional agriculture will not be sufficient to meet the needs of the population [14], [113]. Therefore, these devices allow the optimization of agricultural processes, as they can be used for the premature detection of diseases by detecting the presence of parasites, as well as the amount of nutrients and water in plants to improve irrigation and fertilizer application. In this sense, the current trend is to carry the camera on board unmanned aerial vehicles (UAVs), as the spatial resolution improves with respect to

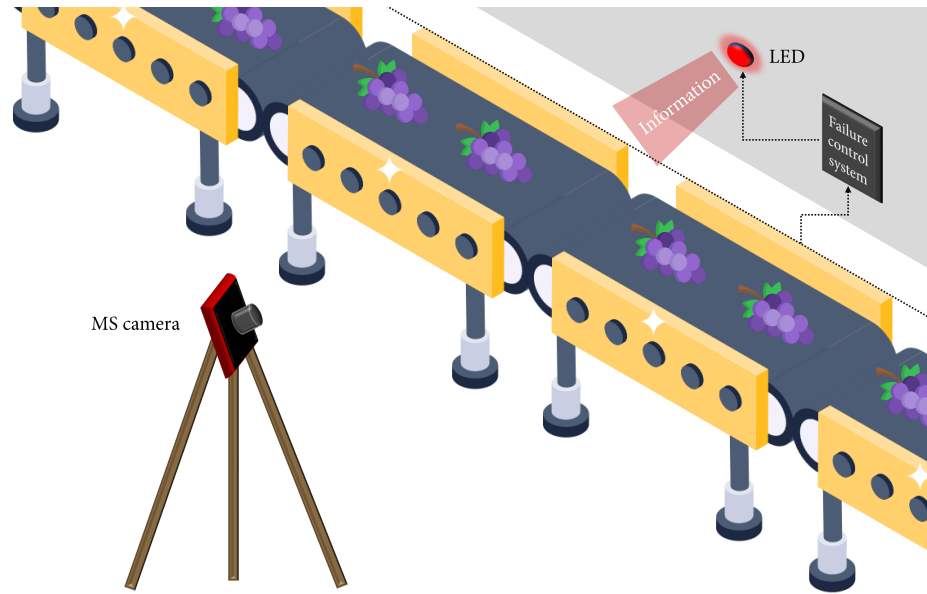


Figure 6.1: A use case example using a multispectral camera for food analysis and monitoring failures in the conveyor belts. Some of the images of this figure are from Flaticon.com.

cameras installed on satellites or aircraft. However, to facilitate the communication with the MS, it would be more suitable to place it in a fixed stand (Fig. 6.2). Thus, the camera could have a dual functionality to monitor crop health and receive useful information from sensors installed in the field to enable necessary actions to be carried out. In addition, the camera mounted in a stand could have an additional function for surveillance. Since the device would be located at a certain height, its field of view (FOV) would cover a large part of the farm, allowing it to be used, for example, to detect the presence of intruders.

6.2 Future work

As seen in previous chapters, the use of multispectral cameras is hardly found in the literature, so this work constitutes an excellent starting point for future experiments that can build upon the results obtained. In this way, it is recommended that further research should be undertaken in the following areas.

First, a potential study that could be performed from this thesis is the application of high-spectral-resolution cameras for underwater communication. In this sense, it is well-known that the transmitter's wavelength affects attenuation underwater. Particularly, the highest wavelengths (red wavelengths) are more attenuated than the blue-green bands. Therefore, the use of an MS camera could provide a higher resolution in those regions taking advantage of the several bands these types of cameras have. Research into solving this problem is already in progress by members of our research group.

Second, the number of LED models employed in this work was limited. Therefore, the findings of this thesis encouraged further studies to validate the results by

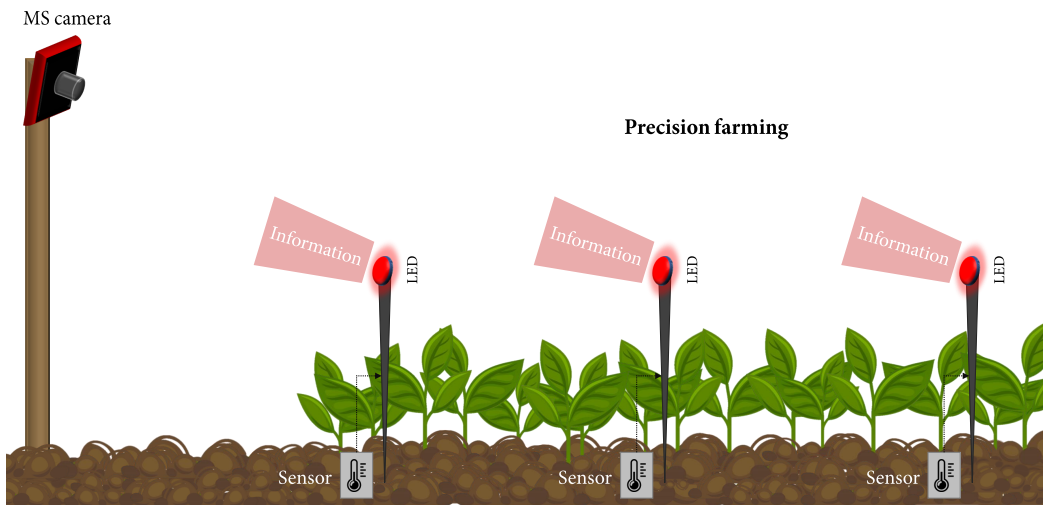


Figure 6.2: A use case example using a multispectral camera for monitoring and analysis in precision farming. Some of the images of this figure are from Freepik.com.

using a larger sample size of different LED models. Furthermore, future studies should aim at analyzing the spectral variability using one model (intra-class) or various models (inter-class).

Moreover, another promising experiment is exploiting the n camera's bands to design a communication system with n transmitters. In order to achieve this goal, it would be necessary to generate a matrix comprising the n spectral signatures, which must be distinguishable from each other to guarantee a successful performance. The most straightforward approach to achieve spectrally different light sources is to use LEDs of different colors. However, if the same emitter were used to exploit the spectral variations induced by changes in the temperature of its p-n junction, it would be highly challenging to achieve as many transmission channels as the number of bands in the camera since the spectral changes would not be significant enough to be detected by the device.

An immediate work that can emerge from this thesis is to employ a device with higher spectral resolution than the MS camera under study, such as a hyperspectral camera. The camera employed in this research possesses nine bands with FWHM between 24 nm and 71 nm. However, HS cameras have more bands and narrower FWHM, which make them suitable for detecting more subtle spectral differences on LEDs.

In relation to the last future research line, it is suggested to optimize the camera performance by applying dimensionality reduction techniques, such as principal component analysis (PCA), usually employed in hyperspectral imaging applications. The main idea is to thoroughly examine the best bands to be used in the channel matrix and evaluate the outcome improvements. These techniques can make it easier to perform analysis on the data, and they can also help to speed up the processing time. Additionally, dimensionality reduction techniques can help to remove noise and redundant information from the data, which can improve the overall accuracy of the results. Consequently, their application can benefit

in hyperspectral imaging applications where the data can be very complex and high-dimensional.

Another possible avenue for future work is fine-tuning the clustering algorithms employed in this thesis. While the current work demonstrated that cluster analysis approaches could improve system performance compared to traditional linear methods, there may be opportunities to optimize the clustering algorithms used. Therefore, it may be possible to further enhance the performance of the OCC system by fine-tuning the algorithm.

An additional possibility for future work is the exploration of using rolling shutter mode in an MS camera communication system. In the current work, only global shutter mode was used, which captures an image all at once. However, rolling shutter mode captures an image progressively, line by line, over a period of time. Using rolling shutter mode in an OCC system could potentially increase the data rate by allowing for faster capture of images. In this particular scenario, it becomes crucial to thoroughly examine the implications of employing an MS camera with a macro-pixel for spectral band filtering, particularly in relation to data reception during the utilization of the rolling shutter mode.

Furthermore, the incorporation of multispectral cameras as a key tool in the concept of joint communication and sensing is proposed for future work. These cameras will not only enable the capture of visual information, but also the acquisition of thermal and spectral data, enriching environmental perception. For instance, their application could be explored in machinery monitoring, where communication between devices and joint sensing can reveal subtle changes in temperature indicative of potential failures, such as excessive friction. This innovative integration has the potential to transform early anomaly detection into an essential component of industrial asset management, improving operational efficiency and reducing costs associated with unplanned corrective maintenance.

Lastly, following a typical approach used in multispectral imaging applications, the integration of pansharpening techniques with high-spectral-resolution cameras in OCC holds great potential for advancing the capabilities this technology. Pansharpening is a fusion technique that combines the high-resolution panchromatic band with lower-resolution multispectral bands in order to enhance the spatial and spectral resolution of the captured images. The improved spatial resolution provide OCC systems with benefits, such as better object recognition, tracking, localization, as well as more accurate ROI selection [114], [115].

Bibliography

- [1] Verified Market Research, **Global optical wireless communication market size by type (visible light communication, infrared communication), by industry (industrial, transportation, healthcare, infrastructure/defense), by geographic scope and forecast global optical wireless communication market size by type (visible light communication, infrared communication), by industry (industrial, transportation, healthcare, infrastructure/defense), by geographic scope and forecast**, 2021 (see page 1).
- [2] M. Z. Chowdhury, M. Shahjalal, M. K. Hasan, and Y. M. Jang, **The role of optical wireless communication technologies in 5G/6G and IoT solutions: Prospects, directions, and challenges**, *Applied Sciences*, vol. 9:no. 20, ISSN: 2076-3417. DOI: 10.3390/app9204367. [Online]. Available: <https://www.mdpi.com/2076-3417/9/20/4367> (see page 1).
- [3] W. Liu and Z. Xu, **Some practical constraints and solutions for optical camera communication**, *Philosophical Transactions of the Royal Society A: Mathematical, Physical and Engineering Sciences*, vol. 378:no. 2169, 20190191. DOI: 10.1098/rsta.2019.0191. eprint: <https://royalsocietypublishing.org/doi/pdf/10.1098/rsta.2019.0191>. [Online]. Available: <https://royalsocietypublishing.org/doi/abs/10.1098/rsta.2019.0191> (see pages 1, 2, 11, 20).
- [4] H. Haas, L. Yin, Y. Wang, and C. Chen, **What is LiFi?** *Journal of Lightwave Technology*, vol. 34:no. 6, 1533–1544. DOI: 10.1109/JLT.2015.2510021 (see page 1).
- [5] S. A. H. Mohsan, **Optical camera communications: Practical constraints, applications, potential challenges, and future directions**, *J. Opt. Technol.*, vol. 88:no. 12, 729–741. DOI: 10.1364/JOT.88.000729. [Online]. Available: <http://opg.optica.org/jot/abstract.cfm?URI=jot-88-12-729> (see page 2).
- [6] C. Jurado-Verdu, V. Guerra, V. Matus, J. Rabadan, and R. Perez-Jimenez, **Convolutional autoencoder for exposure effects equalization and noise mitigation in optical camera communication**, *Opt. Express*, vol. 29:no. 15, 22973–22991. DOI: 10.1364/OE.433053. [Online]. Available: <http://www.opticsexpress.org/abstract.cfm?URI=oe-29-15-22973> (see pages 2, 12).
- [7] J. He, Y. Yang, and J. He, **Artificial neural network-based scheme for 4-PWM OCC system**, *IEEE Photonics Technology Letters*, 1–1. DOI: 10.1109/LPT.2022.3153692 (see page 2).
- [8] S. Arai, S. Mase, T. Yamazato, T. Endo, T. Fujii, M. Tanimoto, K. Kidono, Y. Kimura, and Y. Ninomiya, **Experimental on hierarchical transmission scheme for visible light communication using LED traffic light and high-speed camera**, in *2007 IEEE 66th Vehicular Technology Conference*, 2007, 2174–2178. DOI: 10.1109/VETECONF.2007.456 (see page 2).
- [9] D. Iwase, M. Kasai, T. Yendo, S. Arai, T. Yamazato, H. Okada, and T. Fujii, **Improving communication rate of visible light communication system using high-speed camera**, in *2014 IEEE Asia Pacific Conference on Circuits and Systems (APCCAS)*, 2014, 336–339. DOI: 10.1109/APCCAS.2014.7032788 (see page 2).
- [10] V. Guerra, J. R. Ticay-Rivas, V. Alonso-Eugenio, and R. Perez-Jimenez, **Characterization and performance of a thermal camera communication system**, *Sensors*, vol. 20:no. 11, ISSN: 1424-8220. DOI: 10.3390/s20113288. [Online]. Available: <https://www.mdpi.com/1424-8220/20/11/3288> (see page 2).
- [11] J. Marcello, F. Eugenio, C. Gonzalo-Martín, D. Rodríguez-Esparragón, and F. Marqués, **Advanced processing of multiplatform remote sensing imagery for the monitoring of coastal and mountain ecosystems**, *IEEE Access*, vol. 9, 6536–6549. DOI: 10.1109/ACCESS.2020.3046657 (see page 2).

- [12] J. González-Piqueras, S. Sánchez, J. Villodre, H. López, A. Calera, D. Hernández-López, and J. Sánchez, **Radiometric performance of multispectral camera applied to operational precision agriculture**, in *IGARSS 2018 - 2018 IEEE International Geoscience and Remote Sensing Symposium*, 2018, 3393–3396. DOI: [10.1109/IGARSS.2018.8518786](https://doi.org/10.1109/IGARSS.2018.8518786) (see page 2).
- [13] N. Kobayashi, H. Suzuki, M. Ishikawa, T. Obi, T. Ichimura, H. Yanagisawa, T. Tsuchida, and A. Sasaki, **Telepathology support system with gross specimen image using high resolution 4K multispectral camera**, in *2020 42nd Annual International Conference of the IEEE Engineering in Medicine Biology Society (EMBC)*, 2020, 1388–1381. DOI: [10.1109/EMBC44109.2020.9175398](https://doi.org/10.1109/EMBC44109.2020.9175398) (see pages 2, 16).
- [14] C. Bouyé and C. Tsamba, **Opportunities for hyperspectral and multispectral imaging**, *Optik & Photonik*, vol. 13: no. 4, 28–29. DOI: <https://doi.org/10.1002/opph.201870408>. eprint: <https://onlinelibrary.wiley.com/doi/pdf/10.1002/opph.201870408>. [Online]. Available: <https://onlinelibrary.wiley.com/doi/abs/10.1002/opph.201870408> (see pages 2, 69).
- [15] R. Kumar and Richa, **LED market by product type (LED lamps, LED fixtures), by device configuration (pinned LED, chip on board LED, surface-mounted LED, others), by technology (basic LED, high brightness LED, OLED, ultra violet LED, polymer), by end-user (residential, commercial, industrial, outdoor, architectural) and by application (automotive, general lighting, backlighting, signal signage, others) - global opportunity analysis and industry forecast, 2018-2024**, Allied Market Research, 2018 (see page 3).
- [16] Z. Ghassemlooy, W. Popoola, and S. Rajbhandari, **Optical wireless communications: System and channel modelling with Matlab®**. CRC press, 2019 (see page 3).
- [17] M. E. Raypah, B. K. Sodipo, M. Devarajan, and F. Sulaiman, **Estimation of luminous flux and luminous efficacy of low-power SMD LED as a function of injection current and ambient temperature**, *IEEE Transactions on Electron Devices*, vol. 63: no. 7, 2790–2795. DOI: [10.1109/TED.2016.2556079](https://doi.org/10.1109/TED.2016.2556079) (see page 3).
- [18] S. Chhajer, Y. Xi, Y.-L. Li, T. Gessmann, and E. Schubert, **Influence of junction temperature on chromaticity and color-rendering properties of trichromatic white-light sources based on light-emitting diodes**, *Journal of applied physics*, vol. 97: no. 5, 054506 (see page 3).
- [19] J.-P. M. G. Linnartz, X. Deng, and P. Van Voorthuisen, **Impact of dynamic LED non-linearity on DCO-OFDM optical wireless communication**, *IEEE Communications Letters*, vol. 25: no. 10, 3335–3339. DOI: [10.1109/LCOMM.2021.3102744](https://doi.org/10.1109/LCOMM.2021.3102744) (see page 3).
- [20] J. D. Moreno Gázquez, **Fusión de datos de alta resolución para la obtención de mapas de coberturas terrestres en maspalomas**, B.S. thesis, Universidad de Las Palmas de Gran Canaria, 2016 (see page 4).
- [21] J. D. Moreno Gázquez, **Clasificación de imágenes multiespectrales e hiperespectrales de alta resolución para la obtención de cartografía temática en maspalomas**, M.S. thesis, Universidad de Las Palmas de Gran Canaria, 2018 (see page 4).
- [22] Y. Tanaka, T. Komine, S. Haruyama, and M. Nakagawa, **Indoor visible communication utilizing plural white LEDs as lighting**, in *12th IEEE International Symposium on Personal, Indoor and Mobile Radio Communications. PIMRC 2001. Proceedings (Cat. No.01TH8598)*, vol. 2, 2001, F–F. DOI: [10.1109/PIMRC.2001.965300](https://doi.org/10.1109/PIMRC.2001.965300) (see page 11).
- [23] T. Komine and M. Nakagawa, **Integrated system of white LED visible-light communication and power-line communication**, *IEEE Transactions on Consumer Electronics*, vol. 49: no. 1, 71–79. DOI: [10.1109/TCE.2003.1205458](https://doi.org/10.1109/TCE.2003.1205458) (see page 11).
- [24] N. Iizuka, **OCC proposal of scope of standardization and applications**, *IEEE 802.15 SG7a standardization documents* (see page 11).
- [25] W. A. Cahyadi, Y. H. Chung, Z. Ghassemlooy, and N. B. Hassan, **Optical camera communications: Principles, modulations, potential and challenges**, *Electronics*, vol. 9: no. 9, ISSN: 2079-9292. DOI: [10.3390/electronics9091339](https://doi.org/10.3390/electronics9091339). [Online]. Available: <https://www.mdpi.com/2079-9292/9/9/1339> (see pages 11, 12, 20).

- [26] **IEEE standard for local and metropolitan area networks—part 15.7: Short-range optical wireless communications**, *IEEE Std 802.15.7-2018 (Revision of IEEE Std 802.15.7-2011)*, 1–407. DOI: [10.1109/IEEESTD.2019.8697198](https://doi.org/10.1109/IEEESTD.2019.8697198) (see page 11).
- [27] J. Rabadan, V. Guerra, C. Guerra, J. Rufo, and R. Perez-Jimenez, **A novel ranging technique based on optical camera communications and time difference of arrival**, *Applied Sciences*, vol. 9: no. 11, ISSN: 2076-3417. DOI: [10.3390/app9112382](https://doi.org/10.3390/app9112382). [Online]. Available: <https://www.mdpi.com/2076-3417/9/11/2382> (see page 11).
- [28] K. A. Mahmoodi, A. Gholami, and Z. Ghassemlooy, **Impact of number of LEDs on an optical camera communication based indoor positioning system**, in *2020 3rd West Asian Symposium on Optical and Millimeter-wave Wireless Communication (WASOWC)*, 2020, 1–4. DOI: [10.1109/WASOWC49739.2020.9410069](https://doi.org/10.1109/WASOWC49739.2020.9410069) (see page 11).
- [29] S. Jeong, J. Min, and Y. Park, **Indoor positioning using deep-learning-based pedestrian dead reckoning and optical camera communication**, *IEEE Access*, vol. 9, 133725–133734. DOI: [10.1109/ACCESS.2021.3115808](https://doi.org/10.1109/ACCESS.2021.3115808) (see page 11).
- [30] N. M. Esfahani, A. Gholami, N. S. Kordavani, S. Zvanovec, and Z. Ghassemlooy, **Performance investigation of OCC-based vehicle to vehicle communications**, in *2020 3rd West Asian Symposium on Optical and Millimeter-wave Wireless Communication (WASOWC)*, 2020, 1–5. DOI: [10.1109/WASOWC49739.2020.9410093](https://doi.org/10.1109/WASOWC49739.2020.9410093) (see page 11).
- [31] M. F. Ahmed, M. Shahjalal, M. O. Ali, and Y. Min Jang, **Neural network-based LED detection in vehicular system for high data rate in OCC**, in *2020 International Conference on Information and Communication Technology Convergence (ICTC)*, 2020, 662–665. DOI: [10.1109/ICTC49870.2020.9289325](https://doi.org/10.1109/ICTC49870.2020.9289325) (see page 11).
- [32] X. Sun, W. Shi, Q. Cheng, W. Liu, Z. Wang, and J. Zhang, **An LED detection and recognition method based on deep learning in vehicle optical camera communication**, *IEEE Access*, vol. 9, 80897–80905. DOI: [10.1109/ACCESS.2021.3085117](https://doi.org/10.1109/ACCESS.2021.3085117) (see page 11).
- [33] M. Akram, L. Aravinda, M. Munaweera, G. Godaliyadda, and M. Ekanayake, **Camera based visible light communication system for underwater applications**, in *2017 IEEE International Conference on Industrial and Information Systems (ICIIS)*, 2017, 1–6. DOI: [10.1109/ICIINFS.2017.8300377](https://doi.org/10.1109/ICIINFS.2017.8300377) (see page 11).
- [34] M. Akram, R. Godaliyadda, and P. Ekanayake, **Design and analysis of an optical camera communication system for underwater applications**, *IET Optoelectronics*, vol. 14: no. 1, 10–21. DOI: <https://doi.org/10.1049/iet-opt.2018.5157>. eprint: <https://ietresearch.onlinelibrary.wiley.com/doi/pdf/10.1049/iet-opt.2018.5157>. [Online]. Available: <https://ietresearch.onlinelibrary.wiley.com/doi/abs/10.1049/iet-opt.2018.5157> (see page 11).
- [35] Z. Zhou, S. Wen, and W. Guan, **RSE-based optical camera communication in underwater scenery with bubble degradation**, in *Optical Fiber Communication Conference (OFC) 2021*, Optica Publishing Group, 2021, M2B.2. DOI: [10.1364/OFC.2021.M2B.2](https://doi.org/10.1364/OFC.2021.M2B.2). [Online]. Available: <http://opg.optica.org/abstract.cfm?URI=OFC-2021-M2B.2> (see page 11).
- [36] E. Eso, A. Burton, N. B. Hassan, M. M. Abadi, Z. Ghassemlooy, and S. Zvanovec, **Experimental investigation of the effects of fog on optical camera-based VLC for a vehicular environment**, in *2019 15th International Conference on Telecommunications (ConTEL)*, 2019, 1–5. DOI: [10.1109/ConTEL.2019.8848552](https://doi.org/10.1109/ConTEL.2019.8848552) (see page 11).
- [37] V. Matus, E. Eso, S. R. Teli, R. Perez-Jimenez, and S. Zvanovec, **Experimentally derived feasibility of optical camera communications under turbulence and fog conditions**, *Sensors*, vol. 20: no. 3, ISSN: 1424-8220. DOI: [10.3390/s20030757](https://doi.org/10.3390/s20030757). [Online]. Available: <https://www.mdpi.com/1424-8220/20/3/757> (see page 11).
- [38] V. Matus, S. R. Teli, V. Guerra, C. Jurado-Verdu, S. Zvanovec, and R. Perez-Jimenez, **Evaluation of fog effects on optical camera communications link**, in *2020 3rd West Asian Symposium on Optical and Millimeter-wave Wireless Communication (WASOWC)*, 2020, 1–5. DOI: [10.1109/WASOWC49739.2020.9410076](https://doi.org/10.1109/WASOWC49739.2020.9410076) (see page 11).

- [39] V. Matus, V. Guerra, S. Zvanovec, J. Rabadan, and R. Perez-Jimenez, **Sandstorm effect on experimental optical camera communication**, *Appl. Opt.*, vol. 60: no. 1, 75–82. DOI: 10.1364/AO.405952. [Online]. Available: <http://opg.optica.org/ao/abstract.cfm?URI=ao-60-1-75> (see page 11).
- [40] V. Matus, V. Guerra, C. Jurado-Verdu, S. Zvanovec, and R. Perez-Jimenez, **Wireless sensor networks using sub-pixel optical camera communications: Advances in experimental channel evaluation**, *Sensors*, vol. 21: no. 8, ISSN: 1424-8220. DOI: 10.3390/s21082739. [Online]. Available: <https://www.mdpi.com/1424-8220/21/8/2739> (see page 11).
- [41] C. Jurado-Verdu, V. Matus, J. Rabadan, V. Guerra, and R. Perez-Jimenez, **Correlation-based receiver for optical camera communications**, *Opt. Express*, vol. 27: no. 14, 19150–19155. DOI: 10.1364/OE.27.019150. [Online]. Available: <http://www.opticsexpress.org/abstract.cfm?URI=oe-27-14-19150> (see page 12).
- [42] N. Bani Hassan, Z. Ghassemlooy, S. Zvanovec, M. Biagi, A. M. Vegni, M. Zhang, and P. Luo, **Non-line-of-sight MIMO space-time division multiplexing visible light optical camera communications**, *Journal of Lightwave Technology*, vol. 37: no. 10, 2409–2417, ISSN: 1558-2213. DOI: 10.1109/JLT.2019.2906097 (see page 12).
- [43] O. I. Younus, N. Bani Hassan, Z. Ghassemlooy, P. A. Haigh, S. Zvanovec, L. N. Alves, and H. L. Minh, **Data rate enhancement in optical camera communications using an artificial neural network equaliser**, *IEEE Access*, vol. 8, 42656–42665. DOI: 10.1109/ACCESS.2020.2976537 (see page 12).
- [44] W. Huang, P. Tian, and Z. Xu, **Design and implementation of a real-time CIM-MIMO optical camera communication system**, *Opt. Express*, vol. 24: no. 21, 24567–24579. DOI: 10.1364/OE.24.024567. [Online]. Available: <http://www.opticsexpress.org/abstract.cfm?URI=oe-24-21-24567> (see page 12).
- [45] P. Luo, M. Zhang, Z. Ghassemlooy, H. Le Minh, H.-M. Tsai, X. Tang, L. C. Png, and D. Han, **Experimental demonstration of RGB LED-based optical camera communications**, *IEEE Photonics Journal*, vol. 7: no. 5, 1–12. DOI: 10.1109/JPHOT.2015.2486680 (see page 12).
- [46] W. J. Ryu and S. Y. Shin, **RGB MIMO optical camera communication with histogram equalization**, in *2017 International Conference on Signals and Systems (ICSigSys)*, 2017, 303–307. DOI: 10.1109/ICSIGSYS.2017.7967061 (see page 12).
- [47] C. Jurado-Verdu, V. Guerra, J. Rabadan, R. Perez-Jimenez, and P. Chavez-Burbano, **RGB synchronous VLC modulation scheme for OCC**, in *2018 11th International Symposium on Communication Systems, Networks Digital Signal Processing (CSNDSP)*, 2018, 1–6. DOI: 10.1109/CSNDSP.2018.8471829 (see page 12).
- [48] S.-H. Chen and C.-W. Chow, **Color-shift keying and code-division multiple-access transmission for RGB-LED visible light communications using mobile phone camera**, *IEEE Photonics Journal*, vol. 6: no. 6, 1–6. DOI: 10.1109/JPHOT.2014.2374612 (see page 12).
- [49] H.-W. Chen, S.-S. Wen, X.-L. Wang, M.-Z. Liang, M.-Y. Li, Q.-C. Li, and Y. Liu, **Color-shift keying for optical camera communication using a rolling shutter mode**, *IEEE Photonics Journal*, vol. 11: no. 2, 1–8. DOI: 10.1109/JPHOT.2019.2898909 (see page 12).
- [50] Y. Onodera, H. Takano, Y. Nakayama, and D. Hisano, **Adaptive n+1 color shift keying for optical camera communication**, in *2021 IEEE 94th Vehicular Technology Conference (VTC2021-Fall)*, 2021, 1–5. DOI: 10.1109/VTC2021-Fall52928.2021.9625283 (see page 12).
- [51] P. Das, B.-Y. Kim, Y. Park, and K.-D. Kim, **A new color space based constellation diagram and modulation scheme for color independent VLC**, *Advances in Electrical and Computer Engineering*, vol. 12, 11–18, ISSN: 1582-7445. DOI: 10.4316/AECE.2012.04002. [Online]. Available: <http://www.aece.ro/abstractplus.php?year=2012&number=4&article=2> (see page 12).
- [52] T.-H. Kwon, K.-S. An, P. P. Banik, and K.-D. Kim, **Wearable visual-mimo for healthcare applications**, in *2019 1st International Conference on Advances in Science, Engineering and Robotics Technology (ICASERT)*, 2019, 1–4. DOI: 10.1109/ICASERT.2019.8934600 (see page 12).

- [53] N. T. Le, M. A. Hossain, and Y. M. Jang, **A survey of design and implementation for optical camera communication**, *Signal Processing: Image Communication*, vol. 53, 95–109, ISSN: 0923-5965. DOI: <https://doi.org/10.1016/j.image.2017.02.001>. [Online]. Available: <https://www.sciencedirect.com/science/article/pii/S0923596517300188> (see pages 13, 20).
- [54] H.-T. Chen, D.-Y. Lin, S.-C. Tan, and S. Y. Hui, **Chromatic, photometric and thermal modeling of LED systems with nonidentical LED devices**, *IEEE Transactions on Power Electronics*, vol. 29: no. 12, 6636–6647. DOI: [10.1109/TPEL.2014.2302453](https://doi.org/10.1109/TPEL.2014.2302453) (see page 14).
- [55] P. S. Almeida, V. C. Bender, H. A. C. Braga, M. A. Dalla Costa, T. B. Marchesan, and J. M. Alonso, **Static and dynamic photoelectrothermal modeling of LED lamps including low-frequency current ripple effects**, *IEEE Transactions on Power Electronics*, vol. 30: no. 7, 3841–3851. DOI: [10.1109/TPEL.2014.2340352](https://doi.org/10.1109/TPEL.2014.2340352) (see page 14).
- [56] X. Shen, H. Chen, J. Lin, Y. Li, H. Lin, J. Chen, and C. Chen, **Analysis and modeling of optical and thermal properties of phosphor converted white light emitting diode**, *IEEE Access*, vol. 7, 118679–118689. DOI: [10.1109/ACCESS.2019.2936593](https://doi.org/10.1109/ACCESS.2019.2936593) (see page 14).
- [57] S. Y. Hui, A. T. L. Lee, and S.-C. Tan, **New dynamic photo-electro-thermal modeling of light-emitting diodes with phosphor coating as light converter part I: Theory, analysis, and modeling**, *IEEE Journal of Emerging and Selected Topics in Power Electronics*, vol. 8: no. 1, 771–779. DOI: [10.1109/JESTPE.2018.2889118](https://doi.org/10.1109/JESTPE.2018.2889118) (see page 14).
- [58] M. E. Raypah, M. Devarajan, and F. Sulaiman, **Influence of injection current and ambient temperature on intensity and wavelength of low-power SMD LED**, in *2016 IEEE 37th International Electronics Manufacturing Technology (IEMT) 18th Electronics Materials and Packaging (EMAP) Conference*, 2016, 1–6. DOI: [10.1109/IEMT.2016.7761989](https://doi.org/10.1109/IEMT.2016.7761989) (see page 14).
- [59] M. E. Raypah, B. K. Sodipo, M. Devarajan, and F. Sulaiman, **Estimation of luminous flux and luminous efficacy of low-power SMD LED as a function of injection current and ambient temperature**, *IEEE Transactions on Electron Devices*, vol. 63: no. 7, 2790–2795. DOI: [10.1109/TED.2016.2556079](https://doi.org/10.1109/TED.2016.2556079) (see page 14).
- [60] S. Muthu, F. J. Schuurmans, and M. D. Pashley, **Red, green, and blue LED based white light generation: Issues and control**, in, vol. 1, 2002, 327–333. DOI: [10.1109/ias.2002.1044108](https://doi.org/10.1109/ias.2002.1044108) (see page 14).
- [61] G. S. Spagnolo, D. Papalillo, and A. Martocchia, **LED applications in railway signals: Wavelength and intensity vs temperature variation**, *Journal of Transportation Technologies*, vol. 02, 78–83, ISSN: 2160-0473. DOI: [10.4236/jtts.2012.21010](https://doi.org/10.4236/jtts.2012.21010) (see page 14).
- [62] N. Narendran, Y. Gu, J. Freyssonier, H. Yu, and L. Deng, **Solid-state lighting: Failure analysis of white LEDs**, *Journal of Crystal Growth*, vol. 268: no. 3, ICMAT 2003, Symposium H, Compound Semiconductors in Electronic and Optoelectronic Applications, 449–456, ISSN: 0022-0248. DOI: <https://doi.org/10.1016/j.jcrysgr.2004.04.071>. [Online]. Available: <https://www.sciencedirect.com/science/article/pii/S0022024804004907> (see page 14).
- [63] A. M. Muslu, B. Ozluk, E. Tamdogan, and M. Arik, **Impact of junction temperature over forward voltage drop for red, blue and green high power light emitting diode chips**, in *2017 16th IEEE Intersociety Conference on Thermal and Thermomechanical Phenomena in Electronic Systems (ITherm)*, 2017, 1011–1019. DOI: [10.1109/ITHERM.2017.7992599](https://doi.org/10.1109/ITHERM.2017.7992599) (see page 14).
- [64] B. Lu, Y. Wang, B. R. Hyun, H. C. Kuo, and Z. Liu, **Color difference and thermal stability of flexible transparent InGaN/GaN multiple quantum wells mini-LED arrays**, *IEEE Electron Device Letters*, vol. 41, 1040–1043, ISSN: 15580563. DOI: [10.1109/LED.2020.2994143](https://doi.org/10.1109/LED.2020.2994143) (see page 14).
- [65] N. Narendran and Y. Gu, **Life of LED-based white light sources**, *Journal of Display Technology*, vol. 1: no. 1, 167–171. DOI: [10.1109/JDT.2005.852510](https://doi.org/10.1109/JDT.2005.852510) (see page 14).
- [66] A. Andonova, R. Yordanov, and I. Yordanova, **Thermal stability analysis of power LED during aging**, in *Proceedings of the 2011 34th International Spring Seminar on Electronics Technology (ISSE)*, 2011, 274–278. DOI: [10.1109/ISSE.2011.6053872](https://doi.org/10.1109/ISSE.2011.6053872) (see page 14).

- [67] C.-J. Chan, F.-M. Hsu, Y.-F. Su, and K.-N. Chiang, **Study on current and junction temperature stress aging effect for accelerated aging test of light emitting diodes**, in *2016 International Conference on Electronics Packaging (ICEP)*, 2016, 62–65. DOI: [10.1109/ICEP.2016.7486783](https://doi.org/10.1109/ICEP.2016.7486783) (see page 14).
- [68] V. Becirovic, V. Helac, B. Arslanagic, and H. Samic, **Effects on LEDs during the accelerated ageing test**, in *2019 18th International Symposium INFOTEH-JAHORINA (INFOTEH)*, 2019, 1–6. DOI: [10.1109/INFOTEH.2019.8717756](https://doi.org/10.1109/INFOTEH.2019.8717756) (see page 14).
- [69] S. M. Jameel, A. Rehman Gilal, S. S. Hussain Rizvi, M. Rehman, and M. A. Hashmani, **Practical implications and challenges of multispectral image analysis**, in *2020 3rd International Conference on Computing, Mathematics and Engineering Technologies (iCoMET)*, 2020, 1–5. DOI: [10.1109/iCoMET48670.2020.9073821](https://doi.org/10.1109/iCoMET48670.2020.9073821) (see page 15).
- [70] R. Qureshi, M. Uzair, K. Khurshid, and H. Yan, **Hyperspectral document image processing: Applications, challenges and future prospects**, *Pattern Recognition*, vol. 90, 12–22, ISSN: 0031-3203. DOI: <https://doi.org/10.1016/j.patcog.2019.01.026>. [Online]. Available: <https://www.sciencedirect.com/science/article/pii/S0031320319300366> (see page 15).
- [71] L. Windrim, A. J. Carnegie, M. Webster, and M. Bryson, **Tree detection and health monitoring in multispectral aerial imagery and photogrammetric pointclouds using machine learning**, *IEEE Journal of Selected Topics in Applied Earth Observations and Remote Sensing*, vol. 13, 2554–2572. DOI: [10.1109/JSTARS.2020.2995391](https://doi.org/10.1109/JSTARS.2020.2995391) (see page 15, 16).
- [72] R. T. S., J. Brema Karunya, and G. J. John Wessley, **A novel remote sensing based approach to estimate the water quality index using sentinel-2 multispectral data**, in *2022 International Conference on Smart Technologies and Systems for Next Generation Computing (ICSTSN)*, 2022, 1–4. DOI: [10.1109/ICSTSN53084.2022.9761360](https://doi.org/10.1109/ICSTSN53084.2022.9761360) (see page 15).
- [73] J. Marcello, D. Rodríguez-Esparragón, and D. Moreno, **Comparison of land cover maps using high resolution multispectral and hyperspectral imagery**, in *IGARSS 2018 - 2018 IEEE International Geoscience and Remote Sensing Symposium*, 2018, 7312–7315. DOI: [10.1109/IGARSS.2018.8517878](https://doi.org/10.1109/IGARSS.2018.8517878) (see page 15).
- [74] H. Wilson, B. Boots, and A. Millward, **A comparison of hierarchical and partitional clustering techniques for multispectral image classification**, in *IEEE International Geoscience and Remote Sensing Symposium*, vol. 3, 2002, 1624–1626 vol.3. DOI: [10.1109/IGARSS.2002.1026201](https://doi.org/10.1109/IGARSS.2002.1026201) (see page 15).
- [75] T. Blaschke, **Object based image analysis for remote sensing**, *ISPRS Journal of Photogrammetry and Remote Sensing*, vol. 65: no. 1, 2–16, ISSN: 0924-2716. DOI: <https://doi.org/10.1016/j.isprsjprs.2009.06.004>. [Online]. Available: <https://www.sciencedirect.com/science/article/pii/S0924271609000884> (see page 15).
- [76] V.-E. Neagoe and V. Chirila-Berbentea, **A novel approach for semi-supervised classification of remote sensing images using a clustering-based selection of training data according to their GMM responsibilities**, in *2017 IEEE International Geoscience and Remote Sensing Symposium (IGARSS)*, 2017, 4730–4733. DOI: [10.1109/IGARSS.2017.8128058](https://doi.org/10.1109/IGARSS.2017.8128058) (see page 15).
- [77] M. W. Vannier, R. L. Butterfield, D. Jordan, W. A. Murphy, R. G. Levitt, and M. Gado, **Multispectral analysis of magnetic resonance images**. *Radiology*, vol. 154, 221–224, ISSN: 0033-8419. DOI: [10.1148/radiology.154.1.3964938](https://doi.org/10.1148/radiology.154.1.3964938). [Online]. Available: <http://pubs.rsna.org/doi/10.1148/radiology.154.1.3964938> (see page 16).
- [78] T. Taxt and A. Lundervold, **Multispectral analysis of the brain in magnetic resonance imaging**, in *Proceedings of IEEE Workshop on Biomedical Image Analysis*, 1994, 33–42. DOI: [10.1109/BIA.1994.315868](https://doi.org/10.1109/BIA.1994.315868) (see page 16).
- [79] F. Meriaudeau, V. Paquit, N. Walter, J. Price, and K. Tobin, **3D and multispectral imaging for subcutaneous veins detection**, in *2009 16th IEEE International Conference on Image Processing (ICIP)*, 2009, 2857–2860. DOI: [10.1109/ICIP.2009.5414511](https://doi.org/10.1109/ICIP.2009.5414511) (see page 16).

- [80] P. A. Bautista and Y. Yagi, **Digital staining for histopathology multispectral images by the combined application of spectral enhancement and spectral transformation**, in *2011 Annual International Conference of the IEEE Engineering in Medicine and Biology Society*, 2011, 8013–8016. DOI: [10.1109/IEMBS.2011.6091976](https://doi.org/10.1109/IEMBS.2011.6091976) (see page 16).
- [81] D. C. Liyanage, M. Tamre, and R. Hudjakov, “Hyperspectral/multispectral imaging methods for quality control,” in *Handbook of Research on New Investigations in Artificial Life, AI, and Machine Learning*, IGI Global, 2022, 438–461. DOI: [10.4018/978-1-7998-8686-0.ch017](https://doi.org/10.4018/978-1-7998-8686-0.ch017) (see page 16).
- [82] I. Moscol, G. Peltroche, V. Ruesta, and J. Sanchez, **Prediction of the main quality parameters of fishmeal to automate the drying process using hyperspectral imaging and artificial neural networks**, in *2020 IEEE Engineering International Research Conference (EIRCON)*, 2020, 1–4. DOI: [10.1109/EIRCON51178.2020.9254070](https://doi.org/10.1109/EIRCON51178.2020.9254070) (see page 16).
- [83] F. Gruber, P. Wollmann, B. Schumm, W. Grählert, and S. Kaskel, **Quality control of slot-die coated aluminum oxide layers for battery applications using hyperspectral imaging**, *Journal of Imaging*, vol. 2: no. 2, ISSN: 2313-433X. DOI: [10.3390/jimaging2020012](https://doi.org/10.3390/jimaging2020012). [Online]. Available: <https://www.mdpi.com/2313-433X/2/2/12> (see page 16).
- [84] S. Singh, P. Pandey, M. S. Khan, and M. Semwal, **Multi-temporal high resolution unmanned aerial vehicle (UAV) multispectral imaging for menthol mint crop monitoring**, in *2021 6th International Conference for Convergence in Technology (I2CT)*, 2021, 1–4. DOI: [10.1109/I2CT51068.2021.9418204](https://doi.org/10.1109/I2CT51068.2021.9418204) (see page 16).
- [85] S. Debnath, M. Paul, D. M. M. Rahaman, T. Debnath, L. Zheng, T. Baby, L. M. Schmidtke, and S. Y. Rogiers, **Identifying individual nutrient deficiencies of grapevine leaves using hyperspectral imaging**, *Remote Sensing*, vol. 13: no. 16, ISSN: 2072-4292. DOI: [10.3390/rs13163317](https://doi.org/10.3390/rs13163317). [Online]. Available: <https://www.mdpi.com/2072-4292/13/16/3317> (see page 16).
- [86] Y. Wu, X. Li, Q. Zhang, X. Zhou, H. Qiu, and P. Wang, **Recognition of spider mite infestations in jujube trees based on spectral-spatial clustering of hyperspectral images from UAVs**, *Frontiers in plant science*, vol. 14, 1078676. DOI: [10.3389/fpls.2023.1078676](https://doi.org/10.3389/fpls.2023.1078676) (see page 16).
- [87] S. Hazratov and G. Bilgin, **Mitosis detection in multispectral histopathological images with deep learning**, in *2019 Medical Technologies Congress (TIPTEKNO)*, 2019, 1–4. DOI: [10.1109/TIPTEKNO.2019.8894914](https://doi.org/10.1109/TIPTEKNO.2019.8894914) (see page 16).
- [88] A. Ozdemir and K. Polat, **Deep learning applications for hyperspectral imaging: A systematic review**, *Journal of the Institute of Electronics and Computer*, vol. 2, 39–56, ISSN: 26438240. DOI: [10.33969/JIEC.2020.21004](https://doi.org/10.33969/JIEC.2020.21004). [Online]. Available: <https://iecsce.org/jpapers/49> (see page 16).
- [89] J. Torres-Tello and S.-B. Ko, **Identifying useful features in multispectral images with deep learning for optimizing wheat yield prediction**, in *2021 IEEE International Symposium on Circuits and Systems (ISCAS)*, 2021, 1–5. DOI: [10.1109/ISCAS51556.2021.9401360](https://doi.org/10.1109/ISCAS51556.2021.9401360) (see page 16).
- [90] A. Ren, H. Wang, W. Zhang, J. Wu, Z. Wang, R. V. Penty, and I. H. White, **Emerging light-emitting diodes for next-generation data communications**, *Nature Electronics*, vol. 4: no. 8, 559–572. DOI: [10.1038/s41928-021-00624-7](https://doi.org/10.1038/s41928-021-00624-7). [Online]. Available: <https://doi.org/10.1038/s41928-021-00624-7> (see page 17).
- [91] Toshiba Electronic Devices & Storage Corporation, *Basic knowledge of discrete semiconductor device. Chapter V: Optical semiconductors isolators/solid state relays*, Feb. 2022. [Online]. Available: <https://toshiba.semicon-storage.com/ap-en/semiconductor/knowledge/e-learning/discrete/chap5/chap5-3.html> (see page 17).
- [92] Y. Varshni, **Temperature dependence of the energy gap in semiconductors**, *Physica*, vol. 34: no. 1, 149–154, ISSN: 0031-8914. DOI: [https://doi.org/10.1016/0031-8914\(67\)90062-6](https://doi.org/10.1016/0031-8914(67)90062-6). [Online]. Available: <https://www.sciencedirect.com/science/article/pii/0031891467900626> (see page 18).

- [93] J. Bullough, **Lighting answers: LED lighting systems**, *National Lighting Product Information Program, Lighting Research Center*, vol. 7: no. 3 (see page 18).
- [94] Y. Yang, W. Lien, Y. Huang, and N. Chen, **Junction temperature measurement of light-emitting diodes by voltage-temperature relation method**, in *2007 Conference on Lasers and Electro-Optics - Pacific Rim*, 2007, 1–2. DOI: [10.1109/CLEOPR.2007.4391713](https://doi.org/10.1109/CLEOPR.2007.4391713) (see page 18).
- [95] E. F. Schubert, **Light-Emitting Diodes**, 2nd ed. Cambridge University Press, 2006. DOI: [10.1017/CBO9780511790546](https://doi.org/10.1017/CBO9780511790546) (see page 18).
- [96] C. Negrea, P. Svasta, and M. Rangu, **Electro-thermal modeling of power LED using SPICE circuit solver**, in *2012 35th International Spring Seminar on Electronics Technology*, 2012, 329–334. DOI: [10.1109/ISSE.2012.6273096](https://doi.org/10.1109/ISSE.2012.6273096) (see page 18).
- [97] X. He, Y. Liu, K. Ganesan, A. Ahnood, P. Beckett, F. Eftekhari, D. Smith, M. H. Uddin, E. Skafidas, A. Nirmalathas, and R. R. Unnithan, **A single sensor based multispectral imaging camera using a narrow spectral band color mosaic integrated on the monochrome CMOS image sensor**, *APL Photonics*, vol. 5: no. 4, 046104. DOI: [10.1063/1.5140215](https://doi.org/10.1063/1.5140215). eprint: <https://doi.org/10.1063/1.5140215>. [Online]. Available: <https://doi.org/10.1063/1.5140215> (see page 20).
- [98] Y. S. Hussein, M. Y. Alias, and A. A. Abdulkafi, **On performance analysis of LS and MMSE for channel estimation in VLC systems**, in *2016 IEEE 12th International Colloquium on Signal Processing Its Applications (CSPA)*, 2016, 204–209. DOI: [10.1109/CSPA.2016.7515832](https://doi.org/10.1109/CSPA.2016.7515832) (see page 23).
- [99] A. Anusree and R. K. Jeyachitra, **Performance analysis of a MIMO VLC (visible light communication) using different equalizers**, in *2016 International Conference on Wireless Communications, Signal Processing and Networking (WiSPNET)*, 2016, 43–46. DOI: [10.1109/WiSPNET.2016.7566085](https://doi.org/10.1109/WiSPNET.2016.7566085) (see page 23).
- [100] M. K. Jha, N. Kumar, and Y. V. S. Lakshmi, **NOMA MIMO visible light communication with ZF-SIC and MMSE-SIC**, in *2020 2nd PhD Colloquium on Ethically Driven Innovation and Technology for Society (PhD EDITS)*, 2020, 1–2. DOI: [10.1109/PhDEDITS51180.2020.9315316](https://doi.org/10.1109/PhDEDITS51180.2020.9315316) (see page 23).
- [101] T.-A. Tran and D. C. O'Brien, **Performance metrics for multi-input multi-output (MIMO) visible light communications**, in *2012 International Workshop on Optical Wireless Communications (IWOW)*, 2012, 1–3. DOI: [10.1109/IWOW.2012.6349684](https://doi.org/10.1109/IWOW.2012.6349684) (see page 24).
- [102] D. Xu and Y. Tian, **A comprehensive survey of clustering algorithms**, *Annals of Data Science*, vol. 2: no. 2, 165–193. DOI: [10.1007/s40745-015-0040-1](https://doi.org/10.1007/s40745-015-0040-1) (see page 24).
- [103] Spectral Products, *SM242/SM442 preconfigured CCD spectrometer - Spectral Products*. [Online]. Available: https://www.spectralproducts.com/SM242_442/1776 (see page 28).
- [104] Gigahertz-Optik, *BTS256-LED*. [Online]. Available: <https://www.gigahertz-optik.com/en-us/product/bts256-led/> (see page 28).
- [105] edevis, *edevis® - Thermography - Infrared Camera - A-Series*. [Online]. Available: http://irndt.de/en/thermography_camera_A6xx_series.php (see page 28).
- [106] SILIOS Technologies, *Compact snapshot multispectral cameras*. [Online]. Available: <https://www.silios.com/cms-cameras> (see page 28).
- [107] D. Moreno, J. Rufo, V. Guerra, J. Rabadan, and R. Perez-Jimenez, **Effect of temperature on channel compensation in optical camera communication**, *Electronics*, vol. 10: no. 3, ISSN: 2079-9292. DOI: [10.3390/electronics10030262](https://doi.org/10.3390/electronics10030262). [Online]. Available: <https://www.mdpi.com/2079-9292/10/3/262> (see pages 33, 68).
- [108] D. Moreno, J. Rufo, V. Guerra, J. Rabadan, and R. Perez-Jimenez, **Optical multispectral camera communications using LED spectral emission variations**, *IEEE Photonics Technology Letters*, vol. 33: no. 12, 591–594. DOI: [10.1109/LPT.2021.3078842](https://doi.org/10.1109/LPT.2021.3078842) (see pages 55, 60, 67).

- [109] D. Moreno, V. Guerra, J. Rufo, J. Rabadan, and R. Perez-Jimenez, **Clustering-based data detection for spectral signature multiplexing in multispectral camera communication**, *Opt. Lett.*, vol. 47: no. 5, 1053–1056. DOI: 10.1364/OL.449207. [Online]. Available: <http://opg.optica.org/ol/abstract.cfm?URI=ol-47-5-1053> (see pages 60, 65, 67).
- [110] D. Moreno, B. Majlesein, J. Rufo, V. Guerra, J. Rabadan, and R. Perez-Jimenez, **Thermally-induced spectral variations of LED applied to optical multispectral camera communications**, in *2020 12th International Symposium on Communication Systems, Networks and Digital Signal Processing (CSNDSP)*, 2020, 1–6. DOI: 10.1109/CSNDSP49049.2020.9249518 (see page 65).
- [111] D. Moreno, B. Majlesein, V. Guerra, J. Rufo, J. Rabadan, and R. Perez-Jimenez, **Comparison of clustering algorithms for data detection in multispectral camera communication**, in *2022 4th West Asian Symposium on Optical and Millimeter-wave Wireless Communications (WASOWC)*, 2022, 1–5. DOI: 10.1109/WASOWC54657.2022.9798432 (see page 65).
- [112] D. Moreno, V. Guerra, J. Rufo, J. Rabadan, and R. Perez-Jimenez, **Spectral signature multiplexing in multispectral camera communication**, in *2022 13th International Symposium on Communication Systems, Networks and Digital Signal Processing (CSNDSP)*, 2022, 515–520. DOI: 10.1109/CSNDSP54353.2022.9907907 (see pages 65, 107).
- [113] United Nations Department of Economic and Social Affairs, Population Division, **World population prospects 2022: Summary of results**, 2022 (see page 69).
- [114] M. Guo, P. Zhang, Y. Sun, W. Zhang, Y. Zhou, and Y. Yang, **Object recognition in optical camera communication enabled by image restoration**, *Opt. Express*, vol. 30: no. 20, 37026–37037. DOI: 10.1364/OE.467659. [Online]. Available: <https://opg.optica.org/oe/abstract.cfm?URI=oe-30-20-37026> (see page 72).
- [115] A. Mederos-Barrera, C. Jurado-Verdu, V. Guerra, J. Rabadan, and R. Perez-Jimenez, **Design and experimental characterization of a discovery and tracking system for optical camera communications**, *Sensors*, vol. 21: no. 9, ISSN: 1424-8220. DOI: 10.3390/s21092925. [Online]. Available: <https://www.mdpi.com/1424-8220/21/9/2925> (see page 72).
- [116] D. Moreno, V. Guerra, J. Rufo, J. Rabadan, and R. Perez-Jimenez, **Multispectral optical camera communication links based on spectral signature multiplexing**, *IET Optoelectronics*, vol. 17: no. 4, 91–100. DOI: <https://doi.org/10.1049/ote2.12090>. eprint: <https://ietresearch.onlinelibrary.wiley.com/doi/pdf/10.1049/ote2.12090>. [Online]. Available: <https://ietresearch.onlinelibrary.wiley.com/doi/abs/10.1049/ote2.12090> (see page 107).

This appendix chapter includes the works presented by the author in conference proceedings during the development of this thesis. In the following pages, the camera-ready full papers are attached.

Thermally-induced Spectral Variations of LED applied to Optical Multispectral Camera Communications

Daniel Moreno, Behnaz Majlesein, Julio Rufo, Victor Guerra, Jose Rabadan, Rafael Perez-Jimenez

Photonic Technology and Communications

IDeTIC

Las Palmas de Gran Canaria, Spain

dmoreno, bmajlesein, jrufu, vguerra, jrabadan, rperez@idetic.eu

Abstract—Optical Camera Communication (OCC) applications have intensively risen in recent years. This work proposes using a multispectral or hyperspectral camera as an OCC receiver to take advantage of the high spectral resolution of this type of device with respect to conventional cameras. Furthermore, spectral features of the LEDs, usually used as transmitters in OCC, are affected by temperature. Hence, one of the goals of this work is to benefit from those spectral variations that will be grasped by the multispectral camera and thus achieve a new data channel. Therefore, different communication channels could be obtained from a single light source.

Index Terms—OCC, multispectral, hyperspectral, LED, temperature dependence, peak wavelength

I. INTRODUCTION

IN the last few years, there has been a rapid rise in the use of Optical Camera Communication (OCC). It is foreseen that significant advancement in this technology will be implemented increasingly soon thanks to the massive presence of optical cameras in consumer electronic devices such as smartphones, tablets and laptops. What is more, OCC has been added as an extension of IEEE 802.15.7 standard on Visible Light Communications (VLC) [1]. This technology used a camera or an image sensor to receive data from a light source. The sensor scanning is based on two different modes. On the one hand, global shutter exposes every pixel per frame simultaneously. Moreover, it can only detect waveforms with bandwidths below half the frame rate. On the other hand, rolling shutter scans the image sequentially. Besides, this mode allows higher speed communication because the optical source's waveform can be captured within a single frame [2]. Nevertheless, the maximum obtainable speed is dependent on the projected size of the light source, as OCC is based on image-forming optics [3]. OCC has been proposed as a suitable technology in applications such as the Internet of Things (IoT), Vehicular Communication, and Indoor Positioning Systems (IPS). Positioning accuracy of OCC-based IPS is within the centimeter range [4], [5], outperforming any RF-based positioning technique. Vehicle-to-Anything (V2X) is another promising application field of OCC due to the uprising presence of vehicle-

mounted optical cameras (generally used for surveillance and security).

Apart from this, regarding the camera used as a receiver in OCC, in this technology has been employed several types of cameras such as Single-Lens Reflex (SLR) cameras [6] or smartphones [7]. In all the cases mentioned above, the devices are used to take pictures and videos within the visible range. Their image sensor only permits the capture of RGB images at most, similar to the human eye. However, multispectral cameras (and hyperspectral cameras) can capture a higher number of communication bands than the RGB bands provided by conventional cameras. These have been used in different sectors such as remote sensing [8], agriculture [9] or biotechnology [10]. In this manner, Optical Multispectral Camera Communication (OMCC) would offer a wide range of opportunities.

Furthermore, the behavior of the Light-Emitting Diodes (LEDs) varies depending on temperature. Some of the characteristics affected are emitted wavelength and luminosity. This work analyzes the LED spectral variations caused by heat. The use of a multispectral (or hyperspectral) camera, which has a high spectral resolution, is proposed to take advantage of this typically considered harmful effect. It is expected to get various independent communication channels using a single sort of transmitter, which would lessen the complexity and cost of the system. On the other hand, although this type of camera has a low sampling rate, there are techniques such as spectral signatures extraction to distinguish particular signals at different wavelengths that would improve its performance.

This paper is divided into six sections. Section II gives a brief overview of the theoretical background on which the work is based. The characterization methodology and the results concerning the temperature effects on the used LED devices are presented in Sections III and IV, respectively. In Section V, the application of this characterization is proposed using a multispectral camera. Lastly, some conclusions are drawn in Section VI.

II. TEMPERATURE DEPENDENCE ON LED WAVELENGTH

The working principle of LED is spontaneous emission of light. That light is emitted when an electron obtains

enough energy to traverse the forbidden energy gap of the semiconductor. Then, a photon is emitted when that electron goes back to a lower energy level. The emitted photon has a wavelength that is related to the energy gap by Equation 1. In addition, the energy gap is affected by the p-n junction temperature, depending on the LED's substrate, which is usually modeled using Equation 2. According to [11], in most semiconductor materials energy gap diminishes as temperature increases. Therefore, as wavelength is inversely proportional to energy gap (Equation 1), the peak wavelength of the LED grows with temperature.

$$E_g = hf = \frac{hc}{\lambda} \quad (1)$$

$$E_g = E_0 - \frac{\alpha T^2}{T + \beta} \quad (2)$$

where h is Planck constant, f is frequency, c is the speed of light in vacuum and λ is wavelength. T is temperature, E_0 is energy gap at 0K temperature condition, and α and β are semiconductor-dependent constants, which are empirically determined.

However, the metallic content in the LED material must be considered. For instance, [12] proved that the band gap might not follow the decrement as the LED heats up, but it may increase with temperature depending on Indium (In) content in InGaN alloys (green and blue LEDs).

Apart from this, spectral width and luminous efficiency are affected by temperature as well. Normally, the conversion efficiency decreases and the spectral width increases as temperature grows [13]. Based on this, it is intended to use a high spectral resolution camera, such as a multispectral camera, to check if these slight wavelength changes in the LED emission are detectable by it. Then, grasping these generally undesired variations, this work proposes improving communications by increasing the number of communication channels.

III. METHODOLOGY

The primary goal of this work is to benefit from the spectral variations that temperature effects on LEDs, so that a multispectral camera detects those changes and finally use it for OCC purposes. To accomplish this objective, RGB LEDs have been characterized by focusing on the effect of temperature on their emitted spectrum. Moreover, a multispectral camera has been used to set a communication link with those LEDs as transmitters. Lastly, spectral responses of the emitters have been extracted from the pictures to evaluate the practicability of Optical Multispectral Camera Communications (OMCC) and the use of the LED wavelength variations induced by temperature.

The LEDs under study (common cathode RGB LED) were driven using currents ranging from 10 mA to 130 mA by an Ethernet-controlled current source to induce them different junction temperatures. Additionally, the temperature was previously stabilized for 5 minutes. This experimental characterization consisted of three different

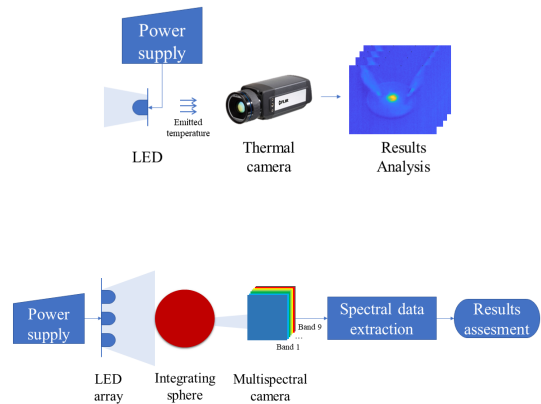


Fig. 1: System setup schemes. Scheme used to get the temperature data (top) and scheme used to get the spectral data (bottom).

processes. Firstly, the junction temperature of the LEDs has been measured by a thermal imaging camera, as shown in Fig. 1 (top). The employed camera was a FLIR A645, whose main features are a pixel resolution of 640 x 480 and a high sensitivity below 50 mK. For each current, the maximum temperature of the LED has been recorded. Secondly, a spectrometer (Spectral Products SM442) has been used to obtain wavelength data of the LED in the visible range. Due to the high intensity of the LED beam, a 15-centimeters ABS-plastic cylinder has been used to distance the LED from the light input, allowing to receive the signal within the dynamic range of the spectrometer. This fix does not affect the measurement, because of the spectrometer is only needed to get the wavelength information of the LED and visualize shape variations (not absolute changes). Finally, the spectral radiant power of the LED in the visible spectral range has been measured using an integrating sphere and a light meter (Gigahertz BTS256). This device also permits to acquire spectral information; however, the spectrometer provided a better spectral resolution (1 nm vs. 5 nm).

After the LEDs' characterization, the aim was to capture the wavelength variation in the LEDs by a camera. It was needed to have a high spectral resolution camera that can detect the slight variations due to temperature; in this case, a multispectral camera, in order to reach this objective. Specifically, the multispectral camera used was the CMS-C1-C-EVR1M-GigE by SILIOS Technologies. It is a 9-bands camera (8 color narrow bands and 1 panchromatic band) that covers the wavelength range from 400 to 1000 nm. It has a CMOS sensor and a resolution of 1280 (H) x 1024 (V) in the raw picture and 426 (H) x 339 (V) in the spectral pictures. Fig. 1 (bottom) depicts the scheme followed to collect the spectral information of the LED using the multispectral camera. The light beam of these LEDs passes through an integrating sphere that

concentrates it on a narrow point. Then, the multispectral camera receives that beam and a picture is taken. The camera parameters were adjusted so that the acquired image would not be saturated. The pictures have been saved as single-band images in ENVI file format, which includes one header and one file with multispectral data. Finally, the pictures were cropped selecting only the part that contains the emitted light and from these, the spectral signatures were extracted. With the spectral response of the LED at various temperatures, an evaluation can be made of how well the several signals are distinguished by the camera.

IV. CHARACTERIZATION RESULTS

In Fig. 2 is presented some examples of the temperature-time behavior of the RGB LEDs. It depicts an exponential growth which is higher as the driving current increases, such as that the highest temperature was obtained on the blue LED, followed by the green and the red LEDs. It also can be seen that at 10 mA the temperature kept almost constant. As an example, Fig. 3 shows several thermal pictures of the red LED at low and high temperatures. Fig. 4 (top) shows the effects of the induced high temperature on the LED emission, by increasing the polarization current, on the peak wavelengths of each RGB color. Table I details the spectral information in Fig. 4 (top) showing the peak wavelengths and the Full Width at Half Maximum (FWHM) values of each spectrum. It can be seen that by rising the temperature the emitted wavelength grew as expected and, consequently, the peak wavelength shifted. The largest shift was obtained in the red LED with a difference of 21.1 nm between the minimum and the maximum temperature (peak wavelength at 659.6 nm at 27 °C and 680.7 nm at 65 °C). It was followed by a 13.5 nm shift in blue (from 486.1 nm at 28 °C to 499.6 nm at 78 °C). In green, the peak wavelength did not increase with temperature in the same way that red and blue did. In this case, the highest peak wavelength was found at the minimum temperature (547.2 nm, 27 °C). The green source color of the employed LED is made with InGaN on Silicon (Si). As seen in Section II, In content in this alloy can affect in such a way that when the temperature increases the energy gap also grows, so wavelength decreases. In addition to the peak wavelength shift, it is noteworthy how the width changed with the temperature variation. The most striking change was acquired in blue, having a difference between the width at 28 °C and 66 °C of roughly 30 nm. Note that the intensity values were normalized in Fig. 4 (top) because the approach was to analyze only the spectral information.

Fig. 4 (bottom) reports the spectral radiant power of the LED in W/nm. The highest levels were obtained for the blue LED, followed by green and red. It can be noted that at the maximum temperature, when the LED is supplied with 130 mA, the power decreased with respect to the second maximum. As a consequence of that, temperature expectedly affected the efficiency of the LED.

Furthermore, it shows the wavelength variations, as well as the FWHM changes on temperatures.

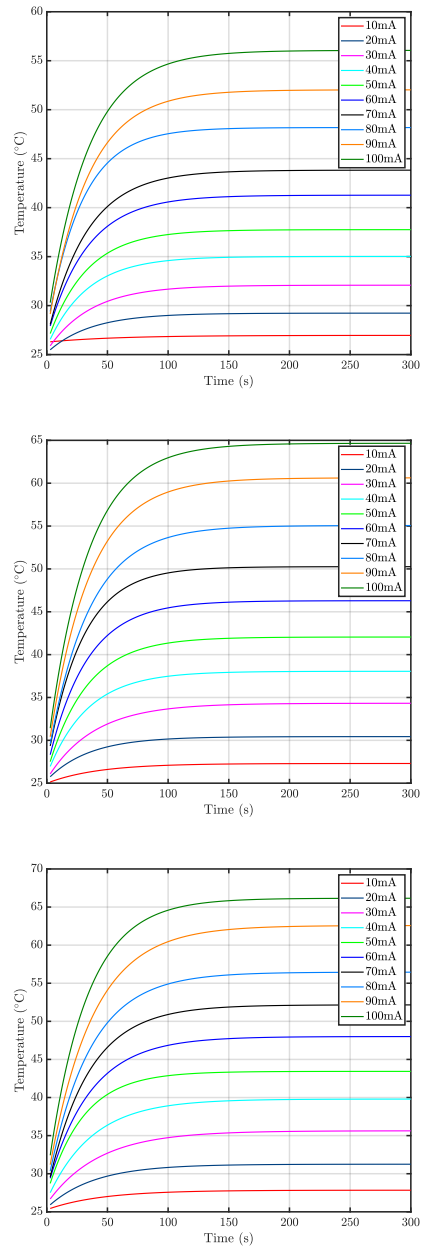


Fig. 2: Temperature behavior of the RGB LED: Red (top), green (middle) and blue (bottom).

V. MULTISPECTRAL CAMERA RESULTS

The images captured by the camera show the spectral variations caused by changing the LED junction temperature. Those changes can be observed in the spectral

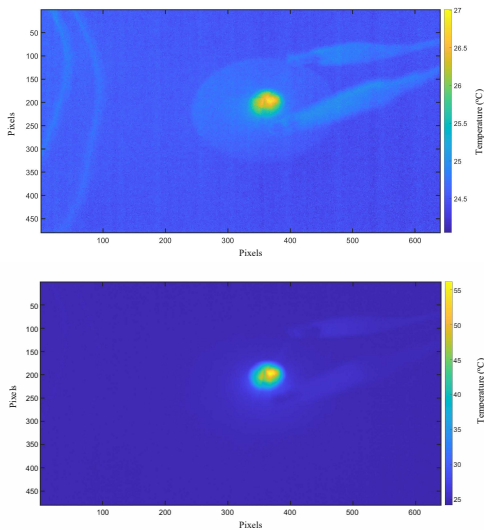


Fig. 3: Examples of images of the red LED driven at different currents, taken by a thermographic camera. LED at 10 mA (top) and LED at 100 mA (bottom).

TABLE I: Spectral information at different temperatures.

LED	Red			
Current (mA)	10 (27 °C)	50 (38 °C)	100 (56 °C)	130 (65 °C)
Peak wavelength (nm)	659.6	663.6	672.5	680.7
FWHM (nm)	8.73	14.97	22.33	24.15

LED	Green			
Current (mA)	10 (27 °C)	50 (42 °C)	100 (65 °C)	130 (76 °C)
Peak wavelength (nm)	547.2	544.9	545.1	546.8
FWHM (nm)	23.73	31.80	40.92	43.18

LED	Blue			
Current (mA)	10 (28 °C)	50 (43 °C)	100 (66 °C)	130 (78 °C)
Peak wavelength (nm)	486.1	486.1	490.5	499.6
FWHM (nm)	16.68	29.62	45.85	32.10

signatures of the LED shown in Fig. 6. As a case in point, Fig. 6 (bottom) depicts the several levels of energy of the blue LED, supplied with various currents (therefore, at different temperatures), with respect to the 9 bands of the multispectral camera. Targeting the bands 1, 2 and 3, centered in 427, 461 and 501 nm, respectively, as the analyzed results were obtained on the blue LED, there are some phenomena to consider. Besides, a high level is placed in band 9, which corresponds to the panchromatic band. However, the focus is not in this band, because the only remarkable consequence is the increase in level due to the increment in current. Firstly, part of the energy captured in the band 1 was captured in the band 2 as temperature grew, causing an increment in the level of this band. The identical happened with bands 2 and 3. It occurred because the peak wavelength of the LED gradually shifted, so the bands 2 and 3, which have an FWHM of the order of 50 nm (see Fig. 5), took more information. Additionally, it is perceptible a growth in level as expected, since the way chosen to raise the temperature is by increasing the driving current, ergo the power of the LED also increases. Figs. 6 (top) and 6

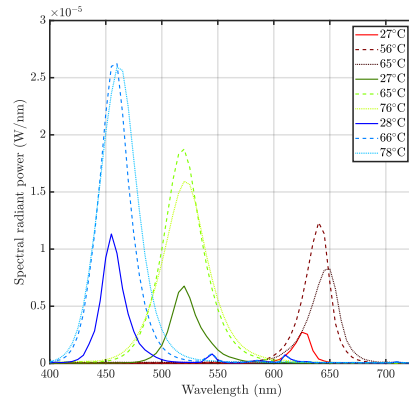
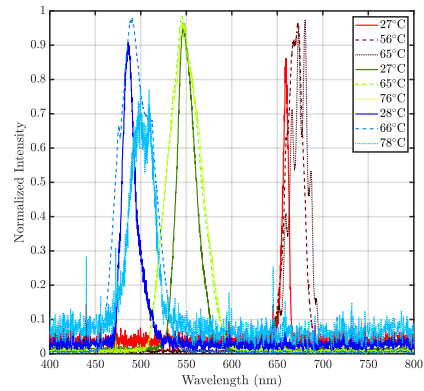


Fig. 4: Characterization of the RGB LED at different temperatures: Normalized RGB LED spectra (top) and spectral radiant power (bottom). Solid line, dashed line, dotted line and dash-dot line correspond to 10 mA, 50 mA, 100 mA and 130 mA, respectively.

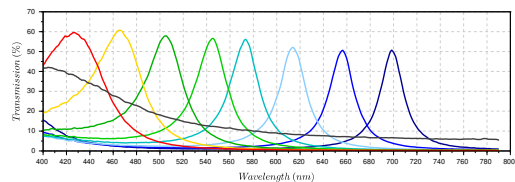


Fig. 5: Filter specifications.

(bottom) depict the spectral signatures of the red and green LED, respectively, showing similar results. These results suggested that several communication channels can be obtained from a single emission source since the slight changes in wavelength are detected by the multispectral camera.

VI. CONCLUSIONS

In this work, several RGB LEDs have been characterized, especially to visualize the effect of the temperature in the wavelength of the emitted light. Furthermore, it has

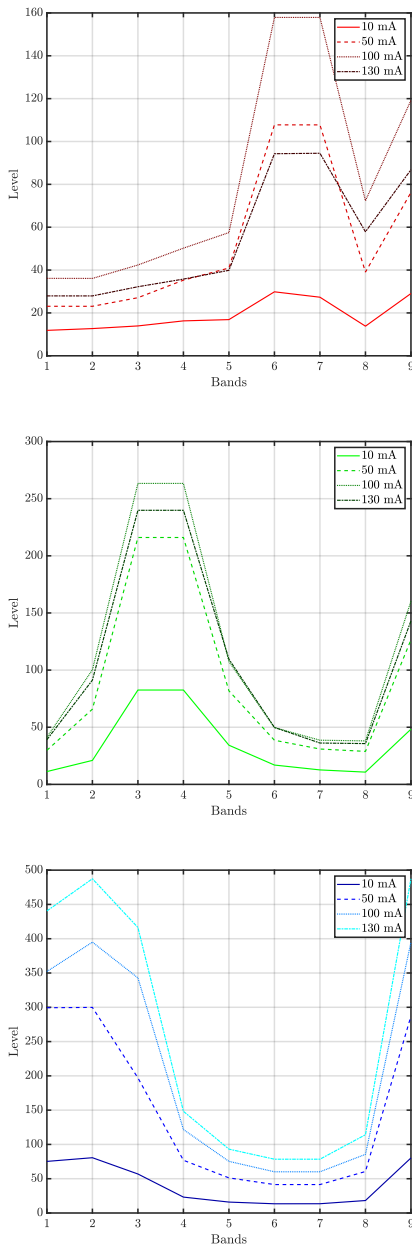


Fig. 6: Spectral signatures of the RGB LED at different temperatures: Red (top), green (middle) and blue (bottom). Solid line, dashed line, dotted line and dash-dot line correspond to 10 mA, 50 mA, 100 mA and 130 mA, respectively.

been utilized a multispectral camera taking pictures of the light beam of the LED and analyzing those wavelength variations. The spectral response of the RGB LEDs has been extracted and how the wavelength shifts have been checked. Therefore, as the spectral changes in the emitted light can be observed by using a multispectral camera, it

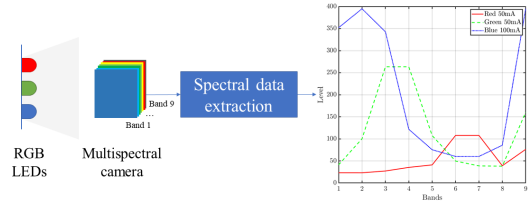


Fig. 7: This figure is an example of a proposed diagram for WDM. By sending three different color signals that are captured by the multispectral camera, after extracting their spectral signatures, each signal could be separated. The same could be performed sending signals of the same color but at different temperatures that shift their spectra and are grasped by the camera.

takes advantage of that phenomenon considered harmful. So, the more variation in the peak wavelength of the LED is affected by temperature, the better. Thus, this paper proposes to use those dissimilarities to create separable communication channels in an OMCC application.

This led us to conclude that employing, for instance, two receivers with two different optical filters, will be feasible to separate each signal by using the same transmitter device. Using the temperature to tune the wavelength of the LED will allow this to be done. It will also be possible to use a camera with enough spectral resolution, such as a multispectral or a hyperspectral camera, which captures the light beam in its several bands with greater or lesser intensity depending on the wavelength shift.

For communication purposes, it would be necessary to do a previous characterization of the transmitters to know how their behavior is affected by the temperature. In this case, the results of this study indicated that the red LED got more considerable spectral variations than green and blue. Moreover, the evidence of this work points towards the idea that temperature effects in emitters, usually considered detrimental, can be detected by high-spectral-resolution cameras and used for applications such as Wavelength Division Multiplexing (WDM) (Fig. 7).

Further studies will focus on the use of different transmitters to compare their performance. Additionally, future work will concentrate on creating a channel matrix in order to numerically demonstrate that those signals from a unique transmitter can be discriminated in separable channels.

ACKNOWLEDGMENT

This work was benefited from the Trainee Predoctoral Research Staff Program (2019) of the Universidad de Las Palmas de Gran Canaria. It has been funded in part by the Canary Islands Regional Government (Project ATICCuA ProID2017010053) and the Spanish Research Administration (MICINN project: OSCAR, ref.: TEC 2017-84065-C3-1-R). It has been funded in part by ENLIGHT'EM European Training Network in Low-Energy Visible Light IoT Systems(Innovative Training Networks (ITN) H2020-MSCA-ITN-2018 grant number 814215).

REFERENCES

- [1] *Short-Range Optical Wireless Communications (802.15.7-2018)*, IEEE Revision of the 802.15.7-2011, Rev. 2018, April 2019.
- [2] Z. Wang, Q. Wang, W. Huang, and Z. Xu, *Visible light communications: Modulation and signal processing*. John Wiley & Sons, 2017.
- [3] C. Jurado-Verdu, V. Matus, J. Rabadan, V. Guerra, and R. Perez-Jimenez, "Correlation-based receiver for optical camera communications," *Opt. Express*, vol. 27, no. 14, pp. 19 150–19 155, Jul 2019. [Online]. Available: <http://www.opticsexpress.org/abstract.cfm?URI=oe-27-14-19150>
- [4] Y. Li, Z. Ghassemlooy, X. Tang, B. Lin, and Y. Zhang, "A vlc smartphone camera based indoor positioning system," *IEEE Photonics Technology Letters*, vol. 30, no. 13, pp. 1171–1174, July 2018.
- [5] J. Xu, C. Gong, and Z. Xu, "Experimental indoor visible light positioning systems with centimeter accuracy based on a commercial smartphone camera," *IEEE Photonics Journal*, vol. 10, no. 6, pp. 1–17, Dec 2018.
- [6] P. Luo, M. Zhang, Z. Ghassemlooy, H. Le Minh, H.-M. Tsai, X. Tang, and D. Han, "Experimental demonstration of a 1024-qam optical camera communication system," *IEEE photonics technology letters*, vol. 28, no. 2, pp. 139–142, 2015.
- [7] S. R. Teli, S. Zvanovec, and Z. Ghassemlooy, "The first tests of smartphone camera exposure effect on optical camera communication links," in *2019 15th International Conference on Telecommunications (ConTEL)*. IEEE, 2019, pp. 1–6.
- [8] J. Marcello, D. Rodriguez-Esparragon, and D. Moreno, "Comparison of land cover maps using high resolution multispectral and hyperspectral imagery," in *IGARSS 2018-2018 IEEE International Geoscience and Remote Sensing Symposium*. IEEE, 2018, pp. 7312–7315.
- [9] M. Rosenberger, "Multispectral edge detection algorithms for industrial inspection tasks," in *2014 IEEE International Conference on Imaging Systems and Techniques (IST) Proceedings*, Oct 2014, pp. 232–236.
- [10] F. Meriaudeau, V. Paquit, N. Walter, J. Price, and K. Tobin, "3d and multispectral imaging for subcutaneous veins detection," in *2009 16th IEEE International Conference on Image Processing (ICIP)*, Nov 2009, pp. 2857–2860.
- [11] Y. P. Varshni, "Temperature dependence of the energy gap in semiconductors," *physica*, vol. 34, no. 1, pp. 149–154, 1967.
- [12] C. Zhao, R. Zhang, B. Liu, D. Fu, H. Chen, M. Li, Z. Xie, X. Xiu, S. Gu, and Y. Zheng, "The temperature dependence of optical properties of ingan alloys," *Science China Physics, Mechanics and Astronomy*, vol. 55, no. 3, pp. 396–399, 2012.
- [13] Jeong Park and C. C. Lee, "An electrical model with junction temperature for light-emitting diodes and the impact on conversion efficiency," *IEEE Electron Device Letters*, vol. 26, no. 5, pp. 308–310, May 2005.

Underwater Optical Camera Communications based on a Multispectral Camera and Spectral Variations of the LED Emission

Behnaz Majleseini*

Julio Rufo*

jruf@lightbeecorp.com

LightBee S.L.

Las Palmas de Gran Canaria, Spain

Victor Guerra

IDeTIC, Universidad de Las Palmas de Gran Canaria

Las Palmas, Spain

vguerra@idetic.eu

Daniel Moreno

IDeTIC, Universidad de Las Palmas de Gran Canaria

Las Palmas, Spain

dmoreno@idetic.eu

Jose Rabadan

IDeTIC, Universidad de Las Palmas de Gran Canaria

Las Palmas, Spain

jrabadan@idetic.eu

ABSTRACT

Optical Camera Communication (OCC) applications have intensively used in recent years. Underwater Optical Wireless Communications (UWOC) are one of the most viable alternatives today in underwater environments, compared to traditional acoustic communications or radio communications. UWOC present important and remarkable advantages such as their available bandwidth and the possibility of using COTS devices already present in underwater environments such as LED lighting lamps. This work proposes using a multispectral or hyperspectral camera as an OCC receiver, in short range underwater links, to take advantage of the high spectral resolution of this type of devices regarding conventional cameras. Furthermore, spectral features of the LEDs, usually used as transmitters in OCC, are affected by temperature. Hence, one of the goals of this work is to benefit from those spectral variations that will be grasped by the multispectral camera and thus achieve a new data channel. Therefore, different communication channels could be obtained from a single light source.

CCS CONCEPTS

• **Computer systems organization** → *Embedded systems*; • **Optical Wireless Communications** → *Visible Light Communications*; Optical Camera Communications; • **Networks** → Network reliability.

KEYWORDS

OCC, multispectral, hyperspectral, LED, UWOC

ACM Reference Format:

Behnaz Majleseini, Julio Rufo, Daniel Moreno, Victor Guerra, and Jose Rabadan. 2020. Underwater Optical Camera Communications based on

*Authors contributed equally to this research.

ACM acknowledges that this contribution was authored or co-authored by an employee, contractor or affiliate of a national government. As such, the Government retains a nonexclusive, royalty-free right to publish or reproduce this article, or to allow others to do so, for Government purposes only.

L¹OT '20, September 21, 2020, London, United Kingdom

© 2020 Association for Computing Machinery.

ACM ISBN 978-1-4503-8099-7/20/09...\$15.00

<https://doi.org/10.1145/3412449.3412554>

a Multispectral Camera and Spectral Variations of the LED Emission. In *Light Up the IoT (L¹OT '20)*, September 21, 2020, London, United Kingdom. ACM, New York, NY, USA, 6 pages. <https://doi.org/10.1145/3412449.3412554>

1 INTRODUCTION

In the last few years, there has been a rapid rise in the use of Optical Camera Communication (OCC). It is foreseen that significant advancement in this technology will be implemented increasingly soon thanks to the massive presence of optical cameras in consumer electronic devices such as smartphones, tablets and laptops. What is more, OCC has been added as an extension of IEEE 802.15.7 standard on Visible Light Communications (VLC) [1]. This technology used a camera or an image sensor to receive data from a light source. The sensor scanning is based on two different modes. On the one hand, global shutter exposes every pixel per frame simultaneously. Moreover, it can only detect waveforms with bandwidths below half the frame rate. On the other hand, rolling shutter scans the image sequentially. Besides, this mode allows higher speed communication because the optical source's waveform can be captured within a single frame [12]. Nevertheless, the maximum obtainable speed is dependent on the projected size of the light source, as OCC is based on image-forming optics [4]. OCC has been proposed as a suitable technology in applications such as the Internet of Things (IoT), Vehicular Communication, and Indoor Positioning Systems (IPS). Positioning accuracy of OCC-based IPS is within the centimeter range [5, 13], outperforming any RF-based positioning technique. Vehicle-to-Anything (V2X) is another promising application field of OCC due to the uprising presence of vehicle-mounted optical cameras (generally used for surveillance and security).

Underwater Optical Wireless Communications (UWOC) are one of the most viable alternatives today in underwater environments. UWOC, compared to traditional acoustic communications or radio communications, present important and remarkable advantages such as their available bandwidth and the possibility of using COTS devices already present in underwater environments such as LED lighting lamps. The current modulation and coding technologies allow that at a short distance between transmitters and receivers transmission speeds reach values that are not possible in both acoustic and radio communications, very limited in underwater

environments. VLC systems offer a compromise between transmission and link distance compared to other technologies, thus, allow high speeds of short or medium distance transmission.

Apart from this, regarding the camera used as a receiver in OCC, in this technology has been employed several types of cameras such as Single-Lens Reflex (SLR) cameras [6] or smartphones [10]. In all the cases mentioned above, the devices are used to take pictures and videos within the visible range. Their image sensor only permits the capture of RGB images at most, similar to the human eye. However, multispectral cameras (and hyperspectral cameras) can capture a higher number of communication bands than the RGB bands provided by conventional cameras. These have been used in different sectors such as remote sensing [7], agriculture [9] or biotechnology [8]. In this manner, Optical Multispectral Camera Communication (OMCC) would offer a wide range of opportunities.

This work analyzes the LED spectral variations caused by heat and the attenuation due to the underwater channel. The use of a multispectral (or hyperspectral) camera, which has a high spectral resolution, is proposed to take advantage of this typically considered harmful effect. It is expected to get various independent communication channels using a single sort of transmitter, which would lessen the complexity and cost of the system. On the other hand, although this type of camera has a low sampling rate, there are techniques such as spectral signatures extraction to distinguish particular signals at different wavelengths that would improve its performance.

This paper is divided into six sections. Section 2 gives a brief overview of the theoretical background on which the work is based. The characterization methodology and the results concerning the temperature effects on the used LED devices are presented in Sections 3 and 4, respectively. In Section 5, the application of this characterization is proposed using a multispectral camera in an underwater environment. Lastly, some conclusions are drawn in Section 6.

2 LED WAVELENGTH DEPENDENCE ON TEMPERATURE

The working principle of LED is spontaneous emission of light. That light is emitted when an electron obtains enough energy to traverse the forbidden energy gap of the semiconductor. Then, a photon is emitted when that electron goes back to a lower energy level. The emitted photon has a wavelength that is related to the energy gap by Equation 1. In addition, the energy gap is affected by the p-n junction temperature, depending on the LED's substrate, which is usually modeled using Equation 2. According to [11], in most semiconductor materials energy gap diminishes as temperature increases. Therefore, as wavelength is inversely proportional to energy gap (Equation 1), the peak wavelength of the LED grows with temperature.

$$E_g = hf = \frac{hc}{\lambda} \quad (1)$$

$$E_g = E_0 - \frac{\alpha T^2}{T + \beta} \quad (2)$$

where h is Planck constant, f is frequency, c is the speed of light in vacuum and λ is wavelength. T is temperature, E_0 is energy gap at 0

temperature condition, and α and β are semiconductor-dependent constants, which are empirically determined[11].

However, the metallic content in the LED material must be considered. For instance, [14] proved that the band gap might not follow the decrement as the LED heats up, but it may increase with temperature depending on Indium (In) content in InGaN alloys (green and blue LEDs).

Apart from this, spectral width and luminous efficiency are affected by temperature as well. Normally, the conversion efficiency decreases and the spectral width increases as temperature grows [3]. Based on this, it is intended to use a high spectral resolution camera, such as a multispectral camera, to check if these slight wavelength changes in the LED emission are detectable by it. Then, grasping these generally undesired variations, this work proposes improving communications by increasing the number of communication channels.

3 METHODOLOGY

The primary goal of this work is to benefit from the spectral variations that temperature effects on LEDs, so that a multispectral camera detects those changes and finally use it for OCC purposes. To accomplish this objective, RGB LEDs have been characterized by focusing on the effect of temperature on their emitted spectrum. Moreover, a multispectral camera has been used to set a communication link with those LEDs as transmitters in an underwater environment. Lastly, spectral responses of the emitters have been extracted from the pictures to evaluate the practicability of Optical Multispectral Camera Communications (OMCC) and the use of the LED wavelength variations induced by temperature.

The LEDs under study (common cathode RGB LED with no heat sinks) were driven using currents ranging from 10 mA to 130 mA by an Ethernet-controlled current source to induce them different junction temperatures. Additionally, the temperature was previously stabilized for 5 minutes. This experimental characterization consisted of three different processes. Firstly, the junction temperature of the LEDs has been measured by a thermal imaging camera, as shown in Fig. 1 (top). The employed camera was a FLIR A645, whose main features are a pixel resolution of 640 x 480 and a high sensitivity below 50m. For each current, the maximum temperature of the LED has been recorded.

Secondly, a spectrometer (Spectral Products SM442) has been used to obtain wavelength data of the LED in the visible range. Due to the high intensity of the LED beam, a 15-centimeters ABS-plastic cylinder has been used to distance the LED from the light input, allowing to receive the signal within the dynamic range of the spectrometer. This fix does not affect the measurement, because of the spectrometer is only needed to get the wavelength information of the LED and visualize shape variations (not absolute changes). Finally, the spectral radiant power of the LED in the visible spectral range has been measured using an integrating sphere and a light meter (Gigahertz BTS256). This device also permits to acquire spectral information; however, the spectrometer provided a better spectral resolution (1 nm vs. 5 nm).

After the LEDs' characterization, the aim was to capture the wavelength variation in the LEDs by a camera. It was needed to have a high spectral resolution camera that can detect the slight

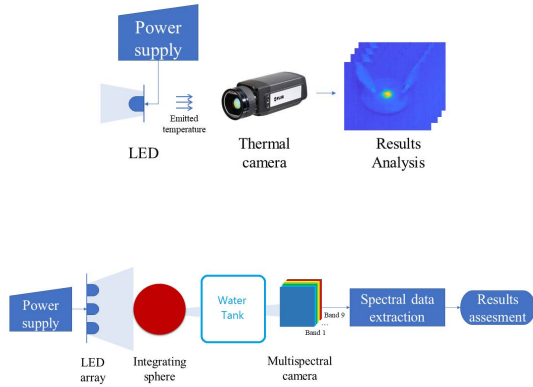


Figure 1: System setup schemes. Scheme used to get the temperature data (top) and scheme used to get the spectral data (bottom).

variations due to temperature; in this case, a multispectral camera, in order to reach this objective. Specifically, the multispectral camera used was the CMS-C1-C-EVR1M-GigE by SILIOS Technologies. It is a 9-bands camera (8 color narrow bands and 1 panchromatic band) that covers the wavelength range from 400 to 1000 nm. It has a CMOS sensor and a resolution of 1280 (H) x 1024 (V) in the raw picture and 426 (H) x 339 (V) in the spectral pictures.

Fig. 1 (bottom) depicts the scheme followed to collect the spectral information of the LED using the multispectral camera. The light beam of these LEDs passes through an integrating sphere that concentrates it on a narrow point. Then the light goes through a water tank that can easily simulate an underwater channel. One of the main characteristics of the underwater channel in terms of its response in wavelength is its low coherence time, that is, the intervals where the channel can be considered quasi-stationary are very small. This renders the linear and temporally invariant channel approximations invalid a priori, as demonstrated in [2]. It should be noted that this is not the same throughout the ocean, since it only occurs in areas where drastic changes in temperature and salinity occur and large amounts of marine particles are concentrated. In other areas such as the seabed, this statement would not be true, since in that case the temperature is uniform and there is hardly any movement, so the channel could be considered quasi-stationary. On the other hand, the interaction between light, water molecules and underwater particles gives rise to two wavelength-dependent effects that involve attenuation of the optical signal: spatial scattering and energy absorption. The main cause of the absorption of light in water is the excitation of the vibration state of water molecules by photons and other dissolved particles. On the other hand, light scattering refers to processes in which the direction of the photon is changed and can take place both in molecules or in dissolved particles. In this way, the absorption and scattering

phenomena are used to characterize the extinction coefficient $c(\lambda)$ at a wavelength determined by equation 3.

$$c(\lambda) = \alpha(\lambda) + \beta(\lambda) \quad (3)$$

where $\alpha(\lambda)$ represents the absorption coefficient and $\beta(\lambda)$ represents the total dispersion coefficient. To calculate the minimum necessary power in an underwater link to induce a detectable signal, assuming no misalignment between both endpoints, we can use Equation 4.

$$P_{tx,min} = \frac{S_{rx} \cdot d^2}{A_{eff} \cdot e^{-c(\lambda)d} \cdot R(\theta, \phi)} \quad (4)$$

where S_{rx} is the receiver's sensitivity, A_{eff} is the effective receiver area, d is the link range, $R(\theta, \phi)$ is a factor that depends on the type of source and its orientation, and $e^{-c(\lambda)d}$ is a coefficient that models the effect of extinction phenomena that occur in the underwater environment [2]. For this work, only clear tap water was used.

Then, the multispectral camera receives that beam and a picture is taken. The camera parameters were adjusted so that the acquired image would not be saturated. The pictures have been saved as single-band images in ENVI file format, which includes one header and one file with multispectral data. Finally, the pictures were cropped selecting only the part that contains the emitted light and from these, the spectral signatures were extracted. With the spectral response of the LED at various temperatures, an evaluation can be made of how well the several signals are distinguished by the camera.

4 CHARACTERIZATION RESULTS

In Fig. 2, some examples of the temperature-time behavior of the RGB LEDs are presented. It depicts an exponential growth which is higher as the driving current increases. Interesting information can be extracted from these graphs, such as that the highest temperature was obtained on the blue LED, followed by the green and the red LEDs. It also can be seen that at 10 mA the temperature kept almost constant. As an example, Fig. 3 shows several thermal pictures of the red LED at low and high temperatures. Fig. 4 (top) shows the effects of the induced high temperature on the LED emission, by increasing the polarization current, on the peak wavelengths of each RGB color. Table 1 details the spectral information in Fig. 4 (top) showing the peak wavelengths and the Full Width at Half Maximum (FWHM) values of each spectrum. It can be seen that by rising the temperature the emitted wavelength grew as expected and, consequently, the peak wavelength shifted. The largest shift was obtained in the red LED with a difference of 21.1 nm between the minimum and the maximum temperature (peak wavelength at 659.6 nm at 27 and 680.7 nm at 65). It was followed by a 13.5 nm shift in blue (from 486.1 nm at 28 to 499.6 nm at 78). In green, the peak wavelength did not increase with temperature in the same way that red and blue did. In this case, the highest peak wavelength was found at the minimum temperature (547.2 nm, 27). The green source color of the employed LED is made with InGaN on Silicon (Si). As seen in Section 2, In content in this alloy can affect in such a way that when the temperature increases the energy gap also grows, so wavelength decreases. In addition to the peak wavelength

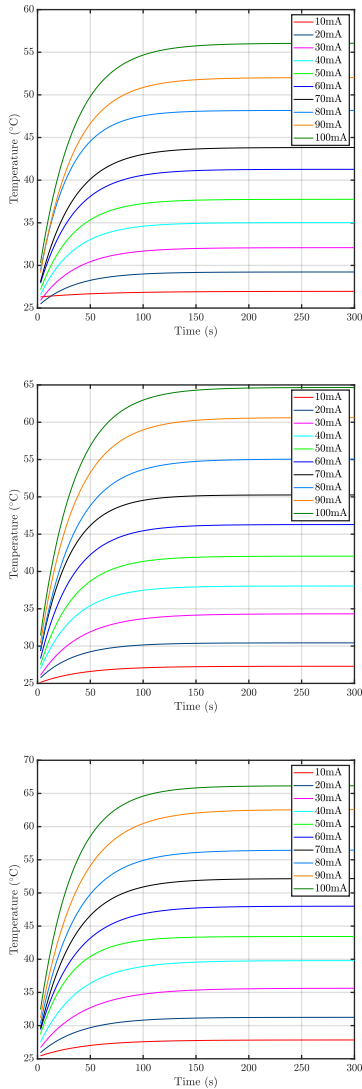


Figure 2: Temperature behavior of the RGB LED: Red (top), green (middle) and blue (bottom).

shift, it is noteworthy how the width changed with the temperature variation. The most striking change was acquired in blue, having a difference between the width at 28 and 66 of roughly 30 nm. Note that the intensity values were normalized in Fig. 4 (top) because the approach was to analyze only the spectral information.

Fig. 4 (bottom) reports the spectral radiant power of the LED in W/nm. The highest levels were obtained for the blue LED, followed by green and red. It can be noted that at the maximum temperature, when the LED is supplied with 130 mA, the power decreased with respect to the second maximum. As a consequence of that, temperature expectedly affected the efficiency of the LED. Furthermore, it shows the wavelength variations, as well as the FWHM changes on temperatures.

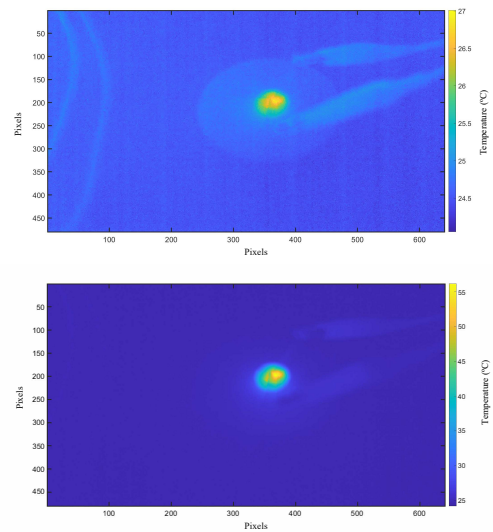


Figure 3: Examples of images of the red LED driven at different currents, taken by a thermographic camera. LED at 10 mA (top) and LED at 100 mA (bottom).

Table 1: Spectral information at different temperatures.

LED	Red			
Current (mA)	10 (27)	50 (38)	100 (56)	130 (65)
Peak wavelength (nm)	659.6	663.6	672.5	680.7
FWHM (nm)	8.73	14.97	22.33	24.15

LED	Green			
Current (mA)	10 (27)	50 (42)	100 (65)	130 (76)
Peak wavelength (nm)	547.2	544.9	545.1	546.8
FWHM (nm)	23.73	31.80	40.92	43.18

LED	Blue			
Current (mA)	10 (28)	50 (43)	100 (66)	130 (78)
Peak wavelength (nm)	486.1	486.1	490.5	499.6
FWHM (nm)	16.68	29.62	45.85	32.10

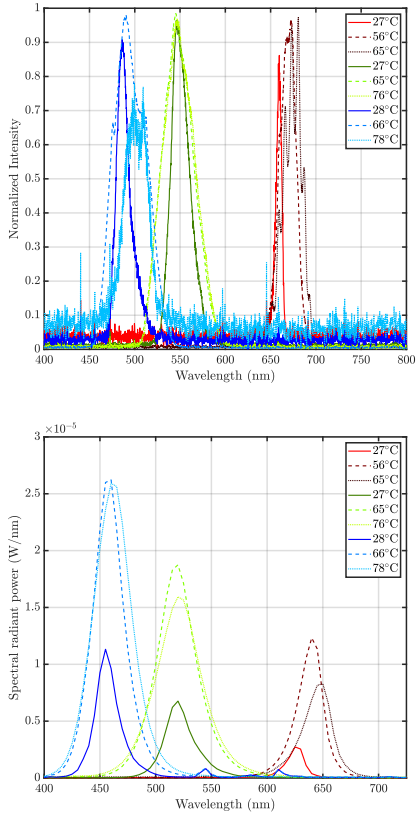


Figure 4: Characterization of the RGB LED at different temperatures: Normalized RGB LED spectra (top) and spectral radiant power (bottom). Solid line, dashed line, dotted line and dash-dot line correspond to 10 mA, 50 mA, 100 mA and 130 mA, respectively.

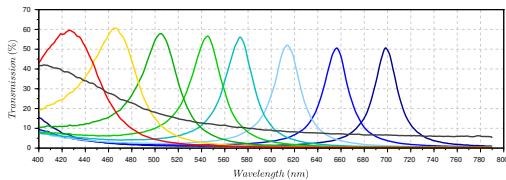


Figure 5: Filter specifications.

5 MULTISPECTRAL CAMERA RESULTS

The images captured by the camera show the spectral variations caused by changing the LED junction temperature. Those changes can be observed in the spectral signatures of the LED shown in Fig. 6. As a case in point, Fig. 6 (bottom) depicts the several levels of energy of the blue LED, supplied with various currents (therefore, at different temperatures), with respect to the 9 bands of the multispectral camera. Targeting the bands 1, 2 and 3, centered in 427, 461 and 501 nm, respectively, as the analyzed results were obtained on the blue LED, there are some phenomena to consider. Besides, a high level is placed in band 9, which corresponds to the panchromatic band. However, the focus is not in this band, because the only remarkable consequence is the increase in level due to the increment in current. Firstly, part of the energy captured in the band 1 was captured in the band 2 as temperature grew, causing an increment in the level of this band. The identical happened with bands 2 and 3. It occurred because the peak wavelength of the LED gradually shifted, so the bands 2 and 3, which have an FWHM of the order of 50 nm (see Fig. 5), took more information. Additionally, it is perceptible a growth in level as expected, since the way chosen to raise the temperature is by increasing the driving current, ergo the power of the LED also increases. Figs. 6 (top) and 6 (bottom) depict the spectral signatures of the red and green LED, respectively, showing similar results. These results suggested that several communication channels can be obtained from a single emission source since the slight changes in wavelength are detected by the multispectral camera.

6 CONCLUSIONS

In this work, several RGB LEDs have been characterized, especially to visualize the effect of the transmitter’s temperature in the wavelength/spectrum of the emitted light. Furthermore, it has been utilized a multispectral camera taking pictures of the light beam of the LED and analyzing those wavelength variations. The spectral response of the RGB LEDs has been extracted and how the wavelength shifts have been checked. Therefore, as the spectral changes in the emitted light can be observed by using a multispectral camera, it takes advantage of that phenomenon considered harmful. So, the more variation in the peak wavelength of the LED is affected by temperature, the better. Thus, this paper proposes to use those dissimilarities to create separable communication channels in an OMCC application.

This led us to conclude that employing, for instance, two receivers with two different optical filters, will be feasible to separate each signal by using the same transmitter device. Using the temperature to tune the wavelength of the LED will allow this to be done. It will also be possible to use a camera with enough spectral resolution, such as a multispectral or a hyperspectral camera, which captures the light beam in its several bands with greater or lesser intensity depending on the wavelength shift.

The evidence of this work points towards the idea that temperature effects in emitters, usually considered detrimental, can be detected by high-spectral-resolution cameras and used for applications such as Wavelength Division Multiplexing (WDM) (Fig. 7). In this case, the results of this study indicated that the red LED got more spectral variations than green and blue.

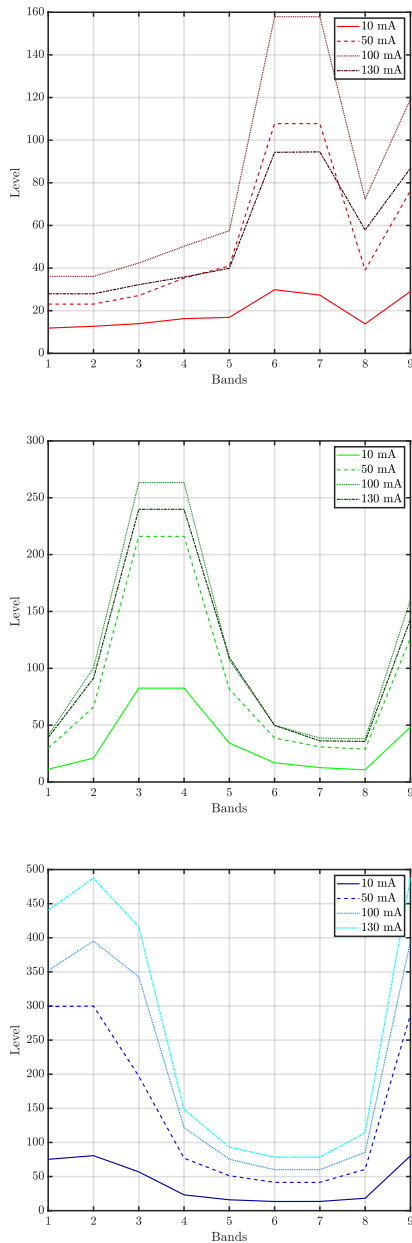


Figure 6: Spectral signatures of the RGB LED at different temperatures: Red (top), green (middle) and blue (bottom). Solid line, dashed line, dotted line and dash-dot line correspond to 10 mA, 50 mA, 100 mA and 130 mA, respectively.

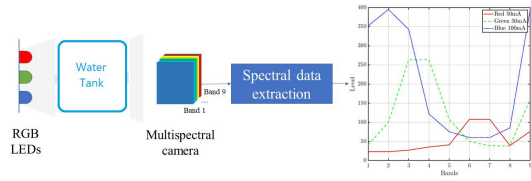


Figure 7: This figure is an example of a proposed diagram for WDM. By sending three different color signals that are captured by the multispectral camera, after extracting their spectral signatures, each signal could be separated.

ACKNOWLEDGMENTS

This work was benefited from Canary Islands Regional Government (Project ATICCuA ProID2017010053). It has been funded in part by the Trainee Predoctoral Research Staff Program (2019) of the Universidad de LasPalmas de Gran Canaria.

REFERENCES

- [1] April 2019. Short-Range Optical Wireless Communications (802.15.7-2018).
- [2] L. Mullen B. Cochenour and A. Laux. 2008. Characterization of the beam-spread function for underwater wireless optical communications links. *OCEANS engineering* 33, 3 (01 Mar 2008), 311–335. <https://doi.org/10.1023/A:1008889222784>
- [3] Jeong Park and C. C. Lee. 2005. An electrical model with junction temperature for light-emitting diodes and the impact on conversion efficiency. *IEEE Electron Device Letters* 26, 5 (May 2005), 308–310. <https://doi.org/10.1109/LED.2005.847407>
- [4] Cristo Jurado-Verdu, Vicente Matus, Jose Rabadan, Victor Guerra, and Rafael Perez-Jimenez. 2019. Correlation-based receiver for optical camera communications. *Opt. Express* 27, 14 (Jul 2019), 19150–19155. <https://doi.org/10.1364/OE.27.019150>
- [5] Y. Li, Z. Ghassemlooy, X. Tang, B. Lin, and Y. Zhang. 2018. A VLC Smartphone Camera Based Indoor Positioning System. *IEEE Photonics Technology Letters* 30, 13 (July 2018), 1171–1174. <https://doi.org/10.1109/LPT.2018.2834930>
- [6] Pengfei Luo, Min Zhang, Zabih Ghassemlooy, Hoa Le Minh, Hsin-Mu Tsai, Xuan Tang, and Dahai Han. 2015. Experimental demonstration of a 1024-QAM optical camera communication system. *IEEE photonics technology letters* 28, 2 (2015), 139–142.
- [7] Javier Marcello, Dionisio Rodriguez-Esparragon, and Daniel Moreno. 2018. Comparison of land cover maps using high resolution multispectral and hyperspectral imagery. In *IGARSS 2018-2018 IEEE International Geoscience and Remote Sensing Symposium*. IEEE, 7312–7315.
- [8] F. Meriaudeau, V. Paquit, N. Walter, J. Price, and K. Tobin. 2009. 3D and multispectral imaging for subcutaneous veins detection. In *2009 16th IEEE International Conference on Image Processing (ICIP)*. 2857–2860. <https://doi.org/10.1109/ICIP.2009.5414511>
- [9] M. Rosenberger. 2014. Multispectral edge detection algorithms for industrial inspection tasks. In *2014 IEEE International Conference on Imaging Systems and Techniques (IST) Proceedings*. 232–236. <https://doi.org/10.1109/IST.2014.6958479>
- [10] Shivani Rajendra Teli, Stanislav Zvanovec, and Zabih Ghassemlooy. 2019. The first tests of smartphone camera exposure effect on optical camera communication links. In *2019 15th International Conference on Telecommunications (ConTEL)*. IEEE, 1–6.
- [11] Yatendra Pal Varshni. 1967. Temperature dependence of the energy gap in semiconductors. *physica* 34, 1 (1967), 149–154.
- [12] Zhaocheng Wang, Qi Wang, Wei Huang, and Zhengyuan Xu. 2017. *Visible light communications: Modulation and signal processing*. John Wiley & Sons.
- [13] J. Xu, C. Gong, and Z. Xu. 2018. Experimental Indoor Visible Light Positioning Systems With Centimeter Accuracy Based on a Commercial Smartphone Camera. *IEEE Photonics Journal* 10, 6 (Dec 2018), 1–17. <https://doi.org/10.1109/JPHOT.2018.2878532>
- [14] ChuanZhen Zhao, Rong Zhang, Bin Liu, DeYi Fu, Hui Chen, Ming Li, ZiLi Xie, XiangQian Xiu, ShuLin Gu, and YouDou Zheng. 2012. The temperature dependence of optical properties of InGaN alloys. *Science China Physics, Mechanics and Astronomy* 55, 3 (2012), 396–399.

Comparison of clustering algorithms for data detection in Multispectral Camera Communication

Daniel Moreno¹, Behnaz Majleseini², Victor Guerra³, Julio Rufo⁴, Jose Rabadan¹, Rafael Perez-Jimenez¹

¹*Photonics Technology and Communications (IDeTIC), Universidad de las Palmas de Gran Canaria (ULPGC)*

35017 Las Palmas de Gran Canaria, Las Palmas, Spain

²*Lightbee, S.L., 35017 Las Palmas de Gran Canaria, Las Palmas, Spain*

³*Pi Lighting Sarl, 1950 Sion, Valais, Switzerland*

⁴*Ramon y Cajal Researcher, Universidad de La Laguna (ULL), 38208 San Cristobal de La Laguna, Santa Cruz de Tenerife, Spain*

Emails: daniel.moreno@ulpgc.es, bmajleseini@lightbeecorp.com, victor.guerra@pi-lighting.com, jrufotor@ull.edu.es, jrabadan@idetec.eu, rperez@idetec.eu

Abstract—In this work, the performance of an optical camera communication (OCC) system is compared using several clustering algorithms in a cluster-based data detection approach. Furthermore, a multispectral camera is utilized to capture the thermally induced spectral variations in light-emitting diodes (LEDs). Thus, more than one channel can be attained from the same device. The results of this paper prove that using a clustering method can enhance the bit error rate (BER). Finally, different training sets were used to fit the clustering models underlining the impact on the system performance.

Index Terms—Clustering, optical camera communication, multispectral, temperature effect.

I. INTRODUCTION

OPTICAL wireless communications (OWC) are believed to be a crucial technology in future wireless communication systems. Besides, as part of the OWC, optical camera communication (OCC) has attracted increasing interest in recent years due to the advances in cameras and image sensors and their ubiquity on consumer electronics devices [1].

For this reason, the last few years have witnessed enormous growth in OCC systems. However, a challenging area in this field is the maximum achievable data rate limited by the camera's scanning method. Therefore, several studies have tended to focus on increasing data rate. For example, in [2], Arai *et al.* improved the data rate of an image sensor communication (ISC) system by designing a rotary light-emitting diode (LED) transmitter that rotates the blinking LEDs during the camera's exposure time. Thus, the camera captures the different LED states as afterimages, increasing the data rate 60 times more than using a conventional ISC system.

It is well-known that temperature has a significant impact on LED devices. Many studies have examined the thermal effects on light sources caused by the LED's p-n junction temperature alterations [3], [4]. One of the most important effects to take

into consideration in OWC is the spectral emission variation. Varshni and Planck-Einstein's relations show that the peak wavelength rises with temperature in general. However, few researchers have addressed this impact and found that it degrades system performance [5], [6].

Nonetheless, recent studies have focused on using this hypothetical negative effect to expand the number of communication channels. A multispectral camera with appropriate spectral resolution to discern the spectral signatures of LEDs at different temperatures could be used to achieve this enhancement [7], [8].

On the other hand, machine-learning-based techniques are gaining popularity in communication systems. Due to recent insights about unsupervised learning, the performance of OWC systems has improved. For instance, Wu and Chi boosted the data rate of an underwater visible light communication (VLC) system to 75 Mbps by correcting the phase deviation of 8-quadrature amplitude modulation (QAM) with a k-means algorithm [9]. In a VLC system based on direct current biased optical orthogonal frequency-division multiplexing (DCO-OFDM), Wang *et al.* used a k-medoids method. The clustering technique was used in the post-equalization step to minimize noise and identify distorted constellation points, improving the system's bit error rate (BER) [10].

Furthermore, Ma *et al.* used a k-means clustering technique to decrease nonlinear distortion effects in a VLC system with Nyquist pulse-amplitude modulation (PAM), significantly enhancing the BER performance over earlier studies [11]. Finally, Shi *et al.* used a density-based spatial clustering of applications with noise (DBSCAN) method in a PAM-7 multiple-input single-output (MISO) underwater VLC system in [12]. DBSCAN was utilized in their proposal to overcome the problem of incorrect assignment caused by the mismatch between the two LEDs used in the transmission.

Similarly, some research has proposed machine learning approaches based on neural networks (NN) to minimize intersymbol interference (ISI) in rolling shutter image sensors evoked by the pixel-row exposure delay [13], [14].

This research was supported the Universidad de Las Palmas de Gran Canaria's Trainee Predoctoral Research Staff Program (2019). It has been funded by the Agencia Estatal de Investigación (PID2020-114561RB-I00).

This paper employs several clustering algorithms to obtain the individual signals from two LEDs with distinct thermally induced spectral characteristics in a multispectral camera communication (MCC) system. The multispectral camera has the spectral resolution required to detect changes in the LED's spectral response caused by temperature variations in the p-n junction. In addition, each transmitter has a different spectral signature at different temperatures; therefore, various communication channels can be established using the same transmitter device. As a result, a multispectral camera that can differentiate signals with distinguishable spectral features permits the use of a temperature-based spectral signature multiplexing technique. Lastly, a cluster analysis using different clustering models is conducted, and the system performance is evaluated.

In this work, the proposed methodology to perform the experiment is described in Section II. Then, Section III presents the obtained results from the methodology and compares the performance of the clustering algorithms. Lastly, some conclusions are drawn in Section IV.

II. METHODOLOGY

The main aim of this work is to experimentally test the performance of a multispectral camera (MS) in a communication link (LED-to-camera) using different clustering algorithms. Besides, in order to take advantage of the high-spectral-resolution capability of this kind of camera, LEDs of a specific wavelength have been employed at different driving currents to modify their working temperature and get different spectral signatures that the MS camera can detect. Furthermore, a cluster-based data detection procedure has been utilized. Some of the most popular types of clustering algorithms were used (hierarchical clustering, centroid-based clustering, and distribution-based clustering) to examine their performance for OCC when different training sets were employed. An in-depth analysis of the algorithms was not performed as it was beyond the scope of this paper.

Two red LEDs were used as transmitters in the system based on the fact that those devices achieved the best results in [8]. The driving current of each LED was controlled by a circuit supplied by a voltage source. Besides, each circuit was connected to a micro-controller that generated a variable pulse position modulation (VPPM) signal depending on the desired temperature to be induced in the LED due to the Joule effect. Finally, the micro-controller devices were connected through the serial port to be controlled by the personal computer (PC), which sent the transmitted data.

On the other hand, the MS camera was connected to the PC via Ethernet in order to manage the capturing process. In addition, a diffuser between the LEDs and the camera was placed to mix the light beams and avoid saturation in the camera. All the setup was located inside a dark chamber to reduce background-light interference. Finally, a Python-based automation script was developed to coordinate all the processes and communicate to the micro-controller devices and the camera.

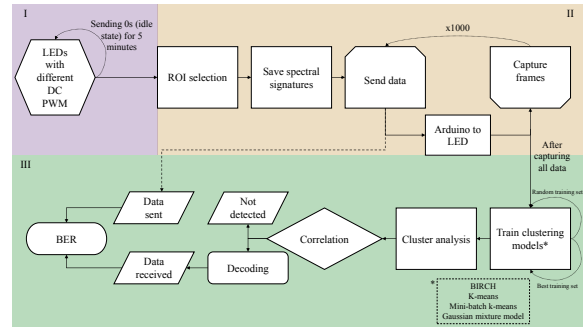


Fig. 1. Flowchart of the experimental procedures. It is split into three phases: Phase I: LED temperature stabilization. Phase II: transmission and reception. Phase III: cluster analysis and performance evaluation.

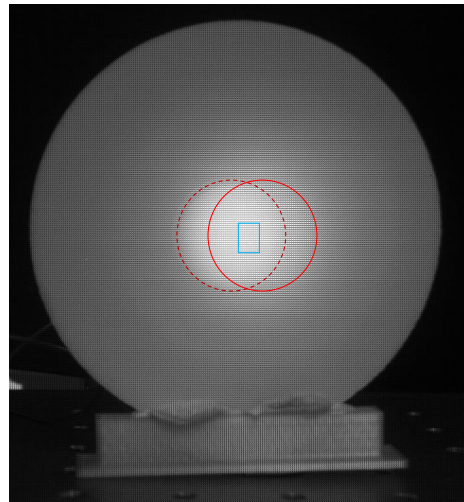


Fig. 2. Example of ROI selection. The red circles represent the LED's light beams. The blue square corresponds to the ROI, which is selected in the region where the beams are mixed.

The core of this experiment consisted of using two LEDs of the same model and changing their p-n junction temperature by the Joule effect to reach different spectral responses. Thus, each LED had a specific spectral signature that an MS camera could capture. Furthermore, in order to have those different signatures, each LED had distinct pulse-width modulation (PWM) duty cycle (DC) values so that the higher the DC value, the higher the junction temperature. No thermal management techniques, such as heat sinks, were used in this work, as they would reduce the variation of the LED spectral characteristics. Once the desired temperature was reached, the data transmission started, and the camera captured the images. Finally, a cluster-based data detection approach was carried out, and the system's performance was assessed. Taking the aforementioned explanation into account, the experiment consisted of three main phases, as shown in Fig. 1.

In Phase I, the goal was to achieve a different LED p-n junction temperature in each device. Therefore, the LEDs were set with 30% and 70% DC values. The frequency of the PWM was set to 5 Hz (bit interval of 200 ms), resulting in one symbol every ten frames since the frame rate was 50 fps. With the purpose of reaching the thermal steady-state on the LEDs, the transmitters were set to an idle state for 5 minutes before sending data because no external thermal management technique was applied to stabilize the temperature. It consisted of keeping the LEDs sending a binary zero with the corresponding DC.

Afterward, in Phase II, the region of interest (ROI), where the light beams of the LEDs were mixed, was determined (Fig. 2). Then, the spectral signatures were stored, and the transmission began. The data transmission involved the following steps. In the first place, a list of 1000 8-bit data was generated for each transmitter. Next, each element in each list was sent to the micro-controller devices in byte format. However, in the micro-controller part, the generated bit sequence was encoded in 8B/10B.

Furthermore, due to the sensitivity of the spectral signature to temperature, it was essential to avoid long sequences of "1" or "0". Therefore, the applied encoding allowed the use of a header consisting of non-consecutive zeros and ones. Moreover, the same header was added after the payload to improve the frame-detection process.

Lastly, Phase III involved cluster analysis and the system performance evaluation. First, several clustering algorithms were used to generate different models and then compare their performance. The employed algorithms were balanced iterative reducing and clustering hierarchies (BIRCH), k-means, mini-batch k-means, and Gaussian mixture model (GMM) [15].

Two distinct strategies were used to train each model. On the one hand, random groups of ten bit streams from the received frames were used to train them. On the other hand, the best set was selected based on the bit error rate (BER) assessment from numerous randomly generated training sets. Once the models were fit according to the training set, they were used to assign a cluster to each sample from the received bit streams. Next, each cluster was assigned to a corresponding symbol (00, 01, 10, or 11) as listed in Table I, obtaining the two LED signals. Subsequently, the resulting signals were correlated (Pearson correlation function) with a matrix comprising all available transmitted signals (a total of 2^{bits}). Finally, the maximum correlation value was taken and compared to thresholds from 0 to 0.95 in steps of 0.05. If the maximum value was less than the threshold, the bit stream was considered undetected. Otherwise, the BER is evaluated by decoding the received signal and comparing it to the transmitted signal. This process was repeated for each clustering model. Table II describes the key parameters of the experiment.

III. RESULTS

In this section, the system performance using several clustering algorithms is analyzed. Figs. 3 and 4 present a comparison

TABLE I
CLUSTER INTERPRETATION.

Symbol	LED state
00	both LEDs OFF
01	one LED ON, one LED OFF
10	
11	both LEDs ON

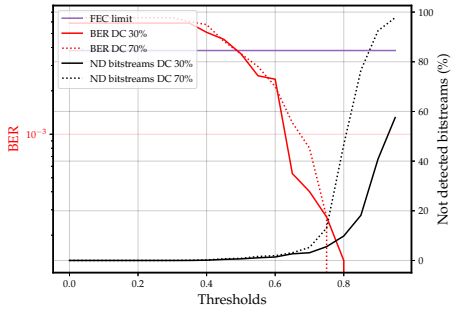
TABLE II
EXPERIMENT KEY PARAMETERS.

Parameter	Value
Transmitter	
Light source	Kingbright L-53SRC-C (Red)
Dominant wavelength [nm]	660
Control device	Arduino UNO
Receiver	
Camera	SILIOS Technologies CMS-C1-C-EVR1M-GigE
Resolution [px]	1280 × 1024 (raw image) 426 × 339 (multispectral images)
Band's center wavelength [nm]	B1: 424
	B2: 464
	B3: 504
	B4: 544
	B5: 573
	B6: 614
	B7: 656
	B8: 699
	B9: 400-800 (pan)
Exposure time [ms]	20
Aperture	f/2.4
Frame rate [fps]	50
Shutter mode	Global shutter
Bit stream	
Coding	8B/10B
Modulation	VPPM
Bit time [ms]	200
Duty cycle	30%, 70%
Bits	Header: 10
	Payload: 8
	Footer: 10
Clustering	
Algorithms	BIRCH (hierarchical CL)
	K-means, mini-batch k-means (centroid-based CL)
	Gaussian mixture model (distribution-based CL)
Number of clusters	4

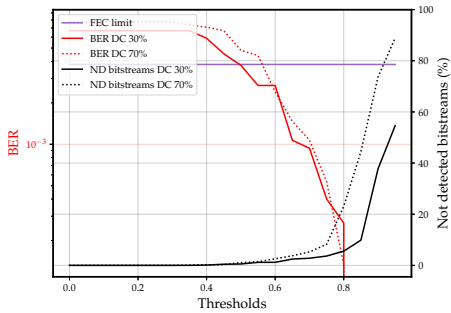
of the distinct models trained with the best training set and with random sets, respectively.

It can be seen that the system performance for each model was similar, achieving slightly better results with the BIRCH algorithm (Figs. 3a and 4a). On the contrary, the GMM model (Figs. 3d and 4d) had a poor performance, especially by not detecting considerable bit streams than the other models for BER below the FEC limit ($3.8 \cdot 10^{-3}$).

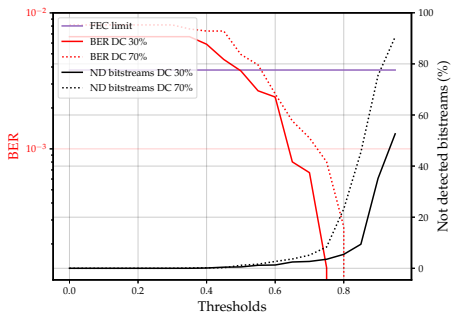
Regarding the training sets employed to fit the models, only BIRCH and mini-batch k-means algorithms obtained acceptable results (Figs. 4a and 4c). However, the used training set considerably marred the other models' performance (Figs. 4b and 4d).



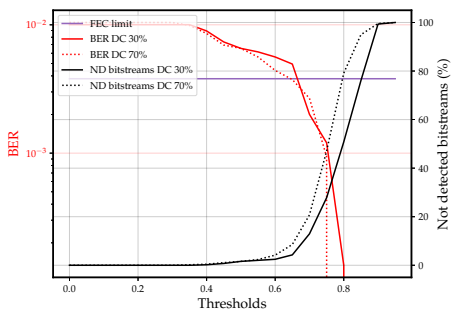
(a)



(b)

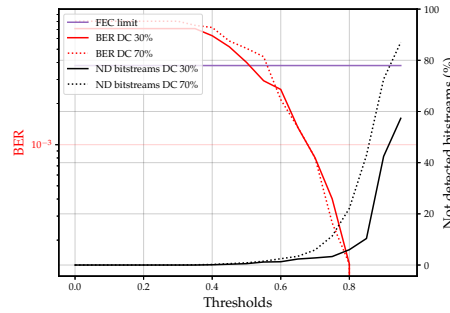


(c)

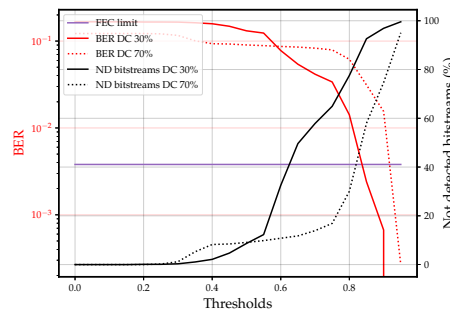


(d)

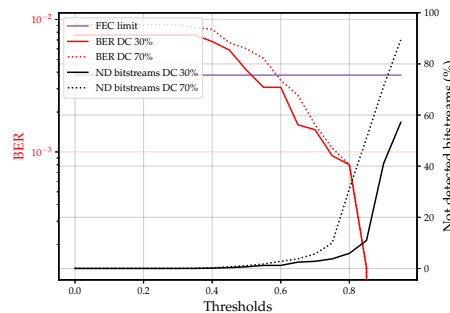
Fig. 3. BER and undetected bit streams at different correlation thresholds using (a) BIRCH, (b) k-means, (c) mini-batch k-means, and (d) GMM algorithms, training the clustering models with the best training set. Solid and dotted lines correspond to the LEDs working at 30% and 70% DC values, respectively.



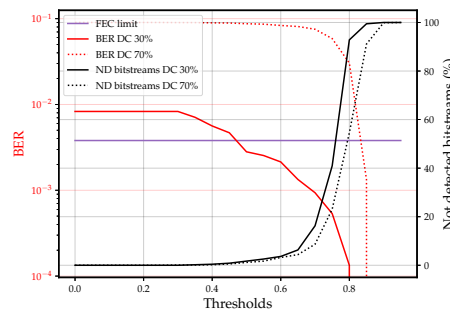
(a)



(b)



(c)



(d)

Fig. 4. BER and undetected bit streams at different correlation thresholds using (a) BIRCH, (b) k-means, (c) mini-batch k-means, and (d) GMM algorithms, training the clustering models with a random training set. Solid and dotted lines correspond to the LEDs working at 30% and 70% DC values, respectively.

IV. CONCLUSION

In this work, a cluster-based data detection approach has been utilized in an MCC system. Besides, the effect of temperature on LED has been used to achieve more than one communication channel from the same device. Therefore, different spectral signatures are obtained from the same light source at different temperatures, allowing the MS camera to distinguish the spectral variation. Moreover, several clustering algorithms were used to analyze the system performance. Finally, the different models were fit by employing distinct training sets: on the one hand, a random group of the bit streams; on the other hand, the best combination of bit streams based on the evaluated BER.

The findings of this study indicate that exploiting the thermally induced spectral variations on LEDs and the use of an MS camera allow getting up to two channels from the same light source.

Furthermore, this paper reinforces the usefulness of supervised learning methods in OCC systems. Satisfactory results have been obtained, proving that BER below the FEC limit can be achieved. Moreover, the results of this work underline the importance of selecting a proper training set in the clustering model for obtaining satisfactory performance. Similar outcomes were achieved with the BIRCH, k-means, and mini-batch k-means algorithms. However, the GMM model did not have a successful performance, suggesting a non-Gaussian nature of the data. Those cases where the random training set obtained poor results intimate that the bit streams used to fit the model did not correctly represent the sample set.

Further work will concentrate on in-depth analyzing the algorithms and fine-tuning their parameters.

REFERENCES

- [1] M. Z. Chowdhury, M. K. Hasan, M. Shahjalal, M. T. Hossain, and Y. M. Jang, "Optical wireless hybrid networks: Trends, opportunities, challenges, and research directions," *IEEE Communications Surveys Tutorials*, vol. 22, no. 2, pp. 930–966, 2020.
- [2] S. Arai, Z. Tang, A. Nakayama, H. Takata, and T. Yendo, "Rotary LED transmitter for improving data transmission rate of image sensor communication," *IEEE Photonics Journal*, vol. 13, no. 4, pp. 1–11, 2021.
- [3] M. E. Raypah, B. K. Sodipo, M. Devarajan, and F. Sulaiman, "Estimation of luminous flux and luminous efficacy of low-power SMD LED as a function of injection current and ambient temperature," *IEEE Transactions on Electron Devices*, vol. 63, no. 7, pp. 2790–2795, 2016.
- [4] R. O. Ocaya, "Thermal tuning of light-emitting diode wavelength as an implication of the Varshni equation," *Measurement*, vol. 162, p. 107910, 2020. [Online]. Available: <https://www.sciencedirect.com/science/article/pii/S0263224120304486>
- [5] E. Tugcu, A. Yazgan, C. Albayrak, and K. Turk, "Red-shift effect in multi-color LEDs based visible light communication," *Optics Communications*, vol. 463, p. 125451, 2020. [Online]. Available: <https://www.sciencedirect.com/science/article/pii/S0030401820301115>
- [6] D. Moreno, J. Rufo, V. Guerra, J. Rabadan, and R. Perez-Jimenez, "Effect of temperature on channel compensation in optical camera communication," *Electronics*, vol. 10, no. 3, 2021. [Online]. Available: <https://www.mdpi.com/2079-9292/10/3/262>
- [7] —, "Optical multispectral camera communications using LED spectral emission variations," *IEEE Photonics Technology Letters*, vol. 33, no. 12, pp. 591–594, 2021.
- [8] D. Moreno, V. Guerra, J. Rufo, J. Rabadan, and R. Perez-Jimenez, "Clustering-based data detection for spectral signature multiplexing in multispectral camera communication," *Optics Letters*, 2022.
- [9] X. Wu and N. Chi, "The phase estimation of geometric shaping 8-QAM modulations based on k-means clustering in underwater visible light communication," *Optics Communications*, vol. 444, pp. 147–153, 2019. [Online]. Available: <https://www.sciencedirect.com/science/article/pii/S0030401819302159>
- [10] Y. Wang, M. Zhang, H. Zhou, X. Wang, C. Qin, W. He, and X. Ren, "Experimental demonstration of OFDM-VLC system employing clustering algorithm," in *2021 2nd Information Communication Technologies Conference (ICTC)*, 2021, pp. 107–111.
- [11] J. Ma, J. He, J. Shi, J. He, Z. Zhou, and R. Deng, "Nonlinear compensation based on k-means clustering algorithm for Nyquist PAM-4 VLC system," *IEEE Photonics Technology Letters*, vol. 31, no. 12, pp. 935–938, 2019.
- [12] M. Shi, Y. Zhao, W. Yu, Y. Chen, and N. Chi, "Enhanced performance of PAM7 MISO underwater VLC system utilizing machine learning algorithm based on DBSCAN," *IEEE Photonics Journal*, vol. 11, no. 4, pp. 1–13, 2019.
- [13] K.-L. Hsu, C.-W. Chow, Y. Liu, Y.-C. Wu, C.-Y. Hong, X.-L. Liao, K.-H. Lin, and Y.-Y. Chen, "Rolling-shutter-effect camera-based visible light communication using RGB channel separation and an artificial neural network," *Optics Express*, vol. 28, p. 39956, 12 2020. [Online]. Available: <https://www.osapublishing.org/abstract.cfm?URI=oe-28-26-39956>
- [14] Y.-S. Lin, C.-W. Chow, Y. Liu, Y.-H. Chang, K.-H. Lin, Y.-C. Wang, and Y.-Y. Chen, "PAM4 rolling-shutter demodulation using a pixel-per-symbol labeling neural network for optical camera communications," *Optics Express*, vol. 29, p. 31680, 9 2021. [Online]. Available: <https://www.osapublishing.org/abstract.cfm?URI=oe-29-20-31680>
- [15] F. Pedregosa, G. Varoquaux, A. Gramfort, V. Michel, B. Thirion, O. Grisel, M. Blondel, P. Prettenhofer, R. Weiss, V. Dubourg, J. Vanderplas, A. Passos, D. Cournapeau, M. Brucher, M. Perrot, and E. Duchesnay, "Scikit-learn: Machine learning in Python," *Journal of Machine Learning Research*, vol. 12, pp. 2825–2830, 2011.

Spectral Signature Multiplexing in Multispectral Camera Communication

Daniel Moreno
IDeTIC-ULPGC

Las Palmas de Gran Canaria, Spain
daniel.moreno@ulpgc.es

Victor Guerra
Pi Lighting

Sion, Switzerland
victor.guerra@pi-lighting.com

Julio Rufo

Universidad de La Laguna (ULL)
San Cristobal de La Laguna, Spain
jrufotor@ull.edu.es

Jose Rabadan
IDeTIC-ULPGC

Las Palmas de Gran Canaria, Spain
jrabadan@idetic.eu

Rafael Perez
IDeTIC-ULPGC

Las Palmas de Gran Canaria, Spain
rperez@idetic.eu

Abstract—Optical camera communication (OCC) is a technology foreseen to have a fundamental role in future communication applications due to the ubiquity of the cameras embedded in most consumer electronic devices and their increasing capabilities (high resolution, scanning frequency, *etcetera*). However, high-spectral-resolution cameras, such as multispectral cameras, present particular characteristics that can be exploited to provide new features to OCC links. Furthermore, as LED spectral responses are different when their temperature changes, more than one communication channel can be achieved using the same LED device if the camera can capture those modifications and distinguish the different LED spectral signatures due to the temperature variation. This novel approach is followed in this research, including some equalization techniques applied to the channel matrix to improve the extraction of the transmitted signal in the receiver reducing the inter-channel interference (ICI). This work shows that up to two distinct channels can be obtained with the same LED at different temperatures, getting a bit error rate (BER) below the forward error correction (FEC) limit.

Index Terms—Optical camera communication, multispectral, light-emitting diodes, temperature effect.

I. INTRODUCTION

OPTICAL camera communication (OCC) is attracting considerable interest due to the widespread use of cameras in smartphones, automobiles, surveillance, and healthcare, among others. The ubiquity of these devices and the recent advances in image sensors have boosted the uses of this technology in terms of research [1]. In addition, OCC has attracted the scientific community's attention in the last few years due to its potential immediate applications to the market. Recent developments have focused on employing novel modulation/demodulation techniques and different types of cameras and transmitters. Shiraki *et al.* developed a demodulation method using a Gaussian-mixture model to estimate the channel of the OCC system without any synchronization devices [2]. An LED-to-camera communication system based on color

shift keying (CSK) was presented by Hu *et al.* [3]. They compared the throughput of several smartphone cameras and obtained a low symbol error rate avoiding color flicker.

Despite the vast amount of literature on OCC, the full potential of the technology has yet to be exploited, especially outside of conventional camera use. For example, some studies proposed using high-speed cameras to increase the data rate. Arai *et al.* put forward a hierarchical transmission scheme based on two-dimensional fast Haar wavelet transform to guarantee data detection when the camera is far from the transmitter [4]. Iwase *et al.* recognized a lighting pattern from a pattern-mixed image, setting the transmitting rate to the same receiver frame rate and reducing flickering by using 8B/10B encoding [5]. On the other hand, regarding the use of LEDs as transmitters, it is well-known that the spectral characteristics of LEDs are affected by temperature, which has a detrimental effect on the communication performance if not accounted for in the reception process [6], [7].

This work proposes an LED-to-camera communication using a multispectral camera as a receiver, which allows taking advantage of the numerous device bands to distinguish signals of different wavelengths. Furthermore, the LED spectral variation due to temperature is leveraged. Since the LED spectral response varies with thermal changes, those modifications can be grasped by a high-spectral-resolution camera. Therefore, new communication channels can be achieved utilizing the same transmitter device, as the LED spectral response modifies with temperature.

This paper is organized as follows. Section II gives a brief overview of OCC and presents the beneficial applications of using a multispectral camera as receiver in OCC. Section III examines the effect of temperature on LEDs. The procedures and techniques applied to carry out the experiments are described in Section IV. The results obtained from the methodology implemented are presented in Section V. Finally, some conclusions are drawn in Section VI.

This research was supported in part by the Universidad de Las Palmas de Gran Canaria's Trainee Predoctoral Research Staff Program (2019) and in part by the Spanish State Research Agency, project OCCAM PID2020-114561RB-I00.

II. MULTISPECTRAL CAMERA COMMUNICATION

OCC is a technology that employs an image sensor or a camera as an optical data receiver instead of a photodiode as used in visible light communication (VLC) links. Hence, one of the principal advantages of OCC is the ease with which cameras embedded in most consumer electronic devices can be used as receivers, permitting this type of OWC to be implemented without any requirement to add or modify the hardware. However, since these cameras are designed for photography, OCC's maximum achievable data rate is limited by the device's pixel clock and scanning method, allowing only low data rate transmissions [8].

Depending on the number of bands a camera can record and their width, the device's spectral accuracy would capture different signals from the same LED at different temperatures [9]. This effect is a fundamental aspect of this work and will be explained in-depth in Section III.

Regarding the channel modeling in OWC, the received power of an OCC system can be expressed as shown in Equation 1.

$$P_{rx} = P_{tx} R(\theta, \phi) \frac{A_{lens}}{d^2} \cos(\Psi), \quad (1)$$

where P_{tx} is the transmitted power, $R(\theta, \phi)$ is the source's radiation pattern at elevation θ and azimuth ϕ , A_{lens} is the main lens' cross section, d is the link range, and Ψ is the impact angle. As image-forming optics must be considered in OCC, neglecting any defocusing effect, the pixel power does not depend on distance when the projected size of the light source on the sensor is greater than one pixel (Equation 2).

$$A_{proj} = \frac{N_x N_y}{FOV_x FOV_y} \frac{A_{tx}}{d^2}, \quad (2)$$

A_{proj} is the projected number of pixels of the light source on the sensor, N_x and N_y define the sensor's pixel resolution, FOV_x and FOV_y are the camera's horizontal and vertical fields of view, respectively, and A_{tx} is the transmitter's effective area (from the receiver's viewpoint). These equations reveal that although P_{rx} decreases as distance increases, A_{proj} decreases as well (constant power density on the image sensor). Joining Equations 1 and 2, the received optical power at each pixel is obtained in Equation 3.

$$P_{px} = P_{tx} R(\theta, \phi) \frac{A_{lens}}{A_{tx}} \frac{FOV_x FOV_y}{N_x N_y} A_{px} \cos(\Psi), \quad (3)$$

where P_{px} is the pixel power (in watts) and A_{px} is the pixel area.

Regarding channel compensation, it is critical in any system subject to inter-channel interference (ICI). Several techniques aim to alleviate ICI, such as multiple-input multiple output (MIMO), wavelength division multiplexing (WDM) and CSK, which require an equalization stage to minimize the interference in VLC systems. Zero-forcing (ZF) and minimum mean square error (MMSE) equalizers are the usual algorithms applied to equalize [10]–[12].

ZF equalizer is a linear algorithm that reduces ICI to zero in a noiseless scenario. In multispectral camera communication (MCC), the channel matrix is formed by the responses of each camera band, i.e., the spectral signature. In most cases, this matrix could be non-square if the number of transmitters is different from the number of bands. For those cases, the Moore-Penrose pseudo-inverse (\mathbf{W}) can be used to get the inverse channel matrix (Equation 4), which is applied to the received signal.

$$\mathbf{W}_{ZF} = \mathbf{H}^T (\mathbf{H} \cdot \mathbf{H}^T)^{-1}, \quad (4)$$

where \mathbf{H} is the channel matrix and T indicates transposition.

On the other hand, MMSE equalizers are typically employed in communication systems instead of ZF ones since they take into consideration the noise in the system to optimize the output signal-to-noise ratio (SNR). Equation 5 reveals the calculation of the matrix that is used to make the received signal close to the transmitted signal.

$$\mathbf{W}_{MMSE} = \mathbf{H}^T \left(\mathbf{H} \cdot \mathbf{H}^T + \frac{1}{SNR} \cdot \mathbf{I} \right)^{-1}, \quad (5)$$

where \mathbf{I} is the identity matrix. It can be noted from Equation 5 that for high SNR values, the Moore-Penrose inverse used in ZF equalization (Equation 4) and the matrix used in MMSE are equivalent.

On the other hand, the received signal y can be represented as:

$$y = \mathbf{H} \cdot x + n, \quad (6)$$

where x is the transmitted signal and n is additive white Gaussian noise (AWGN). Once the compensation matrix \mathbf{W} is calculated, introducing the linear compensation in Equation 6 yields an estimation of the transmitted signal (Equation 7).

$$\hat{x} = \mathbf{W} \cdot (\mathbf{H} \cdot x + n) \quad (7)$$

It must be considered that regardless of the estimation mechanism of \mathbf{W} , its components will be subject to AWGN. Therefore, the compensation mechanism will not be ideal, and an estimation of the compensation performance is needed. In this regard, the condition number of the channel matrix can be used as this performance metric, as shown in [9] (Equation 8). Well-conditioned matrices (values close to one) better estimate the transmitted signal than ill-conditioned ones (values much higher than one).

$$\text{cond}(\mathbf{H}) = \|\mathbf{H}\| \cdot \|\mathbf{H}^{-1}\| \quad (8)$$

III. THERMAL EFFECTS ON LED DEVICES

The impact of temperature on LED devices has been extensively investigated in the literature. It is well-documented that the efficiency and the spectral characteristics of these light sources are severely affected by variations in the p-n junction temperature.

The energy gap of the semiconductor materials depends on the junction temperature, as modeled in Equation 9 [13]. Generally, the energy gap decreases as temperature increases. Thus, since the energy is inversely proportional to the wavelength (Planck-Einstein relation), the latter increases with temperature causing a variation in the LED emission.

$$E_g = E_0 - \frac{\alpha T^2}{T + \beta}, \quad (9)$$

where T is temperature, E_0 is energy gap at 0 K temperature condition, and α and β are semiconductor-dependent constants, which are empirically determined.

As regards photometric parameters, in [14], surface mount device (SMD) LED's optical parameters were measured at various temperature conditions. It revealed that the peak wavelengths were expectedly red-shifted as temperature increased. Besides, intensity, spectral width, and color-coordinates shift were affected. In addition, luminous flux and efficacy on LEDs were analyzed at different operating conditions in [15]. Based on the fact that luminous flux and efficacy decrease as junction temperature grows, the authors determined the optimized conditions of the LEDs.

Considering the temperature effects mentioned above, this work proposes taking advantage of the thermal impact on LEDs, especially those concerning spectral changes, to utilize a multispectral camera that captures the variation. Thus, by inducing a controlled temperature to the LED would be possible to have the same light source with a different spectral signature. As a result, this spectral variation could be used to implement several communication channels in an OCC link with a multispectral camera as a receiver.

IV. METHODOLOGY

The basic concept of the experiment was to use pairs of the same LED model and change their p-n junction temperature by the Joule effect to obtain different spectral responses. Thus, each LED had a specific spectral signature that a multispectral (MS) camera could capture. Furthermore, in order to have those different signatures, each LED had distinct pulse-width modulation (PWM) duty cycle (DC) values so that the higher the DC value, the higher the junction temperature. No thermal management techniques, such as heat sinks, were used in this work, as they would reduce the variation of the LED spectral characteristics. Once the desired temperature was reached, the data transmission started, the camera captured the images, and, finally, the system's performance was evaluated. Taking the aforementioned explanation into account, Fig. 1 depicts the three main phases of the experiment.

In the first phase, several LED p-n junction temperatures must be achieved. Therefore, the LEDs were set with 30% and 70% of DC values. The frequency of the PWM was set to 5 Hz (bit time of 200 ms). In order to reach the thermal steady state on the LEDs, before sending data, the transmitters were set to an idle state for 5 minutes because no external thermal management technique was applied to

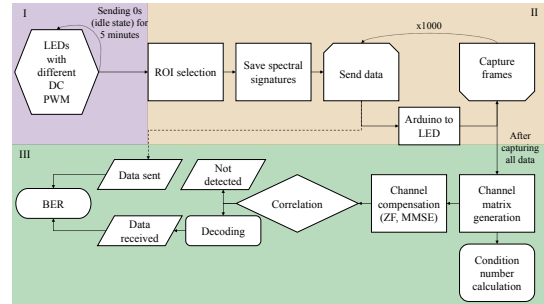


Fig. 1. Flow diagram of the methods. It is divided into three phases. Phase I: stabilization of the LED temperature. Phase II: transmission and reception. Phase III: performance evaluation.

stabilize the temperature. It consisted of keeping the LEDs sending a binary zero with the corresponding DC.

During the second phase, the region of interest (ROI), where the light beams of the LEDs were mixed, was selected. Then, the channel matrix was estimated by capturing the spectral responses of each LED. After that, the transmission began. On the other hand, data transmission was based on the following steps. Firstly, a list of 1000 8-bit pseudo-random integers was generated for each transmitter. Next, the elements of each list were sent to the micro-controller devices in byte format. However, the generated bit sequence was 8B/10B encoded in the micro-controller part. Due to the sensitivity of the spectral signature to temperature, it was essential to avoid long sequences of "1" or "0". Therefore, the applied encoding allowed a header comprising non-consecutive "0" and "1". Moreover, the same header was added after the payload to improve the frame-detection process.

Regarding the MS camera, it has eight narrow bands whose center wavelengths are, from band 1 to band 8: 424, 464, 504, 544, 573, 614, 656, and 699 nm, respectively. Besides, it possesses one panchromatic band that covers the wavelength range from 400 to 800 nm (band 9). The MS camera's frame rate was set to 50 frames per second (fps) and working mode to global shutter. These parameters would allow capturing every 20 ms, so, as the bit time was 200 ms, it permitted ten samples per bit. Although the orchestration script synchronized transmission and data capture, a guard period was added before and after data transmission to ensure that the whole bit stream (header + payload + footer) was captured. Those frames were stored in a ring buffer and saved individually per every data sent. As for the exposure, the aperture setting was $f/2.4$, the maximum allowed by the lens, and the exposure time varied according to the LEDs used (Table I) with the purpose of not saturating the camera with the signals.

Finally, once all the data were taken, the third phase evaluated the system performance. It began with the generation of the channel matrix. The spectral signatures of each LED were normalized by their maximum values and added to the matrix so that it had one signature per row. Alternatively, the condition number of the matrix was

TABLE I
EXPERIMENT KEY PARAMETERS.

Parameter	Value
Transmitter	
Light sources	Kingbright L-53SRC-C (Red)
Dominant wavelengths [nm]	Kingbright L-154A4SUREQBFZGEW (Green, Blue)
Control device	660 (Red), 520 (Green), 460 (Blue) Arduino UNO
Receiver	
Camera	SILIOS Technologies CMS-C1-C-EVRIM-GigE
Resolution [px]	1280x1024 (raw image) 426x339 (multispectral images)
Exposure time [ms]	20 (Red), 6.5 (Green), 0.25 (Blue)
Aperture	f/2.4
Frame rate [fps]	50
Shutter mode	Global shutter
Bit stream	
Coding	8B/10B
Modulation	VPPM
Bit time [ms]	200
Duty cycle	30%, 70%
Bits	Header: 10, Payload: 8, Footer: 10

TABLE II
CONDITION NUMBER OF THE CHANNEL MATRICES.

Condition number (dB)	R	G	B
	24.10	31.29	31.18

calculated as a metric of its performance. Following this, the channel matrix was compensated by applying ZF and MMSE algorithms. At this point, the mixed signals were consequently split into two signals. The resulting signals were then correlated with a matrix comprising all available transmitted signals.

Given that the length of the transmitted signal (header + payload + footer) was shorter than the length of the received signal because the latter included extra frames to avoid missing information, the correlation was performed traversing the template signals through the received signal. As soon as the correlation had been done, the maximum value was then taken. Before decoding the signal, in order to prevent getting a large number of bit errors, a correlation threshold was established. The bit stream was deemed undetected if the maximum coefficient was less than the threshold. Otherwise, if it was greater than the threshold, the received signal was decoded and compared to the sent signal obtaining the bit error rate (BER). The procedure was replicated for several thresholds ranging from 0 to 0.95. Lastly, the whole process was repeated for each LED pair. Table I summarizes the experiment key parameters.

V. RESULTS

Table II compares the condition numbers of all the matrices employed in this work. It is divided into three columns corresponding to the RGB LEDs. It can be seen that the red LED obtained the lowest values, indicating that the spectral response curves of this color are the most separable ones. For the green and the blue LEDs, both obtained similar results. It is mathematically proved because condition number tends to infinity if a spectral signature is close to a linear combination of others. Therefore, the matrices comprising the spectral responses of LEDs at different temperatures whose variability from each other is not significant would be worse conditioned than those

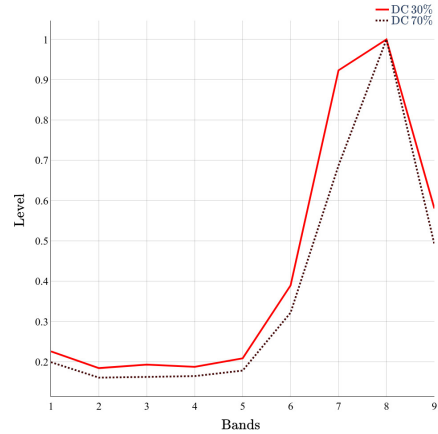


Fig. 2. Normalized spectral signatures of the red LEDs at different temperatures. Solid and dotted lines correspond to the LEDs working at 30% and 70% DC values, respectively.

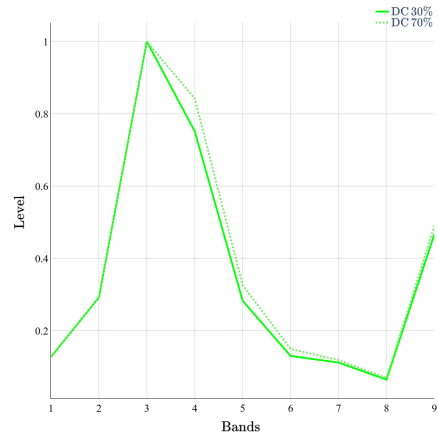


Fig. 3. Normalized spectral signatures of the green LEDs at different temperatures. Solid, and dotted lines correspond to the LEDs working at 30% and 70% DC values, respectively.

matrices formed by the spectral signatures of LEDs with considerable variability.

Figs. 2, 3, and 4 show the spectral signatures of the three LEDs (red, green, and blue, respectively) at different temperatures (several DC values). The x-axis represents the spectral bands, whereas the y-axis represents the normalized camera level. It can be seen that the responses of the red LEDs showed the highest variability from each other, while the green and the blue LEDs presented a higher similarity, respectively.

The system performance for two transmitters is presented in Fig. 5. These pinpoint the BER and the not detected bit streams based on the imposed correlation threshold. The algorithm employed for the channel compensation to obtain these results was the ZF. The MMSE

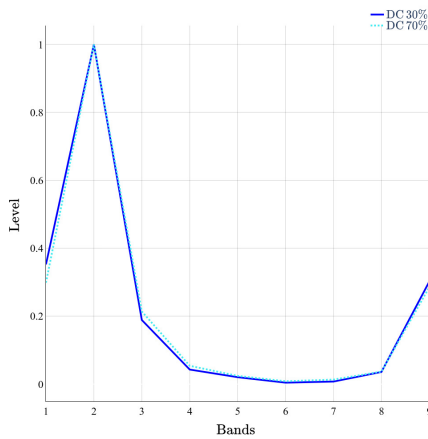


Fig. 4. Normalized spectral signatures of the blue LEDs at different temperatures. Solid and dotted lines correspond to the LEDs working at 30% and 70% DC values, respectively.

results were omitted in this paper because they showed similar performance to the ZF due to the high SNR of the link.

As far as the performance analysis is concerned, the best outcome was obtained for the red LEDs, followed by the green and blue LEDs, as expected. It can be noted from Fig. 5a that the BER of the red LEDs was approximately 10^{-2} for the LEDs at 30% and 70% from thresholds of 0 to 0.25. Besides, from the correlation thresholds of 0.5 and 0.6, the BER was below the forward error correction (FEC) limit ($3.8 \cdot 10^{-3}$) for the LEDs at 30% and 70%, respectively. Using those thresholds, the LEDs reached a BER just under $3.5 \cdot 10^{-3}$, and about 3% of the bit streams were not detected. From the thresholds of 0.85 and 0.9, none of the bit streams were detected for the LEDs at 30% and 70%, respectively.

For the green LEDs (Fig. 5b), the one at 30% got a BER of about $4.7 \cdot 10^{-2}$ for the lower threshold values. It reached a BER below the FEC limit from the thresholds greater than 0.75, reaching a BER of $2.5 \cdot 10^{-3}$ with 17% of the bit streams not detected. The LED at 70% achieved better BER performance than its peer with $3.2 \cdot 10^{-2}$ for the lower threshold values. The BER below the FEC limit was reached from thresholds greater than 0.7. Its most striking results were a BER of $3.7 \cdot 10^{-3}$ and approximately 10% of the bit streams not detected. At a threshold of 0.95, the LED at 30% did not detect the majority of the bit streams, while the LED at 70% missed approximately 35% of them. In the case of the blue LEDs (Fig. 5c), their performance was unsuccessful in getting BER below the FEC limit. On the one hand, the LED at 30% got a BER of $3.3 \cdot 10^{-3}$, missing just over 40% of the bit streams at a threshold of 0.85. On the other hand, the LED at 70% got a BER of about 10^{-4} , discarding more than 90% of the bit streams at a threshold of 0.55. Table III highlights the results above mentioned.

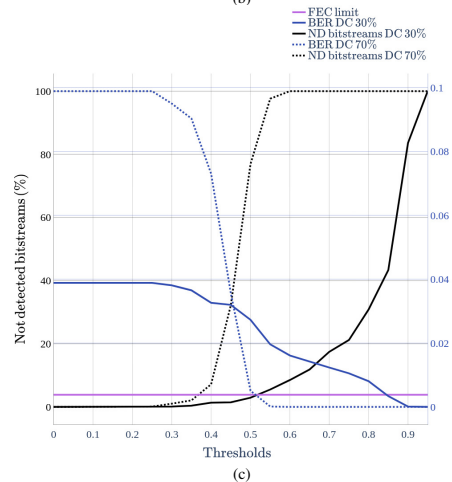
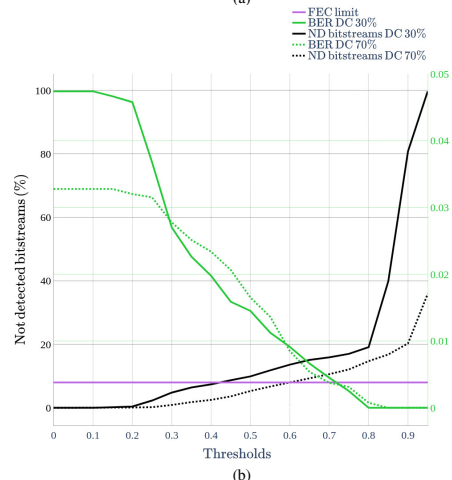
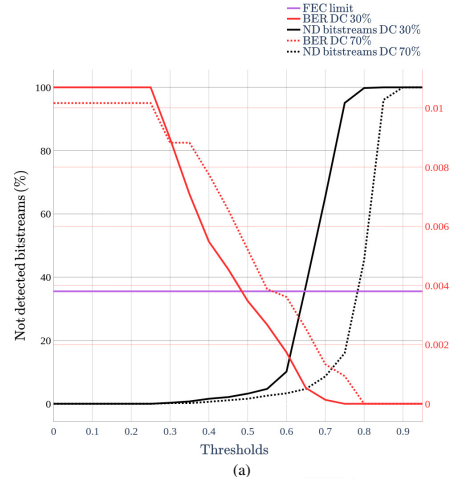


Fig. 5. BER and not detected bit streams at different detection thresholds corresponding to the pairs of (a) red, (b) green, and (c) blue LEDs. Solid and dotted lines correspond to the LEDs working at 30% and 70% DC values, respectively.

TABLE III
LED'S PERFORMANCE COMPARISON

LEDs	DC	BER below FEC limit	Undetected bit streams	Threshold
Red	30%	$3.48 \cdot 10^{-3}$	3.21%	0.50
	70%	$3.61 \cdot 10^{-3}$	3.32%	0.60
Green	30%	$2.50 \cdot 10^{-3}$	17.00%	0.75
	70%	$3.75 \cdot 10^{-3}$	10.60%	0.70
Blue	30%	$3.38 \cdot 10^{-3}$	43.35%	0.85
	70%	$1.30 \cdot 10^{-4}$	97.61%	0.55

VI. CONCLUSIONS

In this research, an experimental OCC link was carried out utilizing a multispectral camera as a receiver. Furthermore, the spectral features of the LEDs employed as transmitters were altered by modifying their p-n junction temperature. Thus, the same LED model would provide different spectral behaviors, which the MS camera would exploit. The LED temperatures were varied because of the Joule effect by supplying various driving currents to the LEDs. No heat sink was used in this work since it would have reduced the thermally-induced spectral variation of the LEDs. Pairs of LEDs with different dominant wavelengths have been used, and their performance has been analyzed.

The strength of this study lies in reaching new channels from the same emitter by changing its temperature. A high-spectral-resolution camera such as a multispectral camera allows grasping the subtle differences in the LED spectral responses. The obtained results prove that BER below the FEC limit can be achieved for those LEDs whose spectral features are considerably affected by thermal changes. It is also fundamental to note that a re-transmission approach must be followed for those cases where the bit streams were not detected.

On the other hand, the performance was somewhat disappointing for the green and the blue LEDs. The prime cause of these undesired results is a consequence of the temperature impact on those light sources. In contrast to the red device, whose peak wavelength was considerably red-shifted, the green and the blue LEDs were less affected by thermal changes. Those results were evidenced in the condition number of their matrices, achieving the worst outcomes for those with greater values. Therefore, the findings of this research suggest that using optical emitters whose spectral characteristics are more affected by thermal variations would improve the achievement of the experiment. However, a trade-off between the degree of spectral variation and the decrease in efficiency caused by temperature must be considered in a scenario where the light sources would be used for both illumination and communication purposes.

The present findings imply that multispectral cameras could be taken advantage of in order to exceed the number of channels that an LED can reach by exploiting the temperature effects on its spectrum.

On a broader level, a combination of LEDs with different dominant wavelengths can be used. Thus, the camera bands centered on a particular wavelength would help to separate the signals following the procedure applied in

this study. Moreover, the prospect of using the thermal effects on LEDs serves as a continuous stimulus for future research. For instance, characterization of various emitting devices could be performed, both the same model as different ones, to analyze the usefulness of each device in this approach.

REFERENCES

- [1] M. Z. Chowdhury, M. Shahjalal, M. K. Hasan, and Y. M. Jang, "The role of optical wireless communication technologies in 5g/6g and iot solutions: Prospects, directions, and challenges," *Applied Sciences*, vol. 9, no. 20, 2019. [Online]. Available: <https://www.mdpi.com/2076-3417/9/20/4367>
- [2] Y. Shiraki, T. G. Sato, Y. Kamamoto, T. Izumi, Y. Nakahara, K. Kondo, and T. Moriya, "A demodulation method using a gaussian mixture model for unsynchronous optical camera communication with on-off keying," *Journal of Lightwave Technology*, vol. 39, no. 6, pp. 1742–1755, 2021.
- [3] P. Hu, P. H. Pathak, H. Zhang, Z. Yang, and P. Mohapatra, "High speed led-to-camera communication using color shift keying with flicker mitigation," *IEEE Transactions on Mobile Computing*, vol. 19, no. 7, pp. 1603–1617, 2020.
- [4] S. Arai, S. Mase, T. Yamazato, T. Endo, T. Fujii, M. Tanimoto, K. Kidono, Y. Kimura, and Y. Ninomiya, "Experimental on hierarchical transmission scheme for visible light communication using led traffic light and high-speed camera," in *2007 IEEE 66th Vehicular Technology Conference, 2007*, pp. 2174–2178.
- [5] D. Iwase, M. Kasai, T. Yendo, S. Arai, T. Yamazato, H. Okada, and T. Fujii, "Improving communication rate of visible light communication system using high-speed camera," in *2014 IEEE Asia Pacific Conference on Circuits and Systems (APCCAS)*, 2014, pp. 336–339.
- [6] E. Tugcu, A. Yazgan, C. Albayrak, and K. Turk, "Red-shift effect in multi-color leds based visible light communication," *Optics Communications*, vol. 463, p. 125451, 2020. [Online]. Available: <https://www.sciencedirect.com/science/article/pii/S0030401820301115>
- [7] D. Moreno, J. Rufo, V. Guerra, J. Rabadan, and R. Perez-Jimenez, "Effect of temperature on channel compensation in optical camera communication," *Electronics*, vol. 10, no. 3, 2021. [Online]. Available: <https://www.mdpi.com/2079-9292/10/3/262>
- [8] W. A. Cahyadi, Y. H. Chung, Z. Ghassemlouy, and N. B. Hassan, "Optical camera communications: Principles, modulations, potential and challenges," *Electronics*, vol. 9, no. 9, 2020. [Online]. Available: <https://www.mdpi.com/2079-9292/9/9/1339>
- [9] D. Moreno, J. Rufo, V. Guerra, J. Rabadan, and R. Perez-Jimenez, "Optical multispectral camera communications using led spectral emission variations," *IEEE Photonics Technology Letters*, vol. 33, no. 12, pp. 591–594, 2021.
- [10] Y. S. Hussein, M. Y. Alias, and A. A. Abdulkafi, "On performance analysis of ls and mmse for channel estimation in vlc systems," in *2016 IEEE 12th International Colloquium on Signal Processing Its Applications (CSPA)*, 2016, pp. 204–209.
- [11] A. Anusree and R. K. Jeyachitra, "Performance analysis of a mimo vlc (visible light communication) using different equalizers," in *2016 International Conference on Wireless Communications, Signal Processing and Networking (WiSPNET)*, 2016, pp. 43–46.
- [12] M. K. Jha, N. Kumar, and Y. V. S. Lakshmi, "Noma mimo visible light communication with zf-sic and mmse-sic," in *2020 2nd PhD Colloquium on Ethically Driven Innovation and Technology for Society (PhD EDITS)*, 2020, pp. 1–2.
- [13] Y. P. Varshni, "Temperature dependence of the energy gap in semiconductors," *physica*, vol. 34, no. 1, pp. 149–154, 1967.
- [14] M. E. Raypah, M. Devarajan, and F. Sulaiman, "Influence of injection current and ambient temperature on intensity and wavelength of low-power smd led," in *2016 IEEE 37th International Electronics Manufacturing Technology (IEMT) 18th Electronics Materials and Packaging (EMAP) Conference*, 2016, pp. 1–6.
- [15] M. E. Raypah, B. K. Sodipo, M. Devarajan, and F. Sulaiman, "Estimation of luminous flux and luminous efficacy of low-power smd led as a function of injection current and ambient temperature," *IEEE Transactions on Electron Devices*, vol. 63, no. 7, pp. 2790–2795, 2016.

This appendix chapter presents the research paper titled “*Multispectral Optical camera communication links based on spectral signature multiplexing*” [116] presented by the author during the course of this thesis development. This paper expands upon one of our previous publications [112]. The article delves into a comprehensive examination of conventional linear equalization techniques, including ZF and MMSE, demonstrating their effectiveness in achieving satisfactory results. The subsequent pages contain the attached camera-ready full paper.

Multispectral Optical camera communication links based on spectral signature multiplexing

Daniel Moreno¹  | Victor Guerra² | Julio Rufo³ | Jose Rabadan¹ | Rafael Perez-Jimenez¹ 

¹Institute for Technological Development and Innovation in Communications (ID²TIC), Universidad de las Palmas de Gran Canaria (ULPGC), Las Palmas de Gran Canaria, Las Palmas, Spain

²Pi Lighting Sarl, Sion, Valais, Switzerland

³Higher Polytechnic School of Engineering and Technology, Universidad de La Laguna (ULL), San Cristóbal de La Laguna, Santa Cruz de Tenerife, Spain

Correspondence

Daniel Moreno.
Email: daniel.moreno@ulpgc.es

Funding information

Agencia Estatal de Investigación, Grant/Award Number: PID2020-114561RB-I00; Universidad de Las Palmas de Gran Canaria, Grant/Award Number: Trainee Predoctoral Research Staff Program

Abstract

Optical camera communication is foreseen to have an essential role in future systems requiring wireless communication capability. In this regard, high-spectral-resolution cameras, such as multispectral (MS) cameras, present specific characteristics that can be exploited to provide new features to optical camera communication links. Using the MS cameras' features to take advantage of the light-emitting diode (LED) behaviour in a novel communication scheme is focussed. Notably, LED spectral response curves are different when their temperature changes. Therefore, these differences can be detected based on the MS cameras' spectral resolution. Thus, more than one communication channel can be attained using the same LED device since the camera can distinguish the different LED spectral signatures. This new approach is analysed in this work, including some equalisation techniques applied to the channel matrix in the receiver to improve the extraction of the transmitted signal reducing the inter-channel interference. For the specific MS camera employed in the experiments, up to two distinct channels could be obtained with the same transmitter at different temperatures, getting a bit error rate below the forward error correction limit. However, obtaining satisfactory results is highly dependent on the variation that temperature causes in the spectral signatures of the LEDs, so further experiments are recommended in future work with different devices.

KEYWORDS

cameras, light emitting diodes, multiplexing, optical communication

1 | INTRODUCTION

Optical camera communication (OCC) has been gaining much attention owing to the widely used types of cameras featured in electronic devices, vehicles, surveillance, and healthcare systems. In addition, the pervasiveness of these devices and the emerging developments in image sensors have prompted this technology for research purposes [1]. Besides, OCC has undergone a revolution in the scientific community over the past decades for its promising immediate applications to the market compared with visible light communication (VLC) systems, which lack commercially available off-the-shelf (COTS)

devices. As a result, new modulation/demodulation approaches and diverse transmitters and cameras have been the subject of recent research. For example, Shiraki *et al.* reported on a demodulation scheme based on a Gaussian-mixture model for an OCC system to obtain the channel states without using synchronization devices in the transmitters [2]. Besides, Hu *et al.* designed an light-emitting diode (LED)-to-camera communication system using colour shift keying (CSK) modulation. The authors evaluated the performance of multiple camera sensors embedded in smartphones achieving low error symbol rates addressing common issues, such as colour flicker, inter-frame data loss, and receiver (RX) diversity [3].

This paper is an extended version of our paper published in: Moreno, D.; Guerra, V.; Rufo, J.; Rabadan, J.; Perez-Jimenez, R. Spectral Signature Multiplexing in Multispectral Camera Communication. In Proceedings of the 13th International Symposium on Communication Systems, Networks and Digital Signal Processing (CSNDSP), Porto, Portugal, 20–22 July 2022.

This is an open access article under the terms of the [Creative Commons Attribution](https://creativecommons.org/licenses/by/4.0/) License, which permits use, distribution and reproduction in any medium, provided the original work is properly cited.

© 2023 The Authors. *IET Optoelectronics* published by John Wiley & Sons Ltd on behalf of The Institution of Engineering and Technology.

Additionally, recent studies utilised neural-network-based approaches to decode information. For instance, Chow *et al.* used a rolling shutter image sensor and an LED light panel for an OCC system. Frame-averaging background removal technique, Z-score normalisation, and neural network were used to achieve non-linear distortion mitigation and satisfactory bit error rate (BER) performance in high inter-symbol interference situations [4]. Furthermore, Tsai *et al.* proposed a pixel-row-per-bit-based neural network to decode data produced by an optical-diffusing-fibre (ODF) transmitter in an OCC link. The authors demonstrated that the proposed algorithm enhanced the BER compared to traditional artificial neural network (ANN) [5].

In spite of the growing body of literature on OCC, the technology's potential still needs to be fully explored, particularly beyond the application of traditional cameras. For instance, several researchers put forward high-speed cameras to boost the bit rate, as in Arai *et al.*'s work, where the authors proposed a hierarchical transmission scheme based on a two-dimensional fast Haar wavelet transform. Thus, data detection is ensured when the camera is distant from the LED emitter [6]. Moreover, Iwase *et al.* proposed a lighting pattern recognition strategy from a pattern-mixed image, adjusting the data rate to the same receiver frame rate and decreasing flickering through 8b/10b encoding [7]. Alternatively, the behaviour of LEDs as optical data transmitters has also been analysed. In particular, temperature-related changes in the LED spectral properties are widely recognized to have a negative impact on communication performance if they are not taken into consideration during the data reception [8, 9].

This paper presents a communication scheme using LEDs as transmitters and a multispectral (MS) camera as a RX. The multiple camera bands provide a higher spectral resolution, permitting the distinction of optical signals with wavelengths. In addition, the LED spectral shift caused by thermal variations is taken advantage of. Given that the spectral signatures of the LEDs vary with temperature modifications, these changes are captured by a high-spectral-resolution camera. The spectral variations will be used to differentiate the LED's transmissions at different temperatures. As a result, new communication channels can be established using the same type of device because the temperature affects the LED's spectral response curves.

To achieve these channels, traditional linear methods have been chosen. This approach may be compared to previous methods that used clustering to obtain communication channels, which have been shown to have better performance than traditional linear methods such as zero-forcing (ZF) equalisation [10]. However, this study provides a deeper analysis of ZF and minimum mean square error (MMSE) equalisation, demonstrating that it can also produce satisfactory results. Additionally, the comparison of this approach to previous methods can provide valuable insight for the research community. Our submission includes experimental results and further analysis to validate the proposed method.

This paper takes a new look at OCC systems by employing an MS camera and thermally induced spectral changes on

LEDs. A novel approach is presented, exploring the possibility of adopting a spectral signature multiplexing based on temperature. It is an innovative method as an alternative to wavelength division multiplexing (WDM), which is detailed in the following sections. Consequently, this study aims to assess the performance of this new proposal by making use of the characteristics of MS cameras that allow discriminating the spectral responses of LEDs at different temperatures.

This paper is divided into six sections. Section 2 provides a brief overview of OCC and discusses the benefits of utilising an MS camera as a receiver in OCC. Section 3 explores the effect of temperature on LEDs. Section 4 outlines the procedures and techniques used to perform the experiments. Section 5 presents the results obtained from the methodology implemented. Finally, Section 6 offers some concluding remarks.

2 | MULTISPECTRAL CAMERA COMMUNICATION

Optical camera communication uses cameras or image sensors to capture optical signals, unlike VLC systems that employ photodiodes. Therefore, this technology takes advantage of the cameras in most electronic devices, making it possible to implement this system without needing additional or modified hardware. Nonetheless, the fact that these cameras are not optimised for communications hinders the bit rate that can be achieved in OCC as it depends on the pixel clock and the scanning method, thereby making this technology oriented to low data rate links [11].

Therefore, one of the main challenges in OCC is data rate improvement, so recent developments have concentrated on proposing different schemes and techniques in this regard. Younus *et al.* implemented an ANN equaliser to reduce intersymbol interference and enhance the data rate. The authors trained the ANN once for several exposure times and stored it in a look-up table [12]. Nonetheless, their result needed to provide more robustness to high exposure time, limiting their usability in applications where visualisation and data gathering were needed. This limitation was overcome in ref. [13] using a convolutional autoencoder for improving signal quality, allowing exposure times up to 7 times greater than the symbol period and with a more computationally efficient architecture than in ref. [12]. Huang *et al.* proposed a real-time OCC system based on colour-intensity modulation multi-input-multi-output (CIM-MIMO). They created a high-dimensional signal constellation and parallel communication channels using spatial, colour, and intensity dimensions to boost data rate and improve the BER performance [14].

As OCC can use the entire light spectrum (ultraviolet, visible light, and infrared), not only visible light, high-spectral-resolution cameras, such as MS or hyperspectral cameras, can provide multiple-wavelength sensitivity utilising one device. Hence, due to the filters centred on different wavelengths that this type of camera has, the application of WDM or MIMO techniques could be simplified.

Moreover, considering the temperature effects on LEDs, which modify their spectral behaviour, MS cameras can turn this a priori detrimental factor into an advantage. The high spectral resolution of those devices would detect multiple signals from the same light source at various temperatures as a function of the band number and their bandwidth [15]. This issue is crucial in this research and will be thoroughly addressed in Section 3.

To the best of the authors' knowledge, the employment of MS cameras as receivers in an OCC system has yet to be exploited. Therefore, multispectral camera communication (MCC) is a field that can be explored and OCC performance is improved because of the natural characteristics of this kind of camera.

For the optical wireless communication's channel modelling, Equation (1) represents the OCC system's received power.

$$P_{rx} = P_{tx} R(\theta, \phi) \frac{A_{lens}}{d^2} \cos(\Psi), \quad (1)$$

where P_{tx} is the transmitted power, $R(\theta, \phi)$ is the source's radiation pattern at elevation θ and azimuth ϕ , A_{lens} is the main lens' cross-section, d is the link range, and Ψ is the impact angle. Considering the image-forming optics theory inherent when employing cameras as receivers for communication, it is demonstrated that the pixel power does not depend on the distance if the LED's projected size on the image sensor is greater than one pixel [16].

$$A_{proj} = \frac{N_x N_y}{FOV_x FOV_y} \frac{A_{tx}}{d^2}, \quad (2)$$

where A_{proj} is the projected number of pixels of the optical emitter on the sensor, N_x and N_y define the sensor's pixel resolution, FOV_x and FOV_y are the camera's horizontal and vertical fields of view, respectively, and A_{tx} is the transmitter's effective area (from the receiver's viewpoint). It can be seen from these equations that P_{rx} and A_{proj} decrease with increasing distance (constant power density on the image sensor). Thus, the received optical power at each pixel is expressed in Equation (3) by combining Equations (1) and (2).

$$P_{px} = P_{tx} R(\theta, \phi) \frac{A_{lens}}{A_{tx}} \frac{FOV_x FOV_y}{N_x N_y} A_{px} \cos(\Psi), \quad (3)$$

where P_{px} is the pixel power (in watts) and A_{px} is the pixel area.

Moreover, channel compensation is critical in any system subject to inter-channel interference (ICI). Several techniques aim to alleviate ICI, such as MIMO, WDM, and CSK, which require an equalisation stage to minimise the interference in VLC systems. ZF and MMSE equalisers are the usual algorithms applied to equalise [17–19].

On the one hand, ZF equalisers are linear algorithms that minimise ICI to zero in noiseless situations. Channel matrices in MCC are formed by the received spectral signatures of the transmitters. Since the channel matrices are likely to be

non-square because the transmitters and the camera's number of bands may differ, the Moore-Penrose pseudo-inverse (\mathbf{W}) can be applied to determine the inverse matrix (Equation 4), thereby estimating the received signal.

$$\mathbf{W}_{ZF} = \mathbf{H}^T (\mathbf{H} \cdot \mathbf{H}^T)^{-1}, \quad (4)$$

where \mathbf{H} is the channel matrix and T indicates transposition.

On the other hand, in scenarios where the signal-to-noise ratio (SNR) is not high and ZF equalisers are limited, MMSE equalisers would be more suitable. Equation (5) shows the calculation of the matrix that is used to approximate the received signal to the transmitted signal.

$$\mathbf{W}_{MMSE} = \mathbf{H}^T \left(\mathbf{H} \cdot \mathbf{H}^T + \frac{1}{SNR} \cdot \mathbf{I} \right)^{-1}, \quad (5)$$

where \mathbf{I} is the identity matrix. It is straightforward to verify from Equation (5) that \mathbf{W}_{ZF} (Equation 4) and \mathbf{W}_{MMSE} are consistent for high SNR values.

Moreover, the received signal y can be expressed as follows:

$$y = \mathbf{H} \cdot x + n, \quad (6)$$

where x is the transmitted signal and n is additive white Gaussian noise (AWGN). After calculating the compensation matrix \mathbf{W} , integrating the linear compensation to Equation (6) estimates the transmitted signal (Equation 7).

$$\hat{x} = \mathbf{W} \cdot (\mathbf{H} \cdot x + n) \quad (7)$$

It is worth noting that \mathbf{W} 's components will be susceptible to AWGN, disregarding the calculation technique used. The compensation approach will thus be flawed, necessitating an evaluation of its performance. In this sense, calculating the condition number of the channel matrix is proposed as an option to assess performance [15] (Equation 8). The transmitted signal is more accurately estimated by well-conditioned matrices (values near to one) than by ill-conditioned ones (values much higher than one).

$$\text{cond}(\mathbf{H}) = \|\mathbf{H}\| \cdot \|\mathbf{H}^{-1}\| \quad (8)$$

3 | THERMAL EFFECTS ON LED DEVICES

In the literature, LED temperature effects have been widely addressed. Some of the main aspects discussed are the impact that changes in the p-n junction temperature cause on the efficiency and the spectral.

Equation (9) is commonly used to model the relationship between the semiconductor material's energy gap and the junction temperature [20]. Accordingly, the energy gap usually

decreases as the temperature rises. In addition, a change in LED emission is caused as the wavelength increases with temperature due to the Planck-Einstein connection (Equation 10).

$$E_g = E_0 - \frac{\alpha T^2}{T + \beta}, \quad (9)$$

where T is temperature, E_0 is energy gap at 0 K temperature condition, and α and β are semiconductor-dependent constants, which are empirically determined.

$$E_g = hf = \frac{hc}{\lambda}, \quad (10)$$

where h is Planck's constant, f is frequency, c is the speed of light in vacuum, and λ is wavelength.

On the other hand, several investigations have studied the impact of temperature on photometric parameters. For instance, optical parameters of surface mount device LEDs were determined under different temperature conditions in ref. [21], revealing a predictable red shift of the peak wavelength when the temperature grew. Likewise, temperature influenced the devices' intensity, spectral width, and colour coordinate shifts. Furthermore, other parameters were examined in [22]. Namely, the LED's luminous flux and efficacy were estimated at different operating conditions. The authors found the optimised conditions of the light sources considering that the aforementioned parameters decrease as junction temperature increases.

Many studies have been conducted on LED lifetime by the accelerated ageing test. These studies conducted tests that subjected LEDs to the leading causes affecting their behaviour, that is, temperature and current through the LED. Most recent evidence shows that luminous flux, colour changes, and lifetime are sensitive to thermal effects, and the current stress degrades the LEDs more than the thermal stress [23–25].

This study suggests utilising an MS camera in light of the thermal impact indicated earlier. Remarkably, it is proposed to capture the spectral shifts caused by temperature.

Considering the temperature effects mentioned above, this work proposes taking advantage of the thermal impact on LEDs, especially those concerning spectral changes, to utilise an MS camera that captures the variation. Therefore, applying a regulated temperature to the transmitter is conceivable to have the same LED with a distinct spectral response curve. Consequently, using an MS camera as a receiver in an OCC link, these spectral changes could be exploited to establish new communication channels.

4 | METHODOLOGY

The main aim of this work is to experimentally test the performance of an MS camera in a communication link (LED-to-camera). In order to exploit the high-spectral-resolution

capability of this kind of camera, LEDs of a specific wavelength have been employed at different driving currents to modify their working temperature and get different spectral signatures that the MS camera can detect.

4.1 | Experimental setup

Different types of LEDs were used as transmitters in the system. Each LED's driving current was adjusted by a circuit powered by a voltage source. In addition, the circuits were linked to a microcontroller that output a variable pulse position modulation signal based on the target temperature to be induced in the LED by the Joule heating effect. Finally, the microcontroller devices and the control PC were paired to send the transmitted data over the serial port.

Additionally, the PC connected to the MS camera managed the image acquisition procedure through Ethernet. It was necessary to use a diffuser between the LEDs and the camera to mix the light beams and prevent pixel saturation. Furthermore, the entire system was set inside a dark room to minimise the influence of background light. Lastly, all the operations were coordinated using a Python-based automation script that enabled communication between the microcontroller devices and the camera.

4.2 | Description of procedures

The basic concept of the experiment was to use groups of the same LED model and change their p-n junction temperature by the Joule effect to obtain different spectral signatures. Since each LED possessed a particular spectral response curve, an MS camera could capture it. Hence, the LEDs were set with distinct pulse-width modulation (PWM) duty cycle (DC) values to have those different signatures. Thus, the higher the DC value, the higher the junction temperature. Because one of the purposes of the experiment was to get the maximum spectral variation caused by temperature, no thermal management techniques, such as heat sinks, were used in this work as they would reduce the changes in the LED's spectral characteristics. After reaching the target temperature, the data transmission started, the camera captured the images, and finally, the system's performance was evaluated. In light of the explanation above, Figure 1 outlines the three main phases of the experiment.

In the first phase, several LED p-n junction temperatures must be achieved. Therefore, the LEDs were set with 30% and 70% of DC values when using two transmitters and 30%, 50%, and 70% when using three transmitters. The frequency of the PWM was set to 5 Hz (bit time of 200 ms). In order to reach the thermal steady state on the LEDs, the transmitters were set to an idle state for 5 min before sending data because no external thermal management technique was applied to stabilise the temperature. It consisted of keeping the LEDs sending a binary zero with the corresponding DC.

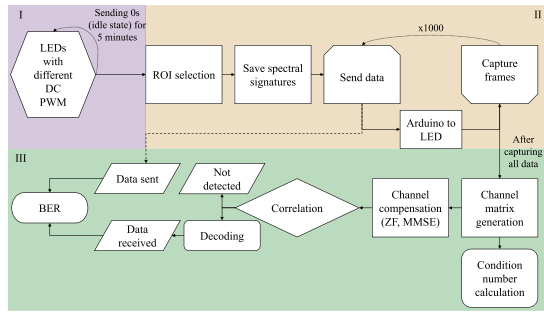


FIGURE 1 Flowchart of the procedures. The methodology is split into three phases. Phase I: LED temperature stabilisation. Phase II: transmit-receive process. Phase III: system performance assessment. LED, light-emitting diode.

During the second phase, the region of interest, where the light beams of the LEDs were mixed, was selected. Then, the channel matrix was estimated by capturing the spectral responses of each LED. After that, the transmission began. On the other hand, data transmission was based on the following steps. First, a list of 1000 eight-bit pseudo-random integers was generated for each transmitter. Next, the elements of each list were sent to the microcontroller devices in byte format. However, the generated bit sequence was 8b/10b encoded in the microcontroller part. Due to the sensitivity of the spectral signature to temperature, it was essential to avoid long sequences of “1” or “0”. Therefore, the applied encoding allowed a header comprising non-consecutive “0” and “1”. Likewise, the same header was added after the payload to improve the frame-detection process. Figure 2 depicts the structure of the bit stream.

Regarding the MS camera, it has eight narrow bands whose centre wavelengths are, from band 1 to band 8: 424, 464, 504, 544, 573, 614, 656, and 699 nm, respectively. Besides, it possesses one panchromatic band that covers the wavelength range from 400 to 800 nm (band 9). The MS camera's frame rate was set to 50 frames per second (fps) and a working mode to global shutter. These parameters would allow capturing every 20 ms, so, as the bit time was 200 ms, it permitted 10 samples per bit. Although the orchestration script synchronized transmission and data capture, a guard period was added before and after data transmission to ensure that the whole bit stream (header + payload + footer) was captured. Those frames were stored in a ring buffer and saved individually per every data sent. As for the exposure, the aperture setting was $f/2.4$, the maximum allowed by the lens, and the exposure time varied according to the LEDs used (Table 1) with the purpose of not saturating the camera with the signals.

Finally, the third phase evaluated the system performance once all the data were taken. It began with the generation of the channel matrix. The spectral signatures of each LED were normalised by their maximum values and added to the matrix so that it had one signature per row. Alternatively, the condition number of the matrix was calculated as a metric of its performance. Following this, the channel matrix was compensated by

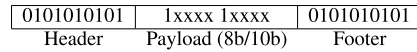


FIGURE 2 Packet structure of the bit streams.

TABLE 1 Key parameters of the experiment.

Parameter	Value
Transmitter	
Light sources	Kingbright L-53SRC-C (Red) Kingbright L-154A4SUREQBFZGEW (Green, Blue)
Dominant wavelengths [nm]	660 (Red), 520 (Green), 460 (Blue)
Control device	Arduino UNO
Receiver	
Camera	SILIOS Technologies CMS-C1-C-EVRIM-GigE
Resolution [px]	1280×1024 (raw image) 426×339 (multispectral images)
Exposure time [ms]	20 (Red), 6.5 (Green), 0.25 (Blue)
Aperture	$f/2.4$
Frame rate [fps]	50
Shutter mode	Global shutter
Bit stream	
Coding	8b/10b
Modulation	VPPM
Bit time [ms]	200
Duty cycle	30%, 50%, 70%
Bits	Header: 10, Payload: 8, Footer: 10

applying ZF and MMSE algorithms. At this point, the mixed signals were consequently split into two (or three) signals. The resulting signals were then correlated with a matrix comprising all available transmitted signals.

Given that the length of the transmitted signal (header + payload + footer) was shorter than the length of the received signal because the latter included extra frames to avoid missing information, the correlation was performed by traversing the template signals through the received signal. As soon as the correlation had been done, the maximum value was then taken. Before decoding the signal, in order to prevent getting a large number of bit errors, a correlation threshold was established. The bit stream was deemed undetected if the maximum coefficient was less than the threshold. Otherwise, if it was greater than the threshold, the received signal was decoded and compared to the sent signal obtaining the BER. The procedure was replicated for several thresholds ranging from 0 to 0.95. Lastly, the whole process was repeated for each LED group. Table 1 summarises the experiment key parameters.

5 | RESULTS

Table 2 shows the condition numbers of all the matrices used in this study. It is divided into two columns corresponding to the number of transmitters, which in turn are subdivided into three columns corresponding to the red-green-blue LEDs. It is apparent that the red LEDs performed the lowest values, revealing that their spectral signatures are the most distinguishable. On the contrary, the green and the blue LEDs obtained similar results. It is mathematically demonstrated that as the condition number approaches infinity when a spectral response curve is close to a linear combination of others. Consequently, matrices comprising the LED spectral signatures at different temperatures whose variability from each other is not significant would be worse conditioned than those matrices formed by the spectral signatures of LEDs with substantial variability.

Figure 3 depicts the spectral signatures of the three LEDs (red, green, and blue) at different temperatures (several DC values). The x -axis represents the spectral bands, whereas the y -axis represents the normalised camera level. It can be seen that the spectral signatures of the red LEDs showed the highest variability from each other, while the green and the blue LEDs presented a higher similarity, respectively.

The system performance for two and three LED emitters is illustrated in Figures 4 and 5. They show the BER and the undetected bit streams depending on the imposed correlation threshold. A ZF algorithm was employed for channel compensation. The results from the MMSE equaliser were left out in this contribution as they performed similarly to ZF because of the high link SNR.

As expected, the red LEDs produced the best results in terms of performance examination, followed by the green and blue LEDs. For the LEDs at 30% and 70%, the BER of the red light sources was roughly 10^{-2} from thresholds of 0–0.25 as shown in Figure 4a. Additionally, from the detection thresholds of 0.5 and 0.6, the BER was below the forward error correction (FEC) limit ($3.8 \cdot 10^{-3}$) for the LEDs at 30% and 70%, respectively. Specifically, a BER slightly less than $3.5 \cdot 10^{-3}$ was achieved, along with approximately 3% of the bit streams not detected. Finally, none of the bit streams were detected for the LEDs from the thresholds of 0.85 and 0.9 at 30% and 70%, respectively.

Figure 4b depicts the green LEDs curves. It can be seen that the transmitter at 30% obtained a BER of approximately $4.7 \cdot 10^{-2}$ for the minimum threshold values. From the thresholds greater than 0.75, this LED achieved a BER of $2.5 \cdot 10^{-3}$, missing 17% of the bit streams. The LED at 70% outperformed its counterpart getting a BER of $3.2 \cdot 10^{-2}$ for the

lower threshold values. The BER was below the FEC limit when the thresholds exceeded 0.7. Its most remarkable outcome was a BER of $3.7 \cdot 10^{-3}$ and about 10% of the bit streams undetected. At a threshold of 0.95, the bulk of bit streams of the LED at 30% was not detected, while about 35% of the bit streams were missed for the LED at 70%.

It can be noted from Figure 4c that the blue LEDs failed to get a BER below the FEC limit. For the LED at 30%, a BER of $3.3 \cdot 10^{-3}$ was achieved, but discarding slightly more than 40% of the bit streams at a threshold of 0.85. For the LED at 70%, a BER of approximately 10^{-4} was reached, not detecting

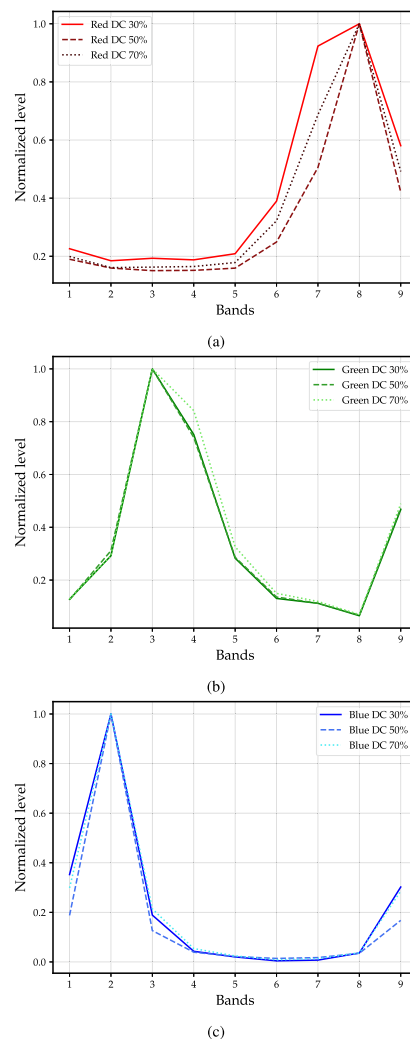


FIGURE 3 Spectral response curves of the three LEDs used in this study at different temperatures. (a) Red LEDs, (b) green LEDs, and (c) blue LEDs. Solid, dashed, and dotted lines correspond to the LEDs working at 30%, 50%, and 70% duty cycle (DC) values, respectively. LED, light-emitting diode.

TABLE 2 Channel matrices condition numbers.

Condition number (dB)	2 TXs			3 TXs		
	R	G	B	R	G	B
	24.10	31.29	31.18	42.80	45.48	50.60

Abbreviation: TXs, diverse transmitters.

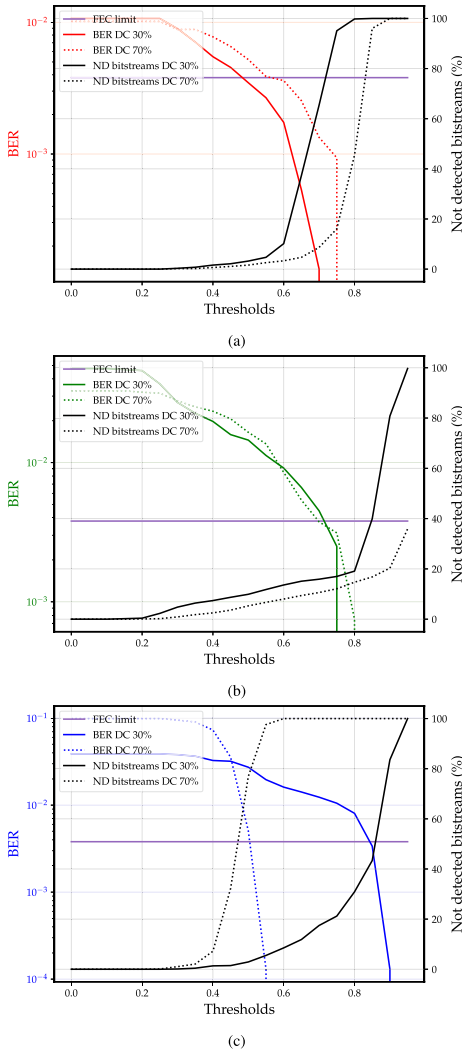


FIGURE 4 Bit error rate (BER) and undetected bit streams at various correlation thresholds corresponding to the (a) red, (b) green, and (c) blue LED pairs. Solid and dotted lines correspond to the LEDs working at 30% and 70% duty cycle (DC) values, respectively. LED, light-emitting diode.

more than 90% of the bit streams at a threshold of 0.55. Table 3 outlines the aforementioned results.

Regarding the three-transmitter case (Figure 5), none of the colours could perform satisfactorily with most of their BER values above the limit.

The quality of the above results depended mainly on the separation by channel compensation of the mixed signals. Figure 6 pinpoints an example of the transmission of the red LEDs. The first row depicts the received signal, that is, the mixed signals of both LEDs. In order to ease the visualisation, only the panchromatic band was shown. The second and third rows show the separated signal after compensation and the data sent corresponding to the LEDs at DC 30% and 70%,

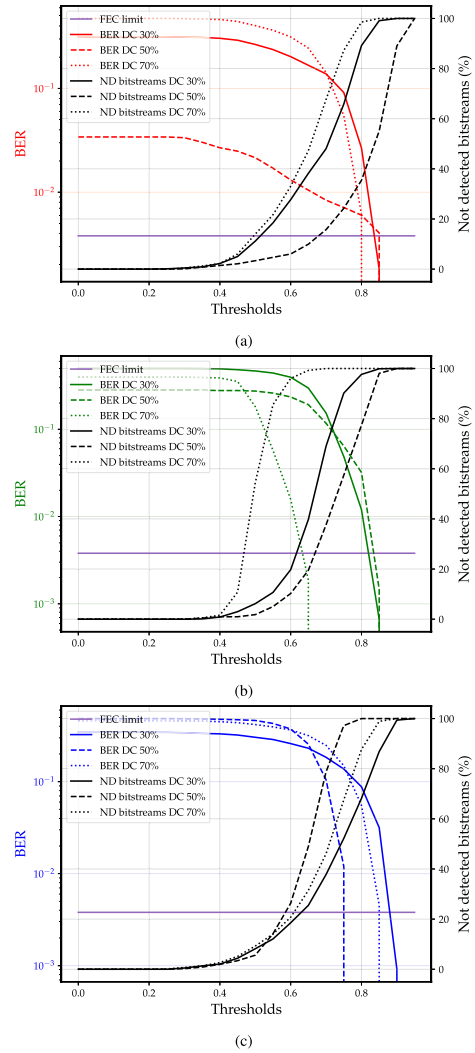


FIGURE 5 Bit error rate (BER) and undetected bit streams at various correlation thresholds corresponding to the (a) red, (b) green, and (c) blue LED trios. Solid, dashed, and dotted lines correspond to the LEDs working at 30%, 50%, and 70% duty cycle (DC) values, respectively. LED, light-emitting diode.

TABLE 3 Comparison of LED performance.

LEDs	DC	BER below FEC limit	Undetected bit streams	Threshold
Red	30%	$3.48 \cdot 10^{-3}$	3.21%	0.50
	70%	$3.61 \cdot 10^{-3}$	3.32%	0.60
Green	30%	$2.50 \cdot 10^{-3}$	17.00%	0.75
	70%	$3.75 \cdot 10^{-3}$	10.60%	0.70
Blue	30%	$3.38 \cdot 10^{-3}$	43.35%	0.85
	70%	$1.30 \cdot 10^{-4}$	97.61%	0.55

Abbreviation: LED, light-emitting diode.

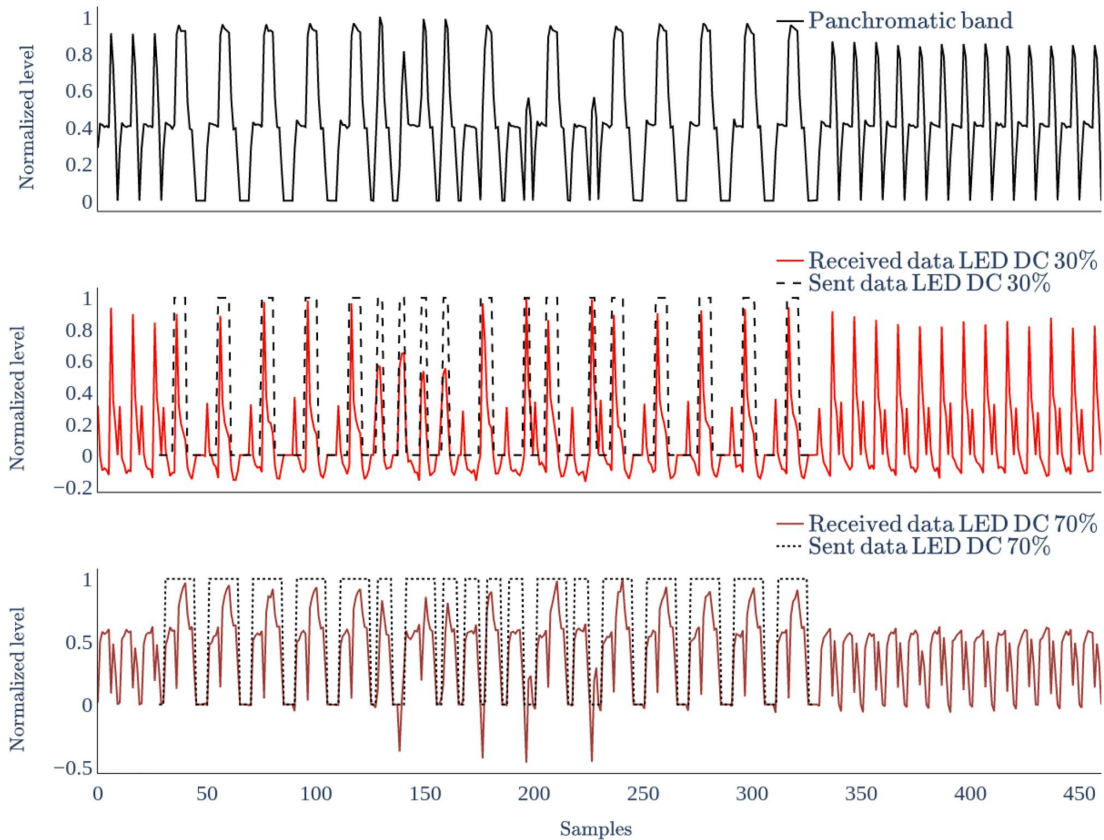


FIGURE 6 Example of transmission of the red LEDs. The first row shows the mixed signal of the LEDs received by the camera. The second and the third rows depict the signals after compensation of the LEDs at 30% and 70%, respectively. The sent data are superimposed for both LEDs.

respectively. In Figure 6, LED 1 (DC 30%) sent a decimal 226 (1110 0010) and LED 2 (DC 70%) sent a decimal 123 (0111 1011). Note that the bit streams show the data after the 8b/10b encoding (LED 1: 11110 10010, LED 2: 10111 11011). It can be seen that the bit streams started at approximately sample 28 and finished at sample 328. For the rest of the samples, the LEDs were in an idle state. It is remarkable to note that, although both signals interfere, the decoding process was successful. Because of that interference, when LED 1 had a peak, LED 2 tended to have a trough and vice versa (for instance, see the peaks between the “1” of the header in LED 1). In the cases where the decoding was not satisfactory, the co-channel interference mentioned above was higher than the one shown in this example, resulting in more bit errors.

6 | CONCLUSIONS

An OCC communication system was conducted in this research employing an MS camera as the data receiver. Furthermore, the spectral features of the light sources employed as transmitters were altered by modifying their p-n

junction temperature. Thus, the same LED model would provide different spectral behaviours, which the MS camera would exploit. The LED temperatures were varied because of the Joule effect by supplying various driving currents to the LEDs. No heat sink was used in this work since it would have reduced the thermally induced spectral variation of the LEDs. Groups of LEDs with different dominant wavelengths have been used, and their performance has been analysed.

The strong point of this contribution lies in attaining multiple channels from the same LED by altering its temperature. A high-spectral-resolution camera, namely an MS camera, makes it possible to capture the slight dissimilarities in the LED's spectral signatures. The findings of this work demonstrate that for certain LEDs whose spectral properties are significantly affected by heat fluctuations in their p-n junction temperature, the BER below the FEC limit can be attained. It is worthwhile noting that in situations where the bit streams were not detected, a re-transmission strategy could be used.

Conversely, the green/blue LEDs' results were below expectations. The foremost factor of this poor performance is the temperature repercussion on those transmitter devices. Notably, the green and the blue devices were less thermally

impacted than the red LEDs, which peak wavelengths were noticeably red-shifted. Besides, it was evident from the condition number of the channel matrices that the ill-conditioned matrices obtained the most unsatisfactory performance. Consequently, the results of this study support the idea that utilising light sources whose spectral features are further influenced by temperature changes would enhance the experiment's success. Nevertheless, in those cases where the optical emitters are employed for illumination and communication, a compromise between the level of spectral changes and the efficiency drop resulting from thermal effects must be taken into account.

Moreover, the performance was unsuccessful when using three LEDs. There are two principal sources for this poor result. First, the slight variation in the spectral response curves brought about by changes in the LED p-n junction temperature limits the capability to obtain new communication channels. Second, the spectral resolution of the camera plays a crucial role in differentiating spectral signatures. Thus, the higher the number of bands and the thinner their width, the higher the resolution. Having considered those aspects, it could be seen in Section 5 by observing the spectral signatures and the condition number for the case of three transmitters that the signals did not present a considerable difference that would make them distinguishable for the employed camera.

An important implication of this research is the increase in the number of channels that can be achieved from a single transmitter by taking advantage of the impact of temperature.

More broadly, light sources with different peak wavelengths can be employed. Accordingly, using the method implemented in this research, the spectral bands of the camera with a specific centre wavelength would facilitate the separation of the signals. Furthermore, the potential for utilising the temperature impact on LEDs is an ongoing spur for further experimental studies. For example, future work should address the analysis of different LEDs (the same model and distinct ones) to assess the value of each device in this technique.

AUTHOR CONTRIBUTION

Daniel Moreno: Data curation, Investigation, Methodology, Software, Visualisation, Writing – original draft. **Victor Guerra:** Data curation, Formal analysis, Software, Validation, Writing – original draft. **Julio Rufo:** Conceptualisation, Supervision, Validation, Writing – review and editing. **Jose Rabadan:** Project administration, Resources, Supervision, Writing – review and editing. **Rafael Perez-Jimenez:** Funding acquisition, Project administration, Supervision, Writing – review and editing.

ACKNOWLEDGMENTS

This research was supported in part by the Universidad de Las Palmas de Gran Canaria's Trainee Predoctoral Research Staff Program (2019) and in part by the Spanish State Research Agency, project OCCAM PID2020-114561RB-I00.

CONFLICT OF INTEREST STATEMENT

The authors declare no conflict of interest.

DATA AVAILABILITY STATEMENT

The data that support the findings of this study are available from the corresponding author upon reasonable request.

ORCID

Daniel Moreno  <https://orcid.org/0000-0003-1336-7365>

Rafael Perez-Jimenez  <https://orcid.org/0000-0002-8849-592X>

REFERENCES

- Chowdhury, M.Z., et al.: The role of optical wireless communication technologies in 5G/6G and IoT solutions: prospects, directions, and challenges. *Appl. Sci.* 9(20), 4367 (2019). [Online]. Available: <https://doi.org/10.3390/app9204367> <https://www.mdpi.com/2076-3417/9/20/4367>
- Shiraki, Y., et al.: A demodulation method using a Gaussian mixture model for unsynchronous optical camera communication with on-off keying. *J. Lightwave Technol.* 39(6), 1742–1755 (2021). <https://doi.org/10.1109/jlt.2020.3043046>
- Hu, P., et al.: High speed LED-to-camera communication using color shift keying with flicker mitigation. *IEEE Trans. Mobile Comput.* 19(7), 1603–1617 (2020). <https://doi.org/10.1109/tmc.2019.2913832>
- Chow, C.-W., et al.: Display light panel and rolling shutter image sensor based optical camera communication (occ) using frame-averaging background removal and neural network. *J. Lightwave Technol.* 39(13), 4360–4366 (2021). <https://doi.org/10.1109/jlt.2021.3073656>
- Tsai, D.-C., et al.: Optical camera communication (occ) using a laser-diode coupled optical-diffusing fiber (odf) and rolling shutter image sensor. *Opt. Express* 30(10), 16069–16077 (2022). [Online]. Available: <https://doi.org/10.1364/oe.449860> <https://opg.optica.org/oe/abstract.cfm?URI=oe-30-10-16069>
- Arai, S., et al.: Experimental on hierarchical transmission scheme for visible light communication using LED traffic light and high-speed camera. In: 2007 IEEE 66th Vehicular Technology Conference, pp. 2174–2178 (2007)
- Iwase, D., et al.: Improving communication rate of visible light communication system using high-speed camera. In: 2014 IEEE Asia Pacific Conference on Circuits and Systems (APCCAS), pp. 336–339 (2014)
- Tugcu, E., et al.: Red-shift effect in multi-color LEDs based visible light communication. *Opt. Commun.* 463, 125451 (2020). [Online]. Available: <https://doi.org/10.1016/j.optcom.2020.125451> <https://www.sciencedirect.com/science/article/pii/S0030401820301115>
- Moreno, D., et al.: Effect of temperature on channel compensation in optical camera communication. *Electronics* 10(3), 262 (2021). [Online]. Available: <https://doi.org/10.3390/electronics10030262> <https://www.mdpi.com/2079-9292/10/3/262>
- Moreno, D., et al.: Clustering-based data detection for spectral signature multiplexing in multispectral camera communication. *Opt. Lett.* 47(5), 1053–1056 (2022). [Online]. Available: <https://doi.org/10.1364/ol.449207> <http://opg.optica.org/ol/abstract.cfm?URI=ol-47-5-1053>
- Cahyadi, W.A., et al.: Optical camera communications: principles, modulations, potential and challenges. *Electronics* 9(9), 1339 (2020). [Online]. Available: <https://doi.org/10.3390/electronics9091339> <https://www.mdpi.com/2079-9292/9/9/1339>
- Younus, O.I., et al.: Data rate enhancement in optical camera communications using an artificial neural network equaliser. *IEEE Access* 8, 42656–42665 (2020). <https://doi.org/10.1109/access.2020.2976537>
- Jurado-Verdu, C., et al.: Convolutional autoencoder for exposure effects equalization and noise mitigation in optical camera communication. *Opt. Express* 29(15), 22973–22991 (2021). [Online]. Available: <https://doi.org/10.1364/oe.433053> <http://www.opticsexpress.org/abstract.cfm?URI=oe-29-15-22973>

14. Huang, W., Tian, P., Xu, Z.: Design and implementation of a real-time CIM-MIMO optical camera communication system. *Opt Express* 24(21), 24567–24579 (2016). [Online]. Available: <https://doi.org/10.1364/oe.24.024567> <http://www.opticsexpress.org/abstract.cfm?URI=oe-24-21-24567>
15. Moreno, D., et al.: Optical multispectral camera communications using LED spectral emission variations. *IEEE Photon. Technol. Lett.* 33(12), 591–594 (2021). <https://doi.org/10.1109/lpt.2021.3078842>
16. Yamazato, T., et al.: Vehicle motion and pixel illumination modeling for image sensor based visible light communication. *IEEE J. Sel. Area. Commun.* 33(9), 1793–1805 (2015). <https://doi.org/10.1109/jsac.2015.2432511>
17. Hussein, Y.S., Alias, M.Y., Abdulkafi, A.A.: On performance analysis of ls and mmse for channel estimation in vlc systems. In: 2016 IEEE 12th International Colloquium on Signal Processing its Applications (CSPA), pp. 204–209 (2016)
18. Anusree, A., Jeyachitra, R.K.: Performance analysis of a MIMO VLC (visible light communication) using different equalizers. In: 2016 International Conference on Wireless Communications, Signal Processing and Networking (WiSPNET), pp. 43–46 (2016)
19. Jha, M.K., Kumar, N., Lakshmi, Y.V.S.: NOMA MIMO visible light communication with ZF-SIC and MMSE-SIC. In: 2020 2nd PhD Colloquium on Ethically Driven Innovation and Technology for Society (PhD EDITS), pp. 1–2 (2020)
20. Varshni, Y.P.: Temperature dependence of the energy gap in semiconductors. *Physica* 34(1), 149–154 (1967). [https://doi.org/10.1016/0031-8914\(67\)90062-6](https://doi.org/10.1016/0031-8914(67)90062-6)
21. Raypah, M.E., Devarajan, M., Sulaiman, F.: Influence of injection current and ambient temperature on intensity and wavelength of low-power SMD LED. In: 2016 IEEE 37th International Electronics Manufacturing Technology (IEMT) 18th Electronics Materials and Packaging (EMAP) Conference, pp. 1–6 (2016)
22. Raypah, M.E., et al.: Estimation of luminous flux and luminous efficacy of low-power SMD LED as a function of injection current and ambient temperature. *IEEE Trans. Electron. Dev.* 63(7), 2790–2795 (2016). <https://doi.org/10.1109/ted.2016.2556079>
23. Andonova, A., Yordanov, R., Yordanova, I.: Thermal stability analysis of power LED during aging. In: Proceedings of the 2011 34th International Spring Seminar on Electronics Technology (ISSE), pp. 274–278 (2011)
24. Chan, C.-J., et al.: Study on current and junction temperature stress aging effect for accelerated aging test of light emitting diodes. In: 2016 International Conference on Electronics Packaging (ICEP), pp. 62–65 (2016)
25. Becirovic, V., et al.: Effects on LEDs during the accelerated ageing test. In: 2019 18th International Symposium INFOTEH-JAHORINA (INFOTEH), pp. 1–6 (2019)

How to cite this article: Moreno, D., et al.: Multispectral Optical camera communication links based on spectral signature multiplexing. *IET Optoelectron.* 17(4), 91–100 (2023). <https://doi.org/10.1049/ote.12090>

C Supplementary scripts for OCC systems

This appendix includes a collection of scripts developed in various programming languages, including Python and MATLAB, to support the research presented in this thesis. The scripts are made available through a dedicated GitHub repository, accessible via the following link: <https://github.com/dmoreno93/optical-camera-communication>. These scripts serve as valuable resources for replicating and extending the experiments conducted in the study.